# Adaptive Reconfigurable Photovoltaic Arrays Based on Spatially Dispersed Irradiance Profiles

**Moein Jazayeri**

Submitted to the
Institute of Graduate Studies and Research
in partial fulfillment of the requirements for the degree of

Doctor of Philosophy
in
Electrical and Electronic Engineering

Eastern Mediterranean University
July 2018
Gazimağusa, North Cyprus

Approval of the Institute of Graduate Studies and Research

Assoc. Prof. Dr. Ali Hakan Ulusoy
Acting Director

I certify that this thesis satisfies all the requirements as a thesis for the degree of Doctor of Philosophy in Electrical and Electronic Engineering.

Prof. Dr. Hasan Demirel
Chair, Department of Electrical and Electronic Engineering

We certify that we have read this thesis and that in our opinion it is fully adequate in scope and quality as a thesis for the degree of Doctor of Philosophy in Electrical and Electronic Engineering.

Prof. Dr. Şener Uysal
Supervisor

Examining Committee

1. Prof. Dr. Hasan Demirel _____

2. Prof. Dr. Şule Erten Ela _____

3. Prof. Dr. Osman Kükrer _____

4. Prof. Dr. Serhat Şeker _____

5. Prof. Dr. Şener Uysal _____

# ABSTRACT

This thesis intends to develop a modeling method for an increased-efficiency adaptive reconfigurable photovoltaic (PV) system. Power generation in PV systems is directly proportional to the incident solar irradiance values on PV module surfaces. High dependency of PV power generation on the incoming solar irradiance values has led the research to develop various models for irradiance estimation purposes. A good model from PV applications point of view should be able to take into account the clouds and their light interaction characteristics in order to generate reliable site-specific irradiance profiles or time-series. This thesis proposes a model for generation of Spatially Dispersed Irradiance Profiles (SDIPs) which utilizes real cloud patterns derived from sky images taken at the application sites and takes into account different cloud types and distributions in the sky together with their sunlight interaction characteristics in order to generate instantaneous irradiance profiles as well as daily irradiance time-series. Utilization of a comprehensive set of cloud types and their sunlight interaction characteristics by the model allows for a precise analysis of the effects of clouds on the incoming irradiance values. Each PV module on the Earth`s surface receives the beam irradiance through circles/ellipses formed when the existing cloud layer in the sky cuts the cones through which the PV module sees the Sun`s disk. The thickness of the circles/ellipses vary according to the variations of the position of the Sun in the sky during a day. The model assumes that the beam irradiance received by each PV module is only affected by the amount of cloud coverage enclosed within the mentioned circles/ellipses. The most appropriate circles/ellipses are determined for each PV module at each time instant and virtually located on the sky images. The beam irradiance component for each PV module is then obtained as a result of taking into

consideration the attenuating effects of the cloud coverage enclosed within the mentioned circles/ellipses. Since the thickness of circles/ellipses and their position on the sky image vary with respect to variations of the Sun`s position in the sky during a day and the geographical location of the PV modules within the PV array, the Ellipse Enclosed Cloud Coverage (EECC) also differs for different PV modules and hence, different irradiance values are obtained for different PV modules. The diffuse and ground-reflected irradiance components are assumed to be identical for all PV modules. In addition to the instantaneous SDIPs, daily irradiance time-series for different PV modules within the array are simulated by the model using a set of consecutive sky images. The results have shown that the obtained instantaneous irradiance values as well as irradiance time-series incident on different geographical locations within a PV array present a dispersed characteristic where the range of dispersion depends on the existing cloud type and its distribution in the sky. The model has been validated using different performance metrics and quite satisfactory validation results have been obtained verifying the model`s capability to generate reliable site-specific irradiance profiles or irradiance time-series to be utilized for different analysis purposes in PV arrays. The results of comparison of the measured and modeled Variability Index (VI) values, as a verification method of the performance of the developed model, show statistics of mean bias error (MBE) of 0.16, root mean square error (RMSE) of 2.394, correlation coefficient of 0.94 and mean absolute error (MAE) of 1.91. The proposed model is presented as a global model, with minimum dependency on sensors or other measurement equipment, which is capable of generation of SDIPs or irradiance time-series for any geographical location on the Earth`s surface under any type and distribution of cloud coverage in the sky, with available sufficient input data.

A simple model is developed in MATLAB/Simulink environment in order to simulate PV modules based on one-diode mathematical model of a PV cell. PV arrays are simulated as combinations of series and parallel connected PV modules with different interconnection architectures and their performances are compared.

A novel adaptive dynamic reconfiguration algorithm is developed in this thesis in order to improve power generation in PV arrays. The proposed reconfiguration algorithm is based on irradiance equalization method aiming at creation of series-connected rows of parallel-connected PV modules in a PV array with average irradiance values similar to the array`s average irradiance value in order to prevent limiting effect of less power generating rows on power generation by the array. The reconfiguration algorithm proposed in this thesis is a simple dynamic algorithm which intends to find near-optimal array configurations, in terms of irradiance equalization principle, based on the existing irradiance profiles as a result of the existing cloud coverage and distribution in the sky. The proposed algorithm is not limited to the number of PV modules included within a PV array and best fits large-scale centralized or distributed PV arrays rather than residential PV applications. The near-optimal array configurations are obtained by considering an irradiance threshold value which is in fact a tolerance shown against current limiting effects of the less power generating rows. The rows with average irradiance values falling within the irradiance tolerance from the array`s average irradiance value are not reconfigured by the algorithm since they do not cause significant limitations on array`s power generation. In this way, the number of reconfigured rows and PV module reconfigurations along with the number of required switching actions to obtain the final array configuration is reduced. Reduction of the number of switching actions also preserves lifetimes of switching devices. Switching actions are performed by a flexible switching matrix which is

capable of connecting each PV module to each row of the PV array. The proposed reconfiguration algorithm is applied to totally four different irradiance profiles or partial shading scenarios and the array`s P-V characteristic curves are obtained before and after PV array reconfiguration considering different irradiance threshold values. The results have shown that the proposed reconfiguration algorithm is able to improve array`s power generation to almost maximum possible amounts under ideal case, in terms of irradiance equalization. In addition to achieving approximately maximum possible power generation in PV arrays, the results have also put forth the smoothing effects of the considered irradiance threshold value on array`s characteristic curves. Lower values of irradiance threshold have results in smoother characteristic curves to the cost of higher number of PV module reconfigurations and switching actions to be performed by the switching matrix. The results show that the reconfiguration algorithm has been able to improve array`s power generation by 4.7%, 6.1% and 2.7%, respectively under three different non-uniform irradiance profiles considered during analysis, where the reconfiguration algorithm is applicable. Although the proposed reconfiguration algorithm is applied to a single geographical location and time instant, it is expected to improve power generation in PV arrays at any geographical location or time interval. The proposed algorithm is also expected to perform better where the existing irradiance profiles contain irradiance values with high dispersion ranges.

**Keywords:** Renewable Energy, Solar Energy, Photovoltaic, PV Module, Partial Shading, PV Power Generation, Spatially Dispersed Irradiance Profile, Irradiance Model, Cloud Cover, PV Array Reconfiguration, Switching Matrix, Adaptive PV System

# ÖZ

Bu tez çalışmasının amacı, yüksek verimli uyarlanabilir ve yeniden yapılandırılabilir güneş enerji sistemleri için bir modelleme yönteminin geliştirilmesinden ibarettir. Güneş enerji sistemlerinde güç üretimi, güneş panelleri yüzeyine ulaşan güneş ışınları ile doğrudan orantılıdır. Güneş enerji sistemlerindeki güç üretiminin güneş panellerinin yüzeyine ulaşan güneş ışınlarına olan yüksek orandaki bağımlılığı literatürde güneş radyasyon oranı tahminleri için birçok modelin geliştirilmesinde etkin rol oynamıştır. Güneş enerjisi uygulamaları açısından uygun sayılabilecek bir modelin uygulama bölgelerine özel güvenilir ve sağlıklı radyasyon haritaları veya radyasyon zaman serilerini üretebilmesi için gökyüzünde bulunan bulutları ve bulutların güneş ışınları ile olan etkileşimlerini dikkate alma kabiliyetinin bulunması gerekmektedir. Bu tez çalışması Uzaysal olarak Dağılmış Radyasyon Haritaları'nı (UDRH) oluşturmak adına anlık radyasyon haritalarının yanı sıra günlük radyasyon zaman serilerini elde etmek amacıyla uygulama alanlarında çekilmiş olan gökyüzü resimlerinden elde edilen gerçek bulut modellerini kullanan ve çeşitli bulut türleri ve gökyüzündeki dağılımları ile birlikte bulutların güneş ışınları ile etkileşim karakteristiklerini dikkate alan bir modeli tanıtmaktadır. Geniş kapsamlı bulut çeşitleri ve bunların güneş ışınları ile etkileşim karakteristiklerinin tez çalışmasında geliştirilmiş olan model tarafından dikkate alınması, bulutların güneş panellerinin yüzeyine ulaşan güneş ışınları üzerindeki etkilerinin hassas bir şekilde analiz edilmesine olanak sağlamaktadır. Direkt güneş ışınları, yeryüzündeki her bir güneş panelinin yüzeyine güneş panelinin güneşi gördüğü koninin gökyüzündeki bulut katmanı tarafından kesilmesi sonucunda oluşan dairelerin/elipslerin içinden geçerek ulaşmaktadır. Bahsi geçen dairelerin/elipslerin kalınlıkları güneşin gökyüzündeki

pozisyonunun gün içerisindeki değişimlerine bağlı olarak değişmektedir. Bu tez çalışmasında önerilen model, her bir güneş panelinin yüzeyine ulaşan direkt güneş ışınlarının yalnızca ilgili dairelerin/elipslerin içinde kalan bulut oranı ve dağılımı tarafından etkilendiğini varsaymaktadır. Model tarafından her bir güneş paneli için her bir zaman aralığındaki en uygun daire/elips belirlenip sanal olarak gökyüzü resimlerinin üzerine yerleştirilmektedir. Daha sonra her bir güneş paneli için direkt güneş ışınları, bahsi geçen dairelerin/elipslerin içinde kalan bulut oranı ve dağılımının zayıflatıcı etkilerinin dikkate alınması sonucunda elde edilmektedir. Bahsi geçen dairelerin/elipslerin kalınlıkları ve gökyüzü resimleri üzerindeki konumlarının güneşin gün içerisinde gökyüzündeki pozisyonunun değişimlerine ve güneş panellerinin uygulama sahasındaki konumuna bağlı olarak değiştiğinden dolayı Elipsler tarafından Çevrelenen Bulut Örtüsü (EÇBÖ) de farklı güneş panelleri için farklı oran ve dağılımlara sahip olup dolaysıyla farklı güneş panelleri için farklı radyasyon oranlarının elde edilmesine neden olmaktadır. Yayılan ve yerden yansıyan güneş ışınlarının uygulama sahası içerisindeki tüm güneş panelleri için aynı olduğu varsayılmaktadır. Anlık UDRH'lara ilaveten günlük radyasyon zaman serileri de bir dizi ardışık gökyüzü resimleri kullanılarak model tarafından modellenmiştir. Elde edilen sonuçlar, anlık radyasyon değerleri konusunda olduğu gibi güneş enerjisi uygulama sahası içerisindeki farklı konumlarda bulunan güneş panellerine ulaşan günlük radyasyon zaman serilerinin dağınık bir karakteristik ortaya koyduğunu ve dağılma aralığının gökyüzünde bulunan bulut örtüsü ve dağılımına bağlı olduğunu ortaya koymaktadır. Tez çalışmasında önerilmiş olan modelin performansı farklı performans ölçüleri kullanılarak doğrulanmış olup güneş enerji sistemlerinde farklı analiz amaçları için kullanılmak üzere modelin uygulama bölgesine özel güvenilir radyasyon haritaları veya radyasyon zaman serilerini üretme kabiliyetini onaylayan

oldukça tatmin edici doğrulama sonuçları elde edilmiştir. Geliştirilen modelin performansının doğrulanması için kullanılan bir yöntem olarak ölçülen ve modellenen Değişkenlik İndeks (Dİ) değerlerinin karşılaştırma sonuçları 0.16 düzeyinde Ortalama Eğilim Hatası (OEH), 2.394 düzeyinde Karesel Ortalama Hata (KOH), 0.94 düzeyinde Korelasyon Katsayısı ve 1.91 düzeyinde Ortalama Mutlak Hata (OMH) istatistiklerini ortaya koymaktadır. Önerilmiş olan model, sensörler veya diğer ölçüm ekipmanlarına minimum düzeyde bağımlılık oranına sahip, herhangi bit bulut türü ve dağılımı altında, yeterli girdi verilerinin mevcut olduğu yeryüzündeki herhangi bir coğrafi konum için UDRH'lar veya radyasyon zaman serilerini üretme kabiliyetine sahip olan global bir model olarak sunulmuştur.

Güneş panellerinin karakteristiklerinin modellenmeleri amacıyla MATLAB/Simulink ortamında bir güneş hücresinin Bir-Diyot matematiksel modelini esas alan basit bir model geliştirilmiştir. Güneş enerji sistemleri farklı iç bağlantıları açısından farklı mimarilere sahip seri ve paralel bağlı güneş panellerinin kombinasyonları halinde modellenmiş olup performansları karşılaştırılmıştır.

Bu tez çalışmasında güneş enerji sistemlerindeki güç üretiminin arttırılması için özgün bir uyarlanabilir dinamik yeniden yapılandırma algoritması geliştirilmiştir. Önerilen yeniden yapılandırma algoritması, daha az güç üreten satırların sistemin toplam güç üretimi üzerindeki sınırlandırıcı etkilerinin önlenmesi amacıyla, bir güneş enerji sisteminde, paralel olarak birbirine bağlanmış olan, ortalama güneş radyasyon değerleri tüm sistemin ortalama radyasyon değerine benzer seri olarak bağlanmış güneş panellerinden oluşan satırların oluşturulmasını esas alan Radyasyon Eşitleme prensibine dayalı olarak çalışmaktadır. Bu tez çalışmasında geliştirilmiş olan yeniden yapılandırma algoritması, gökyüzünde bulunan bulut örtüsü ve dağılımının bir sonucu

olarak oluşan radyasyon haritasına dayanan ve Radyasyon Eşitleme prensibi bakış açısından optimum konfigürasyona yakın bir konfigürasyonun oluşturulmasını amaçlayan basit ve dinamik bir yeniden yapılandırma algoritmasıdır. Geliştirilmiş olan algoritma bir güneş enerji sisteminde bulunan güneş panellerinin sayıları açısından hiçbir bir sınırlamaya tabi olmayıp yerleşim alanlarında kullanılan sistemler ile karşılaştırıldığında büyük çaplı merkezi veya dağıtılmış şekilde bulunan güneş enerji sistemlerinde daha iyi bir performans ortaya koymaktadır. Optimum konfigürasyona yakın sistem konfigürasyonları, gerçek anlamda daha düşük akım üreten satırların sınırlandırıcı etkilerine karşı gösterilen bir tolerans niteliğini taşıyan bir radyasyon eşik değerinin dikkate alınması sonucunda elde edilmektedir. Ortalama radyasyon oranları sistemin ortalama radyasyon değerine göre belirlenen radyasyon eşik sınırları içerisinde kalan satırlar, sistemin güç üretimi üzerinde kayda değer ölçüde sınırlandırıcı etkiye sahip olmadıklarından dolayı, algoritma tarafından yeniden yapılandırılmamaktadır. Böylelikle nihai sistem konfigürasyonunun elde edilmesi için gerekli olan yeniden yapılandırılacak satır ve güneş paneli sayısı ile birlikte gerekli olan anahtarlama eylem sayıları da düşürülmektedir. Anahtarlama eylem sayılarının düşürülmesi aynı zamanda anahtarlama cihazlarının ömür sürelerini de korumaktadır. Anahtarlama eylemleri, her bir güneş panelini sistemin herhangi bir satırına bağlama kabiliyetine sahip olan esnek bir anahtarlama matrisi tarafından gerçekleştirilmektedir. Önerilen yeniden yapılandırma algoritması toplam 4 farklı radyasyon haritası veya kısmi gölgelenme senaryosuna uygulanmış olup sistemin Güç-Gerilim karakteristik eğrileri farklı radyasyon eşik değerleri dikkate alınarak sistemin yeniden yapılandırılması öncesinde ve sonrasında elde edilmiştir. Elde edilen sonuçlar, önerilen yeniden yapılandırma algoritmasının sistemin güç üretimini neredeyse Radyasyon Eşitleme prensibi açısından ideal durum altında mümkün olan en yüksek

değerlere yükseltme başarısını gösterdiğini ortaya koymuştur. Elde edilen sonuçlar aynı zamanda güneş enerji sistemlerinde yaklaşık olarak mümkün olan en yüksek güç üretim değerlerinin elde edilmesinin yanı sıra dikkate alınan radyasyon eşik değerinin sistemin Güç-Gerilim karakteristik eğrisi üzerindeki düzeltici etkisini ortaya koymuştur. Düşük radyasyon eşik değerleri daha yüksek sayıda güneş panelinin yeniden yapılandırılması ve anahtarlama matrisi tarafından daha yüksek sayıda anahtarlama eyleminin gerçekleştirilmesi karşılığında daha düzgün karakteristik eğrilerinin elde edilmesi ile sonuçlanmıştır. Elde edilen sonuçlar, yeniden yapılandırma algoritmasının sistemin güç üretimini analizler sırasında dikkate alınan ve yeniden yapılandırma algoritmasının uygulanabilir olduğu üç farklı homojen olmayan radyasyon haritası altında sırasıyla %4.7, %6.4 ve %2.7 oranında yükseltme başarısını gösterdiğini ortaya koymuştur. Önerilen yeniden yapılandırma algoritmasının tek bir coğrafi konuma ve zaman aralığına uygulanmış olmasına rağmen güneş enerji sistemlerindeki güç üretimini herhangi bir coğrafi konum ve zaman aralığında yükseltmesi beklenmektedir. Ayrıca önerilen algoritmanın mevcut olan radyasyon haritalarının yüksek dağınıklık aralıklarına sahip radyasyon değerlerini içerdiği durumlarda daha iyi bir performans sergilemesi beklenmektedir.

**Anahtar Kelimeler:** Yenilenebilir Enerji, Güneş Enerjisi, Güneş Paneli, Kısmi Gölgelenme, Güneş Enerjisi Güç Üretimi, Uzaysal olarak Dağılmış Radyasyon Haritası, Radyasyon Modeli, Bulut Örtüsü, Güneş Enerji Sistemi Yeniden Yapılandırması, Anahtarlama Matrisi, Uyarlanabilir Güneş Enerji Sistemi

# ACKNOWLEDGEMENT

Firstly I would like to express my very great gratitude and appreciation to my supervisor Prof. Dr. Şener Uysal for his continuous support and advice through my PhD studies. Whom has always shed light on my research with his professional guidance and kind attention.

In addition to my supervisor, also I would like to acknowledge the advice and support of the Head of the Electrical and Electronic Engineering Department Prof. Dr. Hasan Demirel as well as the other honorable jury members, Prof. Dr. Şule Erten Ela, Prof. Dr. Osman Kükrer and Prof. Dr. Serhat Şeker.

I extend my deepest appreciation and admiration to my dear father and mother for their unconditional love, assistance, guidance and support throughout my life. Definitely it was unimaginable to stand where I am today without their endless and limitless faith and trust in me.

Last but not least, my most special thanks and appreciation goes to my dear brother and best friend Kian. I would like to thank him for all the days and sleepless nights we were working together, for all his thoughtful support and helps through various stages of my studies and for all the memories we have shared together. Surely this study could not have been completed without his constant companionship and assistance.

# TABLE OF CONTENTS

# LIST OF TABLES

# LIST OF FIGURES

# LIST OF SYMBOLS AND ABBREVIATIONS

| | |
|---|---|
| $a, b$ | Ångström-Prescott Regression Coefficients |
| *a-Si* | Amorphous Silicon |
| *cc* | Cloud Cover [%] |
| $\overline{cc}$ | Average Cloud Cover [Oktas, tenths] |
| $cc(t)$ | Instantaneous Cloud Cover [Oktas, tenths] |
| $C_x(t)$ | Instantaneous Coordinate of Ellipse Center on X Axis |
| $C_y(t)$ | Instantaneous Coordinate of Ellipse Center on Y Axis |
| $cc_e(t)$ | Instantaneous Value of Ellipse Enclosed Cloud Cover [Oktas, tenths] |
| *CdS* | Cadmium Sulfide |
| *CdTe* | Cadmium Telluride |
| *CI* | Clearness Index |
| *CIGS* | Copper Indium Gallium Di-Selenide |
| *CIS* | Copper Indium Selenium |
| *$CH_4$* | Methane |
| *$CO_2$* | Carbon Dioxide |
| *c-Si* | Crystalline Silicon |
| *Cu2S* | Copper Sulfide |
| *CuInSe2* | Copper Indium Diselenide |
| $\overline{D_o}$ | Mean Daily Clear Sky Diffuse Fraction |
| $D_x(t)$ | Instantaneous Value of Major Axis of Ellipse |
| $D_y(t)$ | Instantaneous Value of Minor Axis of Ellipse |

| | |
|---|---|
| $E_g$ | Bandgap Energy of the Semiconductor Material |
| $e$ | Eccentricity of Ellipse |
| $G$ | Solar Irradiance [W/m$^2$] |
| $G_{STC}$ | Solar Irradiance under Standard Test Conditions [W/m$^2$] |
| $G(t)$ | Instantaneous Value of Cloudy Sky Horizontal Irradiance [W/m$^2$] |
| $\bar{G}_i$ | Average Irradiance of the I$^{th}$ Row [W/m$^2$] |
| $G_{ij}$ | Incident Irradiance on the J$^{th}$ PV Module of the I$^{th}$ Row [W/m$^2$] |
| $\bar{G}$ | Array`s Average Irradiance [W/m$^2$] |
| $G_0(t)$ | Extraterrestrial Solar Irradiance [W/m$^2$] |
| $G_b(t)$ | Instantaneous Value of Clear Sky Horizontal Beam Irradiance [W/m$^2$] |
| $G_{b\beta}(t)$ | Instantaneous Value of Clear Sky Inclined Beam Irradiance [W/m$^2$] |
| $G_d(t)$ | Instantaneous Value of Clear Sky Horizontal Diffuse Solar Irradiance [W/m$^2$] |
| $G_{d\beta}(t)$ | Instantaneous Value of Clear Sky Inclined Diffuse Irradiance [W/m$^2$] |
| $G_g(t)$ | Instantaneous Value of Array Point Cloudy Sky Horizontal Irradiance [W/m$^2$] |
| $G_{g\beta}(t)$ | Instantaneous Value of Array Point Cloudy Sky Inclined Irradiance [W/m$^2$] |
| $G_o(t)$ | Instantaneous Value of Clear Sky Horizontal Irradiance [W/m$^2$] |
| $G_{o\beta}(t)$ | Instantaneous Value of Clear Sky Inclined Irradiance [W/m$^2$] |
| $G_{r\beta}(t)$ | Instantaneous Value of Clear Sky Ground Reflected Irradiance [W/m$^2$] |
| $G_{x,y}(t)$ | Instantaneous Value of Irradiance at Point $(x, y)$ [W/m$^2$] |
| $G_\beta(t)$ | Instantaneous Value of Cloudy Sky Inclined Irradiance [W/m$^2$] |

| | |
|---|---|
| $GaAs$ | Gallium Arsenide |
| $H$ | Daily Horizontal Global Irradiation [J/m$^2$] |
| $H_0$ | Daily Irradiation Outside the Earth`s Atmosphere [J/m$^2$] |
| $\overline{H_b}$ | Mean Daily Clear Sky Horizontal Beam Irradiation [J/m$^2$] |
| $\overline{H_d}$ | Mean Daily Clear Sky Horizontal Diffuse Irradiation [J/m$^2$] |
| $\overline{H_o}$ | Mean Daily Clear Sky Horizontal Global Irradiation [J/m$^2$] |
| $h$ | Elevation Above Sea Level |
| $I_{ph}$ | Photo-Generated Current [A] |
| $I_S$ | Diode Saturation Current [A] |
| $I_{sc}$ | Short-Circuit Current [A] |
| $I_{mp}$ | Current at Maximum Power Point [A] |
| $j$ | Julian Day Number |
| $j`$ | Julian Day Number Defined as the Day Angle |
| $\overline{K_b}$ | Mean Daily Clear Sky Beam Clearness Index |
| $\overline{K_d}$ | Mean Daily Clear Sky Diffuse Clearness Index |
| $K_i$ | Short-Circuit Current Coefficient |
| $\overline{K_o}$ | Mean Daily Clear Sky Clearness Index |
| $K_0$ | Clear-Sky Index |
| $k, l$ | Size of PV Array |
| $k$ | Boltzmann Constant [J/K] |
| $l$ | Number of PV Modules in a Row |
| $m$ | Image Size for Cloud Pattern |
| $N_2O$ | Dinitrogen Oxide |
| $NO_x$ | Nitrogen Oxide |
| $N_P$ | Number of Parallel Connected PV Cells in a PV Module |

| | |
|---|---|
| $N_{PV}$ | Number of PV Modules in the Array |
| $N_{SW}$ | Number of Switching Actions |
| $n$ | Diode Ideality Factor |
| $O_3$ | Ozone |
| $P_{max}$ | Maximum Power Point |
| $P_{NR}$ | Array`s Non-Reconfigured Maximum Power [Watts] |
| $P_{OPT.}$ | Array`s Maximum Power under Ideal Conditions [Watts] |
| $q$ | Electron Charge [c] |
| $R_{cc_e}$ | Range of EECC [Oktas, Tenths] |
| $R_G$ | Range of Array Point Irradiance Values [W/m$^2$] |
| $R_b$ | Ratio between Beam Irradiance on Inclined and Horizontal Surface |
| $R_{cc}$ | Range of Cloud Cover [Oktas, Tenths] |
| $R_d$ | Ratio between Diffuse Irradiance on Inclined and Horizontal Surface |
| $R_S$ | Series Resistance [Ohms] |
| $R_p$ | Shunt Resistance [Ohms] |
| $S$ | Monthly Average Bright Sunshine Hours [Hours] |
| $S_0$ | Monthly Average Day Length [Hours] |
| $S_f$ | Daily Relative Sunshine Duration [Hours] |
| $SIF(t)$ | Instantaneous Value of the Stochastic Insolation Function |
| $Se$ | Selenium |
| $Si$ | Silicon |
| $SO_x$ | Sulfur Oxide |
| $SR$ | Sunrise |
| $SS$ | Sunset |
| $T$ | Working Temperature of a PV Cell [K] |

| | |
|---|---|
| $V_{mp}$ | Voltage at Maximum Power Point [V] |
| $V_{oc}$ | Open-Circuit Voltage [V] |
| $V_t$ | Thermal Voltage of a PV Cell [V] |
| $x,y$ | Coordinates of Ground Coverage Area of Sky Images [Meters] |
| $x', y'$ | Cloud Transmittance Coefficient |
| $\alpha_m$ | PV Module Azimuth Angle [Degrees] |
| $\alpha_p$ | Pixel Azimuth Angle [Degrees] |
| $\alpha_s$ | Solar Azimuth Angle [Degrees] |
| $\beta$ | PV Module Tilt Angle [Degrees] |
| $\gamma_s$ | Solar Altitude Angle [Degrees] |
| $\delta$ | Solar Declination Angle [Degrees] |
| $\Delta G$ | Irradiance Increment, Irradiance Threshold [W/m$^2$] |
| $\Delta H$ | Cloud Height in the Sky [Meters] |
| $\Delta T_{GMT}$ | Difference from GMT Mean Time [Hours] |
| $\theta_p$ | Pixel Zenith Angle [Degrees] |
| $\theta_s$ | Solar Incidence Angle [Degrees] |
| $\theta_z$ | Solar Zenith Angle [Degrees] |
| $\mu_G$ | Mean of Array Irradiance Values |
| $\rho$ | Ground Reflectivity |
| $\tau$ | Time Interval between Irradiance Measurements |
| $\tau_c$ | Cloud Transmittance |
| $\bar{\tau}$ | Cloud Transmission Factor |
| $\varphi$ | Latitude |
| $\omega$ | Hour angle |
| AM | Air Mass |

| | |
|---|---|
| BIPV | Building Integrated PV |
| BOS | Balance of System Equipment |
| BSRN | Baseline Surface Radiation |
| BL | Bridge-Link |
| CBH | Cloud Base Height |
| CC | Cloud Cover |
| CCD | Charged Coupled Device |
| CI | Clearness Index |
| CMSAF | Satellite Application Facility on Climate Monitoring |
| CSP | Concentrated Solar Power |
| EOT | Equation of Time |
| EECC | Ellipse Enclosed Cloud Coverage |
| GHG | Greenhouse Gas |
| GMT | Greenwich Mean Time |
| HDI | Human Development Index |
| IEC | International Electrotechnical Commission |
| LST | Local Solar Time |
| LSTM | Local Standard Time Meridian |
| LT | Local Time |
| MAE | Mean Absolute Error |
| MAPE | Mean Absolute Percentage Error |
| MBE | Mean Bias Error |
| MPP | Maximum Power Point |
| MPPT | Maximum Power Point Tracking |
| NWP | Numerical Weather Prediction |

| | |
|---|---|
| PV | Photovoltaic |
| P&O | Perturb and Observe |
| RBR | Red/Blue Ratio |
| RMSE | Root Mean Square Error |
| SDIP | Spatially Dispersed Irradiance Profile |
| SHS | Solar Home System |
| SP | Series-Parallel |
| SSE | Surface Meteorological and Solar Energy |
| STC | Standard Test Condition |
| TC | Time Correction Factor |
| TCT | Total-Cross-Tied |
| UN | United Nations |
| UVA | Ultraviolet A |
| UVB | Ultraviolet B |
| UVC | Ultraviolet C |
| UNSW | University of New South Wales |
| VI | Variability Index |
| VOC | Volatile Organic Compound |
| WRMC | World Radiation Monitoring Center |

# Chapter 1

# INTRODUCTION

Access to energy, particularly in the form of electricity, is assumed as a vital need in today`s modern human life, whereas energy consumption is directly proportional to the quality of life. The UN defines the Human Development Index (HDI) based on the average life span, educational improvements and per capita Gross Domestic Product for more than 60 countries including more than 90% of the population of the world. Figure 1.1 presents a general picture of the significant role of electricity consumption on the worldwide countries` development status, considering the HDI and electricity consumption amounts.

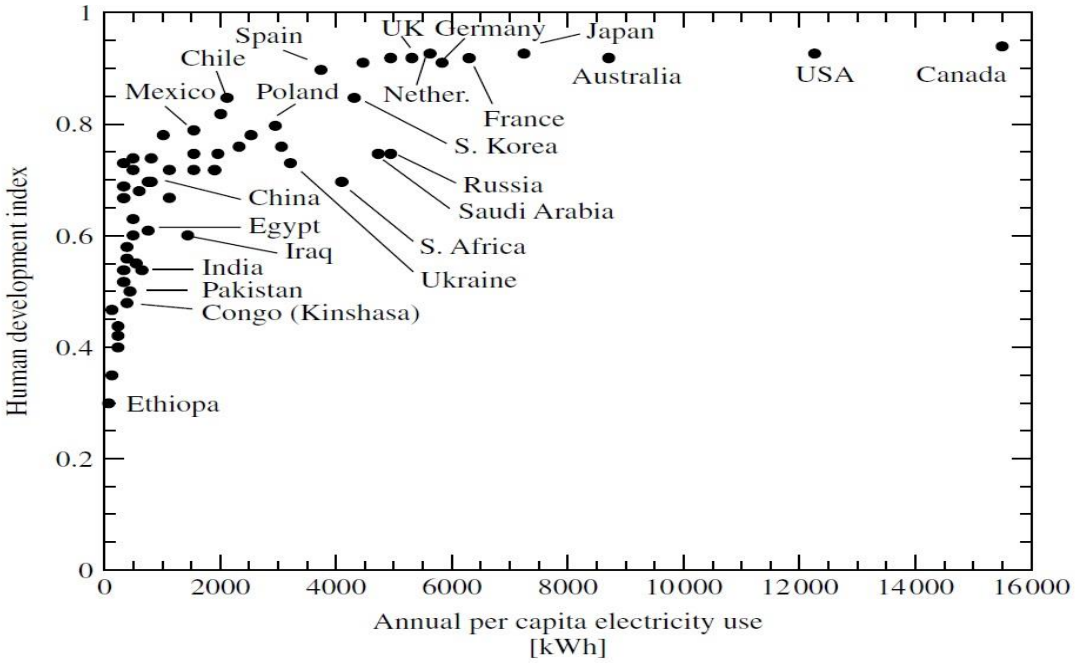

Figure 1.1: HDI vs. Per Capita Electricity Usage [1]

Finite nature of the conventional energy resources and their negative environmental effects together with the increasing energy demand in parallel with the industrial developments have led the modern world to search for new sources of energy. In this regard, utilization of renewable energies has attracted the attentions due to many advantages of these energy sources over the conventional ones. Solar energy is one of the most promising sources of renewable energies having the potential to take the place of conventional energy sources. Generating electricity from solar energy, which is also known as Photovoltaics (PV), does not have any pollution impact on the environment. Also, infinite nature of the energy source, low operational costs, containing no moving parts, high module life-times, quick installation and modularity are all advantages that cause solar energy to be preferred over the existing conventional energy sources. On the other hand, solar energy, like any other source of energy, has also some disadvantages that should be overcome to make possible a wide utilization of this source of energy. Some of the most known disadvantages of solar energy are relatively high installation costs, lack of efficient energy storage and even low, the carbon dioxide emissions that happen during manufacturing stage of PV materials.

## 1.1 History of Photovoltaics

The history of PV goes back to 1839, when Edmund Becquerel, a French physicist, first observed the photovoltaic effect, or electricity generation from light, in liquid electrolytes. The first researches of PV effect in solids, such as Se, was conducted in 1873. The first functional PV device, a solar cell made from Se films, was produced by Fritts in 1883 [1]. The present concept of PV has been prepared with the aid of quantum mechanics in 1920s and 1930s. The Czochralski method developed in 1940s and 1950s is considered as a major development in PV cell technologies. The modern age of PV is assumed to be started in 1954 when the Bell Laboratories in the USA

reported production of a silicon PV cell with 4% light conversion efficiency which was shortly improved to 6% and then 11% [2]. NASA used the first Si solar cells in a space application, the US Vanguard Satellite, in 1958 [1]. This first successful application of solar cells in a space program encouraged researches to develop PV technology for space missions. The Cherry Hill Conference, which was organized in 1973, takes its place in the history as the first PV conference. This conference revealed worthiness of PV to receive government support and consequently the US Energy Research and Development Agency, which finally became the US Dept. of Energy, was formed as the world`s first governmental team established with the aim of conducting research activities on renewable energies. The year 1973 carries a very high importance from PV technology point of view. The oil crisis arisen in October, 1973 as a result of the first World Oil Embargo by the oil producers in the Persian Gulf caused lots of industrialized governments to encourage research activities on renewable energies as reliable replacements for the conventional fossil fuels. Countries such as the USA, Japan and the European countries established facilities to produce Si solar cells and PV technology started to change its phase from research activities to pre-commercial production. The first thin-film solar cell with more than 10% efficiency was produced in the laboratory environment [1]. The first calculator powered by a small-scale consumer-sized solar cell was produced in the early 1980s in Japan. Also, small-scale consumer-sized solar cells utilized to supply power for low-power outdoor lighting applications formed other examples of the very first commercial uses of solar cells, besides the research and development activities. In contrary, MW-scale PV power plants were established in 1980s in developed countries to either provide an additional auxiliary power source to meet the peak power demand during hours with high electricity consumption rate or to act as distributed generation

stations in order to decrease energy transmission or distribution losses [1]. Building Integrated PV (BIPV) introduced by integration of PV cells into buildings in the late 1990s is considered as one of the major developments from PV applications point of view. In 1990s, governmental supports in Europe and Japan have caused them to be the leading countries in terms of grid-connected PV applications. In 1999 the worldwide installed PV capacity has been 1000 MW while this amount is doubled only within 3 years, reaching 2000 MW in 2002. The first Bachelor`s degree in Photovoltaics and Solar Engineering has been granted in 2002 by the UNSW, Australia [1].

## 1.2 PV and Development

The energy requirement has increased along with technology developments. Estimations show that daily energy consumption in very early societies has been approximately 2500 Kilo calories [3] while this amount has reached 70000 Kilo calories in industrialized societies such as the USA, England and Germany during the industrial revolution in 1800s [4]. The mentioned energy sources are replaced by petroleum, natural gas and nuclear energy in late 1900s while the daily energy consumption rate in industrialized countries has increased to approximately 230000 Kilo Calories during these years [4].

Development of electric power industries and entrance of electricity into human`s life can be considered as a basic milestone in today`s modern life. Electricity became the main source of lighting while factories have utilized electrical motors as the main source of power. Also electricity has involved in, and facilitated many areas of today`s human life; from basic communication requirements to small home appliances and

entertainment tools as well as computers and security systems, without which today`s life seems unimaginable.

However, unfortunately, despite the technological developments of today`s modern life, there are lots of people suffering from lack of access to electricity and hence, the very basic opportunities and requirements of today`s life. This ratio may somehow be incredibly high; about 30% of the world`s population [5]. Most of these people live in rural places or in developing countries.

Agricultural applications are considered as major potential areas for electricity usage in rural areas. However, due to limited number of consumers and small amount of electricity usage in rural areas, extension of energy transmission lines to the mentioned areas may not always be economical. The mentioned situation has been the biggest motivation for governments and officials to support rural electrification. Rural electrification in developing countries has followed the developed countries. A big step has been taken by extension of transmission lines to rural areas in 1960s and 1970s. However, unfortunately only a limited number of developing countries managed to extend the electricity grid over rural areas by the end of the $20^{th}$ century and economical and financing problems are still the main obstacles against rural electrification in many developing countries.

Studies have shown that even small amounts of energy, mostly in the form of electricity, may significantly change the lifestyle and improve the quality of life in rural areas. Lighting, communication, clean water and entertainment requirements as well as medical needs are the major areas in which application of electricity may help facilitate the daily life of a rural family. Also external lighting, such as illumination of

streets and social gathering areas provides big opportunities for socializing of the people living in rural places.

Dry batteries, car batteries and small scale generators are some of the energy sources used in rural areas before extension of grid electricity. Economical limitations are considered as reasons for which families in rural places often do not use the grid electricity for luxury or expensive home appliances and entertainment systems. Most of the families in rural areas use grid electricity only for small scale lighting purposes as well as some radios and/or black and white TVs. Taking the mentioned considerations into account together with the previously mentioned economical limitations regarding extension of electricity grid to rural places, it seems that PV technology may be considered as a good alternative to meet rural electricity requirements. As mentioned previously, PV technology can be considered as one of the most suitable sources to supply electricity for rural areas. The modular characteristic of PV technology may be considered as one of the main reasons to prefer this technology for rural electrification. Taking into account the energy requirement for different applications, PV systems can be designed in different sizes and scales in order to meet a wide range of energy requirements in rural areas. Projects installed in India, Mexico and Niger during 1968-1977 are some of the first examples of application of PV technology for rural electrification [5]. Improvements in material, system engineering and electronic devices along with reduction of the price of PV systems due to reduced price of the system components in parallel with a clearer view of energy requirements in a rural place have all resulted in increasing efforts to meet electrification requirements in rural areas of developing countries by using PV technology. As mentioned previously, stand-alone or off-grid PV systems are the best sources of energy to be utilized for rural electrification. Solar Home Systems (SHS)

are examples of such off-grid PV applications which are widely being utilized in rural areas. Estimations show that approximately 500,000 – 1,000,000 solar homes are currently being used in rural areas all-around the world [6]. Moreover, wider utilization of PV technology will bring along improvements in education, health, entertainment, communication and other similar fields in rural areas of developing countries.

## 1.3 The Photovoltaic Effect

Conversion of sunlight into electricity in solar cells is based on the photovoltaic effect. The photons of sunlight received at the surface of a solar cell contain energy, whereas this energy may be higher or lower according to the spectrum of the incident light. The sunlight incident on the surface of a solar cell may be reflected back, absorbed by or pass through the material. The important portion of the sunlight from photovoltaics point of view is the absorbed sunlight. However, not all of the sunlight absorbed by the material is eligible to be converted to electricity. As mentioned previously, the incident light may have different levels of energy. When sunlight with relatively low energy hits the surface of a solar cell it can only create some heat but it is not capable of changing the electrical characteristics of the cell material. However, the case is not the same when sunlight with high energy level is received by a solar cell. In this case, the energy contained in the sunlight is transferred to the electrons of the solar cell material (e.g. silicon) which are generally in the valence band of energy. If this energy is higher than the band gap energy of the material it will excite the electrons and increase their energy levels to the conduction band. The electrons leave their places within the material of the solar cell and can move freely within the material. Movement of the electrons within the material causes them leave electron holes behind. The moving electrons within the material are called charge carriers. The charge carriers and electron holes are separated in a solar cell by a barrier which is formed when

opposite charges face each other. The mentioned separation then creates a voltage at the terminals of a solar cell. Figure 1.2 shows different energy levels in a semiconductor material forming a solar cell.

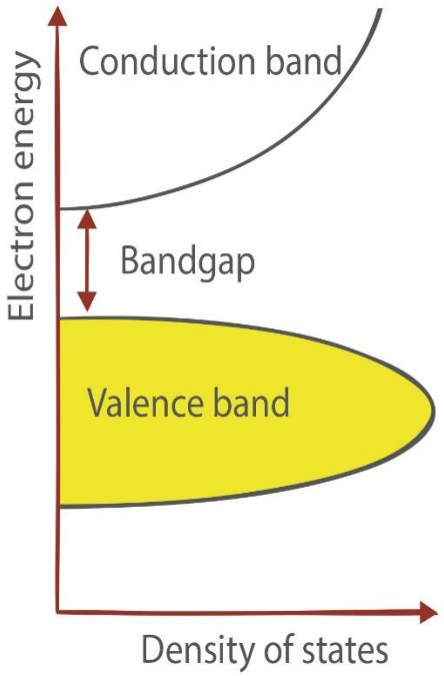


Figure 1.2: Different Electron Energy Bands in a Semiconductor Material

## 1.4 Current Status and Future of Different PV Technologies

This section provides brief information regarding different materials utilized during production of PV modules. The mentioned materials are all semiconductors having different specifications and therefore, efficiency limits. Silicon is the main material that is utilized in today`s PV industry. Most of the produced PV modules use silicon in the form of monocrystalline, multicrystalline or ribbon silicon. Thin-film is another PV technology with a lower share of PV market. Also some novel technologies like dye-sensitized and organic PV cells or III-V multi-junction cells can be considered as emerging PV technologies being at the pre-industrialized stage of development.

The current research and development activities in PV industry are mostly focused on improving PV technologies that currently have the largest share of PV market, such as Si and thin-film PV technologies. Although research and development studies on Si technology provide high significance due to the large market share of the mentioned technology, thin-film technologies are also expected to provide higher efficiency and cost improvements than those of the currently available ones [7].

### 1.4.1 Silicon PV Cells

Silicon is considered as the second most vastly found element in the world following oxygen and the most vastly found semiconductor material on the Earth`s surface. Silicon has found huge application areas in electronics and microelectronics. The global infrastructures for scientific research and technical development of Si begun in 1960s [5]. Governments and industrial organizations have made enormous investments for different purposes such as understanding the chemical and electronical characteristics of Si, development of techniques to obtain Si with the required pureness and crystalline architecture as well as making the devices and equipment required for all the above mentioned purposes. Silicon has widely been utilized for production of electronic chips that played great role in today`s digital electronic developments. The physical properties of silicon are highly suitable to be used in PV industry and the vast amounts of silicon found on the Earth`s surface makes it a very suitable material from PV industry point of view. However, silicon, as the material used in PV industry, can be analyzed and considered under two main categories; Amorphous and Crystalline. Crystalline silicon has also two main types being namely; single or multicrystalline. The dominant role in today`s PV market is played by crystalline silicon, while multicrystalline silicon, that has emerged in 1980s, particularly has earned an increasing market share due to its lower price, despite the slightly lower efficiencies.

Efficiency of a Si PV module ranges from 14% to 20% while technological developments cause continuous cost reductions [8]. Also 25% efficiency limits have been achieved under laboratory conditions [5].

### 1.4.2 Thin-film PV Technology

Beside all the previously mentioned advantages for crystalline silicon to act as the major player of the global PV market, it also has some disadvantages that have led the research to find alternative materials and technologies. The main motivation is to achieve reduced costs and higher possibilities for production in large volumes compared to crystalline silicon solar panels. It is foreseen that silicon technology will not be able to fulfill the final targets purposed for mass global PV production in the future [5]. Some of the disadvantages of silicon for utilization in PV industry can be considered as expensiveness of the crystals and their slow growing speeds. Also it is found that silicon performs weaker than other sunlight absorbing semiconductors. Therefore, higher thicknesses, and hence larger amounts of material, compared to the other semiconductors, are required for silicon PV panels to absorb the same amount of solar irradiance. Taking into account the fact that currently a big portion of silicon that is utilized in PV industry is supplied from waste materials used in the electronic industry, it can be foreseen that in near future, together with the increasing demands of the PV industry, wastes from electronic industry will not be able to meet the silicon requirements of the PV industry. All the above mentioned disadvantages of silicon have led the research to find alternatives for silicon in PV industry.

Evolution of thin-film solar cells as an alternative for c-Si cells turns back to 1950s when some other semiconductors also found to be useful for utilization in PV modules. They are called “Thin-film” because most of the mentioned materials are available in the nature as very thin films (almost 100 times thinner than c-Si technologies) such

that they need to be manufactured on the surface of another material to be supported mechanically. Four different thin-film materials have shown acceptable efficiency (higher than 10%) and found capable to be used as alternatives for c-Si cells as of 1981-1982. The mentioned materials are Copper Sulfide/Cadmium Sulfide (Cu2S/CdS) [9], Amorphous Silicon (a-Si) [10], Copper Indium Diselenide/Cadmium Sulfide (CuInSe2/CdS) [5] and Cadmium Telluride/Cadmium Selenide (CdT/CdS) [11]. Among the mentioned technologies Cu2S/CdS thin-film technology was not considered capable of being utilized in PV industry due to stability issues. Lower cost compared to the c-Si technology has been the main advantage of thin-films from PV industry point of view. However, lower efficiency has been the main disadvantage of thin-film technologies compared to c-Si. Currently the recorded efficiency for thin-film technologies has been approximately 7%, 12% and 14% respectively for a-Si, CIGS and CdTe solar modules [8]. The mentioned disadvantage of thin-film technologies has caused their development face many challenges and still a large share of PV market belongs to c-Si technologies.

### 1.4.3 Emerging PV Technologies

While crystalline silicon and thin-film technologies are considered as the major players of today`s PV market, there are also some novel technologies emerging in PV industry. Although the mentioned novel technologies are not yet widely utilized in PV applications, they are considered to have some specific areas of application such as space programs, PV applications in deserts, building integrated PV systems and different products. Some of the mentioned novel PV technologies along with a brief explanation of each one are as follows;

- ***Dye-Sensitized PV Cells:*** The efficiency of these group of PV cells has reached 11%. However, the main disadvantages associated with these kind of cells are

issues related to stability and production of cells having large surface areas. At present, the mentioned PV cells are mostly utilized in small-scale electronic devices and building integrated PV systems [8].

- ***Organic PV Cells:*** These group of PV cells have been subject to great development during the recent years. Their current efficiency ranges vary from 4% to 8%, for commercial and research oriented cells, respectively. The focus application area of these kind of PV cells is small-scale electronic devices while main barrier against their utilization in the target applications is their sensitivity against sunlight and oxygen which causes them be chemically, physically or mechanically deteriorated. Hence, efforts should be put on manufacturing more stable cells having longer lifetimes than their current efficient lifetime which is 3 to 10 years [8].
- ***High Efficiency III-V Multi-Junction PV Cells:*** These kind of solar cells are generally made of GaAs and have been deployed in space applications for many years. The biggest advantage of these kind of PV cells is their high efficiency limits which even have exceeded 40% in some cases. However, the main disadvantage for these solar cells to be capable of wide utilization in PV market is their very high production costs. Utilization of concentrators has been considered as a solution against high costs of these cells in order to make them capable of being utilized in terrestrial power production applications. The mentioned concentrators are capable of intensifying the beam component of sunlight up to 2000 times and reflect it on the surface of solar cells. Thus, the mentioned technology is mostly utilized in desert areas which receive lots of the incident sunlight as direct solar irradiance [8].

## 1.5 Applications of PV Systems

Applications of PV systems can mainly be analyzed under two categories; 1) Grid-Connected PV Systems, 2) Off-Grid PV Systems. This part of the thesis briefly analyzes the mentioned types of PV systems along with some application examples of each system type. Also different designs and components of a PV system are analyzed.

### 1.5.1 Off-Grid PV Systems

Off-Grid PV systems are the systems without any connection to the main electricity grid. As the cost of energy transmission exceeds the cost of energy generation by off-grid systems, these kind of systems are usually preferred where there is no access to the utility grid, or in places far from the main utility. Also, since these systems do not have high maintenance requirements, they are utilized where maintenance equipment are not readily available or where the chance of regular maintenance of the systems is limited. Another application area for off-grid PV systems is to supply energy for standalone small-scale applications with low energy requirements such as watches, portable radios, traffic signs, calculators or outdoor lightings.

### 1.5.2 Grid-Connected PV Systems

Grid-Connected PV systems are those which are connected to the main electricity grid and capable of transferring the generated electricity to the grid. Although off-grid systems have a significant share among PV applications, significance of PV technology in a wider range seems to be better felt when it is capable to provide energy to the utility grid. The grid-connected PV systems can be considered under two main categories, as follows;

a. ***Grid-Connected Distributed PV Generators:*** These kind of systems are generally individual homes or workplaces with rooftop installed PV modules. They can buy or sell the generated electricity from or to the utility grid. These

systems can be assumed as auxiliary power sources to meet the peak load demand by the utilities. However, the most determinative factor for the utilities to buy electricity from distributed generators is the cost of the generated electricity. On the other hand, possible disturbances in the generated energy, generally due to weather conditions, form another risk factor for the utilities as a potential safety issue.

b. ***Grid-Connected Centralized Power Stations:*** The centralized stations are considered as the main power utilities. However, the most challenging factor for PV technology to be considered as the main power utility is that it should be competitive, in all aspects, with the conventional energy sources.

PV systems, either grid-connected or off-grid, are generally designed with or without battery backups. Figure 1.3 shows a grid-connected PV system design without battery backup. These systems obviously are not capable of storing the generated energy and hence they cannot meet the energy requirements during night or under cloudy sky conditions, especially in case of off-grid systems, when energy production is not possible. Also in case of grid-connected systems, where energy requirements are met by the utility during night or cloudy days, the loads cannot be supplied during a utility power outage situation.

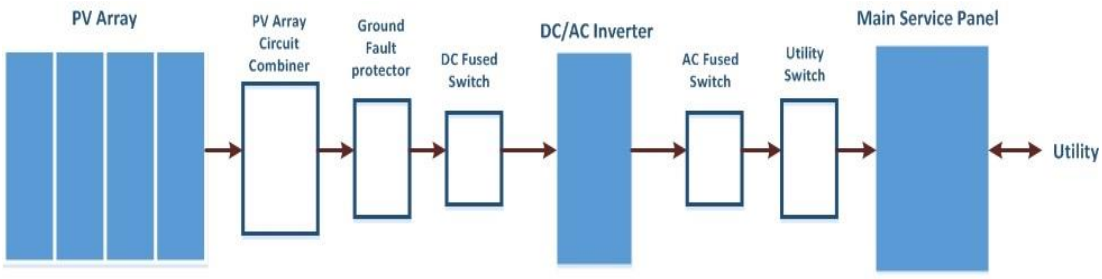


Figure 1.3: Grid-Connected PV System without Battery Backup [12]

On the other hand, the advantage of PV systems with battery backups is that they can store the produced energy. The stored energy can further be used to supply the loads during night or cloudy sky hours in off-grid systems or during utility power outage in case of grid-connected systems. Figure 1.4 shows a grid-connected PV system with battery backup. In such a system, the utility connection is switched-off and the loads are supplied through the battery during a power outage situation.

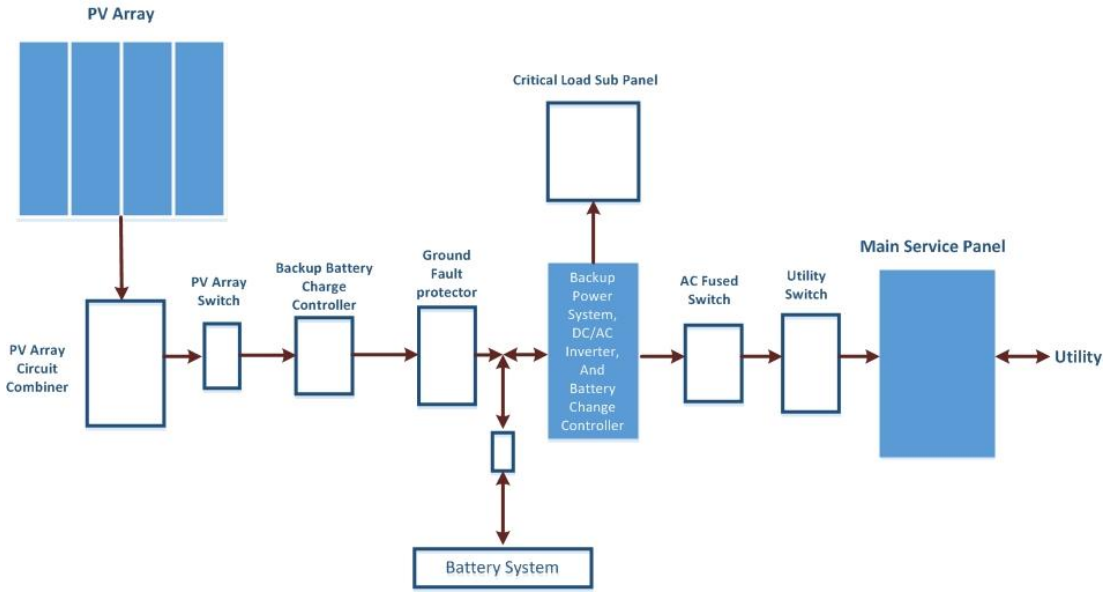


Figure 1.4: Grid-Connected PV System with Battery Backup [12]

Figure 1.5 provides a general scheme showing different application areas of different types of PV systems. Each PV system consists of different components, according to its type and usage area. Different components of a PV system can briefly be described as follows;

- ***PV Arrays:*** PV arrays are the most important part of each PV system. A PV array is a combination of some PV modules which are interconnected with different array architectures, in order to serve different application requirements. PV arrays are responsible for converting the incident sunlight to DC current in a PV system.

- ***Inverters:*** Inverter is also one of the most important components in a PV system. Inverters are responsible for DC-AC current conversion in a PV system.
- ***Balance of System Equipment (BOS):*** Balance of system equipment consist of different components in a PV system. They include mounting and wiring equipment to install and connect different components of the system to each other, metering equipment that are used to measure and monitor the performance of the system, switches with different usages such as connecting or disconnecting the system to or from the main utility, battery charge controllers (for systems with battery backup) and components designed for system protection purposes such as protection against overcurrent, etc.

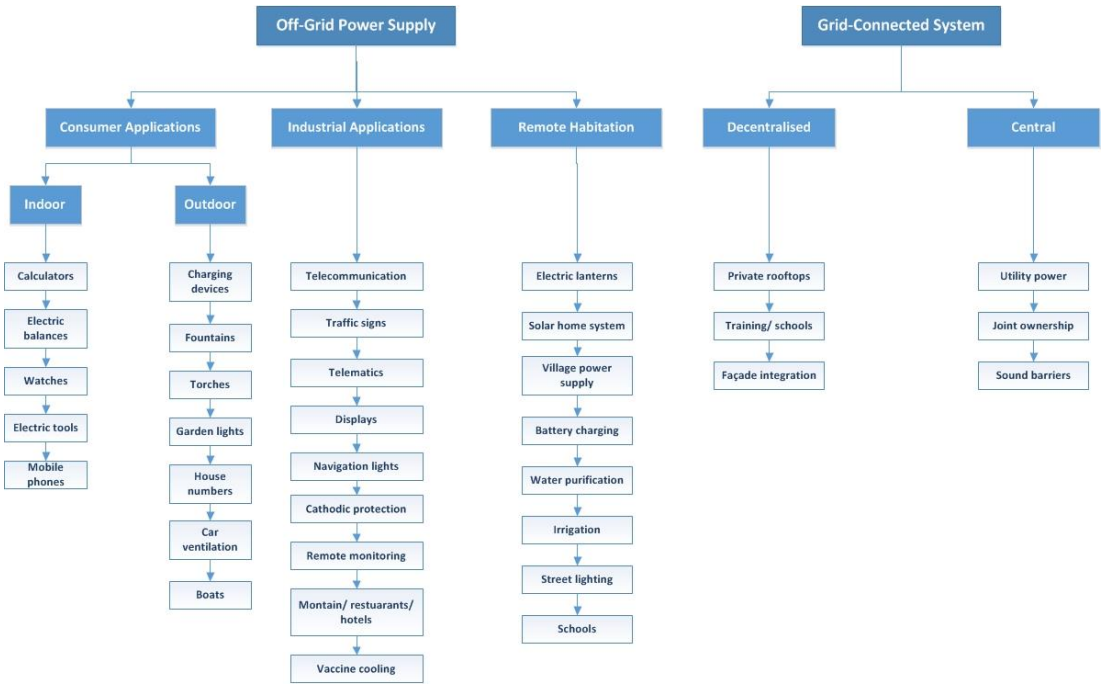

Figure 1.5: Different Application Areas of PV Systems

## 1.6 Global PV Market

As mentioned previously, the global PV market grows day by day owing to developments in PV technology which at the same time results in price reductions, in one hand, and its advantages over the conventional energy sources, on the other hand. Government incentives also play a great role in PV market growth. As an example, PV market has shown an annual growth rate of 60% and 53% during 2007-2012 time period, globally and in the U.S. market, respectively [2]. Results of another research study show 47% increase in DC PV power installation in the USA within the first half of 2016 compared to the same time period in 2015 [3]. Analysists also expect an increasing trend in installed PV capacity from 2014 to 2020 [15]. For example, expectations for growth rate have been approximately 15% - 40% for global PV installation in 2016 in comparison with 2015, while the United States and China are expected to have the largest PV markets until 2020 [3]. Also analysis results have shown 12% and 48% growth in PV module shipments made by PV manufacturers in the 2$^{nd}$ quarter of 2016 compared to the 1$^{st}$ quarter of 2016 and the 2$^{nd}$ quarter of 2015, respectively. Figure 1.6 provides a general overview of the global Concentrated Solar Power (CSP) market by Sept., 2016 [3].

A general scheme of country level PV market growth estimated from 2008 to 2020 in Europe is presented in Figure 1.7. As it is clearly shown in the figure, the European PV market has shown a rapid development from 2008 up to 2011, while the market has experienced a downward trend in 2012-2013 time period. The mentioned downward stream is considered as a result of changes of regulations in some European countries [15].

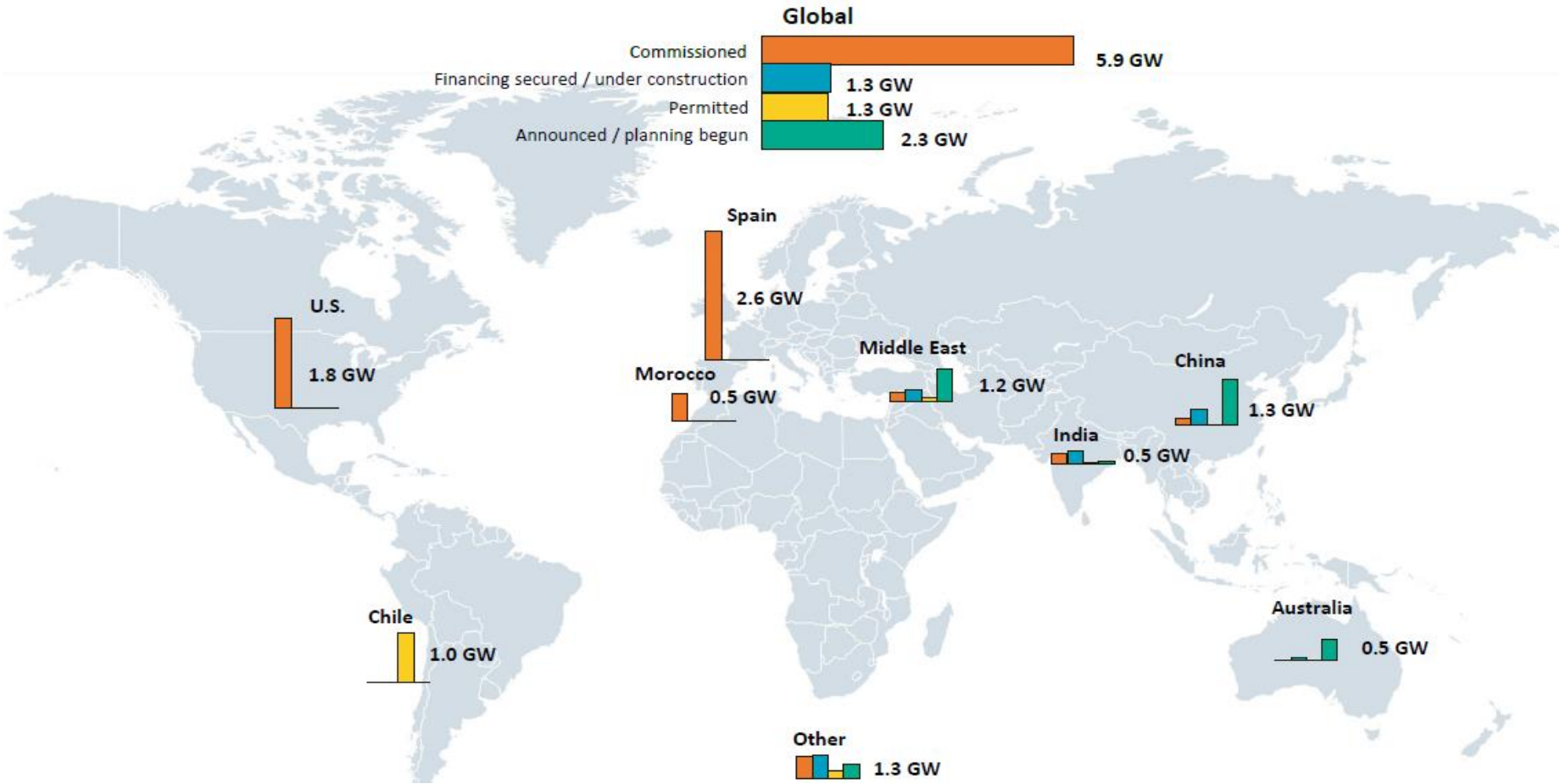


Figure 1.6: Global CSP Market by Sept., 2016 [3]

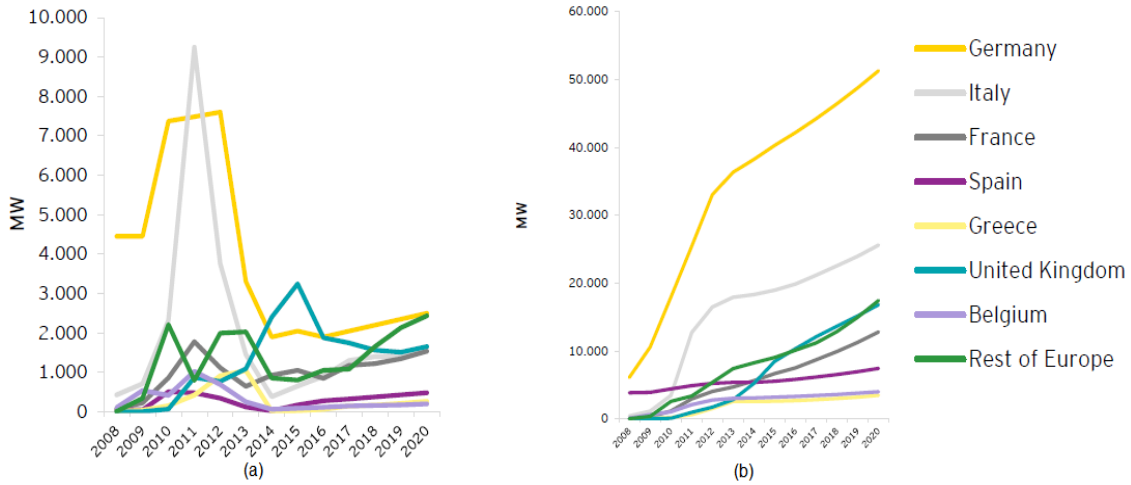


Figure 1.7: Country Level Annual (a) Capacity Installation (b) Cumulative Capacity Installation in Europe [4]

PV systems are generally available under two main types in the global market, being namely; rooftop systems and ground-mounted systems. Rooftop PV systems are generally utilized for commercial, residential or industrial purposes while ground-mounted systems generally serve as utility power plants. The country level distribution of the mentioned system types are shown in Figure 1.8 for some European countries.

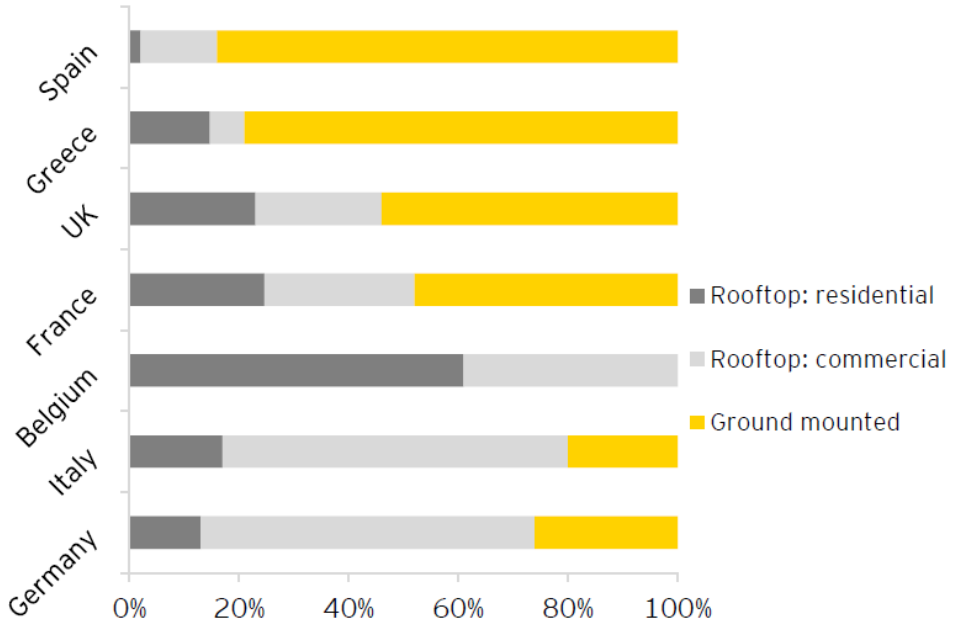


Figure 1.8: Country Level PV Market Distribution in 2014 [4]

### 1.6.1 PV Pricing

Overall price of a PV system can be considered to be consists of the price of BOS, the utilized solar panels and power converter devices, where the highest price belongs to BOS followed by solar panels and finally the power converters. Worldwide PV system prices have generally followed a decreasing trend during the recent years owing to development in technology and government incentives. As an example, the U.S. Department of Energy has initiated a plan aiming at reducing the cost of PV electricity by 75% within a time period from 2010 to 2020. Analysis results show a reduction in global PV module prices from 1.37$ per watt in 2011 to approximately 0.74 $ per watt in 2013 [5]. Results of another study show that PV system prices have been reduced by 70% in 2014 in European countries compared to 2008, where ground-mounted PV systems have been 50% cheaper than rooftop systems for each MW generated power. The lower costs of installation, repair and maintenance of ground-mounted PV systems as a result of the less consumed time and simplicity of the operations have caused the mentioned lower prices. It is estimated that reduction in PV prices has been a result of improvements in PV efficiency together with technology developments in this area as well as competition in the global market [4].

### 1.6.2 PV and Job Creation

Beside all the advantages and benefits, PV technology can be considered from a very different point of view; job creation and employment. Higher number of created jobs can consequently be expected along with developments of PV technology and growth of PV market in many countries. Currently the biggest portion of jobs created by PV technology belongs to European countries, where analysists expect this increasing trend to be continued through 2020 [4]. As an example, totally 110,000 jobs were created in the European PV sector and this amount is expected to exceed 136,000 by

2020 [4]. The number of created jobs for rooftop PV installations are approximately 3 times higher than ground-mounted systems as they require higher number of workforce for installation, repair and maintenance services [4]. Figure 1.9 presents a general scheme of the current direct and indirect jobs created by PV industry in the European market, together with estimations of job creation through 2020. The direct jobs are considered as jobs that are directly involved in the production, installation, repair and maintenance of PV systems while indirect jobs are those related to side services such as transportation, etc. Figure 1.10 shows the current situation along with the estimations for the number of jobs created by PV industry in the European market in terms of rooftop or ground-mounted PV systems. It is obvious from the figure that the number of jobs associated with rooftop PV installations are higher compared to the number of jobs created by ground-mounted PV systems.

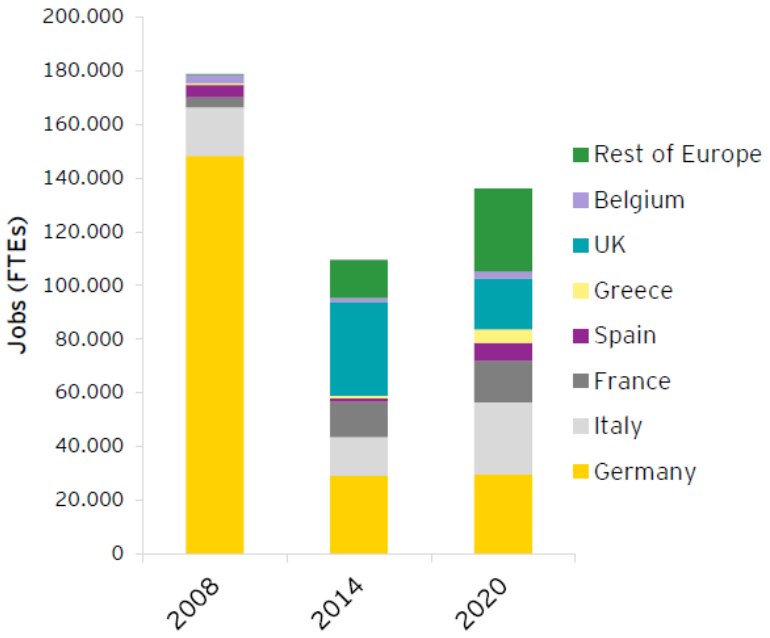


Figure 1.9: A General Overview of the Country Level Job Creation by PV Industry in the European Market [4]

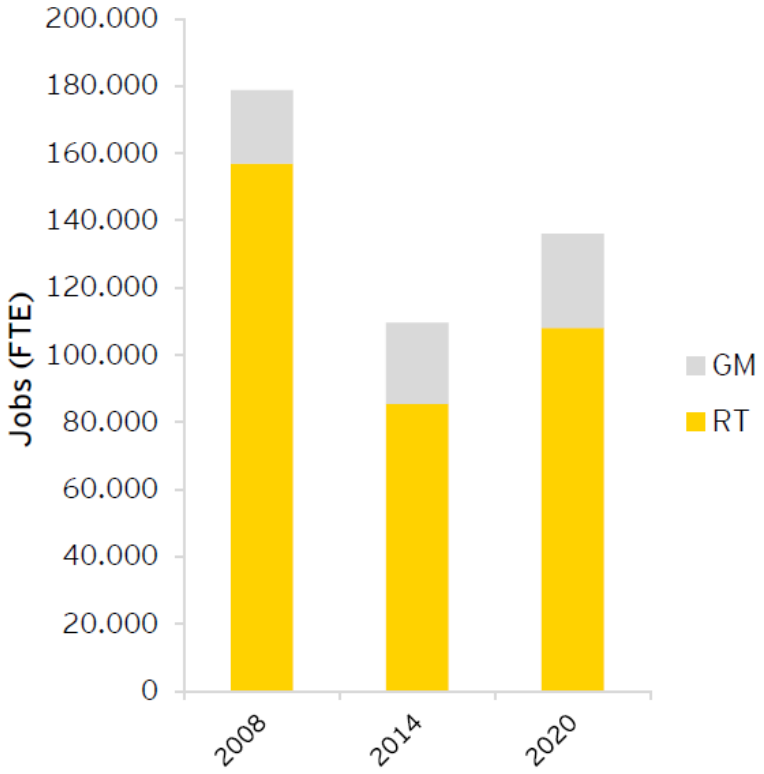


Figure 1.10: Number of Jobs Created by PV Industry in Terms of Rooftop and Ground-Mounted Systems [4]

The number of created jobs by PV industry can also be analyzed and compared in terms of two main process levels, as follows;

i. *Upstream Activities:* Includes processing of PV material, production of solar panels and system components.

ii. *Downstream Activities:* Includes PV system installation, system operation, repair and maintenance and marketing of the generated power.

Taking the above mentioned process levels into account, analysis results have shown that 86% of the total jobs are created during downstream activities. Details on job creation during each step of downstream and upstream application levels can be found in [4].

## 1.7 Environmental Impacts of PV Technology

- ***Greenhouse Gases and Air Pollutants***

Greenhouse gases (GHGs) are the gas components of the atmosphere which absorb or emit solar radiation. The concentration of the mentioned gases in the atmosphere has rapidly increased owing to industrial developments of the modern world. This increasing greenhouse gas emissions has resulted in global warming and consequently climate change, as an undeniable fact of today`s world. The most important GHGs include $CO_2$, $CH_4$, $N_2O$ and fluorinated gases. On the other hand, air pollutants such as different organic or inorganic hazardous solid or liquid particles suspended in air, $O_3$, $SO_x$, $NO_x$ and volatile organic compounds (VOCs) have negative effects on human health and environment by causing acidic rains and smog [6]. Research studies show that PV systems do not lead to any GHG emissions or air pollutants during their normal operation period as well as the recycling stage [7]. The only case of GHG emission associated with PV systems correspond to their production stage.

Research studies report 28-72.4 g/kWh and 18-20 g/kWh $CO_2$ emission ranges in the USA and Europe, respectively for Si and CdTe based thin-film PV technologies during their life cycle that is assumed to be 20-30 years [6]. The results clearly show that CdTe outperforms Si based PV material in terms of GHG emissions. On the other hand, air pollutant emissions during a PV system life-cycle depends on the amount of the fuel burned during its manufacturing process. Thus, the reported air pollutant emissions during manufacturing process of PV systems show variability in the USA and European countries, whereas the air pollutant emissions during PV system manufacturing stage in the USA are generally higher than those in European countries. At the same time CdTe is advantageous over Si based PV technologies from air

pollutant emissions point of view, both in the USA and European countries. Taking the mentioned discussions into consideration it can be concluded that in comparison with PV technology, conventional energy sources, such as coal or natural gas, have dramatically higher amounts of GHG and air pollutant emissions [8].

- ***Heavy Metals and Chemicals***

Research results show that although some materials used during manufacturing process of PV modules are considered as toxic materials, they do not create a risk for human health and environment since the used amounts are very limited. However, toxic material and chemicals used in PV production and the waste produced at the end of their lifetime is a matter of concern which increasingly earns importance in parallel with the rapid growth of PV technology. Taking into consideration 20-30 years estimations for lifetime of a PV module together with the relatively new commercialized utilization of PV modules, it is obvious that the required measures regarding the heavy metal and chemical wastes at the end of lifetime of PV modules should be taken into consideration in the near future [9]. Results of research studies foresee that disposal waste of PV modules at the end of their lifetime poses the most significant environmental impact of PV technology during its lifetime [10]. Also the hazardous wastes of material and substances contained in the BOS equipment should be taken into consideration. Research and development programs and activities are encouraged in order to use materials having smaller negative environmental effects. Deactivation and disposal of PV modules at the end of their lifetimes is still considered as an environmental challenge regarding PV technology. For this purpose, PV CYCLE, an international industrial program aimed at recycling of end-of-life PV modules is established in Europe. The goal of this program is to collect at least 65%

of solar modules at the end of their lifetimes and recycle at least 85% of their material [11].

### *i. Cadmium*

Cadmium, which is a zinc mining spin-off, is considered as one of the most important materials used in PV technology. Research results show that CdTe PV technology is the most beneficial way of taking apart the cadmium element from the environmental aspects point of view. It has been observed that the amount of cadmium exposure is decreased to the minimum levels when it is used within a PV module [12]. Also research results show that the increasing utilization of cadmium in PV technology can potentially decrease the global environmental pollution caused by cadmium due to mining activities. It has been observed that CdTe PV technology, when it replaces the conventional power generation based on coal burning, provides 100-360 times lower cadmium emissions [13].

Since cadmium is generally found in CdTe PV modules as stable compounds, it does not provide any risk or hazard for human health during normal operation of PV modules [13]. However, environmental impacts of cadmium at the end of PV module lifetime has always been a matter of concern. Recycling is recommended as a preferred method of management of the negative effects of cadmium on human health and the environment at the end of PV module lifetimes [11].

### *ii. Monocrystalline and Multicrystalline Silicon*

Silicon is considered as another material which is widely utilized in PV technology as well as electronics and computer industry. Some toxic substances are generated as a result of the manufacturing process of silicon. However, as mentioned previously, the amount of these toxic substances is very small and their release to the environment is very limited owing to improvements in the manufacturing process [12].

### *iii. CIS, CIGS and a-Si Thin-Film Technologies*

CIS and CIGS are PV technologies involving gallium, copper and indium. The mentioned elements are reported to have low toxicity. Research results also show that CIS is found to have less toxicity compared to CdTe technology [6]. Selenium is a substance used in the manufacturing process of CIS and CIGS PV modules. Although selenium can be recovered in high amounts, still some selenium emissions occur [6]. Disposal of wastes and PV modules at their end-of-life also causes some environmental issues. In case of inappropriate disposal of CdTe, CIS and CIGS PV modules, the contained heavy metals and toxic material may gasify and cause some releases into the atmosphere [6].

Some gases used during manufacturing of a-Si PV modules, such as arsine, phosphine and germane, are toxic. However, since these gases are used in very small amounts they do not cause any considerable risk from human health and environmental aspects points of view [6]. Also methane gas, which is considered as a potential GHG, is generated during manufacturing process of a-Si PV modules [6]

Amorphous silicon PV modules are generally used in consumer-sized small-scale applications and devices such as calculators. These modules may negatively affect the environment at the end of their lifetime since they are usually disposed of within household waste. In contrary to the CdTe PV modules, recycling methods for CIS and CIGS PV modules have not been developed behind the pilot and research studies, while recycling processes have been recommended for a-Si modules [6].

Results of a toxicology study has shown that the most toxic substance used during manufacturing process of PV modules is CdTe which is then followed by CIS and

CIGS PV technologies [14]. Research studies show that replacement of conventional electricity utilities with central PV generators may dramatically reduce the negative environmental impacts of utilization of traditional energy production methods. As an example, the magnitude of the mentioned reduction will be 89-98% in terms of GHG emissions, air pollutants and heavy metals, in case of replacement with CdTe PV modules [15].

- ***Impacts on Water***

Electricity production in PV modules does not depend on water. Therefore, PV systems can be installed in locations with limited access to water sources. Water use in PV systems is only limited with the water consumed during PV module manufacturing process. At the same time, research results show that water use during manufacturing process of Si PV modules is higher than the water required for thin-film CdTe modules [16]. Normal operation of PV systems do not require any water usage except from water used for PV module cleaning purposes. Therefore, it is assumed that use of water in PV systems is very low and PV systems are assumed to have almost no impact on water quality. On the other hand, researches show that water requirement for energy production using conventional methods is much higher compared to PV systems [6].

- ***Impacts on Land and Ecology***

The largest impact of electricity generation from PV on land and ecology can generally be thought of as land occupation in solar power plants. Obviously the mentioned impacts will increase together with the growth of PV technology. However, it should not be forgotten that land occupation by PV plants in locations receiving higher amounts of solar insolation is always less than land usage in places having less amounts of sunshine. Also it has been observed that PV power plants in places

receiving high amounts of solar insolation occupy less amount of land compared to the conventional energy sources such as coal, when the land occupation for mining purposes is taken into consideration [16]. An indirect impact of PV technology on landscape and ecosystem, as well as all electronic devices and other types of renewable energies, is that PV modules contain metal substances, whereas mining of the mentioned metal substances poses significant risks from landscape and ecosystem points of view [17]. As above mentioned, direct land occupation by PV systems may somehow be comparable to conventional energy generation methods. The mentioned amount is even less in case of rooftop or building integrated PV systems [18]. On the other hand, indirect land occupation by PV systems is associated with the manufacturing process including use of material and energy. Researches also show that considerable amount of land is indirectly occupied by PV systems compared to their direct land occupation [19].

Consumption of natural and non-renewable material resources is another concern associated with PV technology. For example tellerium, indium and selenium, and germanium are materials with limited availability for CdTe, CIGS and thin-film Si PV modules, respectively. On the other hand, no silicon shortage is foreseen for PV technology in future [31,32]. Soil erosion is another source of concern associated with large-scale PV power plants. However, the amount of the mentioned erosion highly depends on the existing ground coverage. Researches show that PV power plants established using appropriate soil protection methods (e.g. grass covered ground under tilted PV modules) can reduce soil erosion to almost negligible amounts [22]. Obviously, landscape concerns associated with PV power plants increase together with growth of PV market and increased sizes of plants. However, an advantage of PV technology in terms of land impacts is that land usage by PV systems and power plants

is static while energy generation from conventional sources requires continuous resource extraction and thus, land use [19]. Research studies have shown that large-scale PV plants have higher positive effects from wildlife and environmental factors points of view, compared to energy generation using conventional methods [23]. It has even been observed that solar power plants, when appropriately managed, may have positive effects on the number of species in a specific installation area [24]. On the other hand, BIPV does not directly contribute to land use and soil erosion risks as PV modules are installed on existing buildings that already occupy some amount of land.

Soil acidification is another source of concern associated with most of conventional energy resources. This happens when some acidic substances are deposited as a result of fuel combustion. Depending on the type of soil, reclamation of the affected soil may require very long times, whereas soil damage originated from acid deposition is almost negligible in case of PV technology [6].

Recycling of PV modules at the end of their life cycle may be considered as another advantage of PV technology by contributing to supply the previously mentioned materials with limited availability used in the manufacturing process of different types of PV modules [25].

## 1.8 PV Standards

PV market is gradually turning into a global market, owing to recent developments of PV technology. On the other hand, PV manufacturers from all around the world should all follow the same regulations and standards to be able to compete in the global market.

The International Electrotechnical Commission (IEC) is the international organization which is responsible for development of standards for electrical and electronic devices and systems. The 82nd Technical Committee (TC82) is the technical committee that is responsible for preparation of IEC PV standards. List of different standards determined by IEC for PV systems can be found in [26]. The mentioned standards are categorized under 6 different categories, as follows;

i. ***Measurement Standards:*** The measurement standards consist of a series of IEC standards providing procedures for determination of PV module performance in terms of incident solar irradiance and module surface temperature value.

ii. ***Adequacy Test Standards:*** These standards may perhaps be considered as one of the most significant set of PV standards. They consist of different testing standards for Crystalline Silicon and Thin-film PV materials as well as tests regarding safeness of PV modules. The mentioned standards have provided significant help to make PV a reliable global source for meeting energy requirements.

iii. ***PV Panel Energy Rating Standards:*** These sets of standards consist of standards regarding energy or power based evaluation of PV panels. The mentioned standards involve requirements for evaluation of solar panel performances in terms of their power rating for different irradiance and temperature values, measurement of the effect of incidence angle on panel performance and procedures for estimation of panel surface temperature based on the incident solar irradiance, the ambient temperature and wind speed. They also consist of measurement procedures for the effect of spectral response on PV panel performance.

iv. ***Particular Stress Test Standards:*** These sets of standards consist of particular stress tests such as PV panel salt deterioration tests, PV panel shipment tests, the dynamic mechanic load tests, ammonium deterioration test and voltage endurance test. Details regarding the mentioned set of test standards can be found in [26].

v. ***Solar Panel Component Standards:*** The need to prepare the mentioned set of standards has been felt progressively along with developments of the global PV market. The purpose of these standards is to ensure the conformity between the produced PV modules and the components supplied by external sources for PV manufacturers. The mentioned components include junction boxes, cables, connectors and power converters.

vi. ***PV Panel Material Standards:*** These sets of standards are prepared in order to ensure reliability of PV panels for long-time use. The main goal is to reach a life-time of at least 25 years. Details regarding the mentioned standards can also be found in [26].

## 1.9 Thesis Objectives

The main objective of this thesis is to develop a method for modeling of an increased-efficiency adaptive reconfigurable PV system. The mentioned adaptive reconfiguration of PV arrays can be considered as a preventive measure taken against negative effects of partial shading or non-uniform irradiance profiles on the extent of PV array surfaces. Performance analysis in PV systems requires precise and accurate information of the available solar irradiance values at the application sites because of the very high dependency of power generation in PV systems to the incident solar irradiance values. Thus, the first steps towards achieving the mentioned objective

should be obtaining reliable site-specific irradiance profiles on PV application areas and reliable models for analysis purpose of PV module performances under existing environmental conditions.

Taking the above mentioned discussions into consideration, the objectives of this thesis can be considered under three main areas as follows;

i. Development of a model for generation of site-specific spatially dispersed irradiance profiles on PV array surfaces.
ii. Development of a model in order to analyze performance of PV modules under variable environmental conditions.
iii. Development of a dynamic reconfiguration algorithm for PV arrays based on the previously mentioned non-uniform spatially dispersed irradiance profiles.

## 1.10 Thesis Contributions

Contributions of this thesis can be considered in conjunction with the objectives of the thesis. The first contribution of the thesis can be considered as development of a modeling method which utilizes real sky images taken at PV application areas in which cloud shadow patterns are obtained according to the existing cloud coverage and its distribution in the sky. Different cloud types and their light interaction characteristics are considered by the model in order to account for the attenuating effects of the existing clouds on the incoming solar irradiance values. The model generates site-specific instantaneous Spatially Dispersed Irradiance Profiles (SDIPs) as well as irradiance time-series based on the existing cloud coverage and its distribution in the sky for desired PV application areas as a result of process of the inputs. The model is presented as a global model which can be utilized in order to generate site-specific

irradiance profiles or time-series for desired geographical locations on the Earth`s surface, where sufficient input data is available. The proposed model has minimum dependency on irradiance sensors or pyranometers, and other measurement equipment which facilitates its application to any geographical location, particularly locations where measurement equipment are not readily available. The model generates site-specific irradiance profiles or irradiance time-series based on existing cloud coverage in the sky which can be utilized as reliable sources of data for desired PV analysis purposes.

The thesis also contributes by analyzing the effects of movement of the Sun in the sky during a day on power generation in PV modules with different orientations. By means of the mentioned analysis the best alignment for a PV module in the northern hemisphere is determined and the amount of power generation in PV modules with different alignments are compared.

Once the non-uniform irradiance profiles are obtained according to the above mentioned method, the performance of PV modules/arrays can be analyzed under different environmental conditions (non-uniform irradiance profiles, etc.) Development of a model in order to analyze performance of PV modules under variable environmental conditions is considered as another contribution of this thesis. For this purpose, a simple MATLAB/Simulink based simulation model is developed based on One-Diode mathematical model of a solar cell. Performance of PV modules, as a number of series and/or parallel connected PV cells are analyzed under variable environmental conditions using the mentioned models. Also PV arrays are simulated as combinations of a number of series and/or parallel connected PV modules with different interconnection architectures. The performance of different PV array

architectures are analyzed and compared and the array topology having the best performance is determined to be utilized during further analyses of the thesis.

Another main contribution of the thesis can be considered as the development of an adaptive dynamic reconfiguration algorithm for PV arrays as a preventive measure against negative effects of the existing environmental conditions, particularly partial shading effects due to passing clouds. This goal is achieved by the aid of utilization of the previously mentioned SDIPs and simulation models for PV modules. A simple algorithm is developed for dynamic reconfiguration of PV modules within a PV array in order to improve power generation in PV arrays under partial shading conditions. The mentioned reconfiguration algorithm is an adaptive algorithm since it considers and performs PV module reconfigurations based on the existing site-specific SDIPs. The mentioned algorithm works based on irradiance equalization method which aims at creation of series-connected rows of parallel-connected PV modules with average irradiance values similar to the array`s average irradiance value. The developed algorithm seeks near-optimal array configurations, in terms of irradiance equalization, by setting an irradiance threshold value which is a tolerance against limiting effects of less power generating rows in a PV array. In this way the algorithm is prevented from going into an infinite loop to configure rows with average irradiance values being exactly similar to the array`s average irradiance value since it may not always be possible due to wide dispersion of irradiance values contained in an irradiance profile. Also the number of reconfigured rows are reduced as well as the number of required switching actions to form the final array configuration and hence, the lifetime of switching devices are preserved by the algorithm. The proposed PV array reconfiguration algorithm has been able to improve power generation in PV arrays under existing irradiance profiles without any limitation to the geographical area or the

existing partial shading patterns. The mentioned algorithm fits best to large-scale distributed or centralized PV systems and performs better when irradiance values with wider ranges of dispersion are contained within the existing irradiance profiles. Thesis contributions to the literature are given in the Appendices.

## 1.11 Thesis Organization

This thesis is organized under four main chapters which are then followed by the conclusions of the thesis. A general overview of the past, current and future of PV technologies, different applications of PV systems, the PV market and environmental effects of PV technology together with different PV standards is provided in Chapter 1 as the introduction part of the thesis. Chapter 2 of the thesis provides detailed explanations and information regarding the model which is developed in MATLAB/Simulink environment in order to simulate different characteristics of a PV module under variable environmental conditions. Chapter 3 of the thesis provides detailed explanations and information regarding the novel method which is developed for generation of Spatially Dispersed Irradiance Profiles (SDIPs) on the extent of PV arrays based on the existing cloud coverage and distribution in the sky. The mentioned SDIPs are then utilized as shading scenarios or sources of irradiance data to be utilized for further analysis purposes of the thesis. Chapter 4 of the thesis is allocated to development of a novel adaptive dynamic reconfiguration algorithm for PV arrays in order to combat the negative effects of the existing environmental conditions on PV array performances. The mentioned dynamic reconfiguration algorithm considers SDIPs generated in Chapter 3 as partial shading scenarios or non-uniform irradiance profiles. Chapter 4 is then followed by the Conclusions part of the thesis.

# Chapter 2

# MODELING OF PV ARRAYS

Solar energy and consequently, PV systems, as mentioned previously, have the potential to take the place of conventional means of energy production due to plenty of advantages such as clean and unlimited source of energy, etc. However, still there are many disadvantages and issues that should be overcome for an efficient and wide utilization of PV systems, especially for large-scale applications. As an example, power production in PV systems directly depends on the amount of the incident solar irradiance on the surface of PV modules. Therefore, the output power of a PV module, and hence a PV system, varies from time to time according to the temporary or permanent shading effects that are caused by neighboring buildings, trees or other fixed objects as well as partial or full shading effects caused by passing clouds. Installation of PV systems in appropriate places with suitable positions and distances with respect to each other can be considered as an example of preventive actions in order to minimize the permanent negative effects of partial or full shading of PV generators. However, partial or full shading of PV modules due to passing clouds still remains as a complex and temporary issue that has the potential to dramatically reduce power production in PV module(s) subject to the shading effect. The mentioned complexity comes from the fact that the amount and pattern of shading caused by passing clouds is highly variable and somehow unpredictable.

On the other hand, it is obvious that power yield estimation in a PV power plant is a mandatory factor from system design and management points of view and also there should exist some strategies to cope with negative effects of partial shading and to improve system performance under partial shading conditions.

The above mentioned factors have led the research to find appropriate solutions to estimate output power of a PV system under variable environmental conditions. Modeling of PV systems is one of the most preferred methods in order to analyze PV system performance under variable environmental conditions. This chapter of the thesis is allocated to a summary of the available modeling methods for PV systems introduced in the literature along with simulation of a PV array based on the mentioned models.

## 2.1 Mathematical Model of a PV Cell

A PV cell is the first and smallest building block of each PV system. A PV module consists of a number of PV cells that are connected to each other with different interconnection types. Finally a PV array is considered as a combination of PV modules connected to each other using different architectures and interconnections. The mentioned interconnections of PV cells within a PV module or array are combinations of series and parallel connections in order to meet the current and voltage requirements of different applications. Figure 2.1 shows a PV cell, a PV module and a PV array.

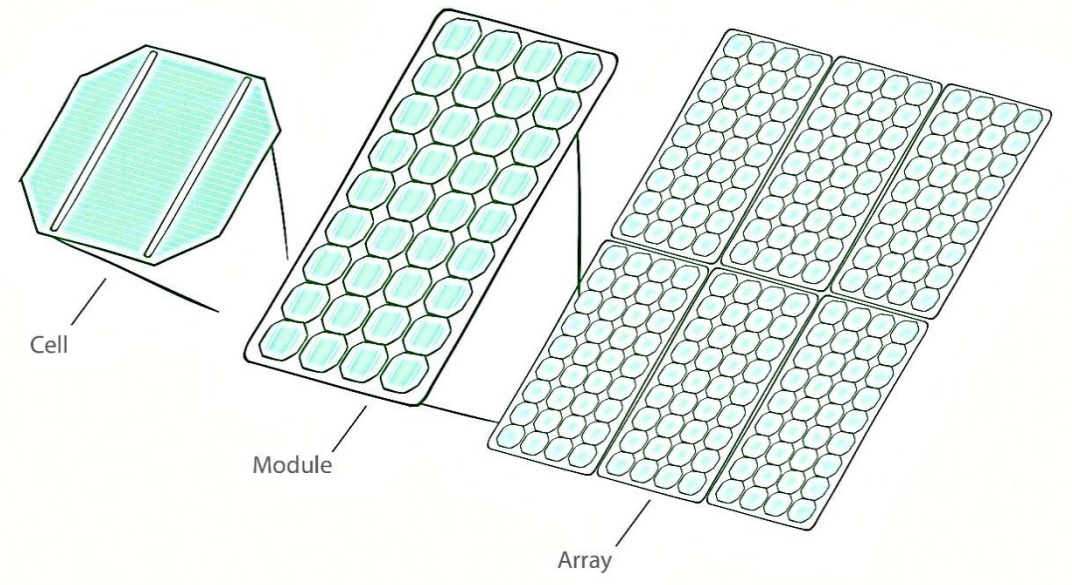

Figure 2.1: A PV Cell, PV Module and PV Array

Series connection of PV cells or modules in a PV module or array, respectively, is generally preferred for applications with higher voltage requirements since the voltage across the terminals of series connected cells or modules is equal to the sum of the voltages of the series interconnected individual cells or modules, respectively. On the other hand, parallel connection type is preferred when the application requires a higher current value as the total current is equal to the sum of the currents produced by individual parallel interconnected cells or modules, respectively. Series and parallel interconnection types are shown in Figure 2.2.

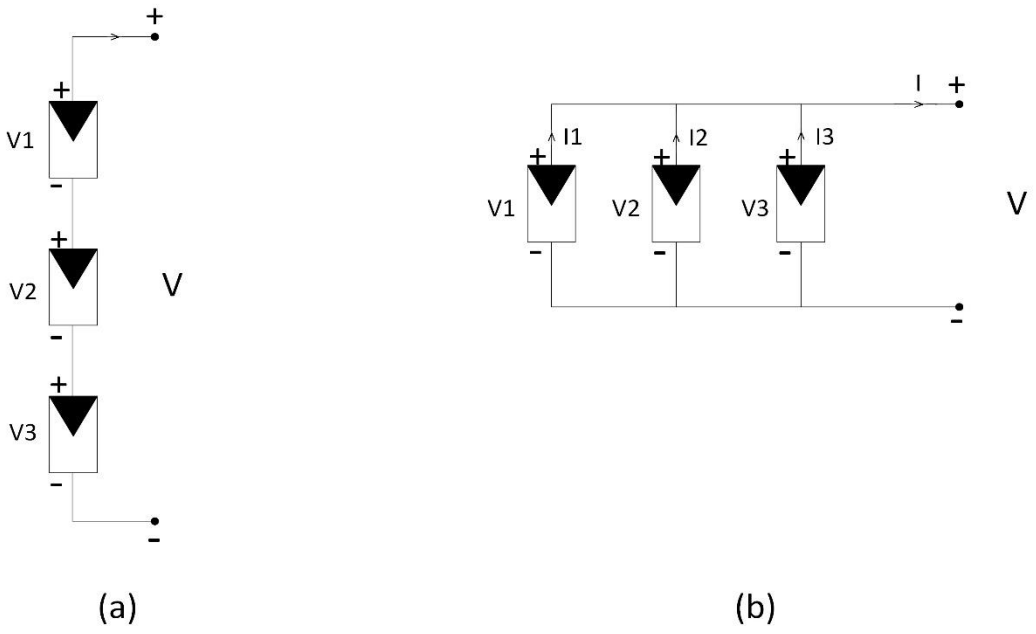


Figure 2.2: (a) Series and (b) Parallel PV Module Interconnection Types

Mathematical modeling of solar cells is a method that has widely been utilized in the literature in order to analyze different characteristics of PV cells, modules or arrays under different environmental conditions. Various models have been introduced in the literature for PV cells. The simplest type of the mentioned models is called the Single-Diode model. This modeling approach is based on a diode which is connected in parallel to a linear independent current source [28,29]. Further improvements are made to the Single-Diode model by adding a series connected resistance to the model which has resulted in formation of $R_s$-Models [30,31]. The more improved version of the $R_s$-Model is called the $R_p$-Model which is developed by adding a parallel connected resistance to this model [32,33,34,35]. This model is also called as the One-Diode model of a PV cell. Another model called the Two-Diode model of a solar cell is also utilized in the literature [36,37,38,39]. This model consists of two diodes and is considered as a more detailed model. The One-Diode mathematical model of a PV cell is utilized in this thesis in order to model different characteristics of a PV cell. The mentioned model is preferred over the others since it is very simple and also

sufficiently reliable for the purposes of the thesis. Figure 2.3 shows the equivalent electrical circuit for the above mentioned One-Diode and Two-Diode mathematical models of solar cells.

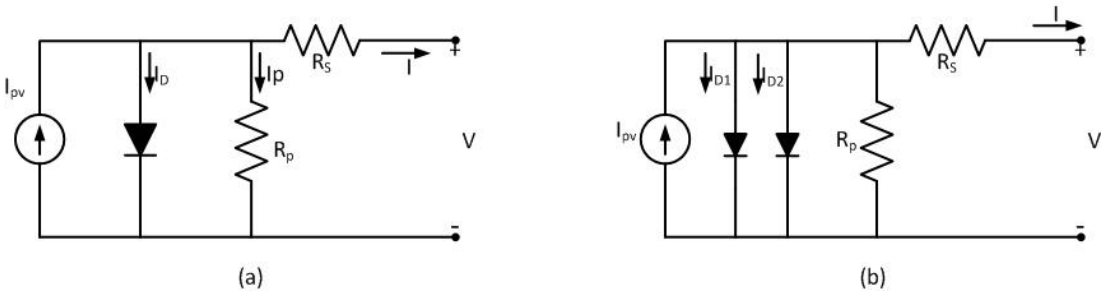


Figure 2.3: The Equivalent Electrical Circuit for (a) One-Diode and (b) Two-Diode Mathematical Model of a Solar Cell

According to the One-Diode mathematical model of a solar cell, the relationship between the cell`s current and voltage values is expressed as;

$$I = I_{ph} - I_S\left(exp\frac{q(V + R_S I)}{nkT} - 1\right) - \frac{(V + R_S I)}{R_P} \tag{2.1}$$

Where;

$I_{ph}$ : Photo-Generated Current (A)

$I_S$ : Diode Saturation Current (A)

$q$ : Electron Charge ($1.60217646 \times 10^{-19}$ C)

$n$ : Diode Ideality Factor

$k$ : Boltzmann Constant ($1.3806503 \times 10^{-23}$ J/K)

$T$ : Working Temperature of the Cell (K)

$R_S$ : Series Resistance (Ω)

$R_P$ : Shunt Resistance (Ω)

Data such as open-circuit voltage ($V_{oc}$), short-circuit current ($I_{sc}$), cell`s voltage and current values at the maximum power point ($V_{mp}$ and $I_{mp}$) and the cell`s maximum

power point ($P_{max}$) are provided within the PV cell`s manufacturer datasheet. The mentioned data are generally provided under the Standard Test Conditions (STC) which is defined as (Solar Irradiance = 1000 W/m$^2$, Cell`s working temperature = 25°C and Air Mass (AM) = 1.5).

A good model from PV analysis point of view should be able to precisely reflect the modeled PV cell`s characteristics, such as I-V and P-V characteristics, under variable environmental conditions. Such a model should be able to accurately calculate different cell parameters taking into account also the effects of the environmental conditions on them. According to the One-Diode mathematical model, which is also considered in this thesis, there are five different unknown parameters that should be calculated by the model. The mentioned parameters are the photo-generated current ($I_{ph}$), the diode saturation current ($I_S$), the diode ideality factor ($n$), the series and parallel resistances, $R_S$ and $R_P$.

### 2.1.1 Determination of PV Cell Parameters

This part of the thesis is allocated to a summary of the calculation methods utilized in the thesis in order to obtain the previously mentioned five unknown cell parameters.

- ***The Photo-Generated Current ($I_{PH}$)***

The photo-generated current of a PV cell is defined as a function of the incident solar irradiance and the cell`s temperature values, as;

$$I_{ph} = [I_{SC} + K_i(T - T_{STC})]\frac{G}{G_{STC}} \tag{2.2}$$

Where;

$I_{sc}$ : Short-Circuit Current (A)

$K_i$ : Short-Circuit Current Coefficient

$T$ : Cell`s Working Temperature

$T_{STC}$ : 25°C

$G$ : Solar Irradiance on the Surface of the Cell ($W/m^2$)

$G_{STC}$ : Solar Irradiance under Standard Test Conditions (1000 $W/m^2$)

It should be noticed that the value of the short-circuit current coefficient ($K_i$) is generally provided in the cell`s manufacturer datasheet.

- ***The Diode Saturation Current ($I_S$) and the Diode Ideality Factor (n)***

The diode saturation current ($I_S$) is obtained according to the following pair of equations taking into account the effects of the variations of the cell`s working temperature;

$$I_S = I_{S,STC}\left(\frac{T_{STC}}{T}\right)^3 exp\left[\frac{qE_g}{nk}\left(\frac{1}{T_{STC}} - \frac{1}{T}\right)\right] \tag{2.3}$$

$$I_{S,STC} = \frac{I_{SC}}{exp\left({}^{V_{oc}}/_{nV_t}\right) - 1} \tag{2.4}$$

Where;

$E_g$ : Bandgap energy of the semiconductor material

$V_t$ : Cell`s Thermal Voltage $\left(V_t = {}^{kT}/_{q}\right)$

The bandgap energy of a semiconductor material is obtained using the following equation [39];

$$E_g = 1.16 - 7.02 \times 10^{-4}\left(\frac{T^2}{T - 1108}\right) \tag{2.5}$$

The value of the diode ideality factor ($n$) is generally dependent on the PV cell`s technology. The value of the ideality factor for silicon PV technologies varies in the range of $n \approx 1 - 2$.

- ***Series ($R_S$) and Parallel ($R_P$) Resistances***

The last two remaining parameters to be calculated by the model are the values of the series and parallel connected resistances. The value of the parallel resistance is assumed to be much higher than the value of the series connected resistance ($R_P \gg R_S$). However, the mentioned values have significant effects on the I-V curve of a modeled PV cell and hence should accurately be calculated by the model. Different approaches are defined in the literature for calculation of the mentioned values. While some research studies propose methods for extraction of these values from the cell`s manufacturer datasheet, other analytical or iteration based approaches are also proposed in different research studies [34,41,38]. However, unavailability of manufacturer`s datasheet values, complexity of calculations, etc. create barriers for accurate determination of the values of the mentioned two parameters from time to time. A simple method for calculation of the values of series and parallel connected resistances based on the cell`s open-circuit voltage, short-circuit current and variations of the cell`s working temperature is utilized in the thesis. The mentioned resistance values are calculated based on the following pair of equations [41];

$$R_P > 10\frac{V_{oc}}{I_{sc}} \tag{2.6}$$

$$R_S < 0.1\frac{V_{oc}}{I_{sc}} \tag{2.7}$$

Also the effect of the incident irradiance on the value of the parallel connected resistance is considered according to the following equation [42];

$$\frac{R_P}{R_{P,STC}} = \frac{G}{G_{STC}} \tag{2.8}$$

## 2.2 Simulation of a PV Module

Once the unknown parameters identified by the One-Diode mathematical model of a solar cell are obtained using Eq.2.2 – Eq.2.8 the I-V and P-V characteristics of a PV cell can be simulated in order to investigate the effects of different factors, such as variations of the cell`s working temperature, the incident solar irradiance, etc., which lead to accurate analysis of the PV system`s performance under variable environmental conditions. As mentioned previously, PV cells are connected in series and/or parallel within a PV module to meet the required current and voltage values. Thus, a PV module can be modeled and simulated as a combination of some series and parallel connected PV cells. A simulation model for a PV module based on One-Diode mathematical model of a PV cell using Matlab/SIMULINK is introduced in our previous study presented in "Appendix G" [43] and utilized in this part of the thesis. The simulation model utilizes Eq.2.2 – Eq.2.8 to calculate different parameters of a solar cell and reflects the I-V and P-V characteristics of the simulated PV module using the data provided in the manufacturer`s datasheet. Figure 2.4 shows a masked implementation of the Matlab/SIMULINK simulation block of the PV module together with the inputs of the model. As it is shown in the figure, the inputs to the model are the PV module`s manufacturer datasheet values along with the number of the series and parallel connected PV cells which form the module and the outputs are I-V and P-V characteristics of the modeled PV module. The main assumption during simulation of the characteristics of the PV module is that the module is not subject to partial shading and hence every single point of the module surface receives identical irradiance values.

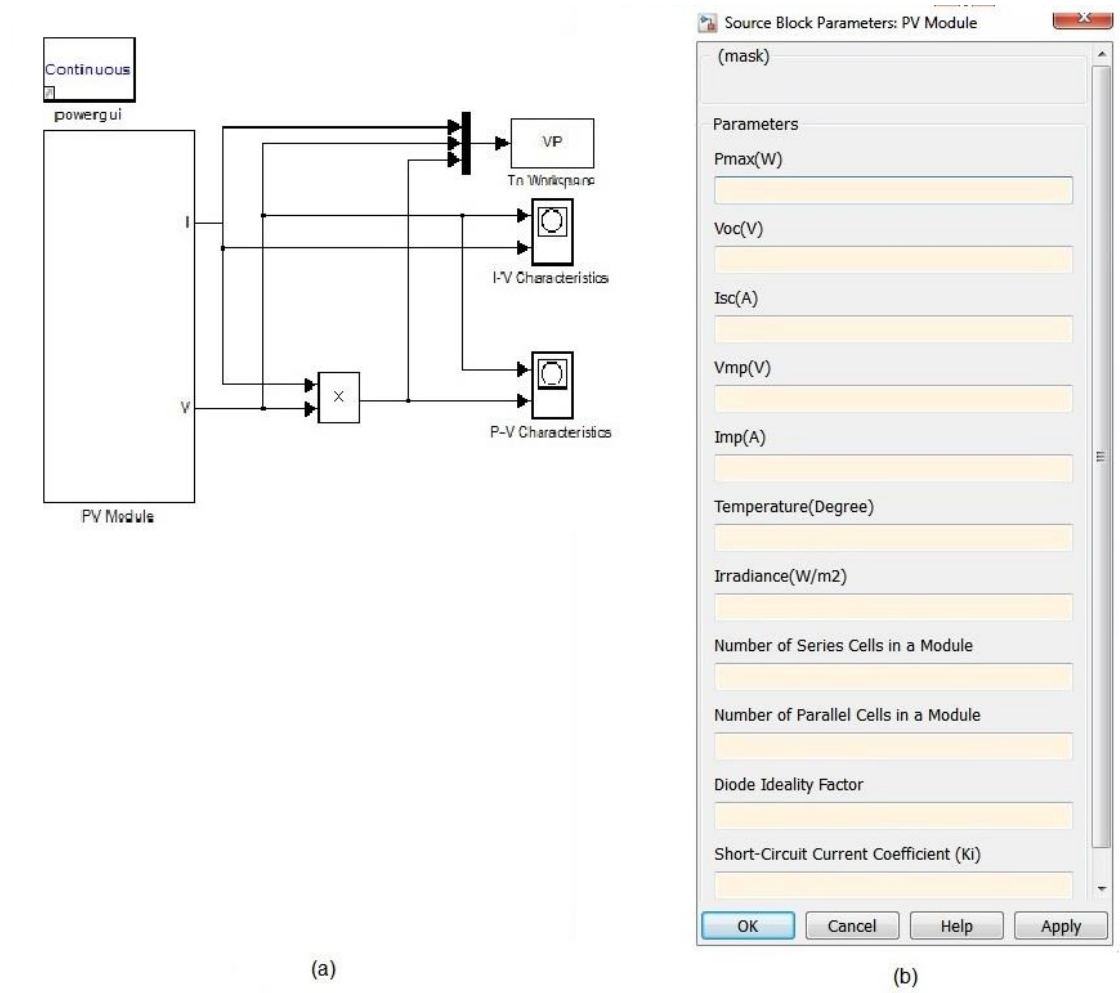


Figure 2.4: (a) Masked Implementation of a PV Module Simulation Block, (b) Model Inputs

Figure 2.5 shows the internal architecture of the masked PV module simulation model as a number of series and parallel connected PV cells together with the architecture of the simulation model of a single PV cell. As it can obviously be observed in the figure, the PV module is modeled as a number of the series and parallel connected solar cells. The output current of the solar cell is multiplied by the total number of the parallel connected cells ($N_P$) while the voltage at the terminals of the module is obtained as a result of multiplication of the voltage of a single PV cell by the total number of the series connected solar cells forming the PV module. The simulated module`s output

current and voltages are converted to physical signals being interfaced with Simulink SymPowerSystem Toolbox elements for further analysis purposes.

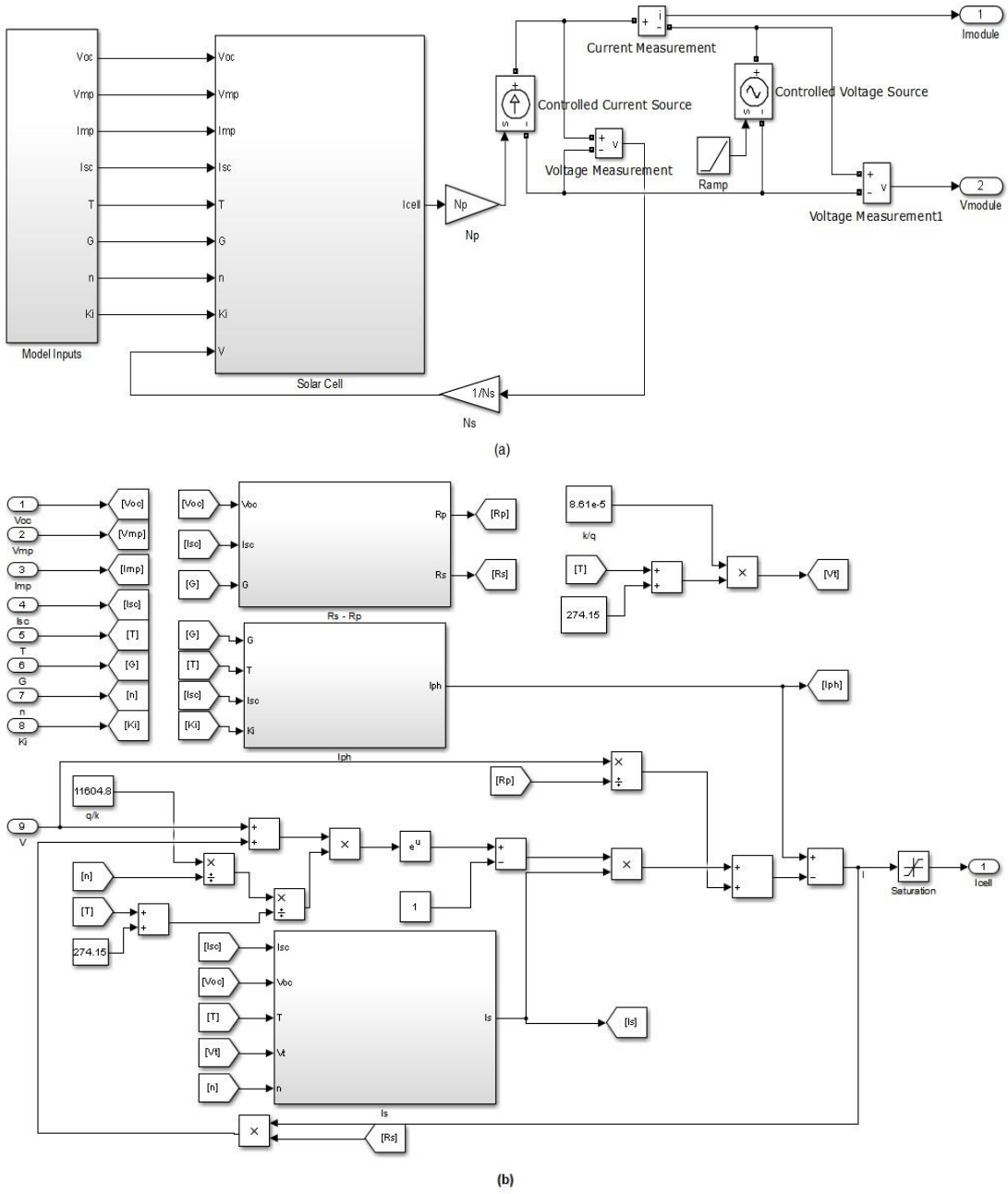


Figure 2.5: (a) Internal Architecture of the Masked PV Module Simulation Block, (b) Architecture of the Single PV Cell Simulation Block

Figure 2.6 shows the detailed internal structures of the building blocks of the solar cell simulation model including the simulation blocks of the series and parallel connected

resistances ($R_S$-$R_P$), the photo-generated current ($I_{ph}$) and the diode saturation current ($I_S$).

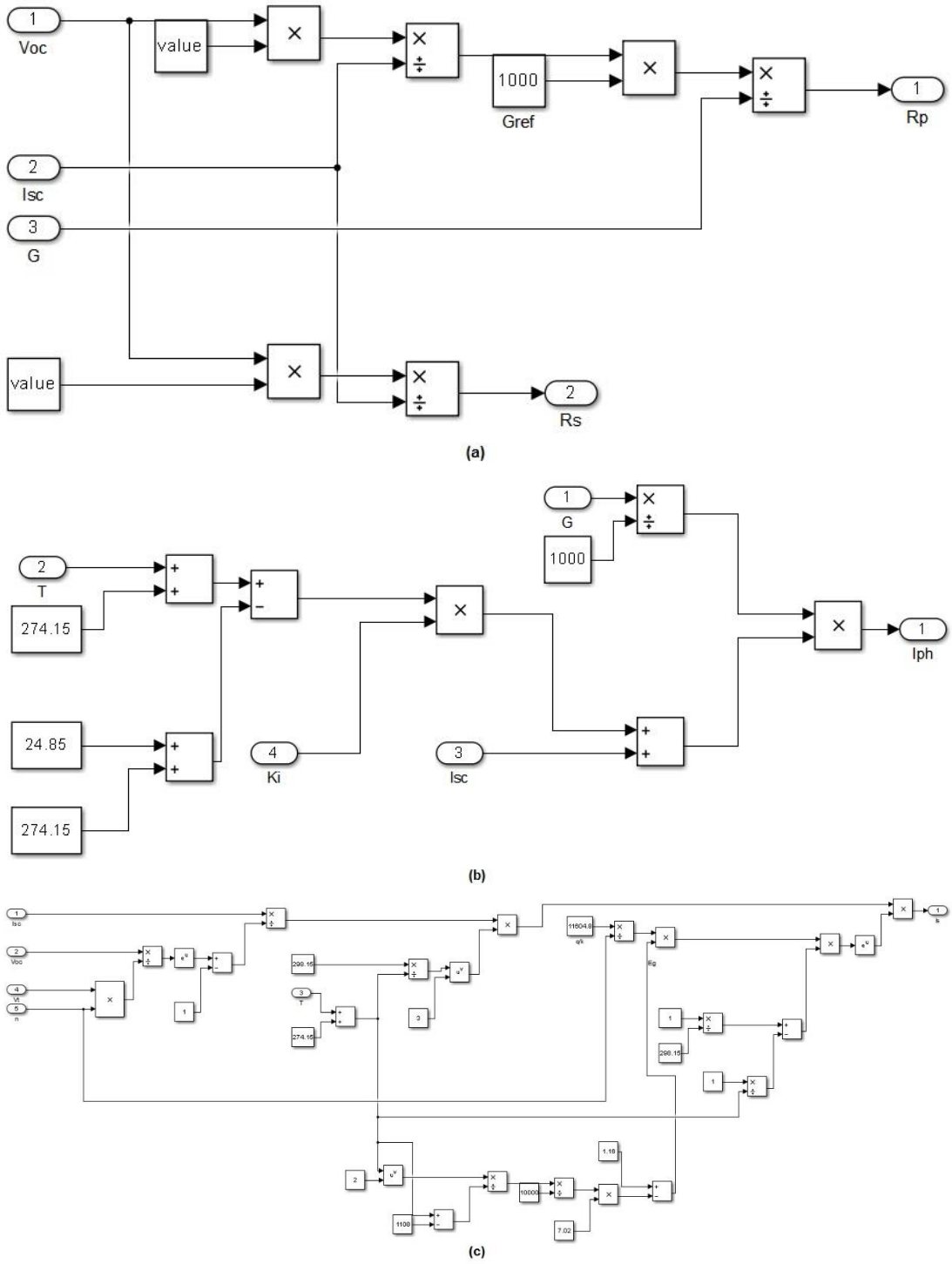


Figure 2.6: Architecture of the (a) $R_S$-$R_P$, (b) $I_{ph}$ and (c) $I_S$ Simulation Blocks

### 2.2.1 Verification of the Simulation Model

The proposed simulation model has been utilized for simulation of the I-V and P-V characteristics of a SOLAREX-MSX60 type PV module. The simulation results are shown in Figure 2.7 and Table 1 provides comparison results between the numerical simulation results and the module`s datasheet values provided by the manufacturer.

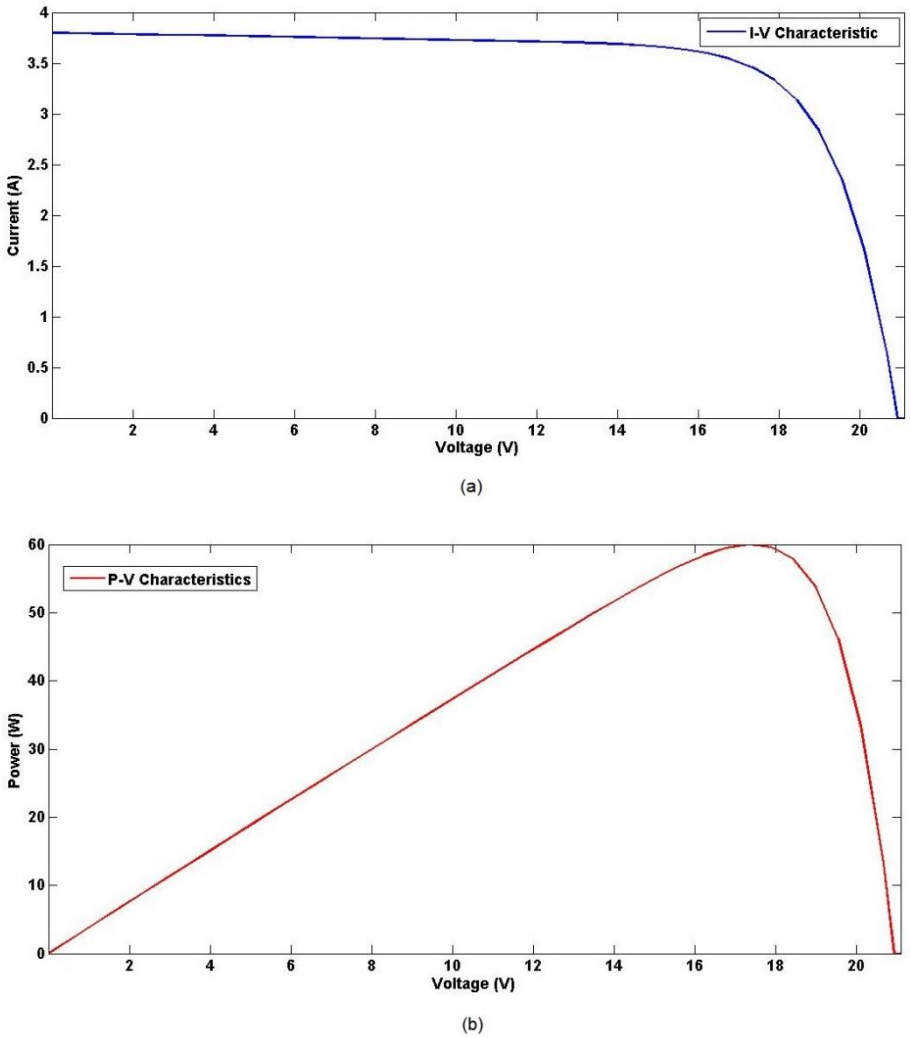


Figure 2.7: Simulated (a) I-V and (b) P-V Characteristics for SOLAREX-MSX60 PV Module

Table 2.1: Simulated vs. Datasheet Parameters for SOLAREX-MSX60 PV Module

| Parameter | Simulated Value | Datasheet Value |
|---|---|---|
| $P_{max}$ | 60 W | 60 W |
| $V_{oc}$ | 20.93 V | 21.1 V |
| $I_{sc}$ | 3.8 A | 3.8 A |
| $V_{mp}$ | 17.09 V | 17.1 V |
| $I_{mp}$ | 3.51 A | 3.5 A |

The simulated characteristic curves and the numerical results show a very good match between the module`s manufacturer datasheet parameters and the simulated ones at three important points being the Maximum Power Point (MPP), the Open-Circuit and the Short-Circuit points, where the module`s output power, current and terminal voltage reach their maximum values, respectively. Hence, the performance of the simulation model is verified and the model is considered to be capable of accurate simulation of characteristics of a PV module.

### 2.2.2 Effects of Different Parameters on a PV Module`s Performance

PV modules are not always operated under identical and/or their standard working conditions. As an example, a PV module may be subject to variable environmental conditions, such as working temperature and the incident solar irradiance values during its field operation. As it was mentioned previously, modeling of PV modules is considered as a method in order to analyze PV modules` performances under different working conditions. Results of such analysis can be utilized for different management and/or planning purposes. This part of the thesis provides brief explanations regarding effects of variations of the values of different parameters of a PV module during its operation. Such variations include variations of the module`s working temperature,

variations of the received solar irradiance on the surface of the module and variations of the values of series and parallel connected resistance. Simulation model of a SOLAREX-MSX60 type PV module is utilized during analyses of this part of the thesis. The datasheet parameters provided by the manufacturer of the module was provided earlier in Table 2.1.

***a. Effects of Temperature Variations***

Effects of variations of the module`s working temperature are shown in Figure 2.8. Four different temperature values are utilized being $0^{\circ}$, $25^{\circ}$, $50^{\circ}$ and $75^{\circ}$, respectively, and the module`s I-V and P-V characteristic curves are obtained for each temperature value. As it is shown in the figure, increasing temperature values cause significant reductions in the module`s performance. Increasing temperature values cause reductions in the module`s open-circuit voltage value and its MPP along with slight increases in the short-circuit current value.

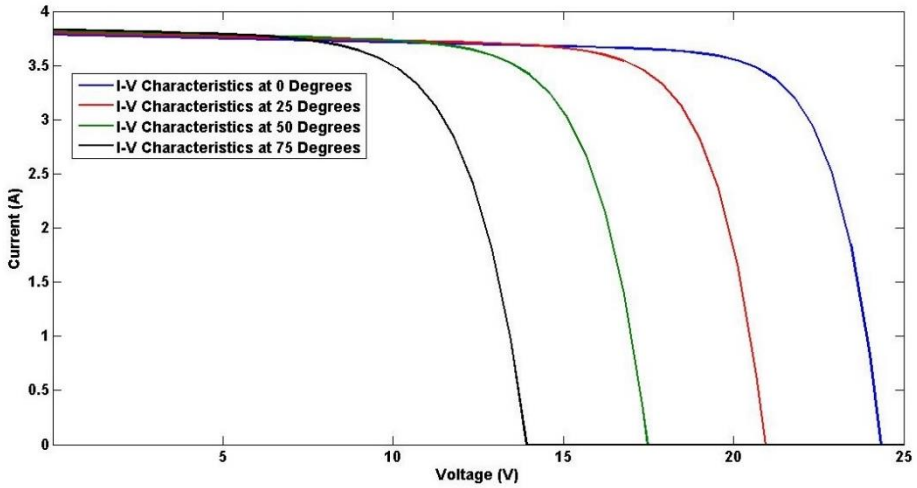


Figure 2.8: Effects of Temperature Variation on a PV Module`s (a) I-V and (b) P-V Characteristics

### *b. Effects of Variations of the Incident Solar Irradiance Value*

As it was discussed previously, PV modules may be subject to different environmental conditions during their field operation. One of the most important factors that affects a PV module`s performance is the solar irradiance received on the surface of the module. Variations of the amount of the incident solar irradiance may be due to permanent obstacles such as neighboring buildings, trees, etc., or temporary factors that are most likely caused by passing clouds. Passing clouds have immediate decreasing effects on the amount of the received solar irradiance and therefore the

performance of PV modules. Such effects may rapidly change and hence the fluctuations in power production by a PV power plant due to rapidly changing partial shading effects is considered as one of the main concerns which should be overcome using appropriate strategies for an efficient and reliable utilization of PV produced energy. Figure 2.9 shows the effects of variations of a PV module`s performance imposed by variations of the incident solar irradiance values. Five different irradiance values are utilized being 200 $W/m^2$, 400 $W/m^2$, 600 $W/m^2$, 800 $W/m^2$ and 1000 $W/m^2$ respectively, and the module`s I-V and P-V characteristic curves are obtained for each irradiance value. It is obvious that the performance of the module is directly proportional to the amount of the incident solar irradiance values. Any reduction in the incident irradiance value cause immediate reduction of the module`s open-circuit voltage, short-circuit current and its MPP.

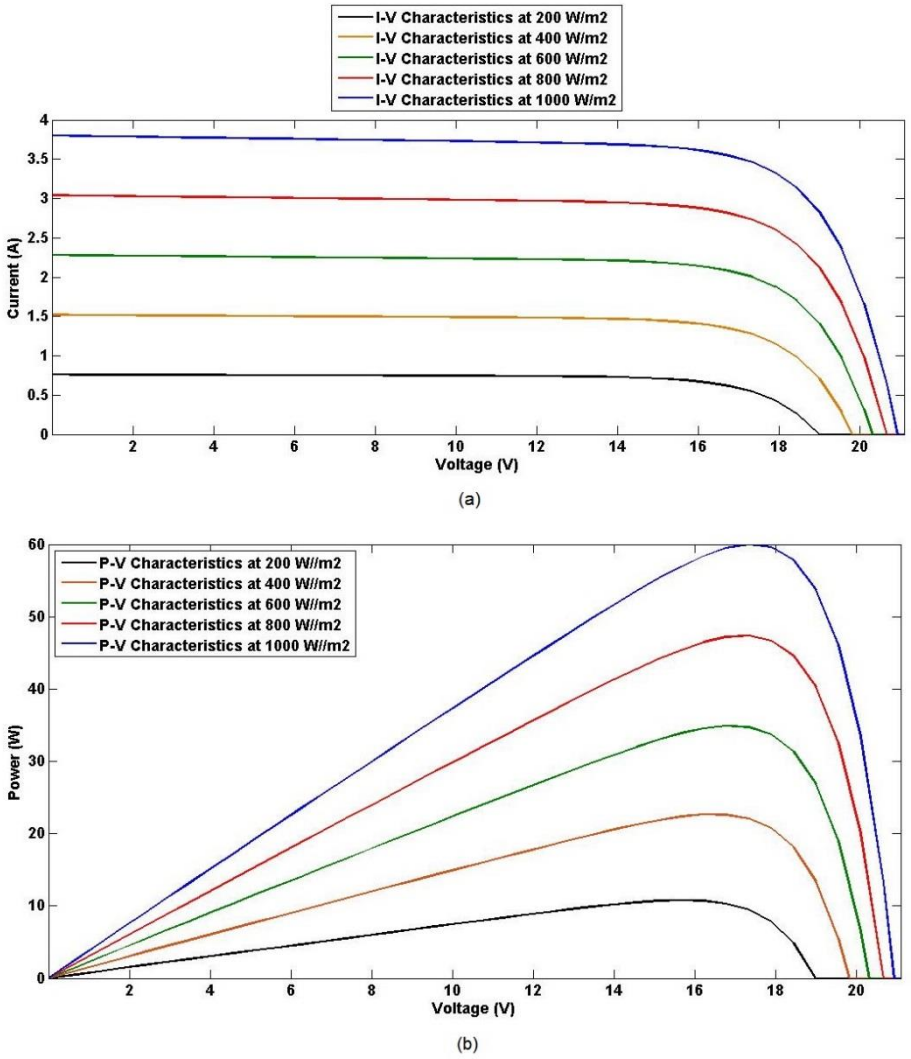


Figure 2.9: Effects of Solar Irradiance Variation on a PV Module`s (a) I-V and (b) P-V Characteristics

### *c. Effects of Variations of the Values of the Series and Parallel Connected Resistances*

Different methods have been suggested in the literature in order to obtain the series and parallel connected resistance values in a PV module. A simple approach is utilized in this thesis based on the module`s open-circuit voltage and short-circuit current value. Appropriate selection of the values of $R_s$ and $R_p$ improves the accuracy of the simulation model to better reflect the simulated PV module`s characteristics. Figure 2.10 shows the effects of variations of the value of the series-connected resistance ($R_s$)

on the performance of a PV module. Totally five different values are utilized for the series-connected resistance corresponding respectively to 0.02 $V_{oc}/I_{sc}$, 0.04 $V_{oc}/I_{sc}$, 0.06 $V_{oc}/I_{sc}$, 0.08 $V_{oc}/I_{sc}$ and 0.1 $V_{oc}/I_{sc}$. It can be observed from the figure that variations of the value of the series-connected resistance change the slope of the characteristic curves of the PV module near its open-circuit point. It is found that higher values of the series-connected resistance cause reductions in the module`s MPP while $V_{oc}$ and $I_{sc}$ values do not change significantly.

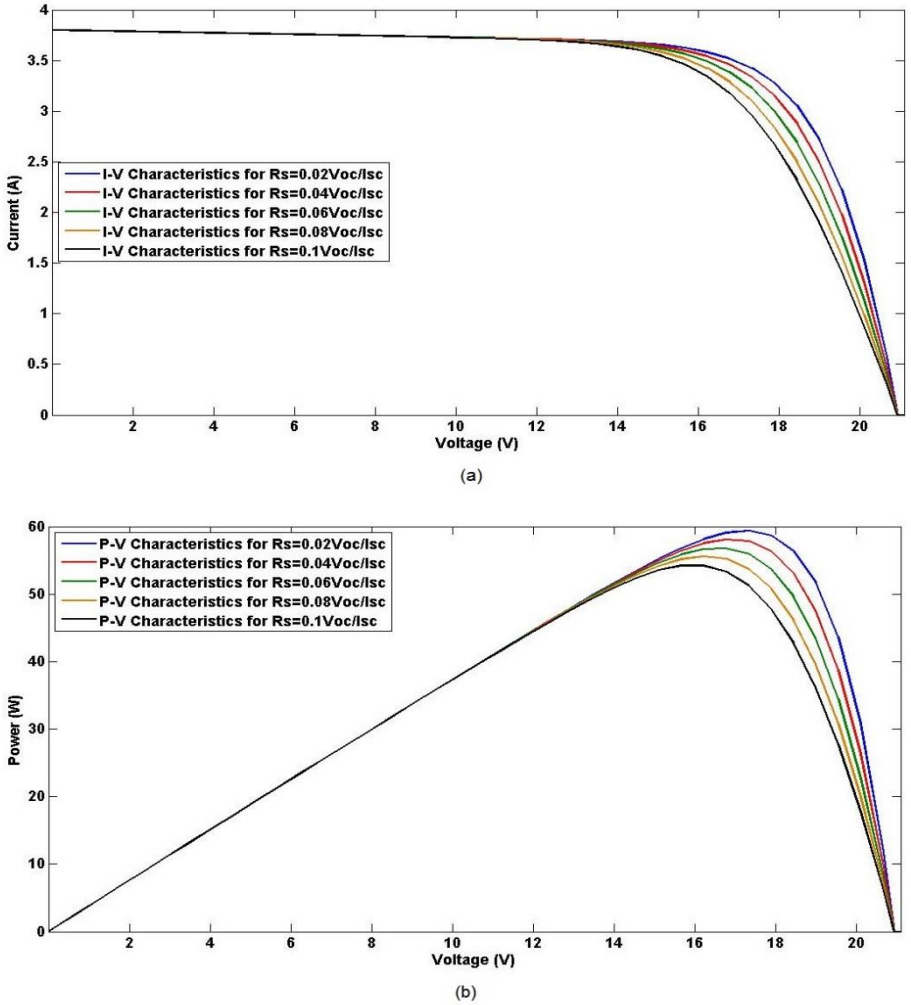


Figure 2.10: Effects of Variation of the Series Connected Resistance Value on a PV Module`s (a) I-V and (b) P-V Characteristics

Figure 2.11 shows the effects of variations of the value of the parallel-connected resistance ($R_p$) on the performance of a PV module. Totally five different values are utilized for the parallel-connected resistance corresponding respectively to 5 $V_{oc}/I_{sc}$, 10 $V_{oc}/I_{sc}$, 20 $V_{oc}/I_{sc}$, 40 $V_{oc}/I_{sc}$ and 60 $V_{oc}/I_{sc}$. The figure shows that, similar to the case of the series-connected resistance, variations of the value of the parallel-connected resistance also change the slope of the characteristic curves of the PV module near the short-circuit point. It is observed that higher values of the parallel-connected resistance increase the module`s MPP.

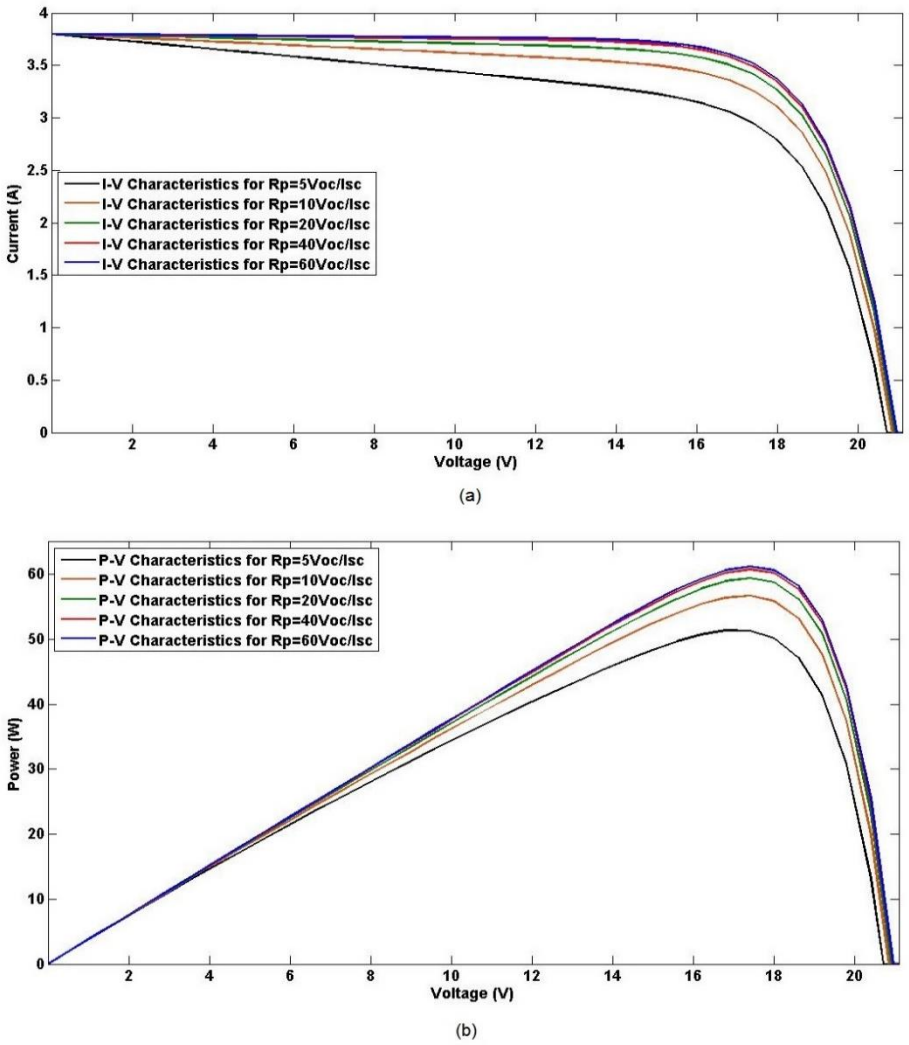


Figure 2.11: Effects of Variation of the Parallel Connected Resistance Value on PV Module Performance

# Chapter 3

# MODELING OF PARTIAL SHADING ON PV ARRAY SURFACES

The amount of power generation by PV modules is directly proportional to the amount of solar irradiance received on their surface. Therefore, having precise and detailed knowledge regarding the irradiance values incident on the surface of each individual PV module within a PV power plant can be considered as a vital need for power yield estimation purposes in PV power plants. An appropriate PV system design and management can only be possible if appropriate and sufficient data are available. Large-scale centralized PV power plants and/or PV power plants distributed within a large geographical area are examples of systems that are highly affected by partial shading effects caused by cloud passages. As it was mentioned previously, the purpose of this thesis is to design an adaptive reconfigurable PV array which is capable of combating the reducing effects of partial shading on PV array surfaces on the generated output power. Significance of such an adaptive system can then be sensed when it comes to large scale PV arrays including large number of PV modules in which shadows caused due to passage of even a very small cloud may cause significant fluctuations in the array`s power generation. It is obvious that the mentioned fluctuations should be coped with for an efficient and reliable operation of the PV power plant. In order to achieve the mentioned goal, firstly the precise value of solar irradiance received by each individual PV module within a PV array should be known, because power yield estimation in PV arrays is only possible when exact and precise

site-specific data of solar irradiance received at each point within the geographical area of the PV array is available. However, the required data for the mentioned analyses and planning purposes may not always be readily available due to some limitations regarding measurement equipment, stations, etc. The mentioned limitations have led the research to develop models for calculation and/or estimation of solar irradiance for desired geographical locations. Modeling of clear-sky irradiance has already been considered in numerous studies and various models have been designed and introduced in order to model solar irradiance values for desired geographical locations. However, a good irradiance model, from solar energy related applications point of view, should be capable of generating solar irradiance profiles, or in other words partial shading patterns, on the surface of PV arrays under cloudy sky conditions. Such a model should also be able to generate realistic cloud shadow patterns on the surface of PV arrays based on the existing cloud coverage in the sky, its shape, distribution and light interaction characteristics. Since the beam or direct irradiance component carries a higher significance from solar energy applications point of view, the emphasis in most of the developed models is put on modeling of the beam or direct solar irradiance component. Models which are introduced in the literature for estimation of beam irradiance can be considered under two main categories, being namely [44];

1. Parametric Models
2. Decomposition Models

The main difference between the parametric models [45,46,47,48] and decomposition models [49,50,51,52,53] is that numerous parameters regarding atmospheric conditions such as cloud type, cloud coverage, distribution of clouds in the sky, sunshine duration, etc. are required by the parametric models for calculation/estimation of solar irradiance while decomposition models only need the

global solar irradiance to estimate the beam and diffuse irradiance components. Wide utilization of the ASHRAE model [45] is due to its simplicity compared to other models while analysis results [44] report that this model suffers from lower accuracy in estimation of the diffuse irradiance compared to the Iqbal model [46] since it does not account for the albedo irradiance and diffuse irradiance generated due to aerosol effects. The Iqbal model has found to be the most accurate parametric irradiance model [54].

This chapter of the thesis is allocated to a model which is proposed to generate Spatially Dispersed Irradiance Profiles (SDIPs) or shadow patterns on the surface of PV arrays based on the existing real clouds in the sky. Real sky images and different cloud types and their light interaction characteristics are utilized by the proposed model in order to generate irradiance profiles on the extent of large-scale centralized or distributed PV arrays. The proposed model is considered as a global model which has the capability of generating site-specific instantaneous irradiance profiles and/or irradiance time-series for any desired geographical location on the Earth with respect to the existing instantaneous cloud coverage at the desired geographical location. The mentioned model generates irradiance values based on the instantaneous position of the Sun in the sky as a result of interaction of sunlight beams with the existing cloud coverage. Thus, the first building block of the model should be considered as calculation of the instantaneous positions of the Sun in the sky during a typical day. The mentioned positions of the Sun in the sky are calculated for the desired instants of time.

## 3.1 Time Systems

Different time systems are currently defined and being utilized. The most commonly used two time systems include the Local Time (LT) of an observation point on the Earth`s surface and the Local Solar Time (LST). The LT depends on the latitude and longitude of each observation point while the LST is independent of the geographical divisions on the Earth`s surface. The LST is the time system which is commonly utilized in solar energy applications. The solar noon is considered as the time instant at which the Sun has its highest elevation in the sky and passes the South axis in LST. However, the local noon may not necessarily match the solar noon due to differences between the LST and LT at different geographical locations on the Earth`s surface. The Local Solar Time (LST) is calculated based on the following equations;

$$LST = LT + (\frac{TC}{60}) \tag{3.1}$$

$$TC = 4 \times (LSTM - Longitude) + EOT \tag{3.2}$$

$$EOT = 9.87\sin(2B) - 7.53\cos(B) - 1.5\sin(B) \tag{3.3}$$

$$B = (360/365.25)(j - 81) \tag{3.4}$$

$$LSTM = 15^{\circ}.\Delta T_{GMT} \tag{3.5}$$

where;

LST : Local Solar Time

LT : Local Time

TC : Time Correction Factor

LSTM : Local Standard Time Meridian

EOT : Equation of Time

$\Delta T_{GMT}$ : Difference from Greenwich Mean Time

Figure 3.1 demonstrates variations of the value of the equation of time during a year.

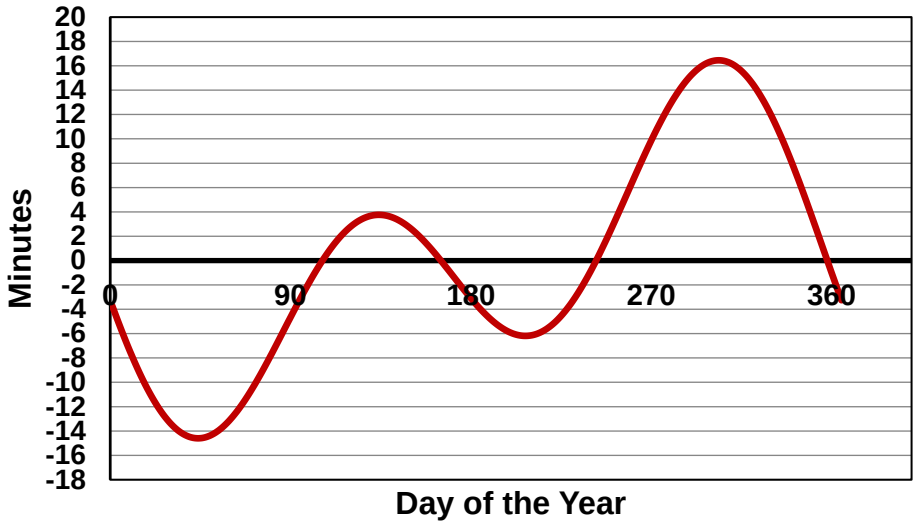


Figure 3.1: Variations of the Value of EOT during a Year

## 3.2 The Sun`s Position in the Sky

The position of the Sun in the sky can be calculated at each time instant for each geographical location on the Earth`s surface, or simply each observation point. The instantaneous positions of the Sun in the sky with respect to different observation points are calculated based on three main parameters as follows;

- The latitude of the observation point
- The day number
- Time of the day

The day number is explained as the Julian day number, ($j$), where the relationship between the $i^{th}$ day of a month and the Julian day number, ($j$), is expressed in Table 3.1.

Table 3.1: Relationship Between the Julian Day Number, (j), and the $i^{th}$ Day of a Month

| **Month** | **The Julian Day Number, (*j*), for the $i^{th}$ Day of the Month** | **Leap Year** |
|---|---|---|
| **January** | i | |
| **February** | 31+i | (+1) |
| **March** | 59+i | (+1) |
| **April** | 90+i | (+1) |
| **May** | 120+i | (+1) |
| **June** | 151+i | (+1) |
| **July** | 181+i | (+1) |
| **August** | 212+i | (+1) |
| **September** | 243+i | (+1) |
| **October** | 273+i | (+1) |
| **November** | 304+i | (+1) |
| **December** | 334+i | (+1) |

The local solar time is utilized in calculations of the Sun`s position in the sky. Time is represented as the hour angle, *w*, as expressed by Eq.3.6 and is set to zero at exact solar noon determining the time at which the Sun is due south.

$$\omega = 15(t - 12) \tag{3.6}$$

The instantaneous position of the Sun in the sky is expressed by its altitude and azimuth angles at a given time instant. Also the solar angle of incidence describes how perpendicular the sunlight beams are received at the surface of a PV module. Detailed explanations regarding the solar altitude, azimuth and incidence angles are provided in the following parts of the thesis.

### *i. The Solar Altitude Angle*

The Sun`s elevation in the sky or the solar altitude angle, $\gamma_s$, is expressed by Eq.3.7 [55] and shown in Figure 3.2;

$$\gamma_s = sin^{-1}(sin\varphi sin\delta + cos\varphi cos\delta cos\omega) \tag{3.7}$$

Where;

$\varphi$ : The latitude of the observation point

$\delta$ : The solar declination angle in degrees

$\omega$ : The solar hour angle

The solar altitude angle is also considered as the complement of the solar Zenith angle, $\theta_Z$, expressed as;

$$\theta_Z = 90^{\circ} - \gamma_s \tag{3.8}$$

The solar declination angle, $\delta$, can be expressed as the angle between the Equatorial Plane and the line joining the center of the Earth`s sphere to the center of the solar disk [55]. The solar declination is a factor that is frequently utilized during calculations of the Sun`s position in the sky. The Sun`s declination is a time dependent variable parameter where a small constant value for each day can be considered as the rate of change. Variations of the value of the Sun`s declination are between (- 23$^{\circ}$27$^{'}$) and (23$^{\circ}$27$^{'}$) corresponding to Winter Solstice and Summer Solstice happening on December 22$^{nd}$ and June 21$^{st}$, respectively. The solar declination angle can be expressed as [55];

$$\delta = \sin^{-1}\{0.3978 sin^{-1}(j` - 80.2^0 + 1.92(\sin(j` - 2.80^0)))\} \tag{3.9}$$

Where j` is the Julian day number defined as the day angle in degrees and expressed as [56];

$$j` = j \times \left(\frac{360}{365.25}\right) \tag{3.10}$$

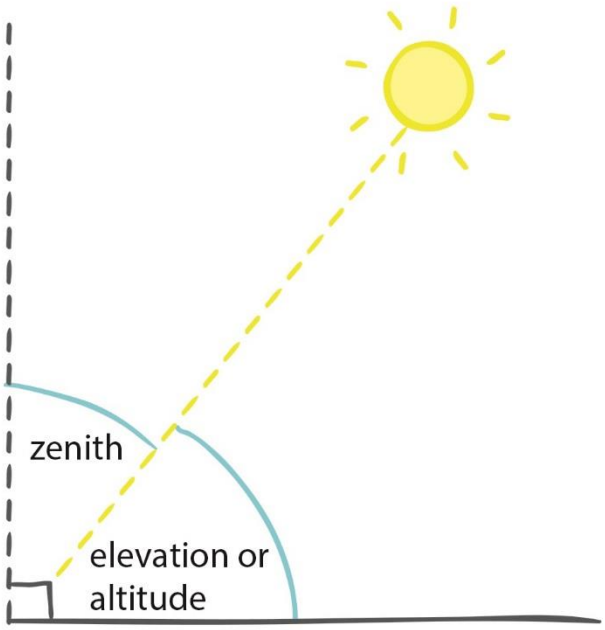


Figure 3.2: The Solar Altitude and Zenith Angles

Figure 3.3 presents variations of the value of the solar declination angle during a whole year.

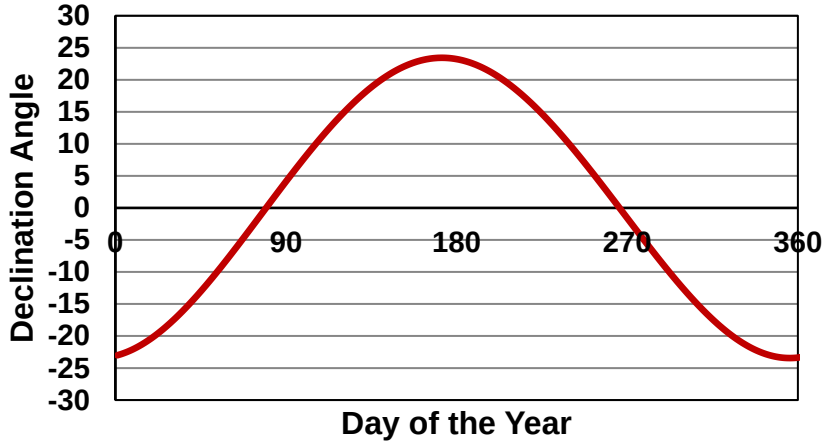


Figure 3.3: Variations of the Solar Declination Angle during a Year

### *ii. The Solar Azimuth Angle*

The solar azimuth angle, $\alpha_s$, is defined as the angle between the position of the Sun with respect to the North axis. In other words the solar azimuth angle takes the values of $180^{\circ}$ and $270^{\circ}$ when the Sun is due South and West, respectively. The Solar azimuth angle can be defined using the following equations;

$$cos\,\alpha_s = (sin\,\varphi\,sin\,\gamma_s - sin\,\delta)/cos\,\varphi\,cos\,\gamma_s \quad (3.11)$$

$$\sin\alpha_s = \cos\alpha_s \sin\omega/\cos\gamma_s \quad (3.12)$$

If $\sin\alpha_s < 0$ $$\alpha_s = 180 - \cos^{-1}(\cos\alpha_s) \quad (3.13)$$

If $\sin\alpha_s > 0$ $$\alpha_s = 180 + \cos^{-1}(\cos\alpha_s) \quad (3.14)$$

The instantaneous position of the Sun in the sky based on the above mentioned solar altitude and solar azimuth angles is provided in Figure 3.4.

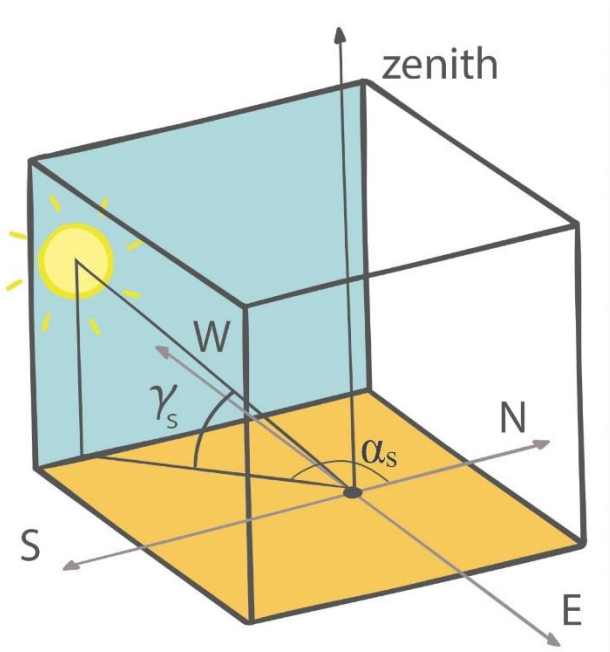


Figure 3.4: The Sun`s Position in the Sky in Terms of Solar Azimuth ($\alpha_s$) and Solar Altitude ($\gamma_s$) Angles

### *iii. The Solar Angle of Incidence*

The solar angle of incidence defines a measure of how perpendicularly sunlight beams hit the PV module surface. The significance of this angle comes from the fact that a PV module generates its highest power when receives the sunlight on its surface perpendicularly. The mentioned angle can be considered as the angle between the sunlight beams and a normal vector on the panel surface. The solar angle of incidence, $\theta_s$, can be defined as;

$$\theta_s = \cos^{-1}[\cos(\beta)\cos(\theta_Z) + \sin(\beta)\sin(\theta_Z)\cos(\alpha_s - \alpha_m)] \quad (3.15)$$

Where;

B : Tilt angle of the PV module (*Horizontal = 0°*)

$\alpha_m$ : Azimuth angle of the PV module *(North = 0°, East = 90°)*

A presentation of the solar angle of incidence is provided in Figure 3.5.

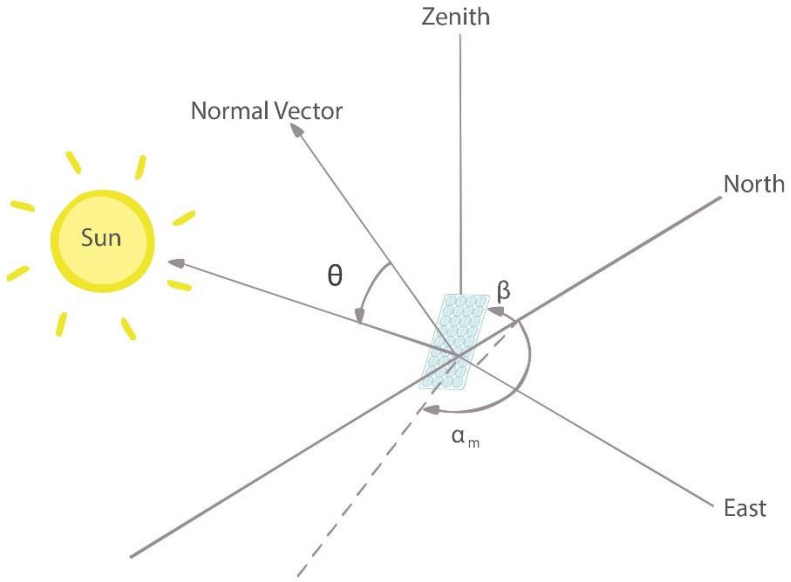


Figure 3.5: The Solar Angle of Incidence

### 3.2.1 Simulation of the Sun`s Position in the Sky

A MATLAB/Simulink based simulation model, as presented in our previous work which is also presented in "Appendix I" [57], is utilized in order to simulate the instantaneous values of the Sun`s position in the sky together with the values of the solar angle of incidence, at any desired time instant and geographical location. Figure 3.6 shows a masked implementation of the mentioned simulation model.

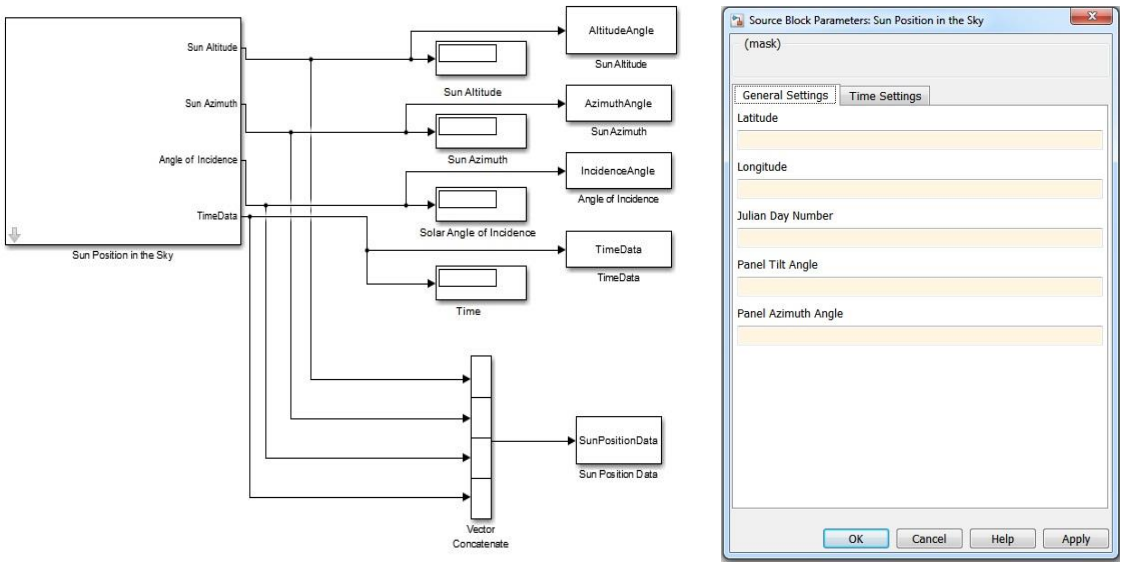


Figure 3.6: A Masked Implementation of the Simulation Model of the Sun`s Position in the Sky

As it is shown in the figure, the inputs to the model are the latitude and longitude of the desired geographical location, the Julian day number, the PV module tilt and azimuth angle values together with the desired time instant or interval. The model calculates the Sun`s position in the sky based on the previously discussed equations. The mentioned calculations are conducted through 5 different sub-systems being responsible for calculation of the hour angle, the declination angle, the solar altitude angle, the solar azimuth angle and the solar angle of incidence. The time input to the model is the local time of the desired geographical area which is internally transformed

by the model to the local solar time based on Eq.3.1 – Eq.3.5. The general overview of the internal structure of the simulation model of the Sun`s position in the sky is provided in Figure 3.7.

***a) Simulation of the Hour Angle***

The model calculates the hour angle according to Eq.3.6 in a separate sub-system as shown in Figure 3.8. The inputs to the mentioned sub-system include the longitude of the geographical area, the local time, the time difference from GMT, the Julian day number and the daylight saving time. For this purpose, the local time input is firstly converted to the local solar time in a separate sub-system based on Eq.3.1 – Eq.3.5. The internal architecture of the "Time Sub-System" is presented in Figure 3.9.

***b) Simulation of Declination Angle***

The declination angle is also simulated by the model through a separate sub-system according to Eq.3.9 and Eq.3.10. The only input to the "Declination Sub-System" is the Julian day number. Figure 3.10 shows the internal architecture of the "Declination Sub-System".

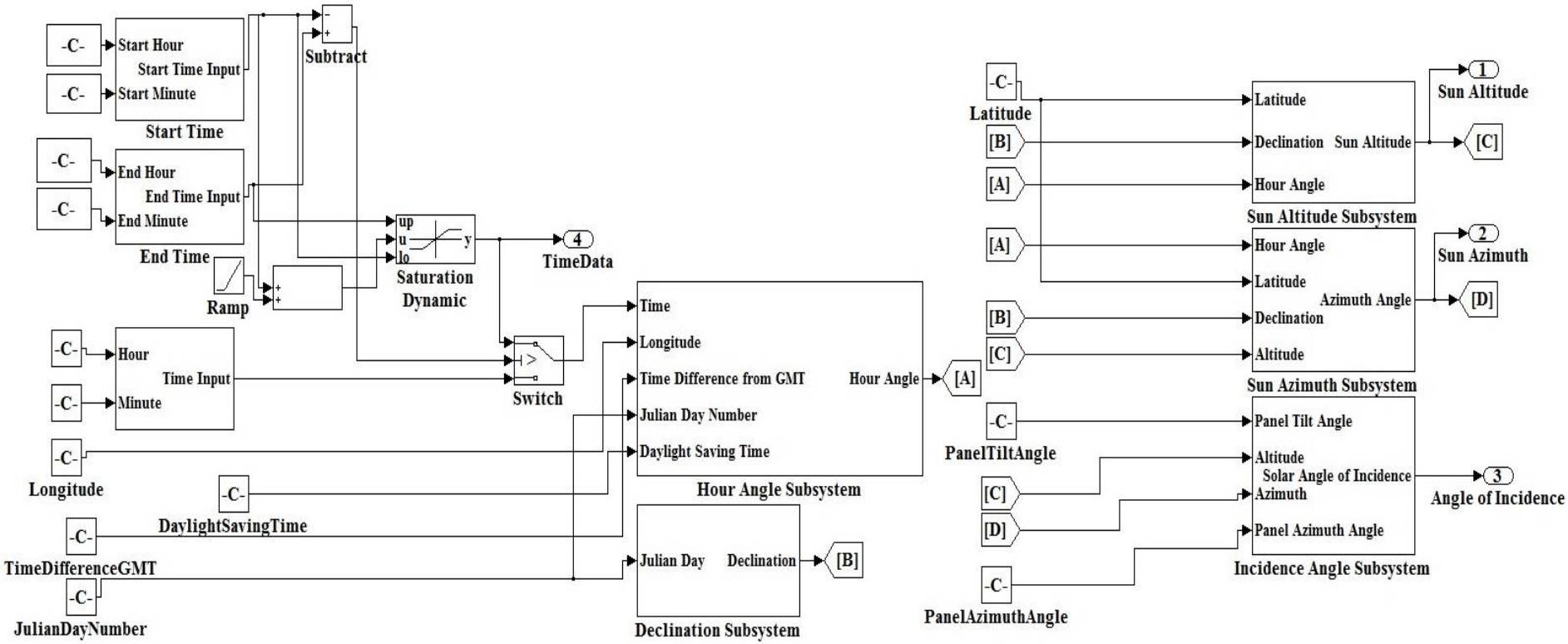


Figure 3.7: General Overview of the Simulation Model of the Sun`s Position in the Sky

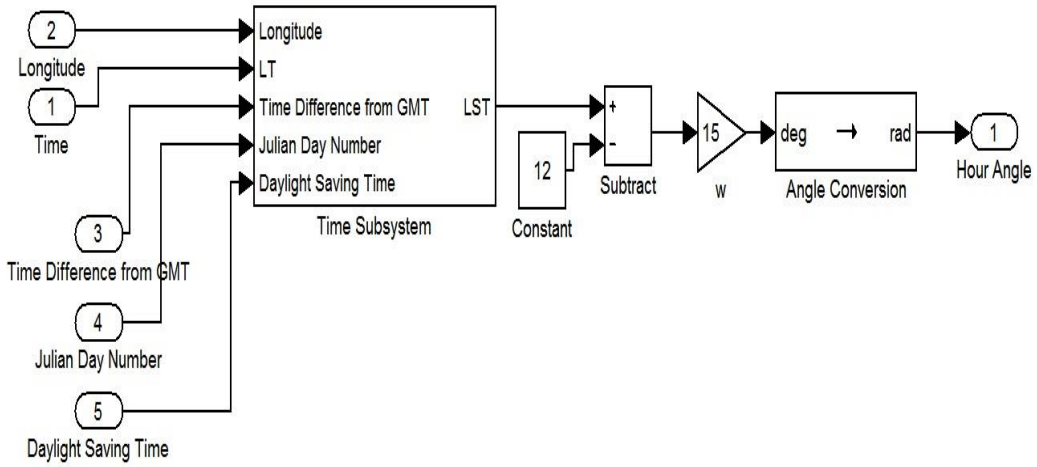


Figure 3.8: The Internal Architecture of the "Hour Angle Sub-System"

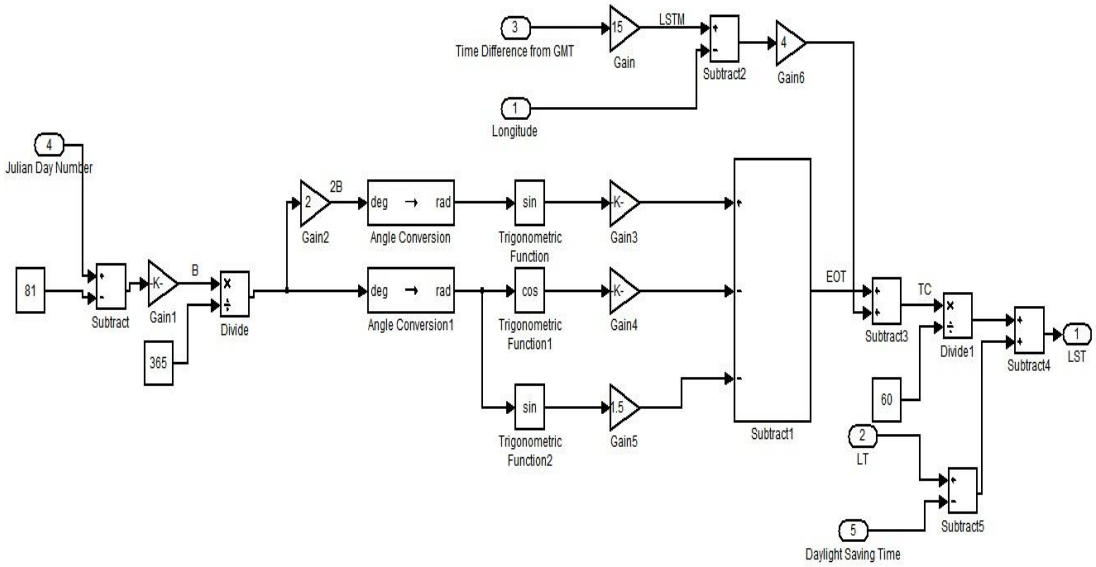


Figure 3.9: The Internal Architecture of the "Time Sub-System"

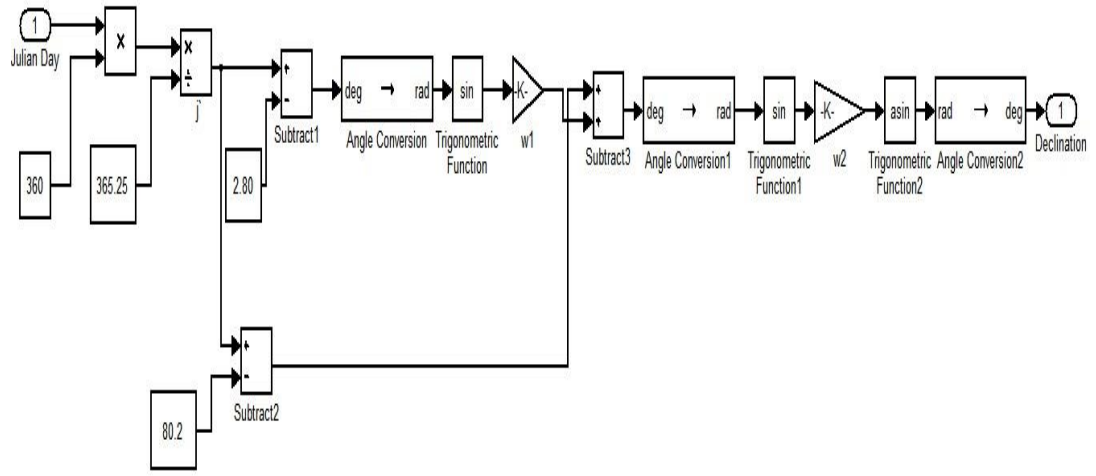


Figure 3.10: The Internal Architecture of the "Declination Sub-System"

### *c) Simulation of the Solar Altitude Angle*

The solar altitude angle is another parameter that is simulated by the model. This value is calculated based on Eq.3.7. Figure 3.11 shows the internal architecture of the "Sun Altitude Sub-System". As it is shown in the figure, the previously simulated solar declination angle and the latitude of the geographical area are the inputs to the "Sun Altitude Sub-System".

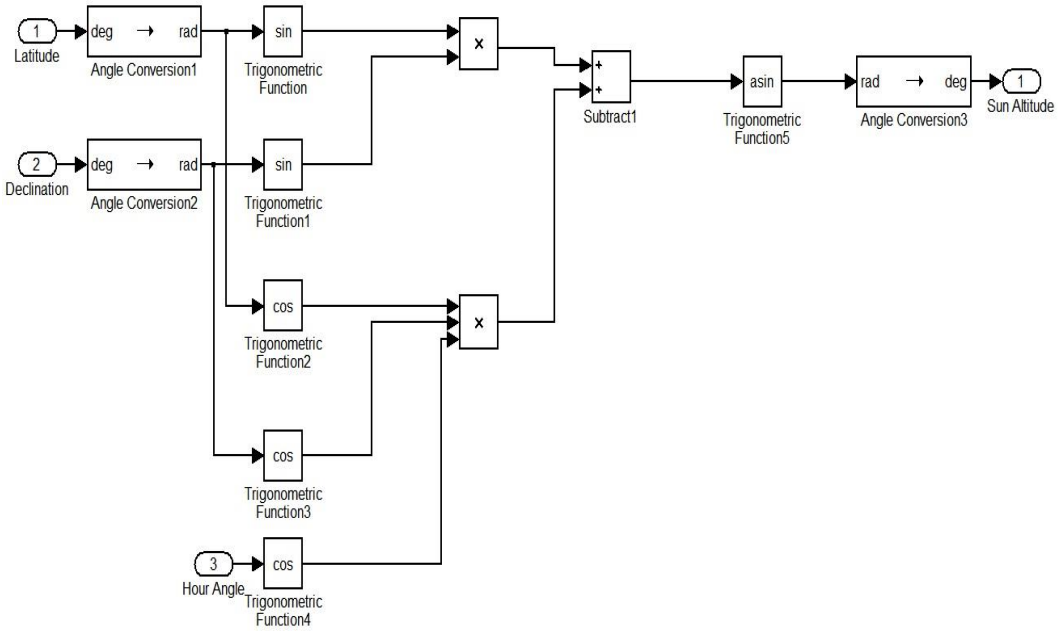


Figure 3.11: The Internal Architecture of the "Sun Altitude Sub-System"

### *d) Simulation of the Solar Azimuth Angle*

Solar azimuth angle is simulated by the model according to Eq.3.11 – Eq.3.14, in "Sun Azimuth Sub-System". The internal architecture of the mentioned sub-system is shown in Figure 3.12. As it is shown in the figure, the latitude of the geographical area, the value of the previously simulated solar declination and solar altitude angles are inputs to the mentioned sub-system.

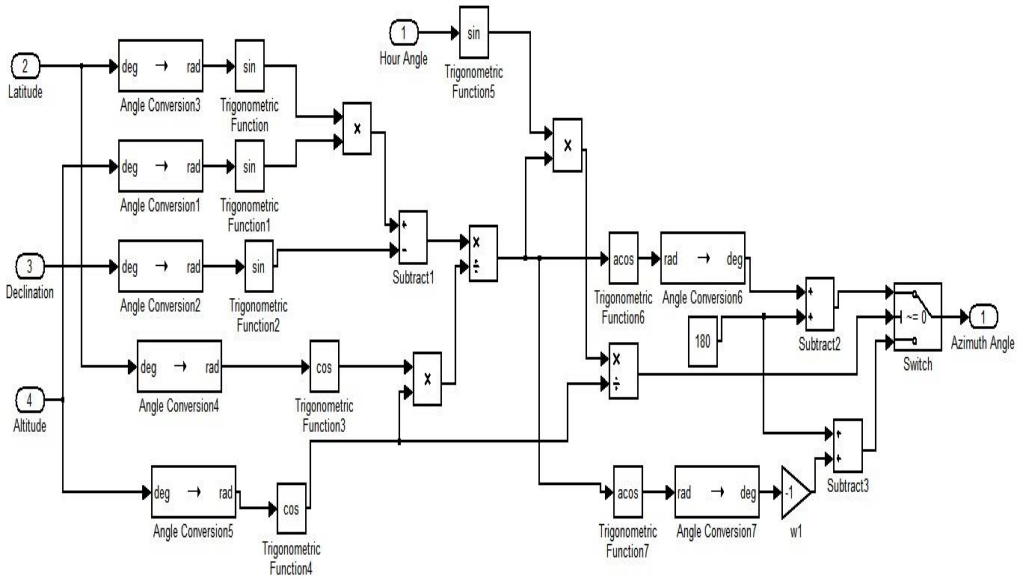


Figure 3.12: The Internal Architecture of the "Sun Azimuth Sub-System"

### *e) Simulation of the Solar Angle of Incidence*

As previously mentioned, solar angle of incidence is another parameter which is simulated by the model based on Eq.3.15. Figure 3.13 shows the internal architecture of the "Incidence Angle Sub-System". As it is obvious from the figure, the previously simulated values of the solar altitude angle, the solar azimuth angle, the value of the panel tilt angle and the panel azimuth angle are the inputs to the simulation sub-system.

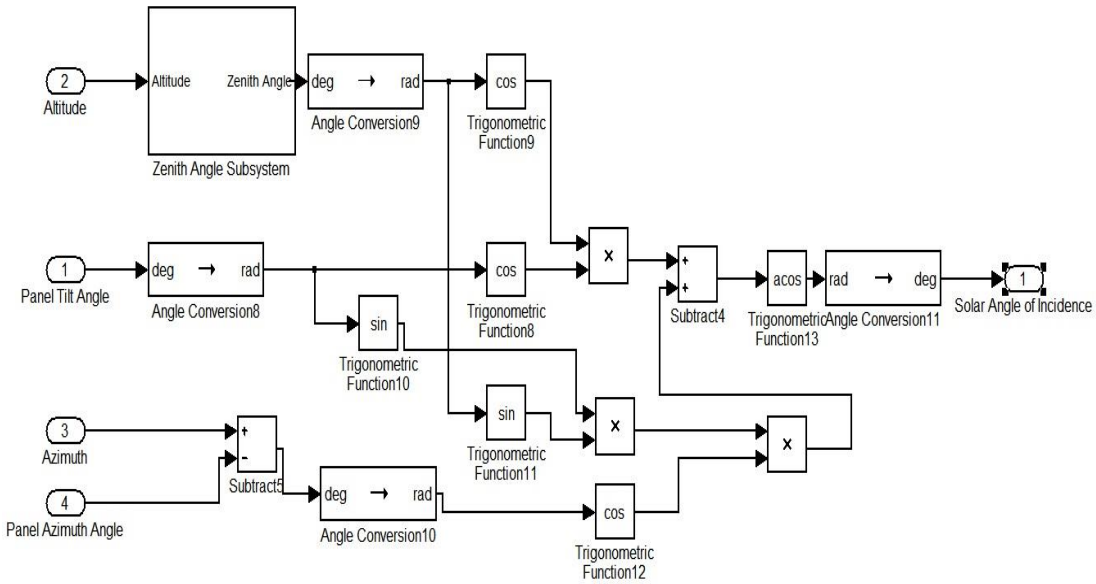


Figure 3.13: The Internal Architecture of the "Incidence Angle Sub-System"

### 3.2.1.1 Sample Results of Simulation of the Sun`s Position in the Sky

The Sun`s position in the sky is simulated using the above mentioned simulation model for Famagusta city, North Cyprus (Latitude: $35^{\circ}8'18''$, Longitude: $33^{\circ}55'45''$), for 4 different sample days being January 1$^{st}$, April 1$^{st}$, July 1$^{st}$ and Oct. 1$^{st}$, representing the 1$^{st}$, 91$^{st}$, 182$^{nd}$ and 274$^{th}$ days of the year. The simulation results are provided in Fig. 3.14 in terms of values of the solar altitude angle, the solar azimuth angle and the angle of incidence.

As it is obviously observed from the results of the simulation, the Sun has its maximum height in the sky at solar noon, which does not exactly match the local noon, for all the sample days. As it is shown, the solar noon happens around the local noon on January, 1$^{st}$ and Oct., 1$^{st}$ whereas it is approximately one hour shifted for April, 1$^{st}$ and July, 1$^{st}$ because of application of daylight saving time on the mentioned dates. It is also observed that the solar azimuth angle takes its lowest value ($180^{\circ}$) when the Sun is due South at exact solar noon for all the sample days. The solar incidence angle also shows a similar behavior to the solar azimuth angle taking the minimum value at exact solar noon, for all the sample days. Lower values of the solar incidence angle, which happen at solar noon, mean that sunlight beams are received on the surface of the PV module closer to perpendicular at the mentioned instant of time. A brief conclusion of the simulation results shows that at exact solar noon the Sun has its maximum elevation in the sky, it is due south and the solar irradiance is received by the solar panel with the closest angle to perpendicular. Therefore it is expected that a south oriented PV module should produce the highest power at exact solar noon.

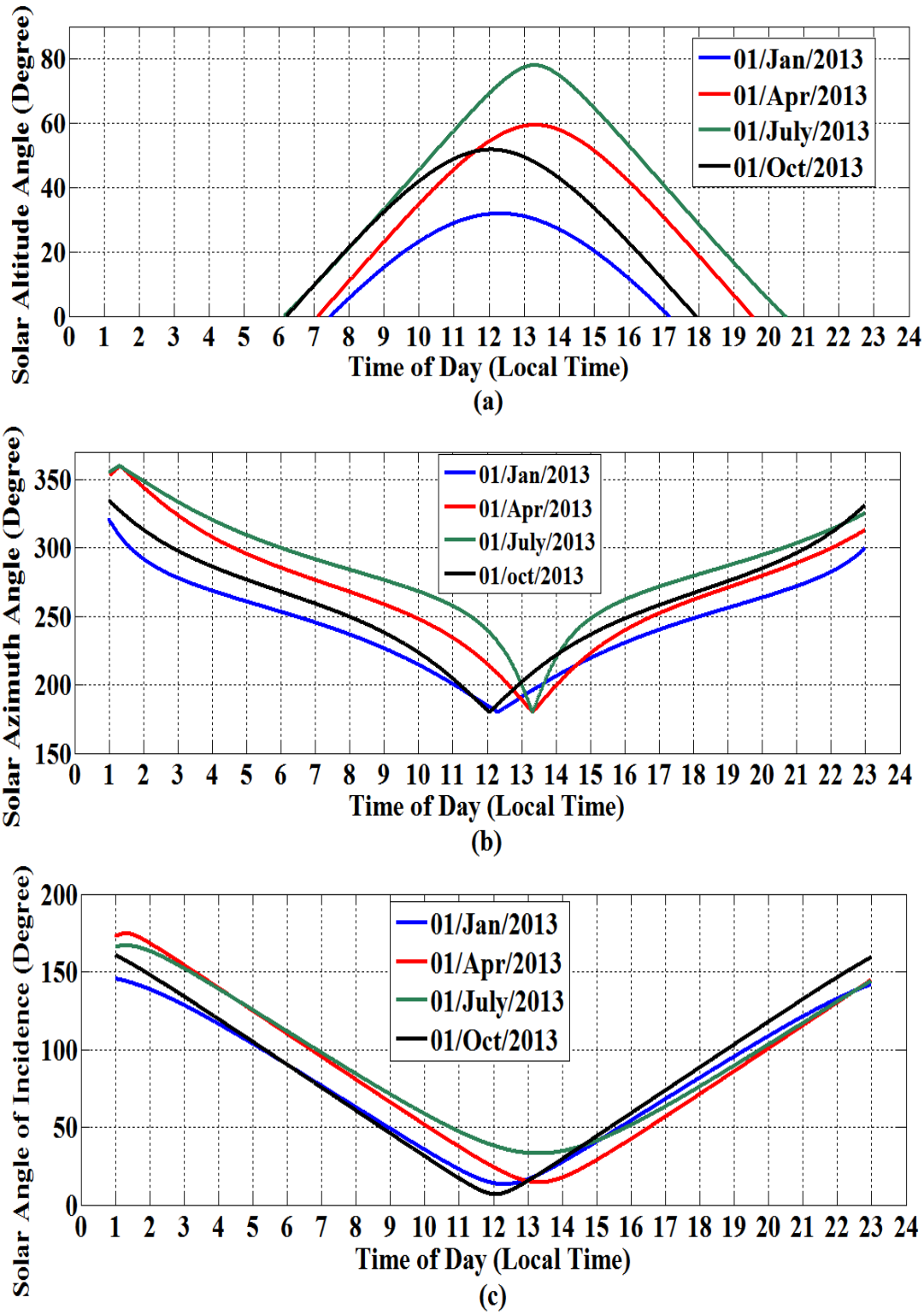


Figure 3.14: Sample Simulation Results of the Sun`s Position in the Sky for Famagusta City, North Cyprus (Latitude: $35^{\circ}8'18''$, Longitude: $33^{\circ}55'45''$)

An experimental analysis, as provided in our previous work which is also presented in "Appendix K" [58], is conducted in order to investigate the effects of the Sun`s

position in the sky and to verify the mentioned prediction regarding power generation in a PV module. The experiment set consists of 6 PV modules, an electronic circuit and a computer. The mentioned PV modules are 45° tilted commercially available crystalline silicon modules ($P_{max}$ = 15 W, $I_{sc}$ = 0.96 A, $V_{oc}$ = 21.6 V) that are located with 6 different orientations as shown in Fig. 3.15, on top of the Electrical and Electronic Engineering Department, Eastern Mediterranean University, Famagusta, North Cyprus (Latitude: $35^{\circ}8'18''$, Longitude: $33^{\circ}55'45''$). The purpose of this arrangement is to create the opportunity to track, compare and analyze the effects of the Sun`s movement in the sky on power generation by PV modules with different orientations during a day. The PV modules directly feed a constant resistive load in order to create the possibility for scaling and measurement of the instantaneous values of the module output power and track the rapid fluctuations in power generation caused by cloud passages. The PV module azimuth angle values are provided in Table 3.2.

Figure 3.15: Arrangement of 6 PV Modules with Different Orientations for Output Power Data Collection

Table 3.2: Azimuth Angles of the PV Modules Utilized for Data Collection Purpose ($North = 0^{\circ}, East = 90^{\circ}$)

| **Panel Orientation** | **Azimuth Angle** |
|---|---|
| South | $175^{\circ}$ |
| South East | $105^{\circ}$ |
| South West | $245^{\circ}$ |
| North | $5^{\circ}$ |
| North East | $47^{\circ}$ |
| North West | $320^{\circ}$ |

An electronic circuit, as shown in Figure 3.16 is designed which is responsible for measuring and sending PV module output power values to a PC. Output power measurements are conducted in per-minute basis. Figure 3.16 shows the circuit diagram of the mentioned electronic circuit.

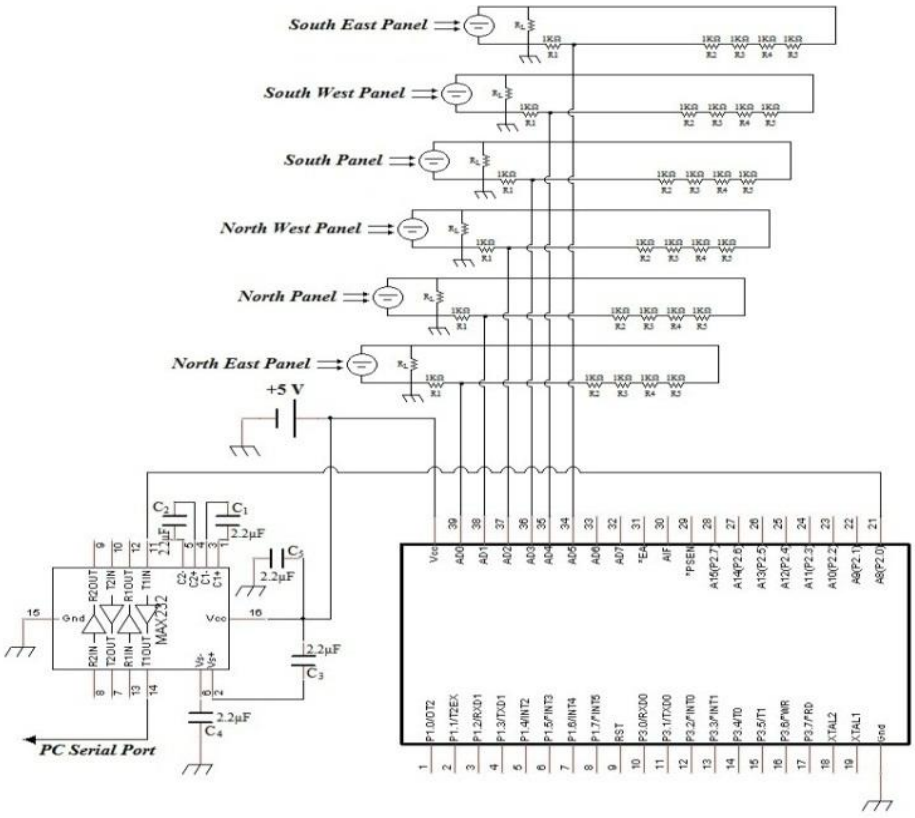


Figure 3.16: The Circuit Diagram of the Electronic Circuit Designed to Measure PV Module Output Power Values and Transfer the Values to a PC

The PV module output power data collection task is carried out for three sample days representing different atmospheric conditions, namely being a sunny, rainy and cloudy day, happening on May 8th, 2012, May 16th, 2012, May 22nd, 2012. The results of the collected output power data for the mentioned three sample days are shown in Figure 3.17. The effects of the Sun`s movement in the sky during a day are obviously visible from the results. It is shown that partial or full shading of PV modules during a rainy or cloudy day has caused significant reductions in power generation by PV modules. However, the situation is not the same for a sunny day (May 8th, 2012). It is obviously visible that the south oriented PV module has the largest amount of power generation while the maximum power is generated by this panel at solar noon which does not exactly match the local noon.

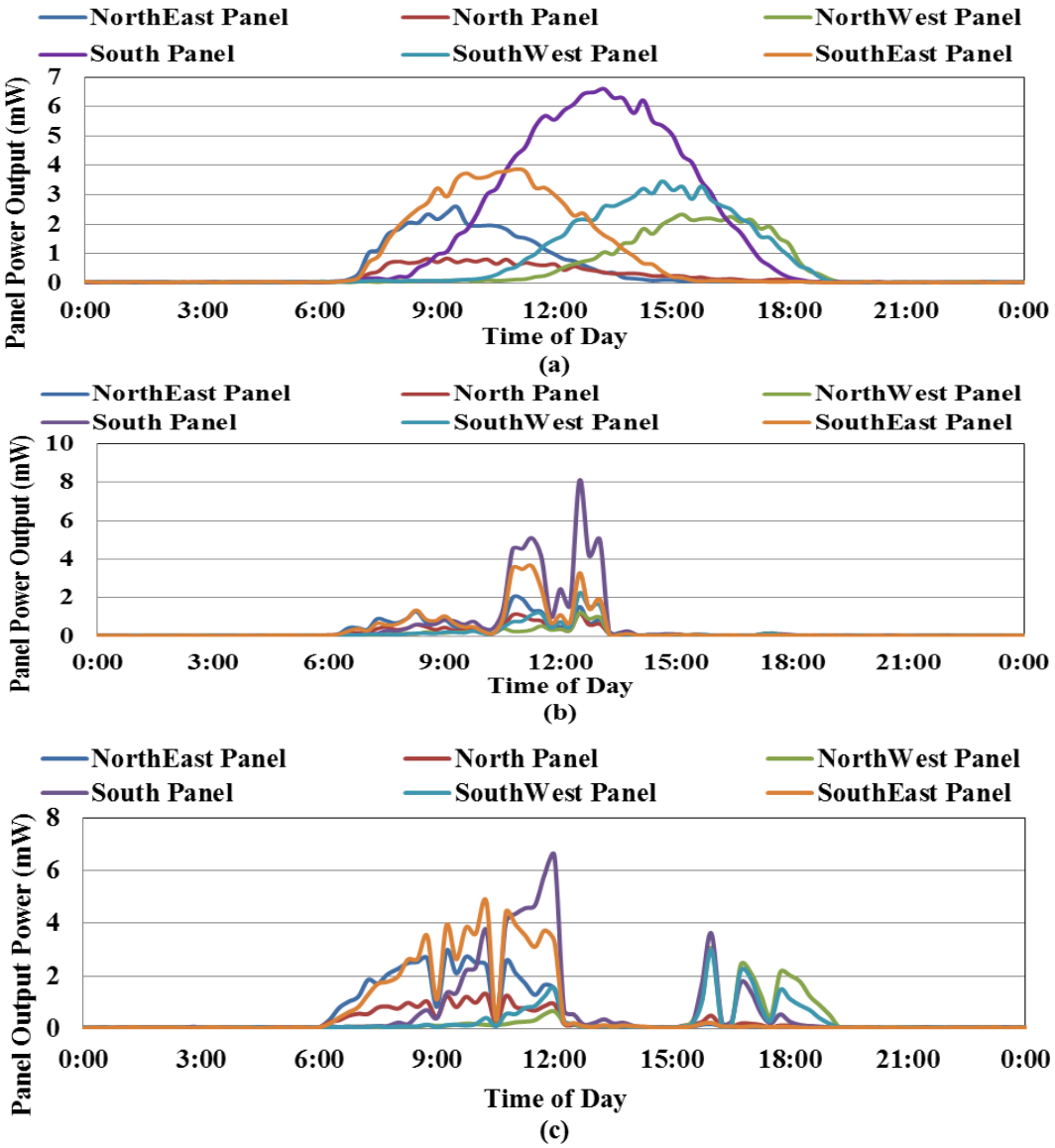


Figure 3.17: Measured PV Module Output Power Values for (a) a Sunny Day (May 8th, 2012), (b) a Cloudy Day (May, 16th, 2012) and (c) a Rainy Day (May 21st, 2012)

The effects of the Sun`s movement in the sky on power generation by other PV modules are also visible from the results, where PV modules on the east side generate their maximum power before solar noon while the situation is completely reversed for the panels on the west side.

## 3.3 Basics of Solar Radiation

This part of the thesis is allocated to a brief discussion and definition of the basic terms and parameters of solar radiation. Solar radiation by itself is a pretty much wide and

comprehensive subject which can be handled as a subject of a separate research study. Therefore, this thesis only considers the topic by its general lines and only particular terms utilized throughout the study are chosen and explained for the sake of simplicity and ease of following of the further discussions and explanations throughout the thesis.

### 3.3.1 Terms and Definitions

This part of the thesis provides the definitions for the terms and parameters utilized throughout the thesis.

- ***Solar Radiation:*** The energy emitted from the Sun towards the Earth`s surface is called solar radiation. Solar radiation is also explained using different words such as; solar irradiation and solar insolation. Solar radiation is measured as the energy received on the surface of a specific area during a specific time period (daily, monthly or yearly). The unit of solar radiation is usually expressed as $Wh/m^2$, $kWh/m^2$. Figure 3.18, Figure 3.19 and Figure 3.20 show the annual mean solar radiation maps of the World, Europe and Cyprus, respectively.

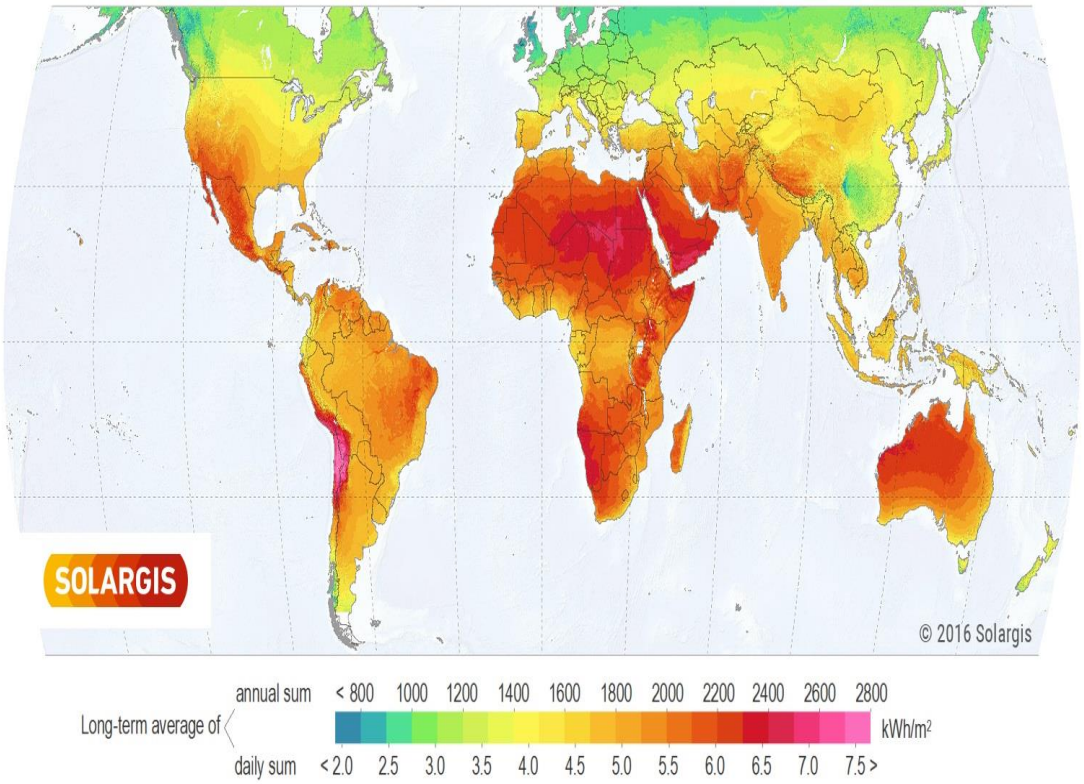


Figure 3.18: Annual Mean Solar Radiation Map of the World

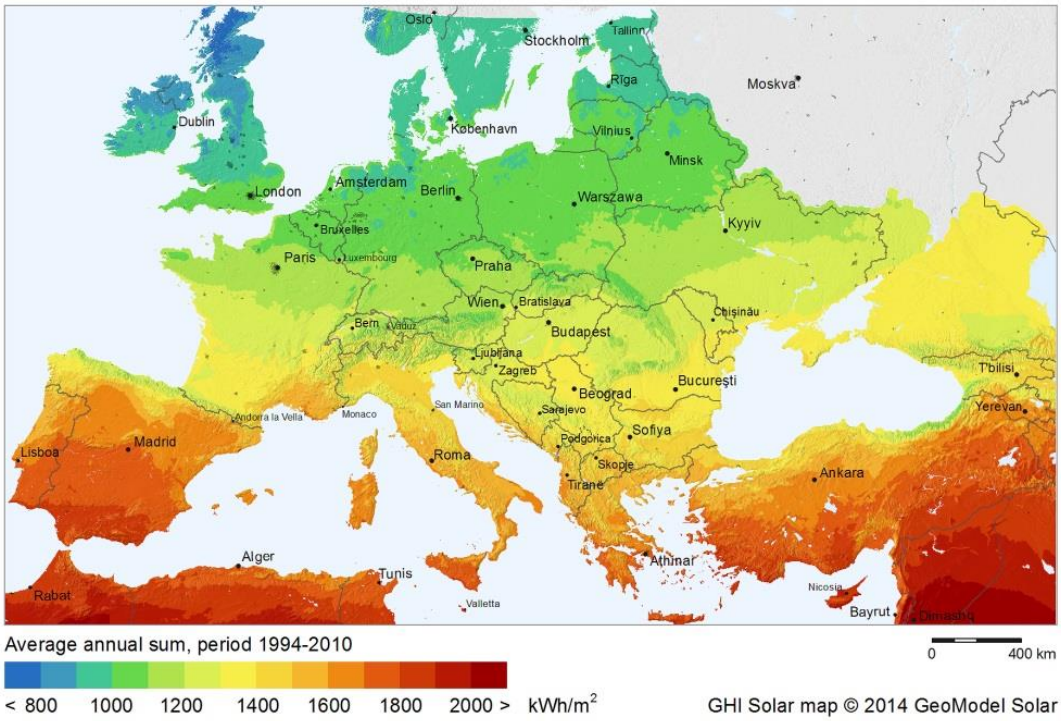


Figure 3.19: Annual Mean Solar Radiation Map of Europe

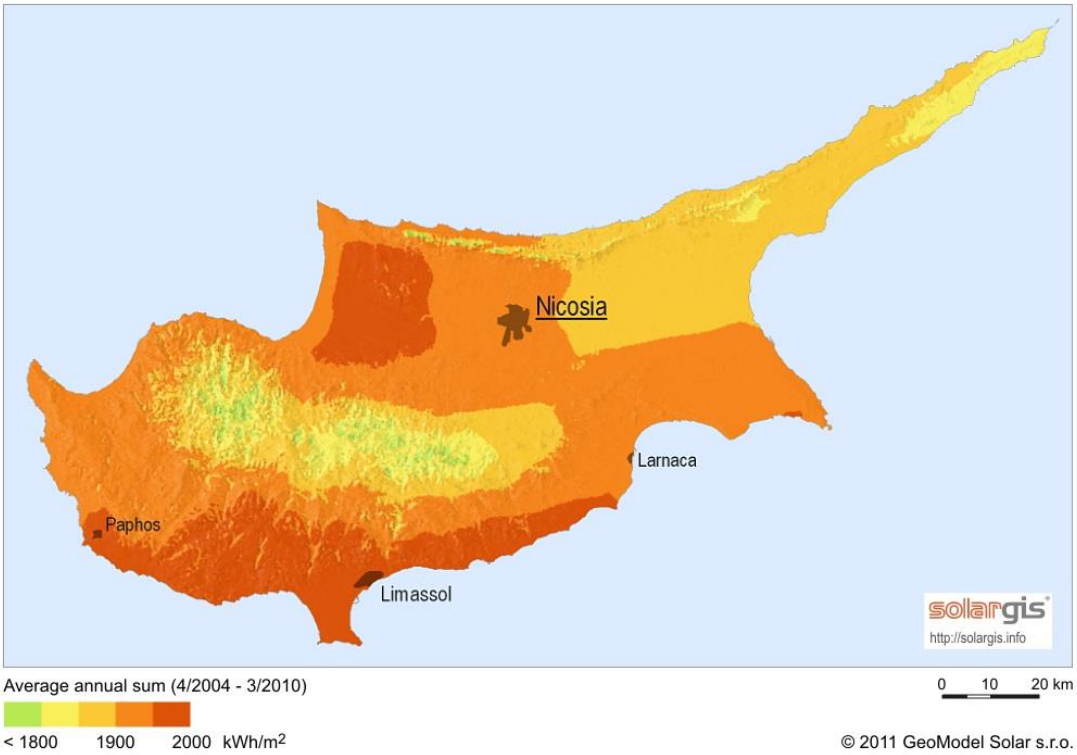


Figure 3.20: Annual Mean Solar Radiation Map of Cyprus

- ***Solar Irradiance:*** Solar irradiance is expressed as the instantaneous power received from the Sun on the surface of a specific area. Solar irradiance is usually expressed in $W/m^2$.
- ***Solar Constant:*** Solar constant is defined as the power reached on the surface of a unit area which is perpendicular to the sunlight beams out of the Earth`s atmosphere. The value of the solar constant is generally assumed as 1367 $W/m^2$.
- ***Air Mass:*** Air Mass (AM) is defined as the length of the path that sunlight beams take through the atmosphere to reach the Earth which is normalized to the shortest possible path length.
- ***Relative Sunshine Duration:*** The relative sunshine duration is defined as the number of sunny hours during a specific time period (daily, monthly and yearly values) at a specific geographical location. It is sometimes provided as the

average value over some years. Thus, the relative sunshine duration can be considered as a good measure for cloudiness of a geographical location. Also the relative sunshine duration expressed in monthly basis can be utilized as a measure for comparison between the cloudiness amounts in a particular location over different time intervals.

- ***Clearness Index:*** Clearness Index (CI) can be considered as a measure of the clearness of the atmosphere. It is defined as the ratio of the global solar irradiance received on a horizontal surface on the Earth to the solar irradiance available out of the atmosphere (extraterrestrial irradiance). Clearness index is expressed as a dimensionless number which is variable between 0 and 1. The value of CI is closer to 1 under clear-sky conditions while lower values are obtained under cloudy sky conditions.
- ***Cloud Cover:*** Cloud Cover (CC) defines the cloudiness of the sky at a specific time interval. It is usually measured in Oktas which varies between 0 and 8, where 0 represents clear-sky and 8 represents overcast sky conditions [59]. Cloud coverage is usually measured and provided by meteorological stations with different time intervals such as hourly, 3-hourly or daily values.

### 3.3.2 Spectrum of Solar Radiation

The Sun emits electromagnetic radiation through almost all of the electromagnetic spectrum. The solar spectrum can be divided into three main areas being namely; the ultraviolet radiation, the visible light and the infrared light. Figure 3.21 presents a general overview of the solar spectrum.

*i. The Ultraviolet Radiation*

The ultraviolet radiation by itself can be divided into three sub-categories being; 1) Ultraviolet C (UVC) spanning in the range of 100-280 nm. The UVC radiation has a

frequency which is higher than the frequency of the violet light. The UVC radiation is invisible to the human eye and very small amounts of this radiation can reach the Earth`s surface due to absorption in the atmosphere. 2) Ultraviolet B (UVB) spanning in the range of 280-315 nm. The UVB radiation together with the UVC radiation causes a reaction which forms the ozone layer. This type of radiation is considered to be very harmful for human health 3) Ultraviolet A (UVA) spanning in the range of 315-400 nm and less harmful to the human health compared to the UVA radiation.

*ii. The Visible Spectrum Range or Sunlight*

The visible light spans in the range of 380-780 nm and is visible to the human eye.

*iii. The Infrared Radiation*

The infrared radiation spans in the range of 700-1,000,000 nm including a significant portion of the radiation received on the Earth`s surface.

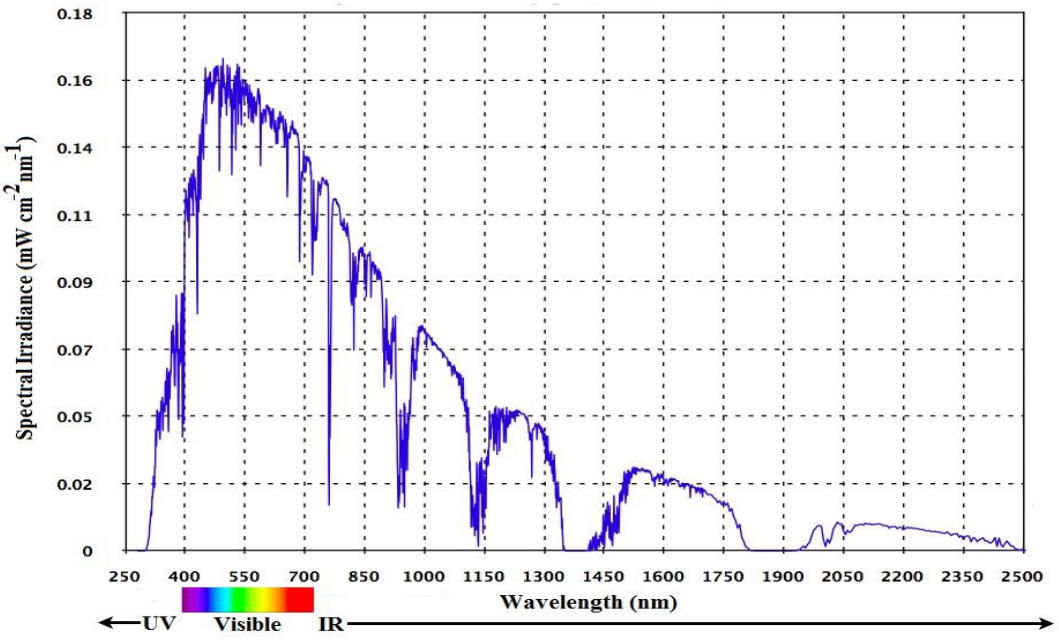


Figure 3.21: Spectrum of Solar Radiation

### 3.3.3 The Extraterrestrial Solar Irradiance

The extraterrestrial solar irradiance is defined as the solar irradiance received on the surface of a horizontal plane out of the Earth`s atmosphere. The extraterrestrial solar irradiance, $G_0$, is obtained as [55];

$$G_0 = \varepsilon 1367 \sin \gamma_s \tag{3.16}$$

Where ;

$$\varepsilon = 1 + 0.0334\cos(\mathrm{j}` - 2.80^{\circ}) \tag{3.17}$$

### 3.3.4 Different Components of Solar Irradiance

The extraterrestrial solar irradiance entering the Earth`s atmosphere passes through a very complicated process to reach the Earth`s surface. This process mainly involves interaction with different components existing in the atmosphere, such as different gases, water vapor, etc. The incoming solar irradiance loses some of its power when reached at the Earth`s surface as a result of the mentioned interactions. What happens when solar irradiance enters the Earth`s atmosphere can mainly be described as follows;

i. A portion of the incoming solar irradiance is absorbed by different components existing in the atmosphere such as different gases, water droplets, etc. As a result of the mentioned absorption 20% of the incoming solar irradiance is converted to heat which causes a heating effect in the atmosphere [55].
ii. Another portion of the incoming irradiance is scattered and reflected back to space mainly due to clouds existing in the atmosphere. The amount of back scattered solar irradiance is approximately 23%[55].
iii. The remaining 57% of the incoming solar irradiance after all absorption and back scattering effects reaches the Earth`s surface [55].

The amount of the solar irradiance that reaches the Earth`s atmosphere forms the Global Solar Irradiance. The mentioned global irradiance is usually measured on a horizontal surface and therefore called the Horizontal Global Solar Irradiance. The global horizontal irradiance consists of two different components being namely; the Direct (or beam) irradiance and the Diffuse Irradiance. The direct component of solar irradiance is defined as the irradiance component that is directly incident on the surface a PV module from the Sun without being subject to any absorption, scattering or reflection. The diffuse irradiance on the other hand can be described as an irradiance component that reaches the surface a PV module after being scattered or reflected by clouds, different particles in the air, neighboring objects, etc.

Since most of PV modules are utilized as tilted panels in solar energy related applications, the global horizontal solar irradiance should be converted to irradiance on a tilted (or inclined) surface to be utilized for the required analysis purposes. The resulting global irradiance on inclined PV module surface contains an extra component compared to the irradiance on a horizontal surface. The mentioned extra component is the ground-reflected (or albedo) irradiance which accounts for a portion of solar irradiance incident on the surface of a tilted PV module that is reflected by the ground. The type of the ground surface (i.e. soil, snow, etc.) has a great role in determination of the amount of the ground-reflected or albedo solar irradiance component.

## 3.4 Modeling of Clear-Sky Solar Irradiance

Dependency of the performance of solar energy systems to the incident solar irradiance is considered as the main reason for which precise information regarding the incident solar irradiance on the surface of PV modules within a PV power plant is required. Obviously clouds, as very complex elements existing in the Earth`s atmosphere, have

significant decreasing effects on the incident solar irradiance. Thus, interactions between clouds and solar irradiance should always be taken into consideration precisely for a good estimation of the amounts of solar irradiance that is received by PV modules. The process of the mentioned irradiance estimation or forecast can therefore be considered to include two main stages. The first stage is to estimate/calculate solar irradiance values under absence of clouds (clear-sky conditions) and the second stage is to account for interactions of the sunlight with clouds and other particles within the atmosphere that form barriers against the incident solar irradiance.

### 3.4.1 Ångström-Prescott Regression

Theoretical establishment of irradiance components requires detailed data regarding meteorological factors and cloud properties. These data are rarely collected and most often not readily available for all stations. On the other hand, data on sunshine hours and cloud coverage are generally recorded and widely available. Hence, correlations have been developed to estimate solar radiation based on sunshine and cloud cover data. The first model of this type was introduced in [60] and then modified in [61]. The model presents a simple relationship between the global irradiation received on a horizontal surface ($\overline{H_o}$), the global irradiation outside the Earth's atmosphere ($H_0$) and the relative sunshine duration as;

$$\frac{\overline{H_o}}{H_0} = a + bS_f \tag{3.18}$$

$$S_f = \frac{S}{S_0} \tag{3.19}$$

Where;

$S_f$ : Daily relative sunshine duration [hours]

$S$ : Monthly average daily bright sunshine hours [hours]

$S_0$ : Monthly average day length [hours]

$a$ , $b$ : Ångström-Prescott regression coefficients

According to [53] $a$ and $b$ are site dependent and respectively being related linearly and hyperbolically to yearly average values of $S_f$ [62]. Different methods for calculation of $a$ and $b$ are available in the literature [62][46][63][64]. The following pair of equations are utilized in this thesis to obtain appropriate values for $a$ and $b$ due to their world-wide applicability [63];

$$a = -0.309 + 0.539\cos\varphi - 0.0693h + 0.29\frac{S}{S_0} \tag{3.20}$$

$$b = 1.527 - 1.027\cos\varphi + 0.0926h - 0.359\frac{S}{S_0} \tag{3.21}$$

Utilizing the Ångström-Prescott Regression, the transmission factor ($\bar{\tau}$), mean daily clear-sky clearness index ($\overline{K_o}$ ), mean daily clear-sky diffuse fraction ($\overline{D_o}$) and mean daily clear-sky diffuse clearness index ( $\overline{K_d}$ ) are expressed as;

$$\bar{\tau} = \frac{a}{a+b} \tag{3.22}$$

$$a + b = \frac{1}{H_0}\int_{SR}^{SS} G_o(t)\,dt = \frac{1}{H_0}\int_{SR}^{SS} G_d(t)\,dt + \frac{1}{H_0}\int_{SR}^{SS} G_b(t)\,dt = \frac{\overline{H_o}}{H_0} = \overline{K_o} \tag{3.23}$$

$$\overline{D_o} = \frac{\overline{H_d}}{\overline{H_o}} \tag{3.24}$$

$$\overline{K_d} = \frac{\overline{H_d}}{H_0} = \frac{\overline{H_o}}{H_0}.\frac{\overline{H_d}}{\overline{H_o}} = \overline{K_o}.\overline{D_o} = (a+b)\overline{D_o} \tag{3.25}$$

$$\overline{K_o} = a + b = \frac{\overline{H_o}}{H_0} = \frac{\overline{H_d}}{H_0} + \frac{\overline{H_b}}{H_0} = \frac{\overline{H_o}}{H_0}.\frac{\overline{H_d}}{\overline{H_o}} + \frac{\overline{H_o}}{H_0}\left(1 - \frac{\overline{H_d}}{\overline{H_o}}\right) = (a+b)\overline{D_o} + (a+b)(1-\overline{D_o}) = \overline{K_d} + \overline{K_b} \tag{3.26}$$

Where;

$\overline{K_b}$ : Mean daily clear-sky beam clearness index

$\overline{H_d}$ : Mean daily clear-sky horizontal diffuse irradiation [J/m$^2$]

Simulated probability functions of daily clearness index for Berlin, Germany (Latitude: 52˚33'56", Longitude: 13˚18'39") in July, using different sets of regression coefficients are compared to observed data, as shown in Figure 3.22, in order to validate and examine the effectiveness of the chosen pair of regression coefficients. The mentioned observed data consist of the observed daily relative sunshine duration data for Berlin, Germany utilized in order to calculate the regression coefficients provided in Eq.3.20 and Eq.3.21, and as a result, the clearness index values and the observed clearness index data for the same location utilized for comparison purposes against the simulated ones. Observed clearness index data for Berlin, Germany (Latitude: 52˚33'56", Longitude: 13˚18'39"), as a data source utilized in this thesis, has been obtained from the NASA Langley Research Center Atmospheric Science Data Center Surface meteorological and Solar Energy (SSE) web portal supported by the NASA LaRC POWER Project [65]. A data pack provided by the European Climate Assessment & Dataset [66] is utilized to achieve the daily relative sunshine duration data for Berlin, Germany (Latitude: 52˚33'56", Longitude: 13˚18'39"). The data pack spans the time period from 1979 to 2014. More information regarding these coefficient sets is provided in Table 3.3. Obviously the results achieved with Eq.3.20 and Eq.3.21 have been the closest results to the observations. Standard methods are provided in the literature to obtain the diffuse fraction based on values of clearness index. The method recommended in [51] is utilized in this thesis due to its consistency with the considered latitudes. The method expresses the diffuse fraction as;

$$\overline{D_o} = \begin{cases} 1.02 - 0.248\overline{K_o} & \overline{K_o} \leq 0.3 \\ 1.45 - 1.67\overline{K_o} & 0.3 < \overline{K_o} < 0.78 \\ 1.47 & \overline{K_o} \geq 0.78 \end{cases} \quad (3.27)$$

Where;

$\overline{K_o}$ : Mean daily clear-sky clearness index

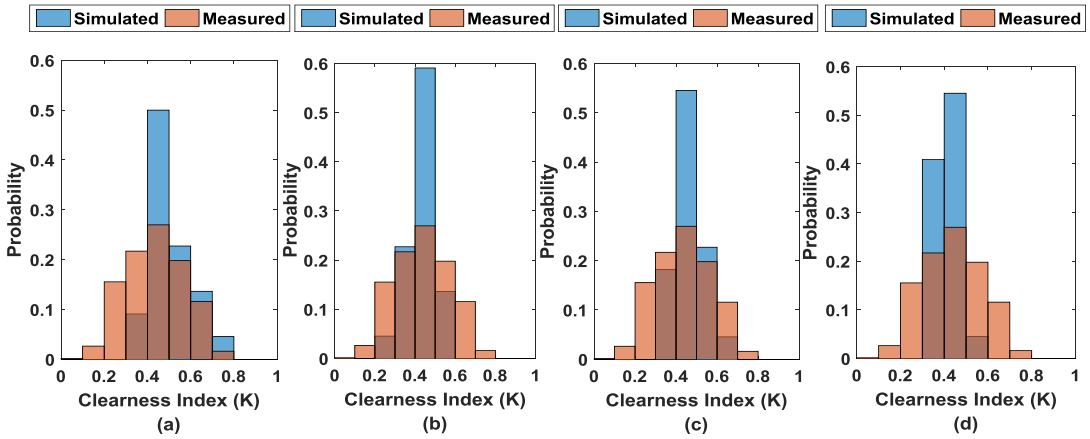


Figure 3.22: Probability Functions of Observed vs. Simulated Clearness Index, $K$, using (a) Gopinathan [63], (b) Iqbal [46], (c) Gueymard et. al. [64] (d) Rietveld [62] Method, for Berlin, Germany (Latitude: 52°33'56", Longitude: 13°18'39") in July. Observed Data Sample Size: 682 days (22 years), Simulated Data Sample Size: 682 Days (22 years)

Table 3.3: List of Different Regression Coefficietns Compared in the Thesis

| **Reference** | ***a*** | ***b*** | **Data Coverage** |
|---|---|---|---|
| Gopinathan [63] | $-0.309 + 0.539\cos\varphi - 0.069 + 0.29\frac{S}{S_0}$ | $1.527 - 1.027\cos\varphi + 0.0926h - 0.359\frac{S}{S_0}$ | $(5^\circ < \varphi < 54^\circ)$ |
| Gueymard et. al. [64] | 0.18 | 0.62 | $(6^\circ < \varphi < 69^\circ)$ (42 locations) |
| Iqbal [46] | $0.29cos\varphi$ | 0.52 | $\varphi < 60^\circ$ |
| Rietveld [62] | $0.1 + 0.24\langle\frac{S}{S_0}\rangle$ | $0.38 + 0.08\langle\frac{S}{S_0}\rangle$ | $(6^\circ < \varphi < 69^\circ)$ (42 locations) |

$\langle\frac{S}{S_0}\rangle$: Yearly average of $S_f$ $\varphi$: Latitude of the geographical location

### 3.4.2 The Clear-Sky Model

Numerous models have been introduced in the literature in order to model solar irradiance under clear-sky conditions. The main emphasize in these models is mostly put on modeling of the beam or direct irradiance component due to its importance from solar energy related applications point of view. A comprehensive review on different clear-sky models is provided in [67]. The mentioned study concludes that the Berland formula which is introduced in [68] outperforms the other clear-sky irradiance models. Clear-Sky models are utilized generally in order to calculate the beam and diffuse irradiance components on a horizontal surface under clear-sky conditions. The clear-sky model introduced in [69] is used in this thesis in order to model the above mentioned irradiance components. This model is chosen due to its simplicity and conformity to the previously mentioned Berland Formula. According to this model the global, direct and diffuse irradiance components are expressed as;

$$G_b(t) = G_0(t) exp \frac{-\alpha}{cos\theta_z(t)} \tag{3.28}$$

$$G_d(t) = c\big(G_0(t) - G_b(t)\big) = G_0(t)c(1 - exp \frac{-\alpha}{cos\theta_z(t)}) \tag{3.29}$$

$$G_o(t) = G_0(t)\left(c + (1-c) exp \frac{-\alpha}{cos\theta_z(t)}\right) \tag{3.30}$$

Where $c = \frac{(a+b).\overline{D_o}}{1-(a+b)(1-\overline{D_o})} = \frac{\overline{K_d}}{1-\overline{K_b}}$ is an adjustment constant and the value of $\alpha$ is chosen in such a way that it ensures the following equation;

$$\frac{\overline{H_b}}{H_0} = (a+b)(1-\overline{D_o}) = \frac{1}{H_0}\int_{SR}^{SS} G_0(t) exp \frac{-\alpha}{cos\theta_z(t)} dt \tag{3.31}$$

Where;

$SS$ : Sunset

$SR$ : Sunrise

## 3.5 Conversion of Horizontal Irradiance to Irradiance on an Inclined PV Module Surface

As it was discussed earlier, the solar irradiance received on a horizontal plane on the Earth`s surface should be converted to irradiance incident on an inclined surface in order to be utilized in solar energy related applications [70,71,72]. This part of the thesis provides brief information on how the horizontal irradiance is converted to irradiance on an inclined PV module surface. The global irradiance incident on the surface of an inclined PV module can be expressed as;

$$G_{o\beta}(t) = G_{b\beta}(t) + G_{d\beta}(t) + G_{r\beta}(t) \tag{3.32}$$

### 3.5.1 Direct Irradiance on Inclined PV Module Surface

The direct irradiance under clear-sky conditions is converted into beam irradiance on inclined PV module surface by multiplying the beam irradiance component on horizontal surface by the ratio of direct irradiance on inclined surface to direct irradiance incident on a horizontal surface, $R_b$, given as;

$$G_{b\beta}(t) = G_b(t)R_b = G_b(t)\frac{\cos\theta_S(t)}{\cos\theta_Z(t)} \tag{3.33}$$

Where;

$G_b(t)$ : The instantaneous value of the clear-sky beam irradiance on a horizontal surface

$G_{b\beta}(t)$ : The instantaneous value of the beam irradiance on an inclined surface

### 3.5.2 Diffuse Irradiance on Inclined PV Module Surface

Due the complicated nature of the diffuse component of solar irradiance, calculation of the diffuse irradiance component on an inclined PV module surface is not as easy and straightforward as calculation of the bam and albedo components. The value of the diffuse irradiance component on an inclined PV module surface is obtained by

multiplying the diffuse irradiance on a horizontal surface by the ratio of the diffuse irradiance incident on the surface of a tilted PV module to the diffuse irradiance component on a horizontal surface, $R_d$. In general, there are two main categories of models that are developed to estimate $R_d$, being namely Isotropic and Anisotropic models. The isotropic models [73,74,75,76] consider a uniform intensity for the diffuse solar irradiance over the sky dome and hence assume that the diffuse irradiance incident on the surface of an inclined PV module depends on the sky portion seen by the module. On the other hand, anisotropic models [77,78,72,79,80,81] assume that the diffuse irradiance is not isotropic in the sky area close to the solar disk while it is considered to be isotropically distributed in the rest of sky dome. As it can be estimated, the advantage of the isotropic models are their simplicity against the anisotropic models but they have shown underestimation in the case of estimation of diffuse irradiance on PV module surface aligned towards the equator. Table 3.4 presents a list of different isotropic and anisotropic models introduced for calculation of the diffuse irradiance component on an inclined PV module surface. The diffuse irradiance incident on the surface of an inclined PV module can be expressed as;

$$G_{d\beta}(t) = G_d(t)R_d \tag{3.34}$$

Where;

$G_d(t)$ : The instantaneous value of the clear-sky diffuse irradiance on a horizontal surface

$G_{d\beta}(t)$ : The instantaneous value of the diffuse irradiance on an inclined surface

Table 3.4: Different Isotropic and Anisotropic Diffuse Irradiance Models

| **Model Name** | **Model Type** | $R_d$ |
|---|---|---|
| Badescu [73] | ISO | $[3+\cos(2\beta)]/4$ |
| Tian et. al. [74] | ISO | $1-\beta/180$ |
| Koronakis [75] | ISO | $1/3[2+\cos(\beta)]$ |
| Liu and Jordan [76] | ISO | $[1+\cos(\beta)]/2$ |
| Perez et. al. [77] | ANI | $0.5(1-F_1')[1-\cos(\beta)]+F_1'\left(\frac{a}{b}\right)+F_2'\sin(\beta)]$ |
| Hay [78] | ANI | $\frac{\overline{H_b}}{H_0}R_b+\left(1-\frac{\overline{H_b}}{H_0}\right)[1+cos\beta]/2$ |
| Reindl et. al. [72] | ANI | $\frac{\overline{H_b}}{H_0}R_b+\left(1-\frac{\overline{H_b}}{H_0}\right)[(1+\cos\beta)/2]\left[1+\sqrt{\overline{H_b}/\overline{H_o}}\,\sin^3(\beta/2)\right]$ |
| Skartveit and Olseth [79] | ANI | $\frac{\overline{H_b}}{H_0}R_b+\Omega^1 cos\beta+\left(1-\frac{\overline{H_b}}{H_0}-\Omega\right)[1+cos\beta]/2$ |
| Stevenand and Unsworth [80] | ANI | $0.51R_b+([1+cos\beta]/2)-1.74/1.26\pi\times[sin\beta-(\beta\times\pi/180)cos\beta-\pi\sin^2(\beta/2)]$ |
| Temps and Coulson [81] | ANI | $\cos^2\left(\frac{\beta}{2}\right)[1+\sin^3\left(\frac{\beta}{2}\right)[(1+\cos^2(\theta_S))\sin^3(\theta_Z)$ |

[1]: $\Omega=max\left\{0,(0.3-2)\frac{\overline{H_b}}{H_0}\right\}$

Where;

$H_0$ : The daily irradiation outside the Earth`s atmosphere [J/m$^2$]

$\overline{H_b}$ : Mean daily clear-sky horizontal beam irradiation [J/m$^2$]

$\overline{H_o}$ : Mean daily clear-sky horizontal global irradiation [J/m$^2$]

Performance of different anisotropic models in estimating the irradiance value incident on an inclined PV module surface has been compared using measured irradiance data and the model providing the best estimation performance has been chosen for calculation purposes in the thesis.

### 3.5.3 Ground Reflected (Albedo) Irradiance on an Inclined Surface

The ground reflected irradiance (albedo) has a small share of the global solar irradiance due to the low reflectivity level of the ground. The ground is assumed to be horizontal and reflecting solar irradiance in a homogeneous manner. The ground reflected irradiance can be expressed as;

$$G_{r\beta} = G_o(t)\rho R_r = G_o(t)\rho \frac{1-\cos\beta}{2} \tag{3.35}$$

Where;

$G_o(t)$ : The instantaneous value of the clear-sky global horizontal irradiance

$G_{r\beta}(t)$ : The instantaneous value of the ground reflected irradiance on an inclined PV module surface.

Figure 3.23 shows a general overview of the mentioned different irradiance components incident on the surface of an inclined PV module.

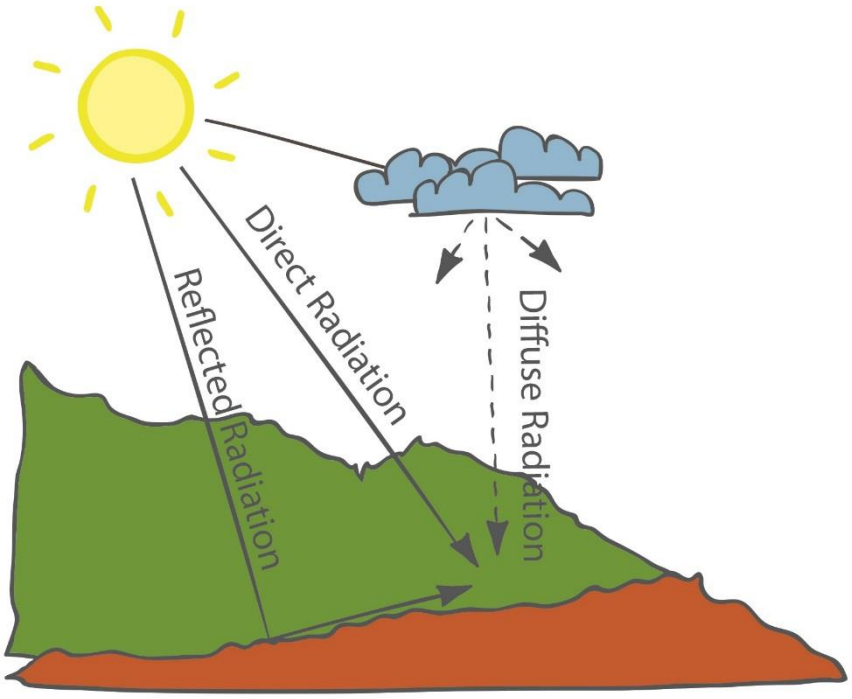


Figure 3.23: Different Irradiance Components Incident on the Surface of an Inclined PV Module

Conversion of the irradiance on horizontal surface to irradiance incident on inclined PV module surface is conducted in this thesis using Eq.3.34 and Eq.3.35, for the beam and ground reflected irradiance components, respectively. Also the model introduced in [72] is utilized in this thesis to convert the diffuse irradiance on a horizontal surface to diffuse irradiance on inclined PV module surface. The accuracy of the utilized conversion method is verified against measured solar irradiance data on a clear day in November on a 45° tilted PV module surface in Famagusta, North Cyprus (Latitude: 35°8'18", Longitude: 33°55'45"). For this purpose the clear-sky irradiance values incident on a horizontal surface for the same day were calculated using Eq.3.28 – Eq.3.30. The mentioned horizontal irradiance values were then converted to irradiance values on an inclined PV module surface using the above mentioned method and the measured and modeled values were compared. The comparison results are provided in Figure 3.24. The comparison results of the performance of 4 different

anisotropic diffuse irradiance conversion models, as specified in Table 3.4, are also provided in the figure. A threshold of 50 W/m$^2$ is also applied to irradiance values in the figure and the values below this threshold are omitted in order to avoid data uncertainty as recommended in [70].

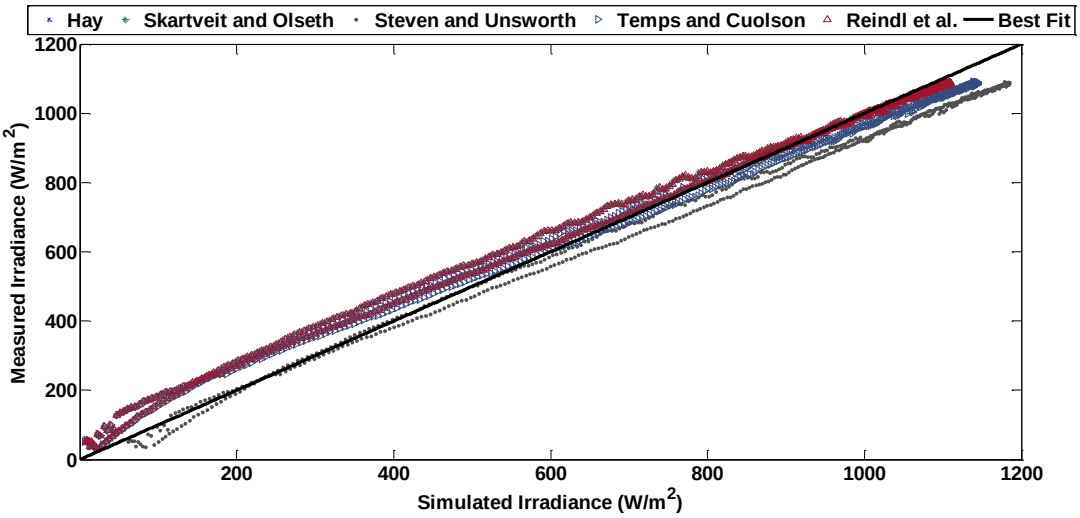


Figure 3.24: Comparison Results of the Modeled and Measured Solar Irradiance Values Incident on a 45° Inclined PV Module Surface on a Typical Clear Day in November in Famagusta, North Cyprus

The conversion performance of the compared models have also been examined and compared using different performance metrics, defined as follows;

$$Mean\ Absolute\ Error\ (MAE) = \frac{1}{n}\sum_{n}^{i=1} M_i - E_i \tag{3.36}$$

$$Root\ Mean\ Square\ Error\ (RMSE) = \sqrt{\frac{1}{n}\sum_{n}^{i=1}(M_i - E_i)^2} \tag{3.37}$$

$$Mean\ Absolute\ Percentage\ Error\ (MAPE) = \frac{1}{n}\left(\sum_{n}^{i=1}\frac{M_i - E_i}{M_i} \times 100\right) \tag{3.38}$$

$$Root\ Mean\ Square\ Percentage\ Error\ (RMSPE)$$

$$= \sqrt{\frac{1}{n}\sum_{n}^{i=1}\left(\frac{M_i - E_i}{M_i} \times 100\right)^2} \tag{3.39}$$

The numerical comparison results of different performance metrics for the compared 5 different anisotropic diffuse irradiance conversion methods are provided in Table 3.5

Table 3.5: Comparison Results of Different Performance Metrics for 5 Different Diffuse Irradiance Conversion Methods

| **Model** | **MAE** $(W/m^2)$ | **RMSE** $(W/m^2)$ | **MAPE** **(%)** | **RMSPE** **(%)** |
|---|---|---|---|---|
| Hay [78] | 33.0062 | 43.1067 | 10.2670 | 18.7669 |
| Reindl et al. [72] | 32.4287 | 42.1637 | 9.9690 | 18.1157 |
| Skartveit and Olseth [79] | 33.3397 | 43.7528 | 10.3217 | 18.6814 |
| Steven and Unsworth [80] | 53.2710 | 62.6140 | 8.1557 | 13.7442 |
| Temps and Coulson [81] | 40.7762 | 45.1770 | 10.0820 | 17.2402 |

It has been observed from the comparison results that the models provided by Steven and Unsworth [80] and Temps and Coulson [81] generally overestimate the data beside their better estimation performance for lower solar altitude angle values. The remaining 4 models have almost provided the same estimation performance while they have provided the best performance for high altitude angles. The model introduced by Reindl et. al. [72], which has also been chosen for irradiance conversion purposes in this thesis, has provided relatively low errors compared to the measured irradiance values. The obtained low error values verify conformity of the selected model for irradiance conversion and calculation purposes in this thesis.

## 3.6 Data

This part of the thesis includes brief explanations regarding different data used by the model during the process of generation of SDIPs. The mentioned data include measurements of solar irradiance values, irradiance data obtained from satellite observations, sky images, cloud coverage data, clearness index values and daily relative sunshine duration data for desired geographical locations. Each data source is described in the further parts together with its utilization purpose.

*i. Measured Solar Irradiance Data*

Irradiance measurements for Famagusta city, North Cyprus (Latitude: $35^{\circ}8'18''$, Longitude: $33^{\circ}55'45''$) are used throughout the modeling process. The mentioned measurements are conducted with 1 Min. time resolution using a $45^{\circ}$ inclined pyranometer. The mentioned measurements are utilized in order to validate the performance of the chosen clear-sky irradiance model and the method which is selected to convert horizontal irradiance values to irradiance values incident on inclined PV module surfaces, as previously described in details in Section 3.5.

Measured irradiance data for Lindenberg, Germany (Latitude: $52^{\circ}12'34''$, Longitude: $14^{\circ}07'13''$) form another source of the utilized measured irradiance data. The mentioned measurements are also conducted with 1 Min. time resolution and are retrieved from WRMC-BSRN (World Radiation Monitoring Center – Baseline Surface Radiation Network) website [82]. These data are also used for verification purposes as further described in details in section 3.8.9.

*ii. Solar Irradiance Retrieved from Satellite Observations*

Hourly mean global horizontal irradiance values for 5 neighboring points in Berlin, Germany (Latitude: $52^{\circ}33'56''$, Longitude: $13^{\circ}18'39''$) retrieved from METEOSAT observations are also used for verification purposes as described in details in section

3.8.9. These data are extracted from a data set that is provided by Satellite Application Facility on Climate Monitoring (CMSAF) [83]. The mentioned data have a spatial resolution of 0.03 × 0.03 degrees.

*iii. Sky Images*

Sky images are another source of data utilized during the modelling procedure. The mentioned sky images are taken in a per-minute basis in Lindenberg (Latitude: 52°12'34", Longitude: 14°07'13") and Berlin (Latitude: 52°33'56", Longitude: 13°18'39"), Germany. The mentioned sky images consist of 720 ×576 RGB images taken by a commercial camera. The mentioned sky images are utilized by the model in order to determine the cloud distribution in the sky and obtain cloud shadow patterns on the ground, as described in details in section 3.8.1.

*iv. Cloud Coverage Observations*

Cloud coverage data for Lindenberg, Germany (Latitude: 52°12'34", Longitude: 14°07'13") provided in [84] are also utilized for model verification purposes as explained in details in section 3.8.9.

*v. Clearness Index*

Clearness Index (CI) data from another source of data utilized during the modeling procedure. Observed clearness index data for Berlin, Germany (Latitude: 52°33'56", Longitude: 13°18'39") was obtained from the NASA Langley Research Center Atmospheric Science Data Center Surface meteorological and Solar Energy (SSE) web portal supported by the NASA LaRC POWER Project [65]. The mentioned clearness index values are utilized to verify the accuracy of the method which is selected for calculation of the Ångström-Prescott Regression coefficients as explained in Section 3.4.1.

*vi. Daily Relative Sunshine Duration*

A data pack provided by the European Climate Assessment & Dataset [66] is utilized to achieve the daily relative sunshine duration data for Berlin, Germany (Latitude: 52°33'56", Longitude: 13°18'39"). The data pack spans the time period from 1979 to 2014. These values are utilized to calculate the Ångström-Prescott Regression coefficients which form the basis for calculation of the clear-sky global, beam and diffuse irradiance values according to the model introduced in [85].

Different data and their utilization purpose during the modeling procedure are briefly explained in Table 3.6.

Table 3.6: Summary of the Utilized Data during Modelling Procedure

| Data | Location of Utilization | Utilization Purpose |
|---|---|---|
| Measured Global Irradiance | - Famagusta, North Cyprus<br><br>- Lindenberg, Germany | - Model Validation (Section 3.5)<br><br>- Model Validation (Section 3.8.9) |
| Hourly Mean Global Solar Irradiance Values Retrieved from Satellite Observations | - Berlin, Germany | - Model Validation (Section 3.8.9) |
| Sky Images | - Berlin, Germany<br>- Lindenberg, Germany | - Determination of Cloud Shadow Patterns (Section 3.8.3) |
| Cloud Coverage Observations | - Lindenberg, Germany | - Model Validation (Section 3.8.9) |
| Clearness Index | - Berlin, Germany | - Model Validation (Section 3.4.1) |
| Daily Relative Sunshine Duration | - Berlin, Germany | - Calculation of the Ångström-Prescott Regression Coefficients (Section 3.4.1) |

## 3.7 Modeling of Solar Irradiance Components on a Horizontal Surface

As mentioned previously, different components of the global solar irradiance incident on a horizontal surface at the desired geographical location are estimated using the model introduced in [85]. The mentioned model has firstly been introduced in [86] and then an improved version of the model has been provided in [69]. This model is utilized in this thesis due to its simplicity and conformity to the goals of the thesis. The mentioned irradiance components are then utilized as inputs to the model which is proposed to generate SDIPs on the extent of PV arrays. Therefore, estimation of different irradiance components under all-sky conditions is considered as the first step for determination of SDIPs. The utilized model is a stochastic model which is adjusted on the Ångström-Prescott regression coefficients and calculates time-series of global solar irradiance incident on a horizontal surface. It considers the global irradiance to be consists of three main parts as follows;

*i.* *Beam irradiance coming from the clear part of the sky.*

The value of the beam irradiance coming from the clear portion of the sky is determined according to a stochastic function, $SIF(t)$, which takes values of 0 and 1 corresponding to absence and presence of clouds in the sky at each time instant, respectively. The beam irradiance incident from the clear part of the sky is calculated as the result of multiplying the mentioned stochastic function by the clear-sky beam irradiance value that is calculated by the clear-sky model which was previously described in Section 3.4.2.

*ii.* *Diffuse irradiance coming from the clear part of the sky*

The diffuse irradiance is considered to be consist of two main parts; the diffuse irradiance coming from the clear and cloudy portions of the sky, respectively.

The diffuse irradiance incident from the clear part of the sky is calculated as the result of multiplication of the instantaneous value of the clear-sky diffuse irradiance, calculated by the clear-sky model as described in Section 3.4.2, by the complement of the existing cloud cover percentage.

*iii. Diffuse irradiance coming from the cloudy part of the sky*

The portion of the diffuse irradiance which is considered to be coming from the cloudy sky portion is calculated as the result of multiplication of the instantaneous value of the clear-sky global irradiance, calculated by the clear-sky model as described in Section 3.4.2, by the existing cloud coverage, in percentage, and the cloud transmission factor, $\bar{\tau}$, to account for the effect of the cloud coverage on the incoming solar irradiance value.

Considering the above mentioned explanations, the model calculates the global solar irradiance incident on a horizontal surface as a result of summation of the above mentioned components, as follows;

$$G(t) = SIF(t)G_b(t) + \big(1 - cc(t)\big)G_d(t) + cc(t)\bar{\tau}G_o(t) \tag{3.40}$$

$$G_o(t) = G_d(t) + G_b(t) \tag{3.41}$$

Where;

$G(t)$ : The instantaneous value of the global horizontal solar irradiance

$SIF(t)$ : The stochastic function

$cc(t)$ : The instantaneous value of the existing cloud coverage percentage

$\bar{\tau}$ : The cloud transmission factor

The original model which is introduced in [85] considers hourly mean values of the clear-sky beam, diffuse and global irradiance values due to very small variations of the

mentioned values during an hour. However, this thesis considers the calculated instantaneous values of the mentioned irradiance components for higher accuracy purposes.

## 3.8 Generation of Spatially Dispersed Irradiance Profiles (SDIPs)

This thesis proposes a novel global model, as also explained in our previous work which is also presented in "Appendix A" [87], to generate Spatially Dispersed Irradiance Profiles (SDIPs) or shadow patterns over the extent of a PV power plant which may be a large-scale centralized PV power plant or a distributed PV system within a large geographical area. In order to achieve this goal, primarily an irradiance model is utilized in order to estimate different all-sky irradiance components. The mentioned model utilizes parameters such as cloud coverage, sunshine duration and cloud transmittance for the mentioned estimation purposes. The outputs of this model are then utilized as inputs to the model which is proposed in the thesis for generation of SDIPs. Numerous models are introduced in the literature to generate all-sky irradiance components by utilizing the above mentioned parameters [69,86,88,89,85,90]. These models generate irradiance time-series on a horizontal surface as a result of process of the input parameters. The mentioned time-series then should be converted to irradiance time-series on inclined PV module surfaces to be utilized in desired solar energy related analysis and applications. The model introduced in [85], as described in Section 3.7 is chosen in this thesis for the mentioned calculation/estimation of different irradiance components due to its simplicity and conformity to the aims of this thesis.

Most of the current approaches introduced in the literature for solar radiation forecast purposes are based on two main methods, being Numerical Weather Prediction (NWP)

methods and methods that are based on process of real-time measured satellite or ground-based sensor data [91]. The biggest disadvantage of ground-based measurement equipment is that they are mostly consist of point sensors (e.g. pyranometers, etc.) that are not capable of providing data with spatial details [92]. An advantage of satellite-based measurements against NWP methods is that they provide data that is more reliable for determination of the exact position and distribution of clouds in the sky. In contrary to the mentioned point, the advantage of NWP methods over satellite measurements is that NWP methods are capable of providing data with longer forecast periods [93]. Also factors such as infrequent data acquisition periods, coarse spatial resolution and long times required to transfer and process the measured data (images, etc.) all cause satellite-based data to be not ideal for very short-term or high resolution forecast purposes. Another weak point of all of the above mentioned methods is that they are not capable of determination of the existing cloud distribution in the sky and considering the interactions of sunlight and clouds and hence taking into account the effects of the existing clouds on the incident solar irradiance on a specific geographical location. Taking all the above mentioned factors into consideration, design and development of a more accurate model which is capable of short-term forecasts with high spatial and temporal resolutions seems to be quite necessary for better and more precise analysis of PV power yield estimation and other solar energy related applications.

Sky cameras or, in other words, sky imagers are examples of devices that can be benefited for data acquisition in solar energy related applications. These kind of devices are relatively economic equipment and since they do not require periodical maintenance they can also be utilized in stand-alone applications. Owing to their fish-eye lenses, sky imagers are capable of providing whole sky images with high temporal

and spatial resolutions and therefore can be considered as appropriate devices to be utilized for cloud analysis [94]. Typical components of a sky imager can be considered as a charge coupled device (CCD) camera, fish-eye lens, a housing to protect the device against environmental effects and a CCD sensor. Also a solar occultor may be included within the device based on the application requirements [92]. Sky cameras have been utilized in various applications in the literature. The main utilization area of sky cameras can be considered as analysis of the atmospheric parameters such as analysis of aerosol properties and cloud analysis (cloud optical depth, cloud cover, cloud type and Cloud Base Height (CBH)) [95,96,97,98,99,100,101]. An example of utilization of sky imagers is provided in [102] where they are utilized for determination of CBH with an improved resolution and reduced cost compared to the current CBH determination technologies such as radiosonde, ceilometer, Dropler LIDAR and cloud radars. Sky imagers have also been utilized in [91] for irradiance forecasting purposes. They have also been benefited in [92] for intra-hour, sub-kilometer cloud forecast and solar irradiance nowcast purposes.

A very recent application of sky imagers is provided in [103] where they have been utilized in order to produce irradiance profiles over 5 different PV power generation stations distributed in different geographical locations in San Diego, CA, USA. Sky imagers are used in the mentioned study in order to obtain sky images with 30 sec. time resolution. These sky images are processed using cloud detection algorithms in order to identify cloudy and clear sky regions and hence determine the distribution of existing clouds in the sky. The ground coverage area of each sky image depends on the height of the clouds in the sky which is also calculated using a specific cloud base height detection algorithm. The mentioned sky images are transformed to 2D latitude-longitude images and the ray tracing method is used to reflect cloud shadow maps over

PV generation areas on the ground. In this way, PV generators (PV modules) on the ground which are affected by shadows caused by each sky image are determined on the ground. After determination of shadow patterns caused by clouds on the ground, the amount of solar irradiance incident on the surface of PV modules subject to the shadow patterns should be determined. For this purpose firstly clear-sky irradiance values are calculated using a clear-sky model. In parallel, a network of pyranometers are utilized to measure irradiance values within the extent of the desired geographical location. The irradiance values measured by pyranometers are classified under three main categories to represent the cloudiness condition of the sky. The mentioned cloudiness classes are defined as; a) no clouds (clear-sky), b) thin clouds (partly cloudy sky) and thick clouds (overcast sky). A histogram of the measured irradiance levels by pyranometers is prepared and the irradiance measurements are normalized by the modeled clear-sky irradiance values. Three values from the mentioned histogram are selected as representatives for the mentioned three cloudiness conditions. In this way the clear-sky indices that correspond to each cloudiness condition are formed. Clear-sky index values in the range of 0.9-1.1, 0.6-0.9 and 0.1-0.5 are chosen respectively for clear-sky, partly cloudy and overcast sky conditions. The global horizontal irradiance for each PV module is calculated by multiplying the clear-sky index by the calculated clear-sky global horizontal irradiance for the desired PV module. The mentioned global horizontal irradiance values are then converted to irradiance values incident on inclined PV module surfaces. A main weak point or limitation associated with this work is that cloudiness of the sky is classified under three categories as mentioned above, being clear-sky, partly cloudy or overcast sky conditions. This type of classification makes impossible a comprehensive consideration and analysis of the effects of the existing clouds on the incident solar irradiance on PV module surfaces.

Another limitation associated with the mentioned study is that the proposed model is dependent on irradiance measurements made by pyranometers, which makes the model a sensor dependent model. Such a sensor dependent model may not always be applicable to desired geographical locations and applications due to lack of measurement equipment (pyranometers) or irregular or infrequent measurements. The above mentioned limitations or weak points are overcome in the model which is proposed in this thesis for generation of SDIPs. Firstly, the proposed model considers various types of clouds (totally 9 different cloud classes) and their light interaction characteristics (cloud transmitivities) to account for a comprehensive and detailed analysis of effects of the existing clouds in the sky on the incident solar irradiance. Another advantage of the proposed model is that the model is not dependent on irradiance measurement by pyranometers and hence, it is designed as a global model which can be applied to any desired geographical location without any limitation.

Another recent study is introduced in [104] where a fractal cloud model is utilized and clear-sky index increment correlations are simulated under all-sky conditions. A pervasive set of sky images obtained from sky imagers and satellite observations along with irradiance measurements obtained from two different pyranometer networks is utilized in the mentioned study. Also Cloud Base Height (CBH) estimations are obtained using a ceilometer in the vicinity of the sky imagers. The proposed method firstly calculates clear-sky index time-series for each pyranometer using the measured irradiance values and clear-sky irradiance for the desired geographical location obtained from a clear-sky model. The clear-sky index values are obtained according to the following equation;

$$K_0 = \frac{G(t)}{G_o(t)} \tag{3.42}$$

The ratio of the scattered red light to the blue light, as discussed in further parts of this thesis, is utilized to identify and separate cloudy and clear parts of the sky in each sky image. CBH measurements obtained from a ceilometer are utilized to estimate the ground coverage area of each sky image. Satellite observed images with 15 Min. time intervals are utilized to produce cloud index maps and cloud motion vectors. Clouds are simulated as fractals under which cloud shadow maps are formed on the ground. Wind speed is derived from satellite observations and cloud shadows are moved in the direction of wind on a network of pyranometers which is virtually located on the ground. An experimentally obtained relationship is utilized at the last step to convert cloud indices to clear-sky index time series. By this way, the modeled and measured clear-sky index values are compared. The comparison results have shown both similarities and differences between the modeled and measured values. The observed similarities are associated with the modeled and measured field statistics. Also it has been observed that the mean values of the modeled and measured sensor data show very similar variabilities. On the other hand, it has been observed that the experimental relationship which is utilized to convert cloud indices to clear-sky index values is not fully compatible with the utilized satellite observations and the mentioned incompatibility has been the main reason behind the observed differences. The results obtained from the mentioned study approves the previously mentioned discussions of the thesis regarding inadequacy of satellite observations for very short-term irradiance forecasting purposes. Also as mentioned in the earlier discussions of this thesis, the authors of the study, once again, conclude that sky imager data outperform satellite observations during estimation of cloud edge dimensions. A main disadvantage of this study is that, similar to the previously discussed study, clouds are considered as a

whole and classified under only one category. As discussed previously, this kind of classification does not allow for consideration of different cloud types and their sunlight interaction characteristics. The mentioned disadvantage in the recent study has caused higher dispersion range of spatial autocorrelation structures of clear-sky index values obtained from observations compared to those obtained from measurements, around the median values. Another disadvantage of the mentioned study can be considered as its high dependency on measured/observed data such as irradiance measurements by pyranometers, cloud base height measurements by ceilometers, sky images obtained from satellite or sky imagers. The mentioned dependency makes application of the introduced model difficult to geographical locations where the required measurement data are not readily available due to lack of measurement equipment, irregular or infrequent measurements, etc.

The mentioned drawbacks regarding the above mentioned two recent research studies are overcome in the proposed model in this thesis. The proposed model takes into account site-specific sky images, different cloud types existing in the sky and light interaction characteristics associated with each cloud type along with the position of the Sun in the sky at each time instant in order to generate instantaneous site-specific realistic irradiance profiles for desired geographical locations. The SDIPs generated by the model can therefore be utilized as reliable sources of irradiance data to be utilized particularly for partial shading analysis and analysis of fluctuations in power generation by PV power plants. At the same time, since the model utilizes real-time sky images to generate instantaneous shadow patterns on the extent of PV power plants and therefore to estimate the instantaneous values of the incident irradiance on PV module surfaces, it also can be utilized to generate irradiance time-series using consecutive sky images taken at the desired geographical location.

The model which is chosen for estimation of different irradiance components under cloudy sky conditions, as discussed in Section 3.7, is a model that considers the effects of cloud coverage on the incident solar irradiance values. As also mentioned previously, cloud coverage has significant effects on the incident solar irradiance and power generation in a PV array and therefore should absolutely be considered by the solar irradiance model. Cloud properties can be considered under two main categories being namely; Dynamic and Radiometric cloud properties [105]. The significance of dynamic properties of clouds from PV applications point of view comes from the fact that movement of clouds in the sky is the main reason for partial shading of PV arrays and fluctuations in the generated power. On the other hand, radiometric properties of clouds account for interactions of sunlight with the existing clouds. A comprehensive overview of cloud radiometric properties is provided in [106]. As mentioned previously, ground based measurements and satellite observations are utilized for cloud detection and classification purposes. A general review on the cloud detection and classification methods introduced in the literature, along with the equipment used for the mentioned purposes is provided in [107].

According to the earlier discussions of the thesis, having detailed and precise knowledge of the instantaneous values of the incident solar irradiance on the surface of each individual PV module within a PV array is a necessity for power yield analysis and management purposes in a PV power plant. Such irradiance values can easily be calculated under clear-sky conditions using clear-sky irradiance models. However, the main problem shows up under cloudy sky conditions. Existing clouds, their shape and distribution in the sky and different light interaction characteristics associated with different cloud types are all factors that affect solar irradiance values incident on the surface of PV modules in a PV array and cause fluctuations in power generation by

the array. Therefore, analysis of partial shading effects in PV arrays requires a model that is capable of considering the effects of the existing clouds in the sky along with their light interaction characteristics on the incident solar irradiance values. The model which is proposed in this thesis integrates the existing cloud patterns in the sky and their sunlight interaction characteristics to the irradiance model introduced in Section 3.7 in order to generate site-specific SDIPs based on the existing clouds in the sky. These site-specific irradiance profiles can be considered as realistic sources of irradiance data to be utilized in power yield and partial shading analysis in PV power plants for desired geographical locations. The model utilizes a clear-sky irradiance model as introduced in Section 3.4.2, different data as introduced in Table 3.5 and the model introduced in [85] together with different cloud classifications and cloud transmittivity values to generate the proposed SDIPs based on instantaneous positions of the Sun in the sky.

Each individual observer, or PV module, on the Earth`s surface sees the Sun`s disk through the base of a cone with opening angle of $0.5^{\circ}$ [108]. Therefore it can be assumed that at solar noon ($\theta_Z = 0^{\circ}$) when the existing cloud layers in the sky cut the mentioned cones a circle is formed through which the Sun`s disk is viewed by each PV module. Each PV module receives the beam irradiance component through the mentioned circle. However, the Sun in not always standing exactly above PV modules. Variations of the position of the Sun in the sky during a day change the shape of the mentioned circles and they transform to ellipses together with the variations of the position of the Sun in sky. It is obvious that the mentioned ellipses get narrower towards sunset or sunrise due to high values of the solar zenith angle. Therefore, it can be assumed that thickness of the ellipses varies proportional to the variations of the

solar zenith angle values during a day. Also obviously it can be assumed that the beam irradiance component incident on the surface of each PV module is only affected by the portion of the existing clouds in the sky which falls within ellipses through which the module receives the beam irradiance, not by the total cloud coverage in the sky. The mentioned assumption is the factor that separates the proposed model in this thesis from the other models introduced in the literature for solar irradiance estimation purposes. According to the previous discussions of the thesis, the beam irradiance component is the most significant component from PV applications point of view. This thesis proposes a novel method for generation of SDIPs over the extent of PV arrays by only considering the attenuating effects of the cloud coverage enclosed within circles/ellipses through which each individual PV module receives the beam irradiance. The diffuse irradiance components coming from the cloudy and the clear parts of the sky are assumed to remain unchanged. The thickness of the ellipses/circles varies with respect to variations of the solar zenith angle as a result of movement of the Sun in the sky during a day. Hence, the first step towards generation of the SDIPs can be considered to be detection of the clear and cloudy parts of the sky included in the sky image. The next step then should be determination of circles/ellipses through which the beam irradiance is received by each individual PV module, based on the instantaneous positions of the Sun in the sky. Detection of the cloudy parts of the sky falling within each obtained circle/ellipse and calculation of the attenuating effects of the mentioned cloud coverage on the beam irradiance component received by each PV module can be considered as the next steps. The irradiance components calculated by the model then should be converted to irradiance values incident on inclined PV module surfaces.

Figure 3.25 shows a summary of different steps of the model developed for generation of SDIPs over the extent of PV arrays.

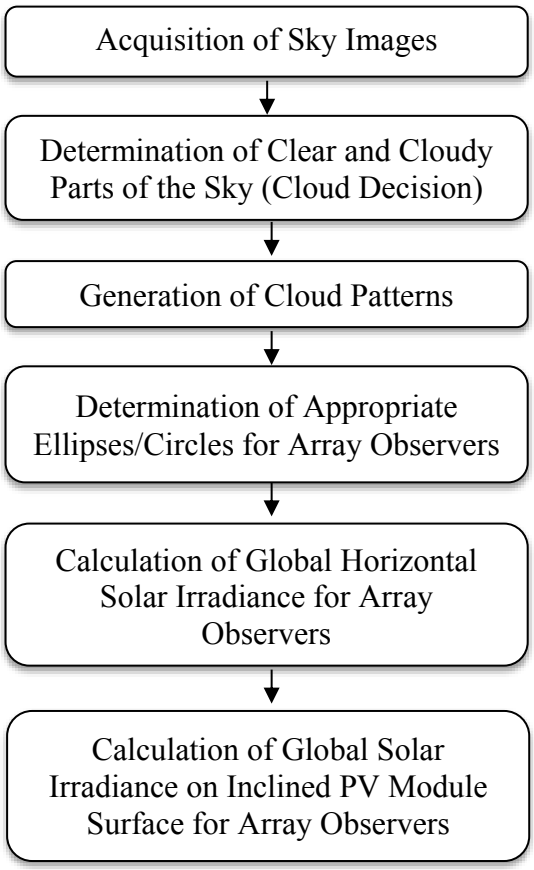


Figure 3.25: Flow Chart of Different Steps of the Modeling of SDIPs over PV Application Areas

### 3.8.1 Sky Images

As mentioned during the earlier discussions of the thesis, different models and methods have been introduced in the literature in order to estimate the cloud coverage and the resulting cloud shadow patterns. However, in this thesis, it is believed that the existing cloud coverage and its distribution in the sky at each time instant is the best driver for cloud shadow patterns over the desired application areas. Also it was mentioned previously that sky imagers or sky cameras outperform satellite observations or other methods utilized during analysis of cloud coverage. Hence, sky

images are utilized in this thesis in order to obtain cloud distributions and cloud shadow patterns on the extent of PV arrays.

The spatial resolution of different parts of cloud shadow maps depends on the distance of each pixel from the center of the sky image, due to the fish-eye nature of the sky images. A pseudo-Cartesian transformation method is introduced in [94] and further utilized in [91] to convert sky images to 2D latitude-longitude images, or "*cloud maps*", over the extent of geographical areas in which the image is taken. The mentioned cloud maps are centered at the position of the sky camera within the application areas. The proposed model in this thesis utilizes local 2D sky images in order to obtain cloud shadow maps over the desired application areas. The mentioned 2D sky images are assumed as the above mentioned latitude-longitude cloud maps derived from whole sky images. The instantaneous positions of the Sun in the sky are calculated for each desired instant of time and the Sun is located virtually on the sky image.

### 3.8.2 Determination of Cloudy and Clear Parts of the Sky

Once the sky image at each desired instant of time is obtained, the clear and cloudy pixels of the image should be classified in order to generate cloud patterns and the resulting cloud shadow maps. The mentioned task is conducted by utilization of an image processing method which is widely used in cloud cover estimation studies. The mentioned method is basically based on the ratio of the red light to the blue light scattered by the clouds. This method was firstly developed at the Scripps Institution of Oceanography [109,110,101]. In general, the amount of the scattered blue light is higher under clear-sky conditions whereas in contrast, more red light is scattered under cloud sky conditions. The utilized method obtains the amount of red and blue light and examines the Red/Blue Ratio (RBR) for each individual pixel of the sky image. The

cloud decision for each pixel is made considering a threshold value. If the RBR for any pixel exceeds the mentioned threshold value, which is determined according to the existing atmospheric conditions and the image capturing equipment, the pixel is considered as a “cloudy” pixel.

### 3.8.3 Determination of Cloud Pattern

Once the cloud decision is made according to the method introduced in Section 3.8.2, cloud patterns are obtained by assigning 1`s and 0`s to cloudy and clear pixels of sky images, respectively. The obtained cloud patterns in this way are also 2D latitude - longitude images. In order to ensure uniformity, facilitate the further calculations and create the opportunity of application of the model to sky images with different resolutions, the obtained cloud patterns are resized to $m \times m$ images in this thesis. The size of the image, $m$, can arbitrarily be chosen. Higher values result in higher precision which has high significance, particularly from cloud edges point of view, while in contrary increases the computational time and the required memory allocation.

### 3.8.4 Clouds and Sunlight Interactions

This thesis utilizes a comprehensive cloud classification and considers sunlight interaction characteristics of various cloud types in order to analyze the effect of the existing clouds in the sky on the incident solar irradiance. The utilized cloud classification is the same as the classification introduced in [111]. The attenuating effect of clouds on the incoming solar irradiance is taken into consideration based on cloud transmittance value, $\tau_c$. The magnitude of cloud transmittance value, $\tau_c$, is calculated based on cloud transmission coefficients, $x'$and $y'$, as provided in Table 3.6 for different cloud types using the following pair of equations [111];

$$\tau_c = (AM \times y') + x' \tag{3.43}$$

$$Airmass = AM = \frac{35}{(1224\cos^2\theta_Z + 1)^{1/2}} \quad (3.44)$$

Where;

$x'$, $y'$ : Cloud transmission coefficients

The decision regarding the cloud type to be utilized for calculation of the cloud transmittance value is manually made based on visual observations according to cloud classification provided in [112], where the shapes of different cloud types are provided together with their approximate heights in the sky.

Table 3.6: Cloud Transmission Coefficients for Different Cloud Classes

| **Cloud Type** | $x'$ | $y'$ |
|---|---|---|
| Fog | 0.163 | 0.005 |
| Stratus Nimbostratus | 0.268 | 0.101 |
| Stratocumulus | 0.366 | 0.015 |
| Cumulus | 0.366 | 0.015 |
| Cumulonimbus | 0.236 | 0.015 |
| Altostratus | 0.413 | 0.001 |
| Altocumulus | 0.546 | 0.024 |
| Cirrostratus | 0.905 | 0.064 |
| Cirrus | 0.872 | 0.018 |

### 3.8.5 Cloud Heights in the Sky

Cloud height in the sky or in other words, Cloud Base Height (CBH), is utilized in the thesis for calculation of the area on the ground which is covered by each sky image. The ground coverage area of sky images is determined based on cloud types included

within each sky image. As mentioned in the previous section, the mentioned cloud types are manually evaluated based on visual observations of cloud shapes and distributions according to the classification provided in [112]. Each cloud type belongs to a cloud class considered under three main categories being namely; high clouds, middle clouds and low clouds according to the mentioned cloud classification. The minimum and maximum cloud heights in the sky are provided for each cloud class. The mentioned minimum and maximum cloud base height values are utilized in this thesis to approximately calculate the minimum and maximum areas on the ground that can be covered by each sky image according to the existing cloud type. As an example, four different cloud types, representing three different cloud classes are chosen and provided together with their base height values in Table 3.7.

Table 3.7: Examples of Cloud Types, Corresponding Cloud Classes and Cloud Base Heights Analyzed in the Thesis

| **Cloud Type** | **Cloud Class** | **Cloud Height (ft)** |
|---|---|---|
| Cumulus | Low Clouds | 2000-3000 |
| Stratocumulus | Low Clouds | 2000-6500 |
| Altocumulus | Middle Clouds | 6500-18000 |
| Cirrus | High Clouds | 16500-45000 |

As an example, the cloud types, their corresponding cloud classes and their base height values are utilized in order to calculate the lower and upper limits of areas on the ground covered by sky images provided in Figure 3.33. It should also be noticed that the cloud types provided in Table 3.7 are only some representatives of different cloud classes which are utilized for calculation purposes in this thesis. Each cloud class may

also include some other cloud types. A comprehensive list of different cloud types was previously provided in Table 3.6.

### 3.8.6 Determination of Ellipses/Circles

Once the sky images are obtained, cloud maps and cloud patterns are derived and cloud classes and their corresponding cloud transmittance values are determined, the ellipses/circles through which each individual array observer, or in other words each PV module, receives the beam irradiance should be determined in order to proceed to generation of SDIPs. As it was discussed previously, the size of ellipses/circles depends on the instantaneous positions of the Sun in the sky during a day and varies proportional to the values of the solar zenith angle. Thus, in order to determine the appropriate circle/ellipse at each desired time instant, the instantaneous position of the Sun in the Sky should be determined in the utilized sky images. For this purpose, the instantaneous position of the Sun in the sky is calculated at each desired time instant based on the method provided in Section 3.2 and the Sun is virtually located on each sky image which is assumed to cover the whole sky dome and cover a full cycle of the movement of the Sun in the sky during a day from sunrise to sunset. PV arrays which are considered as the application areas of the model for generation of SDIPs are considered to be located in the northern hemisphere and include PV modules that are south oriented. The area covered by each PV array on the ground is considered to be limited by the size of the ground coverage area of the utilized sky images. In order to maintain simplicity and facilitate further calculations, the mentioned size of ground coverage area of PV arrays is assumed to be limited by the size of cloud maps that was previously defined as an $m \times m$ area. Hence, the size of PV arrays is determined as a $k \times l$ area on the ground, where $0 < k \leq m,\ 0 < l \leq m$. Again, for the sake of simplicity and in order to express the clear and cloudy sky portions as well as the

position of PV modules within PV arrays by percentage values, a size of 100 is considered for the mentioned sizes of cloud maps and ground coverage areas ($m = k = l = 100$). In this way, all utilized sky images, regardless of their resolutions, are resized to fixed-size cloud maps and the cloudy and clear sky portions are expressed by their corresponding percentage values within the whole cloud map. On the other hand, geographical sizes of PV arrays or ground coverage areas corresponding to each cloud map are also expressed by percentage amounts, instead of their actual sizes in meters, kilometers, etc., since the exact value of the ground coverage area of each sky image or cloud map may not be precisely calculated due to unavailable or insufficient information regarding cloud base height values. In this way, the area on the ground which is subject to different and non-identical irradiance levels caused by the existing cloud coverage in the sky can also be expressed as certain percentage values within the ground coverage area of each sky image.

As it was mentioned previously, each PV module within a PV array on the Earth`s surface sees the Sun`s disk through the base of a cone with opening angle of $0.5^{\circ}$. Ellipses/circles are formed when the mentioned cones are cut by the cloud layer in the sky and the thickness of the mentioned ellipses vary together with the variations of the solar zenith angle as a result of the Sun`s movement in the sky during a day from sunrise to sunset. Figure 3.26 shows the position of the Sun in the sky, PV module on the ground, the existing cloud coverage and the size of ellipse/circle for different time instants during a day.

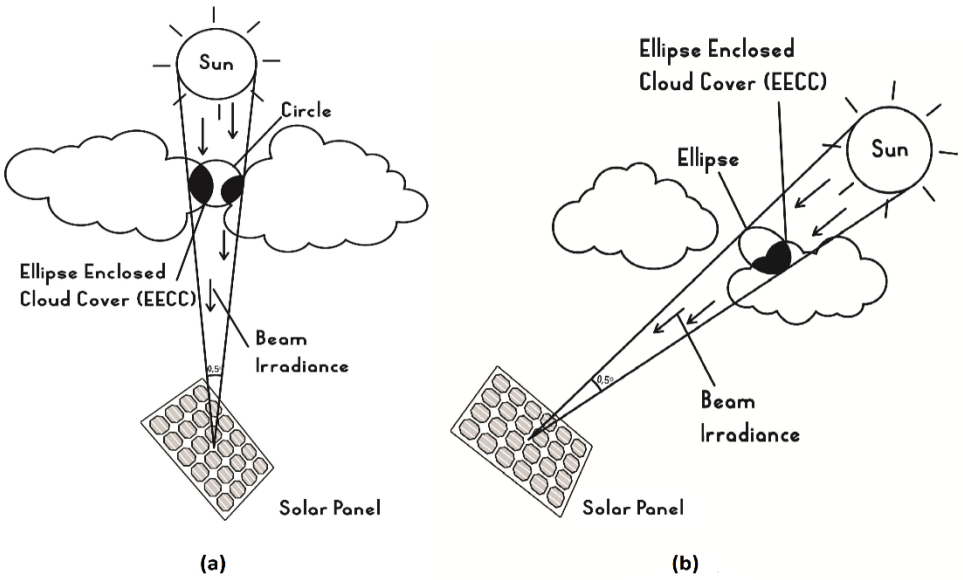


Figure 3.26: Position of the Sun in the Sky, PV module on the Ground and the Resulting (a) Circle at Solar Noon, (b) Ellipse at a Time Instant towards Sunrise/Sunset

As it is also obviously shown in the figure, the attenuating effect of the cloud coverage on the incident solar irradiance only corresponds to the amount of cloud coverage which is enclosed within the ellipse/circle through which the PV module receives the beam irradiance, not the whole cloud coverage existing in the sky. This fact has been the motivation to develop the proposed model in this thesis for generation of SDIPs over the extent of the geographical area of PV arrays on the ground. The proposed model determines the most appropriate circle/ellipse at each instant of time according to the position of the Sun in the sky with respect to each individual PV module on the ground and accounts for the attenuating effect of the cloud coverage enclosed within each ellipse/circle on the beam irradiance incident on the surface of each PV module.

According to the discussions of Section 3.2 the Sun`s position in the Sky is defined based on two main factors; the solar zenith angle and the solar azimuth angle. On the other hand, the thickness of the above mentioned ellipses/circles is assumed to vary

together with the variations of the Sun`s position in the sky. Determination of appropriate ellipses can be considered from two different perspectives; calculation of thickness of the ellipse/circle and determination of the position of the center of the ellipse/circle at each time instant. Therefore, it can be assumed that the thickness and position of the appropriate ellipses/circles at each time instant should also be determined based on variations of the values of solar zenith and solar azimuth angles. The method which is proposed in the thesis for determination of the most appropriate ellipse/circle at each time instant adjusts the thickness of the ellipse/circle and the position of its center point based on the mentioned two angle values. As mentioned previously, the thickness of ellipse/circle varies together with variations of the solar zenith angle. Therefore, Eq.3.45 is developed for calculation of the thickness of the ellipse/circle. The mentioned equation calculates the major axis of the ellipse and takes into account also the opening angle of the cone through which the Sun`s disk is viewed by the observers. The equation calculates the major axis of the ellipse as the ratio of the instantaneous value of the solar zenith angle to its maximum possible value and scales it according to the size of the cloud map, $m$, on which the ellipse will be located. In this way the major axis of the ellipse takes its minimum value and the thus, the thickness of the ellipse reaches its maximum value at solar noon, ($\theta_z = 0^{\circ}$). This is the most similar form of the ellipse to a circle. In contrast, the ellipse takes its thinnest shape when the solar zenith angle reaches the maximum value towards sunrise or sunset. The minor axis of an ellipse is geometrically determined based on the major axis. The minor axis of the ellipse is defined by Eq.3.46 with respect to the major axis. Once the thickness of the ellipse/circle at each time instant is determined, the location of the ellipse/circle center on the utilized sky image or cloud map should also be determined. For this purpose, the location of the ellipse/circle center on the x-axis is

assumed to be proportional to the Sun`s movement in the sky during a day from sunrise to sunset (east to west). The mentioned movement of the Sun in the sky is defined by solar azimuth angle. Hence, the variations of the position of the ellipse/circle center on the x-axis at each time instant is adjusted based on and calculated according to the variations of solar azimuth angle during a day. Eq.3.47 is developed for the mentioned purpose. The mentioned equation calculates the location of the ellipse/circle center as the ratio of the instantaneous values of the solar azimuth angle to values of the mentioned angle at sunrise/sunset and scales it according to the size of the sky image or cloud map, *m*, on which the ellipse/circle center will be located. Hence, at solar noon, ($\alpha_S = 180^{\circ}$), the ellipse/circle center is located exactly above each PV module within the PV array. Also position of the ellipse/circle center on the y-axis is considered proportional and adjusted based on the values of the solar zenith angle. The instantaneous position of the ellipse/circle center on the y-axis is determined using Eq.3.48 as the ratio of the instantaneous value of the solar zenith angle to its maximum value scaled according to the size of the sky image or cloud map, *m*, on which it will be located. The most appropriate ellipse/circle corresponding to each array observer or PV module is thus determined based on Eq.3.45 – Eq.3.48 and located virtually on the utilized sky image or cloud map at each time instant.

$$D_x(t) = 2\left[\left((\theta_z(t) + 0.25)/(90^{\circ})\right) \times m\right] \tag{3.45}$$

$$D_y(t) = D_x(t)\sqrt{(1 - e^2)} \tag{3.46}$$

$$C_x(t) = \begin{cases} [(180 - \alpha(t))/\alpha(t_{sunrise})] \times m, & t < 12\ LST \\ [(180 - \alpha(t))/\alpha(t_{sunset})] \times m, & t \geq 12 LST \end{cases} \tag{3.47}$$

$$C_y(t) = [\theta_z(t)/90^{\circ}] \times m \tag{3.48}$$

Where;

$D_x(t)$ : Instantaneous value of the major axis of the ellipse

$D_y(t)$ : Instantaneous value of the minor axis of the ellipse

$C_x(t)$ : Instantaneous position of the ellipse/circle center on the x-axis

$C_y(t)$ : Instantaneous position of the ellipse/circle center on the y-axis

### 3.8.7 Modeling of Solar Irradiance Values

Once the most appropriate ellipse/circle for each array observer at each time instant is obtained based on the above mentioned approach, the irradiance values incident on the surface of each PV module within the array should be determined in order to form the SDIPs for the desired application area. For this purpose, firstly the horizontal global irradiance value incident on each PV module is obtained using Eq.3.49 which is developed as a modified version of the model introduced in [85]. The model considers the beam irradiance component received on the surface of each PV module through the previously mentioned ellipses/circles to be consist of two main components; the beam irradiance coming from the clear part of the sky and the beam irradiance from the cloudy sky part. The beam irradiance incoming from the cloudy sky portion is affected by the existing clouds enclosed within the ellipses/circles. The attenuating effect of clouds is considered by cloud transmittance, $\tau_c$, as defined in Section 3.8.4. Finally the global horizontal irradiance incident on each individual PV module is obtained as;

$$G_g(t) = \left[\left(\left(1 - cc_e(t)\right).G_b(t)\right) + cc_e(t).\tau_c.G_b(t)\right] + \left(1 - cc(t)\right).G_d(t) + cc(t).\bar{\tau}.G_o(t) \quad (3.49)$$

Where;

$G_g(t)$ : Instantaneous value of the all-sky global horizontal irradiance received by each PV module [W/m$^2$]

$cc_e(t)$ : Ellipse Enclosed Cloud Coverage (EECC) [percentage]

The ellipse enclosed cloud coverage, $cc_e(t)$, is obtained as the ratio of the cloudy pixel numbers to the total pixel numbers enclosed within each ellipse. Cloud transmittance values are calculated based on Eq.3.43 – Eq.3.44 and Table 3.6.

Once the global horizontal irradiance received by each PV module is determined with the aid of Eq.3.49, it should be converted to irradiance value on inclined PV module surface. This task is held using the method described in Section 3.5. Finally, the global irradiance value incident on the surface of each inclined PV module within the PV array is obtained as;

$$G_{g\beta}(t) = \left[\left(1 - cc_e(t)\right)G_{b\beta}(t) + cc_e(t)\tau_c G_{b\beta}(t)\right] + \left(1 - cc(t)\right)G_{d\beta}(t) + cc(t)\bar{\tau}R_d G_o(t) + \rho R_r G_g(t) \quad (3.50)$$

Where;

$G_{g\beta}(t)$ : Instantaneous value of the global solar irradiance incident on the surface of each inclined PV module [W/m$^2$]

It is obvious that using the above mentioned approach, non-identical values of solar irradiance can be obtained for different PV modules within a PV array at each time instant. Thus, the resulting irradiance profile can be expected to include different values of solar irradiance at each time instant which cause it be a reliable source of data to be utilized in partial shading and power yield analysis purposes in PV power plants.

### 3.8.8 Ground Coverage Area of Sky Images

According to the previous discussions of Section 3.8.5, the Cloud Base Height (CBH) is the main factor for determination of the area on the ground which is covered by each sky image. Unfortunately, limitations such as unavailability of appropriate measurement equipment, insufficient data regarding cloud types, etc. may create obstacles against accurate and precise determination of the exact coordinates of area

on the ground, e.g. in meters, etc., which is covered by each sky image. This fact is the main reason for which the area covered by PV arrays on the ground that is considered to be the ground coverage area of each utilized sky image is expressed in this thesis using percentage values instead of the exact coordinates in meters, etc. Also the cloud maps derived from the utilized sky images are resized and expressed by percentage values. Thus, the proposed model for generation of SDIPs over the extent of PV arrays is provided as a global model which can be applied to any sky image, regardless of its resolution, and generates irradiance profiles on 100% area on the ground which is covered by the utilized sky image. On the other hand, the ground area covered by each sky image can be calculated based on the cloud base height, zenith and azimuth angle values of pixels of the utilized sky image, using a method introduced in [92] as;

$$\begin{Bmatrix} x \\ y \end{Bmatrix} = \Delta H tan\theta_p \begin{Bmatrix} sin\alpha_p \\ cos\alpha_p \end{Bmatrix} \tag{3.51}$$

Where;

$x$ , $y$ : Coordinates of the coverage area of each sky image on the ground

$\Delta H$ : Cloud base height [meters]

$\theta_p$ : Pixel zenith angle [degree]

$\alpha_p$ : Pixel azimuth angle [degree]

Obviously higher clouds in the sky cover a wider area on the ground. However, as mentioned before, precise calculation of the coordinates of the ground coverage area of each sky image may not always be possible due to unavailable or insufficient information regarding cloud types and their base height values. Approximate base height values for different cloud types and classes as provided in [112] are utilized in this thesis in order to obtain the maximum and minimum areas on the ground which may be covered by each utilized sky image.

### 3.8.9 Verification of the Model

This part of the thesis is allocated to validation of the proposed model for generation of SDIPs. The mentioned model is developed as a novel model which can be utilized in order to generate site-specific irradiance profiles based on real cloud patterns obtained from sky images for desired geographical locations. Performance of the model has been verified using different measures such as the Variability Index (VI), Autocorrelation Function and Irradiance Increments. The model has provided successful results in terms of the above mentioned performance metrics. A summary of the results of verification of the proposed model is provided in this section of the thesis.

The Variability Index (VI) is a performance metric which has been utilized to verify the performance of the model. The VI metric has firstly been introduced in [113] and can be considered as a measure for variability of the irradiance values during a specific period of time. The VI index is defined as;

$$VI = \frac{\sum_{t=2}^{n} \sqrt{(G(t) - G(t-1))^2 + \Delta t^2}}{\sum_{t=2}^{n} \sqrt{(G_o(t) - G_o(t-1))^2 + \Delta t^2}} \tag{3.52}$$

Where;

$G(t)$ : The instantaneous value of the all-sky global horizontal solar irradiance

$G_o(t)$ : The instantaneous value of the clear-sky global horizontal solar irradiance

$\Delta t$ : Time interval between two consecutive irradiance measurements

According to Eq.3.52 high VI values are expected for cloudy days while clear days are expected to result in lower VI values since clouds do not have significant impacts on the incident irradiance values during clear days.

Berlin, Germany has been considered as the target application area of model proposed for generation of SDIPs. The model has been applied to and samples of irradiance profiles have also been generated for the mentioned geographical location. However, since the measured irradiance time-series required during model verification process have not been available for the above mentioned location, measurements of irradiance time-series for Lindenberg Station (Latitude: 52°12'34", Longitude: 14°07'13") [82], as described in Table 3.5, have been utilized during verification phase of the model. Lindenberg meteorological station has been chosen since it is the closest station to Berlin, Germany which is the main application area of the model. The mentioned irradiance measurements are conducted in per-minute basis. The main assumption here is that once the performance of the model is validated for a specific geographical location, it can be considered as a model which is capable of generation of reliable irradiance profiles for any desired geographical location supported by appropriate and sufficient data. VI values calculated using both per-minute measured and modeled irradiance time-series for Lindenberg, Germany are compared to each other during a time period including totally 117 days from April to August. The days for which irradiance time-series have not been provided by the meteorological station are not taken into consideration during calculations of VI values. The reason for using the above mentioned time period is that highly variable cloud coverage amounts have been reported by the meteorological station during this time-period. The mentioned variable cloudiness amounts during model validation time period would result also in highly variable values of VI. The cloud coverage amounts during the model validation time period have been reported in [84]. Figure 3.27 shows a histogram of the utilized cloud coverage amounts during model validation time period.

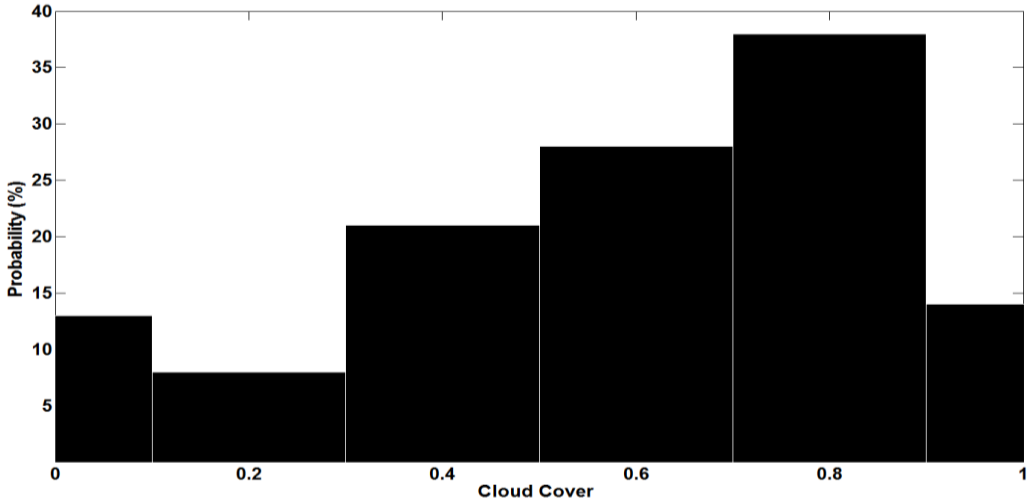


Figure 3.27: Cloud Coverage during Model Validation Time Period

The daily VI values calculated using both measured and modeled per minute irradiance time-series for the mentioned geographical location between 07:00-19:00 are compared to each other during the validation time period. For this purpose, clear-sky irradiance time-series are calculated based on the method discussed in Section 3.4. Modeled daily irradiance time-series are obtained according to Eq.3.49 during the validation time period. For this purpose, a set of sky images, as discussed in Table 3.5, are utilized as representatives of the existing cloud coverage during each day. The mentioned set of sky images are arranged in a manner that they present the same cloud coverage as the observed hourly values for each day during the validation time period. The modeled irradiance time-series are obtained for the observation point located at the center of the ground coverage area of sky images because the pyranometer which measures the irradiance values at the meteorological station is also located at the center point of the ground area covered by local sky images. The cloud coverage during the validation time period is considered to be of Cumulus cloud type since it is a common cloud type at the desired geographical location and the validation period. The comparison between the VI values calculated using both the modeled and observed

irradiance time-series results in Mean Bias Error (MBE) of 0.16, Root Mean Square Error (RMSE) of 2.39, Correlation Coefficient of 0.94 and Mean Absolute Error (MAE) of 1.91. The above mentioned obtained values for different performance metrics are quite satisfactory and considered as indicators of adequacy of the proposed method for estimation of irradiance values under all-sky conditions.

Comparison between probability distribution of both measured and modeled irradiance increments during the validation time period is another means of model validation utilized in this thesis. For this purpose, the same measured and modeled irradiance time-series as above mentioned ones utilized for VI calculations are taken into consideration. An irradiance increment is considered as the difference between two consecutive instantaneous measured or modeled irradiance values. An irradiance increment can be expressed as [104];

$$\Delta G_{\tau} = G(t+\tau) - G(t) \tag{3.53}$$

Where;

$\Delta G_{\tau}$ : Irradiance increment

$\tau$ : Time difference between two irradiance values

Figure 3.28 shows the results of comparison between probability distributions of both measured and modeled irradiance increments during the validation time period.

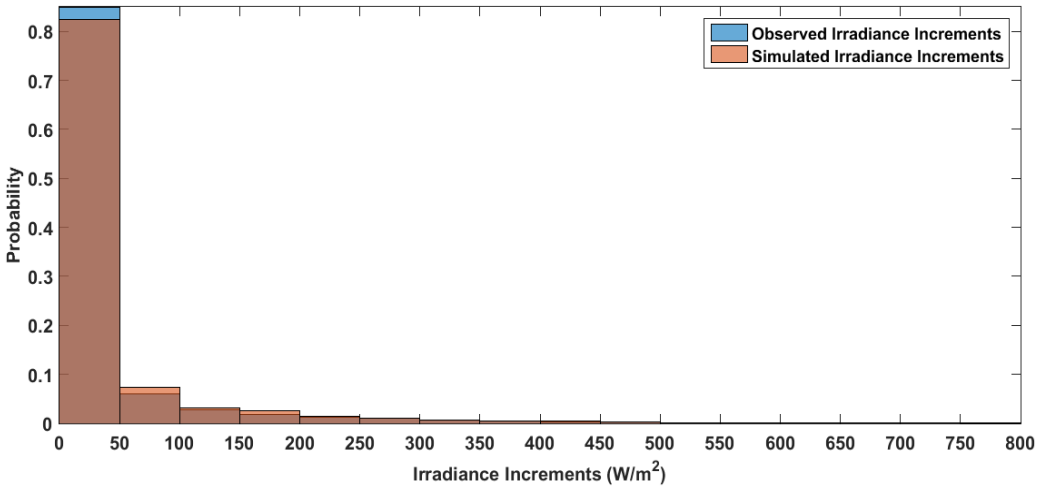


Figure 3.28: Comparison between Probability Distribution of Irradiance Increments, $(\tau = 1\ min.)$ for Measured and Modeled Irradiance Time-Series during Validation Time Period for Lindenberg, Germany

The lag-1 autocorrelation function is another factor that is taken into consideration for model validation purpose. The autocorrelation describes the correlation between values of the irradiance time-series at different time instants as a function of the time difference. The same measured and modeled irradiance time-series as those utilized for calculation of VI values as well as magnitude of irradiance increments are utilized and the results of comparison of autocorrelation coefficients during the validation time-period are provided in Figure 3.29.

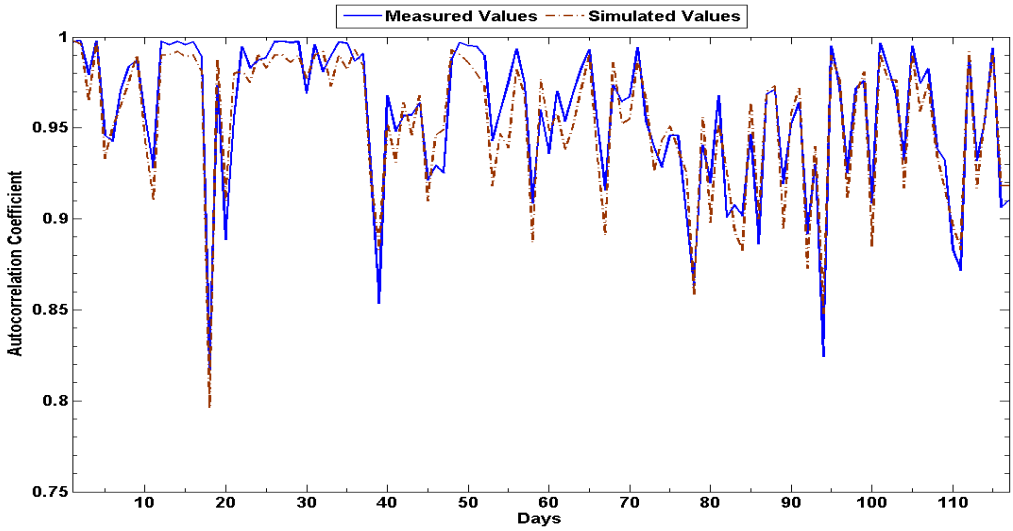


Figure 3.29: Comparison between Lag-1 Autocorrelation Coefficient of Measured and Modeled Irradiance Time-Series during Validation Period for Lindenberg, Germany

As it can obviously be observed from the figure, the lag-1 autocorrelation coefficients of both simulated and measured irradiance time-series are in a good match similar to the case of VI and irradiance increment values. All the obtained results provide a good conformity between the modeled and measured irradiance values and are considered as indicators of statistical closeness of the mentioned data. The mentioned conformity proves the adequacy of the developed model for generation of SDIPs which can be considered as a reliable source of data during analysis of partial shading effects and power yield estimations in PV arrays.

### 3.8.10 Sample Results of the Model

The results of application of the model are provided in this section of the thesis. The developed model is utilized and applied for different irradiance modeling purposes. Different samples of application of the model are particularly selected in a manner that each sample application examines and presents a different capability of the proposed model. The model has firstly been utilized together with an unchanged identical cloud pattern during a day in order to simulate irradiance time-series at different observations points on the ground. The purpose of this application is to examine the capability of the model to reflect the effects of movement of the Sun in the sky during a day on irradiance time-series at different observation points. The model has also been utilized together with different cloud patterns and distributions in the sky in order to examine its capability for generation of instantaneous SDIPs based on the existing cloud patterns and reflect the attenuating effect of different cloud types on the incident irradiance values. Finally the model has been utilized together with a set of sky images in order to simulate irradiance time-series incident on different observation points within the application area and to show its capability to reflect the variable and dispersed characteristics of the irradiance time-series received at different points as a

result of the existing cloud distribution in the sky. The mentioned applications of the model are provided together with their sample results as follows;

a) *Simulation of Daily Irradiance Time-Series Incident on Different Observation Points under Identical Cloud Coverage*

The model has been utilized together with an identical unchanged cloud pattern during a day and irradiance time-series are obtained for different observation points on the ground. The goal here is to examine the model`s capability to reflect the effects of variations of the Sun`s position in the sky during a day on irradiance values incident on different observation points on the ground. Figure 3.30 shows an example of the utilized 2D latitude-longitude sky image, or the cloud map, the all-sky image which is reconstructed from the 2D sky image according to the previously mentioned pseudo-Cartesian transformation and the resulting cloud pattern.


(a) (b) (c)

Figure 3.30: (a) All-Sky Image, (b) Utilized 2D Sky Image (Cloud Map), (c) Obtained Cloud Pattern (Cloud Cover (*cc*) = 45%, m = 100)

As mentioned above, the cloud pattern is kept identical during the day and daily irradiance time-series are obtained for different array observation points during a typical day in July for Berlin, Germany (Latitude: 52°33'56", Longitude: 13°18'39"). Cumulus cloud type is considered as the cloud type during simulations. Figure 3.31 shows the Ellipse Enclosed Cloud Cover (EECC) observed by different array observers at different time instants during the day under identical, unchanged cloud

pattern. Also the resulting SDIPs generated by the model at the same time instants on the extent of the PV array are demonstrated. The utilized time instants are particularly selected to represent instants of time before, close to and after solar noon, respectively.

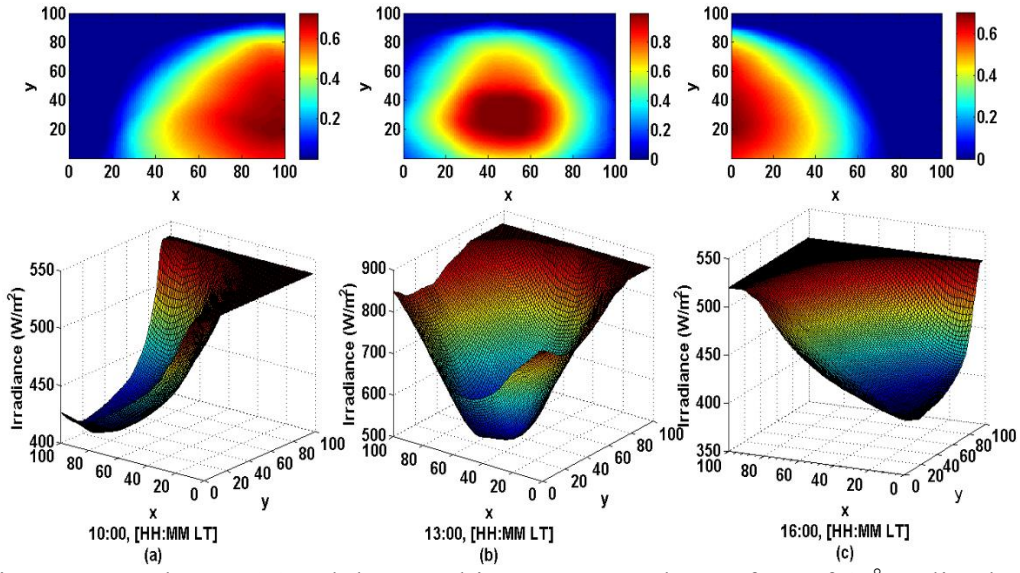


Figure 3.31: The EECC and the Resulting SDIPs on the Surface of 45° Inclined PV Modules within a PV Array at (a) 10:00, (b) 13:00, (c) 16:00 for Berlin, Germany (Latitude: 52°33'56", Longitude: 13°18'39") in July. ($k = l = m = 100$)

The figure clearly shows the effects of variations of the Sun`s position in the sky during a day on the resulting EECCs and the generated SDIPs at different instants of time. It is demonstrated that observers located on the east side of the PV array are almost not affected by the cloud cover existing in the sky at 10:00 AM (before solar noon) when the sunlight coms from the same direction. The array observers located at the middle of the array are mostly affected by the cloud cover around solar noon (13:00 PM) when the Sun is almost above the panels. It is shown that array observers located on the west side of the array are not affected by the existing cloud coverage at 16:00 PM (after solar noon) when the sunlight comes from the same direction.

The model`s capability to reflect the effects of movement of the Sun in the sky on solar irradiance time-series is examined by determination of the incident irradiance sequences on the surface of array observers with different locations within the array.

Figure 3.32 shows irradiance sequences incident on the surface of three PV modules having different locations within the array, under identical cloud coverage during a day.

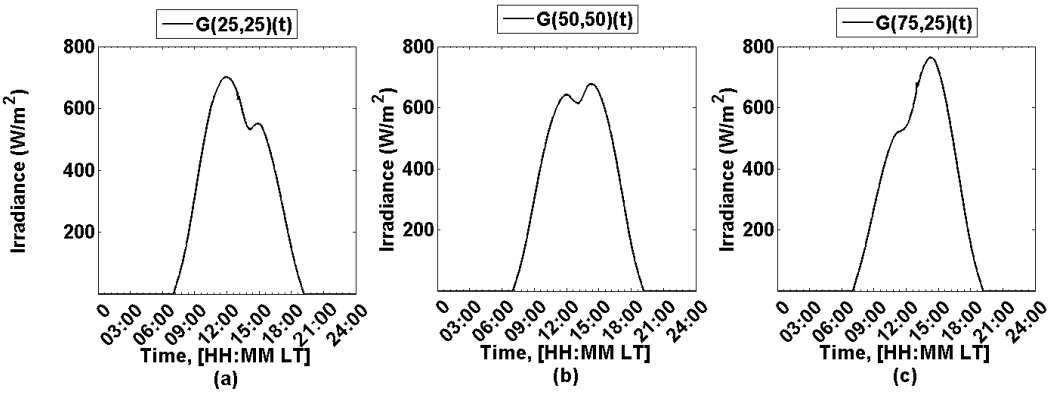


Figure 3.32: Daily Global Irradiance Sequences on the Surface of 45° Inclined Three PV Modules with Different Location within the PV Array in July, for Berlin, Germany (Latitude: 52°33'56", Longitude: 13°18'39"), *cc* = 45%

As mentioned previously, the observer locations are expressed as percentage values. The observation points are particularly selected to represent different locations on the east, center and west sides of the PV application area. The figure clearly shows the effects of variations of the Sun`s position in the sky on different locations within the application area. The cloud coverage is kept unchanged and it is observed that the observation point located on the east side is affected by the existing unchanged cloud coverage after solar noon, while the observation point at the center experiences the effect of partial shading earlier, during noon and the PV module located on west side is affected by the existing cloud coverage before solar noon.

According to the previous discussions of Section 3.8.8, the ground coverage area of each sky image is determined by the cloud heights in the sky. Also it should be taken into consideration that determination of ground coordinates for solar zenith angles near the horizon (high values of solar zenith angle) is not valid. Cumulus clouds are classified as low level clouds with maximum height of approximately 1000 meters [112]. Thus, considering maximum height of 1000 meters and $\theta_P < 65°$, the ground coverage area of the sky image utilized in Figure 3.30 will approximately be 4 km$^2$. Hence, the location of the considered observation points on the ground will also be as follows; $a = (500m, 500m)$, $b = (1000m, 1000m)$ and $c = (1500m, 500m)$.

*b) Simulation of Instantaneous SDIPs based on Different Cloud Types and Characteristics*

Capability of the model for generation of SDIPs based on different cloud types and their light interaction characteristics is examined in this part of the thesis. The model is utilized together with different sky images each including a different cloud type and the resulting SDIPs are compared at the same time instant. Figure 3.33 shows the results of application of the model to different cloud types and distributions at the same time instant.

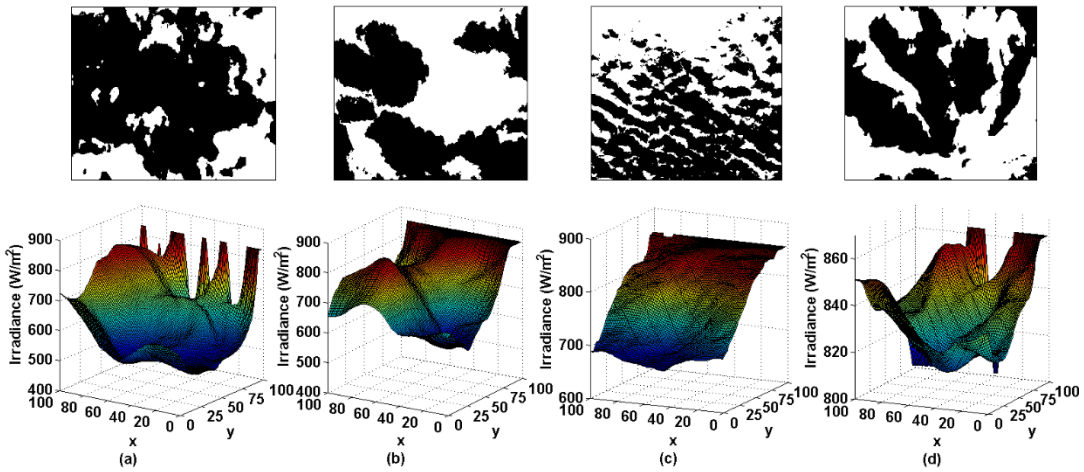


Figure 3.33: Samples of Different Sky Images and the Resulting SDIPs at 13:00 for (a) Stratocumulus Cloud ($\mu_G = 608.6\ W/m^2, R_G = 347.6\ W/m^2$), (b) Cumulus Cloud ($\mu_G = 730.8\ W/m^2, R_G = 293\ W/m^2$), (c) Altocumulus Cloud ($\mu_G = 787.4\ W/m^2, R_G = 189.5\ W/m^2$) and (d) Cirrus Cloud ($\mu_G = 832.6\ W/m^2, R_G = 61\ W/m^2$) on 45° Inclined PV Module Surface for Berlin, Germany in July. ($k = l = m = 100$)

According to the previous discussions regarding the ground coverage area of each sky image, the range of ground coverage areas for the utilized sky images in Figure 3.33 obtained based on the minimum and maximum cloud heights specified in [112] are approximately 1.5-18.5 km$^2$, 1.5-4 km$^2$, 18.5-140 km$^2$ and 115-860 km$^2$, respectively, for Stratocumulus, Cumulus, Altocumulus and Cirrus clouds. Also it was previously discussed that the magnitude of attenuation of the beam irradiance component depends on the cloud type and its corresponding light interaction characteristics. The mentioned attenuating effect is the main factor that cause differences in the range of irradiance levels included within each SDIP. It is observed that Cirrus clouds have the least attenuating effect on the magnitude of the incident solar irradiance while Stratocumulus and Cumulus clouds have presented almost the same effects on the range of the incident irradiance values.

*c) Daily Irradiance Time-Series on Different Observation Points*

This part of the thesis is allocated to a comparison of daily irradiance time-series incident on the surface of five different PV modules having different locations within the PV array. The goal here is to examine and present the model`s capability to generate irradiance sequences for different geographical locations and reflect their differences and variable characteristics caused by the existing cloud distribution in the sky during a day. For this purpose, a set of sky images, as discussed earlier in Table 3.5, is utilized which includes totally 720 images. The cloud type is considered to be Cumulus due to is conformity to the utilized sky images and irradiance sequences are simulated from 07:00 to 19:00 in per-minute basis. Figure 3.34 shows the distribution of cloud coverage presented by the set of sky images during the day together with the EECC for an observation point located at the center of the application area.

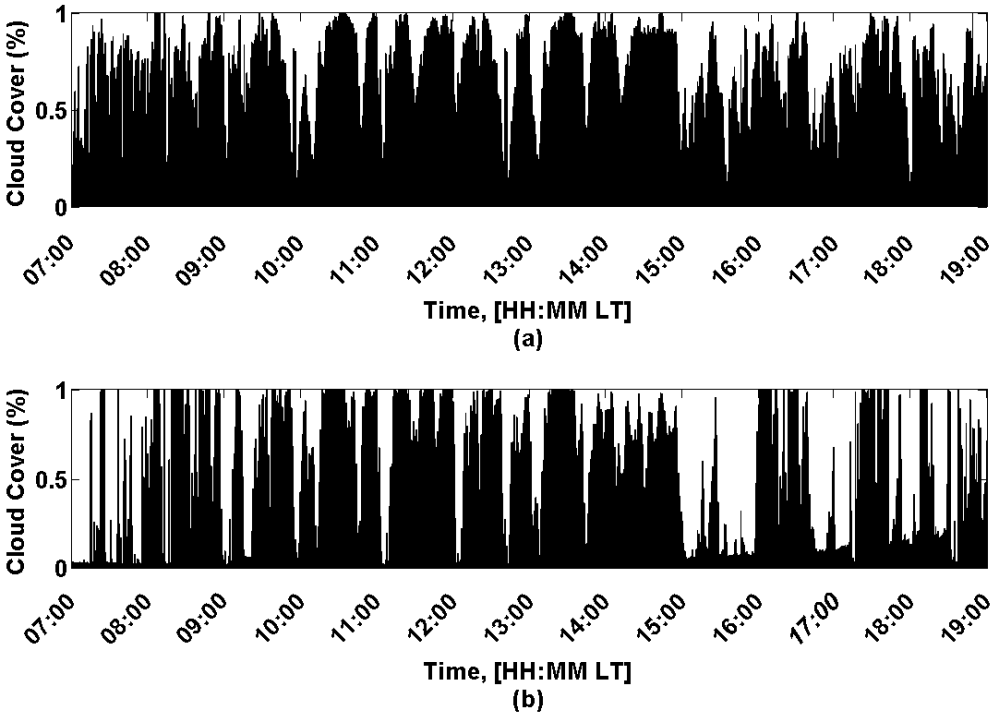


Figure 3.34: (a) Total Cloud Coverage (cc), (b) EECC for the Observation Point at $(x, y) = (50,50)$ Presented by the Utilized Sky Image Set. Time Resolution ($\Delta t$): 1 Min.

According to the earlier discussions, the ground coverage area of a sky image containing Cumulus clouds is approximately 4 km$^2$. Hence, the coordinates of the considered observation points can be considered to be as follows; $a = (500m, 1500m), b = (1500m, 500m), c = (1000m, 1000m), d = (500m, 500m)$ and $e = (1500m, 1500m)$. Figure 3.35 presents the daily irradiance sequences incident on different array observers using the set of sky images provided in Figure 3.34.

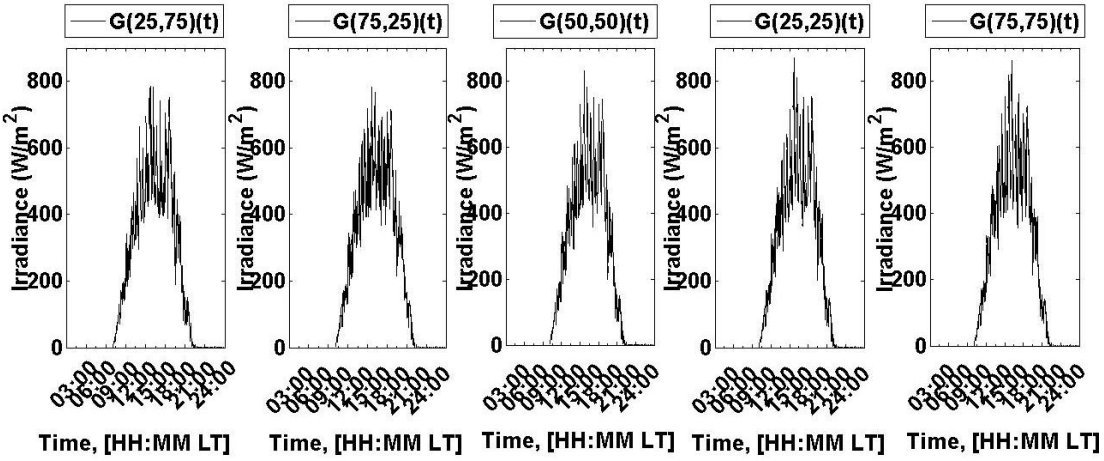


Figure 3.35: Daily Irradiance Time-Series Incident on the Surface of 45° Inclined 5 PV Modules with Different Locations within the PV Array, for Berlin, Germany, in July, Time Resolution ($\Delta t$): 1 Min.

The figure clearly shows that although the cloud coverage is identical for all observation points at each time instant, different irradiance time-series are obtained at different observation points within the PV array. The difference in the time-series for different observation points is a direct result of the distribution of clouds in the sky and the instantaneous values of EECC for each observation point. Obviously, instantaneous values of EECC differ from point to point within the PV array due to different geographical locations of the considered observation points. Therefore, the attenuating effect of EECC on solar irradiance received by each observer at each time

instant differs from point to point which causes fluctuations in the irradiance time-series and different instantaneous values of solar irradiance received by different array observers.

*d) Variable Characteristics of the Incident Solar Irradiance Time-Series at Different Observation Points*

According to the above mentioned discussions, irradiance time-series received at different observation points within the geographical extent of a PV array can be expected to differ from each other due to distribution of the existing cloud coverage in the sky. This part of the thesis is allocated to a comparison between the obtained daily irradiance time-series for different array observers during a day as well as the examination of the developed model to reflect the variable characteristics of the mentioned irradiance time-series. Scatter graphs are utilized for this purpose and the simulated irradiance time-series presented in Figure 3.35 for 5 different observation points within the PV array are compared. The comparison results are shown in Figure 3.36.

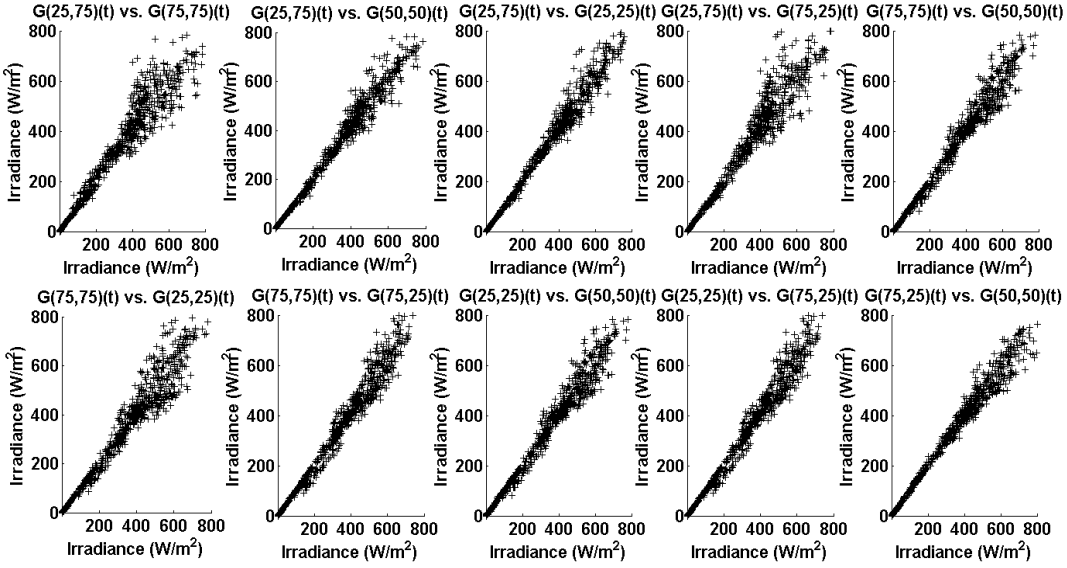


Figure 3.36: Comparison of the Simulated Irradiance Time-Series Incident on the Surface of 5 Different 45° Inclined PV Modules within the PV Array, for Berlin, Germany, in July. Time Resolution ($\Delta t$): 1 Min.

The utilized observation points are located on the diagonals of the application area and particularly selected to cover the area from north to south and from east to west. The comparison results clearly show that while the irradiance time-series incident on closer observation points provide less dispersion ranges, none of the obtained daily irradiance time-series are exactly similar to each other. The figure clearly shows the variable characteristic and dispersion of the daily irradiance time-series incident on the surface of PV modules with different geographical locations within the application area. Obviously the mentioned dispersion and variable characteristics are caused by the existing cloud distribution in the sky. The observed range of dispersion of the irradiance time-series, which also varies from point to point, is a direct result of the EECC values for different observation points since they vary according to the existing cloud distribution and geographical location of the observer on the ground.

The model`s capability to reflect the variable characteristics and dispersion of irradiance time-series received at different observation points on the ground is also examined and verified in the following part of the thesis. For this purpose, irradiance measurements obtained from satellite observations, as described in Table 3.5, are utilized. The coordinates of the observation points considered in Figure 3.35 and Figure 3.36 are utilized to virtually locate the mentioned points on the ground. A sample day in July representing the same cloud coverage as the one considered in Figure 3.34 is selected and the satellite-observed mean hourly irradiance values for the mentioned observation points are derived from satellite data. Figure 3.37 shows comparison results of the mentioned mean hourly irradiance values derived from satellite observations for 5 different observation points on the ground. It can be expected that mean hourly irradiance values present relatively less dispersion from point to point compared to the simulated per-minute irradiance time-series. However,

the figure clearly shows the variable characteristics and dispersion of the hourly mean irradiance values derived from satellite observations for different observation points on the ground, despite their relatively less dispersion compared to per-minute simulated irradiance time-series for the same observation points. It is observed that hourly mean irradiance values obtained from irradiance observations during a day also vary from point to point. Although the ranges of variations are less compared to the simulated per-minute irradiance time-series, the mentioned variability and dispersed characteristics of the observed data verifies the model`s capability to reflect the variable and dispersed characteristics of the irradiance time-series.

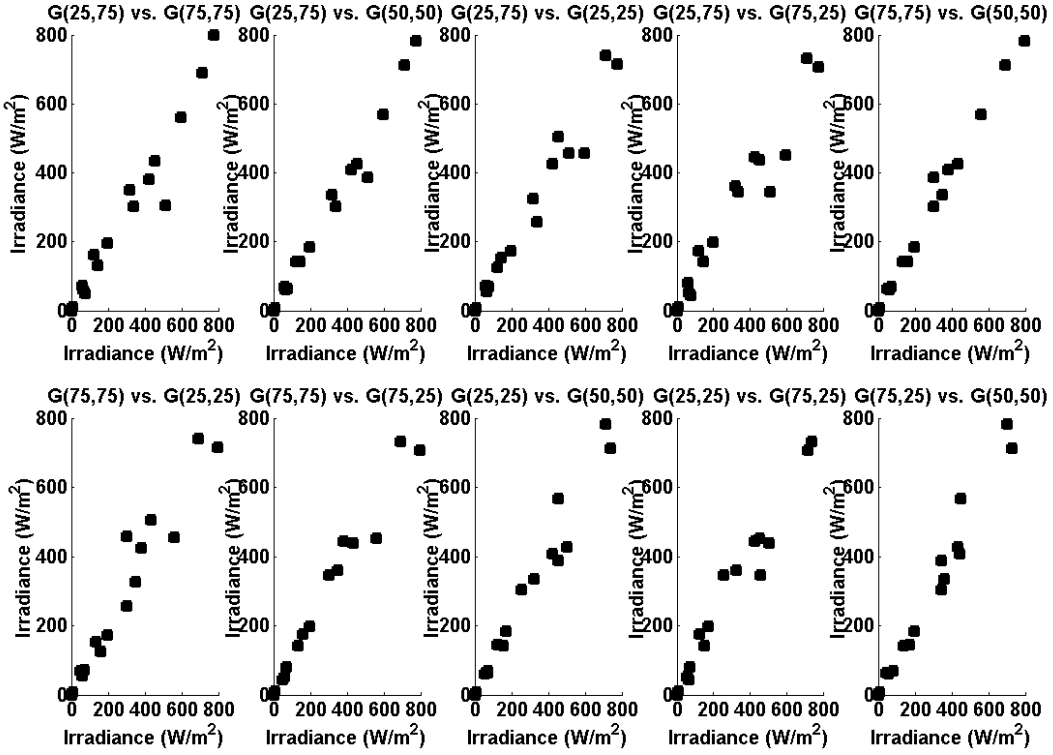


Figure 3.37: Comparison Results of Mean Hourly Irradiance Values Obtained from Satellite Observations for 5 Different Observation Points within the PV Array, for Berlin, Germany, in July

Obviously the main factor affecting the incident irradiance values is the existing cloud coverage in the sky and its shape and distribution. Different irradiance time-series and

dispersion ranges can be expected on an individual observation point on the ground even during days with the same cloud coverage as a result of different cloud distributions in the sky.

# Chapter 4

# MODELING OF ADAPTIVE RECONFIGURABLE PV ARRAYS BASED ON REAL CLOUD PATTERNS

According to the previous discussions of the thesis, high dependency of power generation in PV systems to the incident solar irradiance values causes a vital need for precise and accurate knowledge of the incident solar irradiance values on the surface of each individual PV module within a PV array. Once the incident irradiance values are obtained, different strategies can be determined and considered to cope with the negative effects of partial shading of PV arrays and to increase power generation in PV power plants. Application of bypass diodes, utilization of different PV array interconnection types and reconfiguration of PV arrays are all examples of measures taken against negative effects of partial shading on PV power plants. This chapter of the thesis provides brief explanations regarding the currently utilized coping strategies and introduces a novel adaptive dynamic reconfiguration algorithm for PV arrays based on the existing cloud patterns in the sky in order to increase power generation in PV power plants. The mentioned reconfiguration algorithm is a dynamic algorithm based on the irradiance equalization method introduced in [114] which adjusts the locations of different PV modules within a PV array according to the existing partial shading patterns determined by the SDIPs described in Chapter 3. The mentioned algorithm aims to provide near-optimal array configurations in terms of irradiance equalization, as discussed in further parts of the thesis, under almost all types of partial shading conditions and hence improves array`s power generation to approximately the

highest possible amounts. Preserving lifetimes of switching devices and being not limited by the number of PV modules included in the array are some of the most important advantages of the proposed PV array reconfiguration algorithm.

## 4.1 Partial Shading Problem in PV Arrays

Partial shading of PV arrays, which is mostly caused by passing clouds, is considered as one of the most significant issues that have direct effects on power production in a PV array. Power generation in PV modules is directly proportional to the value of the incident irradiance and hence, partial shading of a PV array makes a number of PV modules within the array unable to generate as much current as the unshaded modules. The current generated by a series-connected string of PV modules is limited by the current value of the module producing the smallest current. Therefore, the shaded modules do not contribute to the array`s power production and limit the power produced by the other modules. Hence, the direct result is reduction of the array`s output power. Partial shading effect in a PV array also may cause other issues such as hotspot problems. A hotspot occurs in a series-connected string of PV modules when one or more than one of the modules are shaded and cannot produce the same current as the others. When the shaded PV module in a series string is forced to pass a higher current than what it is capable to, the module becomes reverse biased and dissipate power instead of power production. This issue increases the temperature of the shaded module and causes the problem which is referred to as the hotspot problem. A hotspot problem may also cause physical damages to the shaded module. Taking all the above mentioned concerns into consideration, an efficient and reliable use of PV produced power depends on utilization of appropriate coping strategies against negative effects of partial shading in PV arrays. Various methods have been proposed in order to cope with the mentioned negative effects. Utilization of bypass diodes and Maximum Power

Point Tracking (MPPT) techniques are some of the widely utilized coping strategies in order to overcome the reductions of PV arrays` power production under partial shading conditions. The mentioned strategies are summarized throughout this part of the thesis.

### 4.1.1 Bypass Diodes

Application of bypass diodes is widely considered as an effective method to overcome the hotspot problem and increase power production amount in a PV array [38,44]. It relies on parallel connection of a diode with reverse polarity to a shaded PV module or group of shaded PV modules in a PV array. Figure 4.1 shows an example of bypass diode application in a series-connected string of PV modules. The bypass diode that is connected in parallel to the shaded PV module(s) becomes forward biased when the mentioned module(s) are reverse biased due to partial shading effects. Therefore, the shaded module(s) are bypassed and the current produced by the unshaded cells passes through the bypass diode. Application of bypass diodes leads to a small voltage reduction (≈ 0.6 V) across the bypassed PV module(s). Figure 4.2 shows the simulated I-V and P-V characteristics of a string of 5 series-connected SOLAREX-MSX60 type PV modules including 3 shaded modules, before and after application of bypass diodes. As it is shown in Figure 4.2, application of bypass diode causes multiple peak points in the array`s characteristic curves. It is observed that each different irradiance value results in a peak point in the array`s characteristic curves. The figure clearly highlights the effective role of bypass diode application resulting in improvement of the array`s MPP.

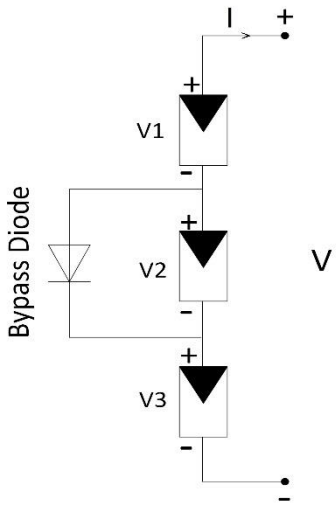


Figure 4.1: Bypass Diode Application in a String of Series-Connected PV Modules

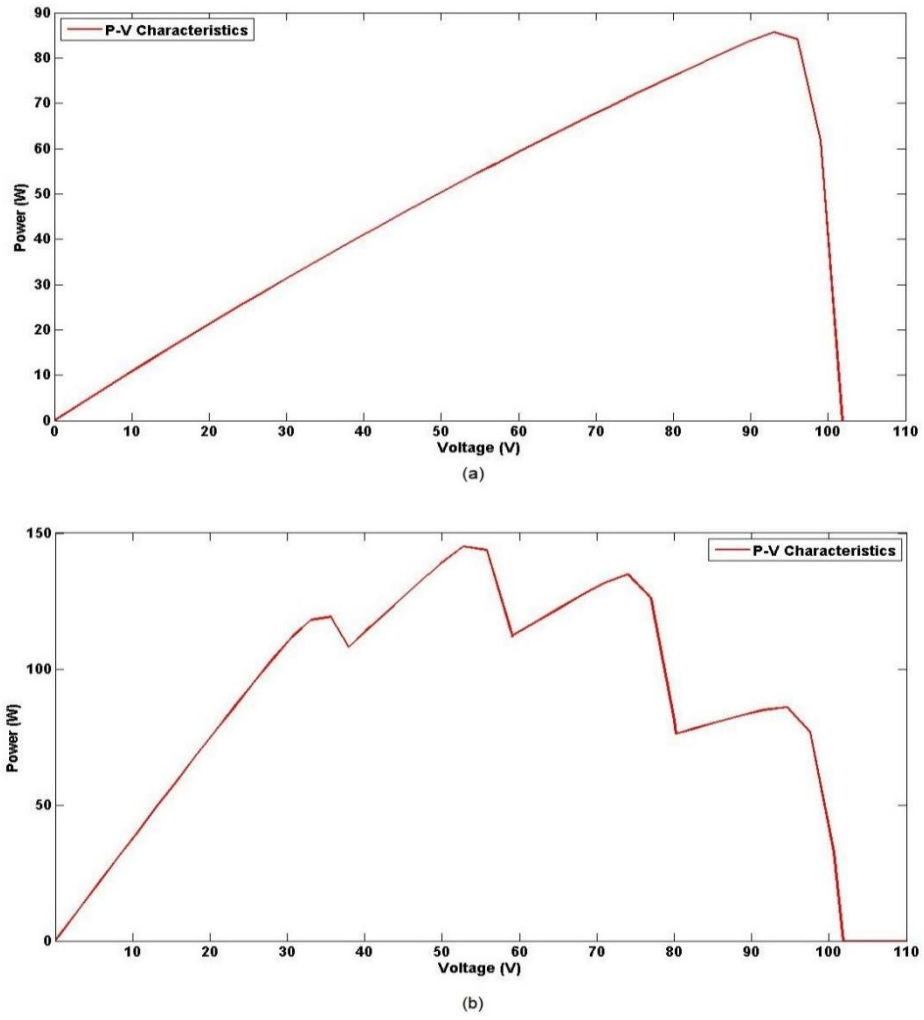


Figure 4.2: P-V Characteristics of a String of Series-Connected PV Modules (a) Before and (b) After Bypass Diode Application

### 4.1.2 Maximum Power Point Tracking

Maximum Power Point Tracking (MPPT) is another method which is developed and widely utilized in order to improve power production in PV arrays under partial shading conditions. Different MPPT algorithms are introduced in the literature [116, 117,118]. Despite differences in the efficiency and working principles, the common purpose of all the mentioned techniques is to operate PV module(s) at their MPP and hence to extract the maximum possible power from the module(s) under variable environmental conditions. Figure 4.3 shows a general diagram of a MPPT system. As it is shown in the figure, a MPPT system includes a DC/DC converter and a MPPT algorithm which controls operation of the converter in order to obtain the optimum load voltage. Perturb and Observe (P&O) algorithms are considered as the most widely preferred MPPT algorithms due to their simplicity while their main disadvantage is the oscillations around the MPP. Improved versions of P&O algorithms are also developed in order to overcome the mentioned disadvantage [119,120,121,122]. An evaluation of the performance of different MPPT algorithms is provided in our previous work which is also presented in "Appendix F" [123]. Utilization of artificial intelligence to control operation of the MPPT system has also been proposed in some research studies [52,53].

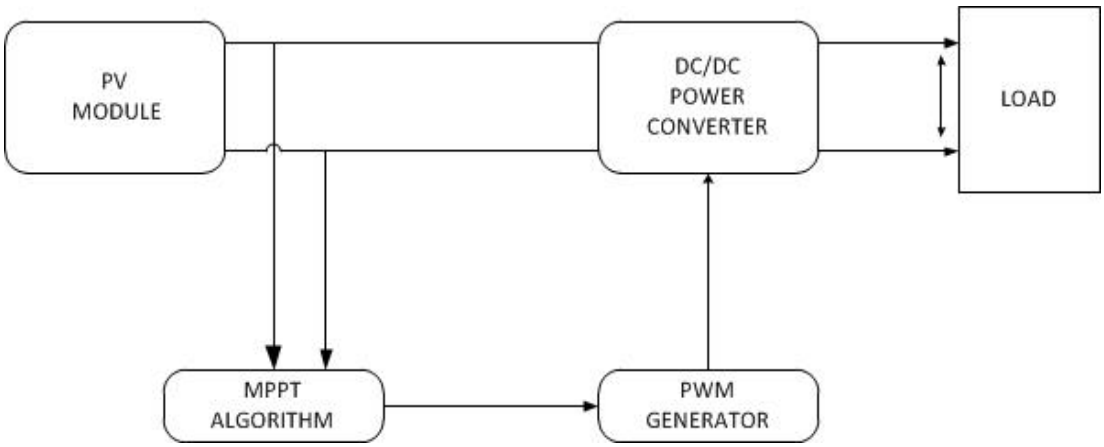


Figure 4.3: General Diagram of a MPPT System

### 4.1.3 Different PV Array Architectures

According to the earlier discussions of the thesis, performance of PV arrays is directly proportional to the amount of solar irradiance incident on the surface of the array. Partial shading of PV arrays due to passing clouds is one of the most significant concerns about performance of PV arrays. The matter becomes more complex and significant when power production in large-scale PV power plants is taken into consideration. The affected part of the PV power plant by partial shading effects due to passing clouds becomes larger in parallel with increases in the area of the PV plant. Thus, precise and reliable knowledge regarding behavior of a PV array under cloudy sky conditions is a vital need for efficient use and management of a PV power plant. Moving clouds in the sky cause fluctuations in the output power of a PV array. As the moving direction and speed of clouds is highly variable, prediction of their effect on the performance of PV arrays becomes very difficult. It is obvious that prediction of cloud behaviors and their effects on the value of the solar irradiance received at different points within a PV power plant may provide a remarkable help for power yield estimation in PV power plants. However, taking the above-mentioned concerns into consideration, it is necessary to find out solutions to decrease the negative effects of partial shading on a PV array`s performance. In addition to solutions such as application of bypass diodes and/or MPPT techniques, different architectures for interconnections between PV modules forming a PV array are introduced as a measure to combat the negative effects of partial shading. Different interconnection types have been proposed in the literature for this purpose. Series-Parallel (SP), Bridge-Link (BL) and Total-Cross-Tied (TCT) interconnections are the most preferred array architectures [126,127,128,129]. The SP array architecture provides series connected strings of PV modules that are connected to each other in parallel. The SP

interconnection is considered as the simplest array interconnection. In a TCT interconnection type all PV modules are both series and parallel connected to each other at the same time. Contrary to the SP architecture, the TCT architecture is the most complex array architecture type with the highest wiring and connector costs. The number of interconnections in the BL architecture is reduced to half compared to the TCT architecture and consequently the wiring and connector costs are reduced as well. Figure 4.4 shows a general overview of the mentioned three PV array interconnection types.

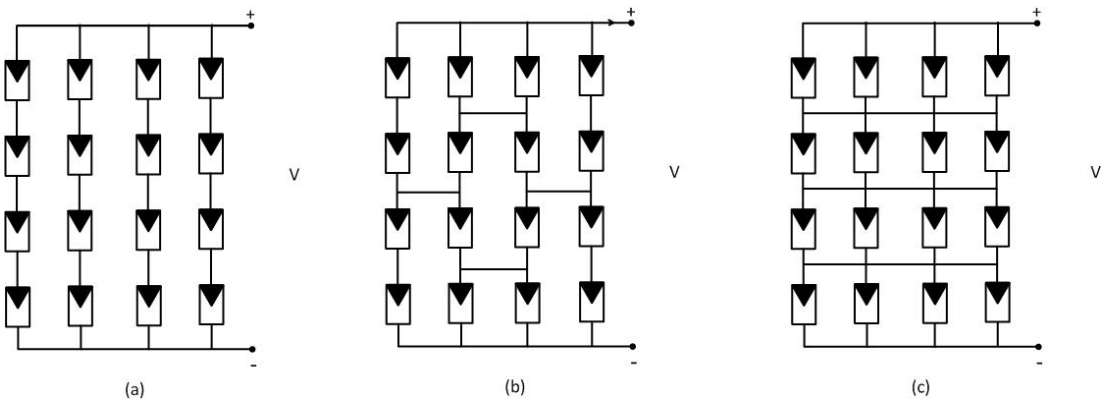


Figure 4.4: General Overview of (a) Series-Parallel, (b) Bridge-Link and (c) Total-Cross-Tied PV Array Architectures

It was mentioned previously that PV modules in a PV array are connected in series and parallel in order to meet the application`s current and voltage requirements. Therefore, taking into account that shading of a single PV module in a series-connected string affects and limits current production by all the modules in the string, it can roughly by assumed that TCT and BL architectures should provide better performances than SP architecture under partial shading conditions. However, a tradeoff will always exist between the better performance provided by more complex architectures such as BL and TCT and their higher costs.

Performance of the mentioned three array architectures under some different partial shading conditions is analyzed and compared and the results, as described in our previous work which is also presented in "Appendix E" [129], are provided in the following part of the thesis. Different partial shading patterns on the surface a PV array are considered here as simple shading scenarios under which the performance of PV arrays with different interconnection types are analyzed. The mentioned shading scenarios are chosen in a manner that each scenario contains three different levels of received solar irradiance on the surface of a PV array. The mentioned irradiance levels are considered as 200 W/m$^2$ corresponding to the irradiance level under the cloud center (the darkest area), 600 W/m$^2$ corresponding to cloud edge causing a more clear area and the clear-sky irradiance represented by 1000 W/m$^2$. The utilized shading scenarios are provided in Figure 4.5. Irradiance characteristics of different shading scenarios are provided as bellow;

i. Shading Scenario "a"

   The cloud center is located above the corner of the PV array. 4 PV modules are subject to 200 W/m$^2$ while 12 PV modules receive 600 W/m$^2$ and the remaining 20 modules experience no shading at all.

ii. Shading Scenario "b"

   The bottom side of the array is affected by the shading caused by the cloud center which receives 200 W/m$^2$. 12 PV modules receive 600 W/m$^2$ caused by the cloud edge and the remaining 12 modules are subject to clear-sky conditions.

iii. Shading Scenario "c"

The left side of the array is affected by the shading under the cloud center. 12 PV modules are illuminated by 200 W/m$^2$ while 12 modules receive 600 W/m$^2$ and the remaining 12 modules are subject to clear-sky conditions.

iv. Shading Scenario "d"

12 modules at the center of the array are subject to clear-sky conditions receiving 1000 W/m$^2$. 12 PV modules receive 600 W/m$^2$ and the remaining 12 modules are subject to 200 W/m$^2$.

v. Shading Scenario "e"

4 PV modules located at the center of the array are affected by the cloud center and receive 200 W/m$^2$. 12 PV modules are illuminated by 600 W/m$^2$ and the remaining 20 modules receive 1000 W/m$^2$.

vi. Shading Scenario "f"

4 PV modules at the center of the array receive 1000 W/m$^2$ while 12 modules around the center receive 600 W/m$^2$ and the outer 20 PV modules are subject to 200 W/m$^2$.

Irradiance characteristics for the mentioned different shading scenarios are provided in Table 4.1

Table 4.1: Irradiance Characteristics of Different PV Array Shading Scenarios

| **Shading Scenario** | **Number of fully shaded PV modules (200 W/m$^2$)** | **Number of partially shaded PV modules (600 W/m$^2$)** | **Number of fully illuminated PV modules (1000 W/m$^2$)** |
|---|---|---|---|
| a | 4 | 12 | 20 |
| b | 12 | 12 | 12 |
| c | 12 | 12 | 12 |
| d | 12 | 12 | 12 |
| e | 4 | 12 | 20 |
| f | 20 | 12 | 4 |

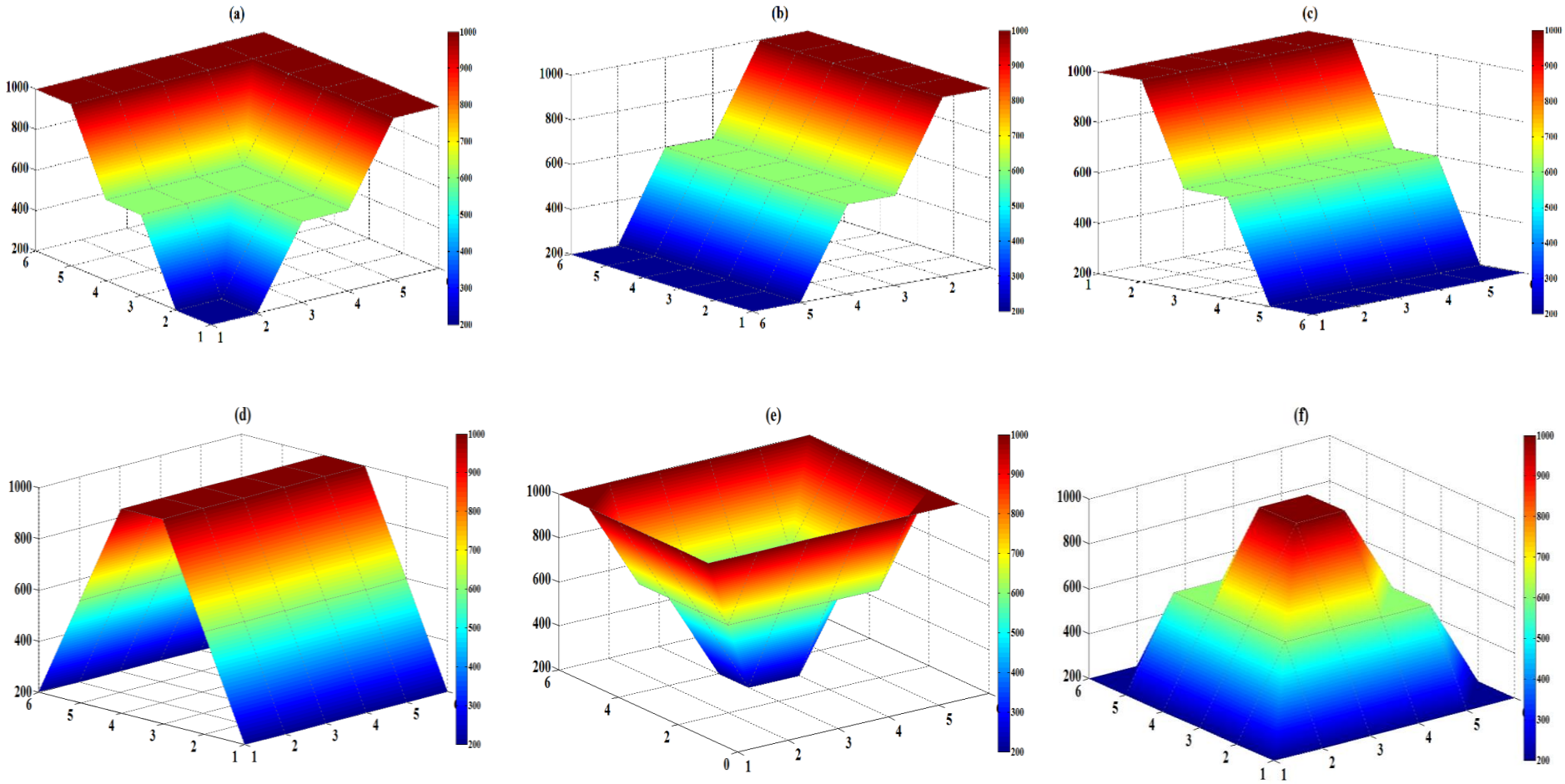


Figure 4.5: Different Shading Scenarios Utilized to Represent Partial Shading Effects Caused by Cloud Passage over a PV Array

The mentioned shading scenarios are applied to a PV array including totally 36 SOLAREX MSX60 type PV modules having three different architectures being; SP, BL and TCT interconnections types. The simulation models utilized for the mentioned PV arrays with different array architectures are provided in Figure 4.6. Each PV module utilized in the simulation models within the array includes a bypass diode across its terminals.

Figure 4.7 shows array`s I-V and P-V characteristics under uniform irradiance levels while array`s I-V and P-V characteristics under the above mentioned 6 different partial shading scenarios are presented in Figure 4.8. As it is shown in Figure 4.7, all the mentioned three different array interconnections provide the same performance under identical irradiance levels. However, the results of Figure 4.8 show that performance of PV arrays vary under different partial shading conditions depending on their interconnection types. The results show that performance of the array under shading scenarios “b”, “c” and “d”, where equal number of PV modules are subject to each irradiance level, does not differ for different array architectures. However, different array topologies have shown variable performance under other partial shading scenarios. (Shading Scenario “a”, “e” and “f”). It is observed that TCT interconnection has outperformed the other two array architectures (SP and BL) under all non-identical irradiance conditions.

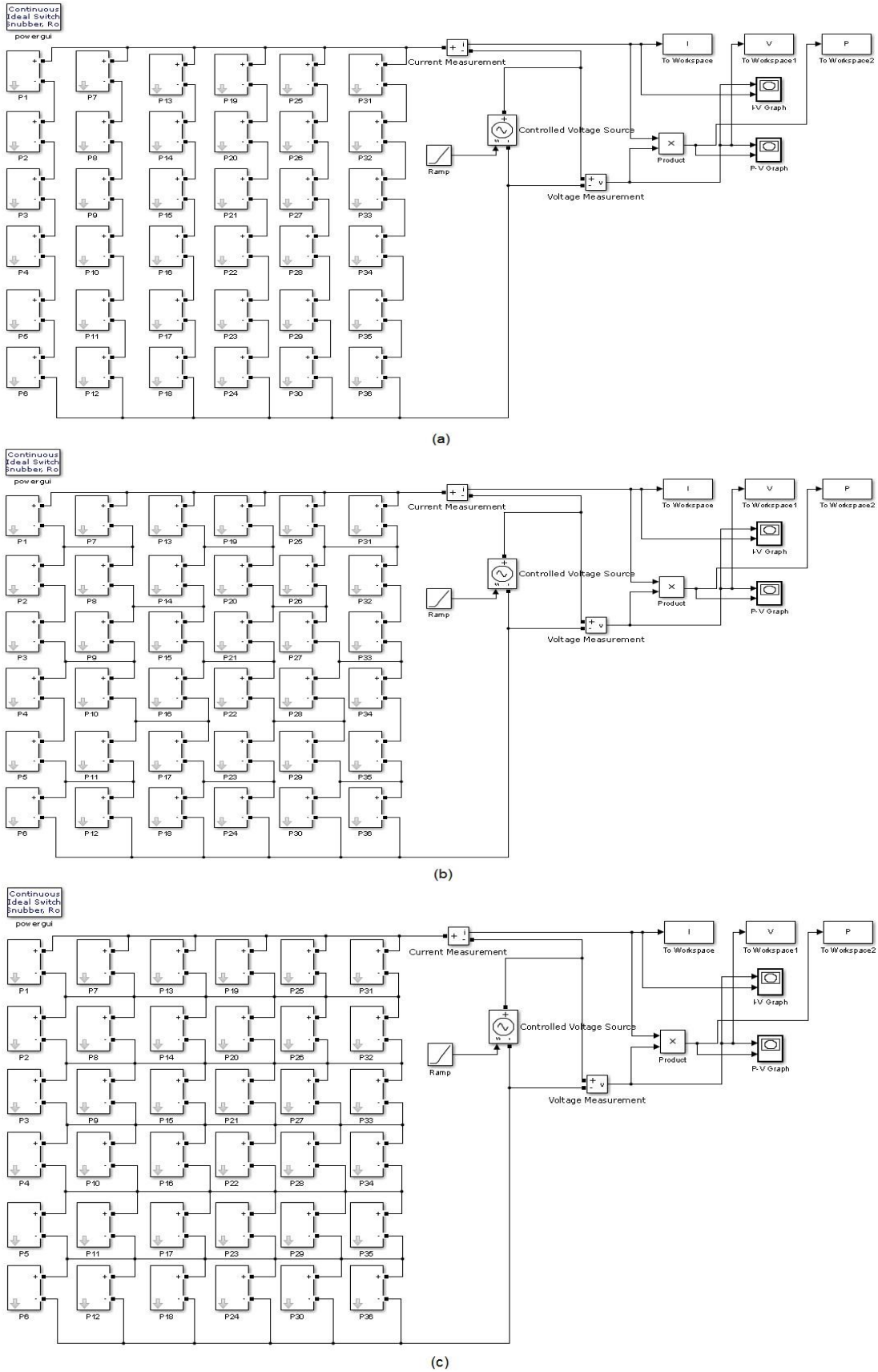


Figure 4.6: Simulation Models Utilized for (a) SP, (b) BL and (c) TCT Interconnected PV Array

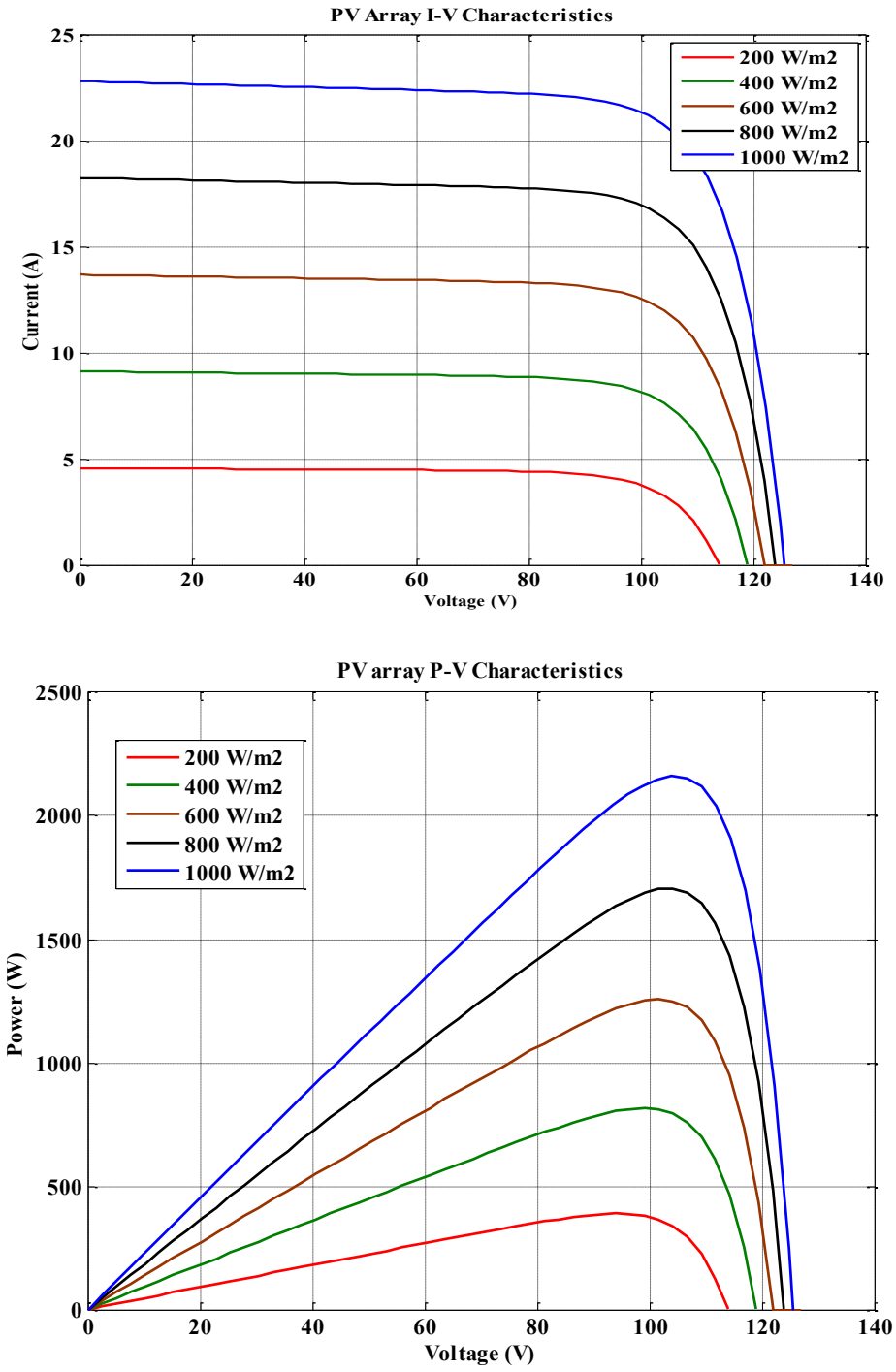


Figure 4.7: PV Array I-V and P-V Characteristics under Identical Irradiance Levels

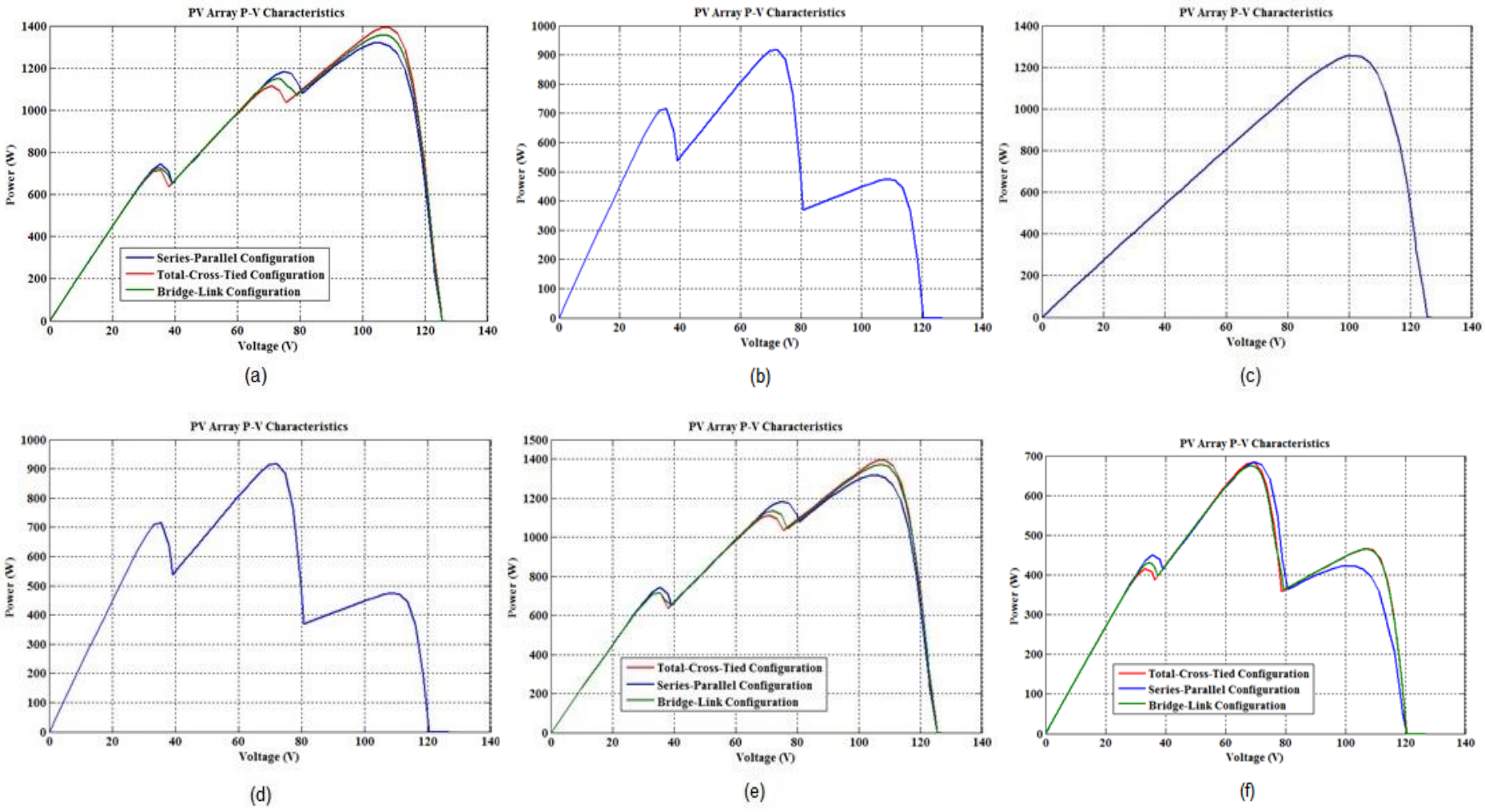


Figure 4.8: Simulation Results for Different Array Architectures under Different Shading Scenarios

Although the TCT interconnection shows a better performance with respect to other array topolgies, the high number of switches and complex wiring is the main disadvantage of this array interconnection. The number of switches are reduced to half in a BL topology with respect to TCT interconnection while its performance may slightly be lower under some certain shading conditions. It is also shown that SP interconnection has the lowest performance under partial shading conditions. As it is shown in the array design and the obtained results, there always exists a tradeoff between the complexity of the array topology, from wiring and number of switches point of view, and the array`s performance under partial shading conditions. The higher MPP reached with TCT makes it advantegous over the other two array topologies to be utilized to improve array`s performance where negative effects of partial shading due to passing clouds and variable shading patterns cause significant power drops in PV power plants.

Therefore, taking the above mentioned points into consideration, TCT interconnection is assumed as the preferred array topology to be utilized during design process of a dynamic and adaptive reconfigurable PV array in order to tackle the negative effects of partial shading and improve array`s power generation under partly cloudy sky conditions, as described in details in further parts of the thesis.

## 4.2 Dynamic Photovoltaic Array Reconfiguration

Dynamic reconfiguration of PV arrays is a leading-edge research area aiming at dynamically changing the location of PV modules within a PV array according to the existing partial shading patterns or non-identical irradiance profiles in order to increase power generation in a PV array. Most of the currently available methods and algorithms introduced for PV array reconfiguration rely on Irradiance Equalization

method. The mentioned Irradiance Equalization method was firstly introduced in [114]. The method aims at creation of series-connected rows of parallel-connected PV modules within a PV array which have average irradiance values equivalent to the array`s average irradiance value. In this way, power production by series-connected rows of parallel-connected PV modules within the array would be balanced due to the balanced average row irradiance values and hence, none of the rows generates less power which limits power generation by the other rows. Hence, it can be expected that PV modules with different or similar irradiance values are connected in parallel to each other in such a manner that they form series-connected rows of PV modules having the same or very close average irradiance values to each other. This goal is achieved by continuous relocation of PV modules within the array until the desired balanced-irradiance series-connected rows are obtained. The mentioned method is hence expected to improve power generation in PV arrays under various types of partial shading. The reconfiguration algorithm introduced in [114] considers all possible configurations of a PV array and finally selects the most appropriate one in terms of output power generation. PV array reconfiguration is also considered in [130] as a mixed integer quadratic programming problem. The algorithm introduced in this study provides the advantage of utilization of non-equal number of PV modules in each row of the array. The matter has also been considered in [131] as an iterative hierarchical sorting algorithm which is based on the previously mentioned irradiance equalization method. The aim of the mentioned algorithm is to achieve near-optimal array configurations in terms of irradiance equalization and the algorithm also considers minimizing the number of switching actions, $N_{SW}$. PV array reconfiguration is also considered in another research study in which a model-based control algorithm is utilized in order to connect an adaptive bank of PV modules to a fixed part of PV array

through a switching matrix [132]. A flexible switching matrix topology is utilized in another study for real-time power generation improvement in PV arrays [133]. Complex structure and/or limitations associated with the mentioned PV array reconfiguration algorithms are the main drawbacks of almost all of the mentioned algorithms.

The algorithm which is proposed for PV array reconfiguration in this thesis, as also presented in our previous work which is also presented in "Appendix B" [134], is a dynamic reconfiguration algorithm which aims at finding of near-optimal array configurations in terms of irradiance equalization and the number of the required switching actions to perform the mentioned array configuration. The adaptive characteristic of the algorithm comes from the fact that it seeks and obtains the near-optimal array configurations based on real-time site-specific cloud shadow patterns or non-identical irradiance profiles existing at the application areas. SDIPs introduced in Chapter 3 form the mentioned non-identical irradiance profiles or cloud shadow patterns on the extent of PV arrays according to which the proposed algorithm performs array reconfiguration. The reconfiguration algorithm is developed as a simple dynamic algorithm which at the same time considers and preserves lifetime of switching elements by reducing the number of the required switching actions in order to perform the reconfiguration task. The main advantages of the proposed algorithm can be considered as being a very simple algorithm without any limitation regarding the number of PV modules included within the PV array. Also the near-optimal PV array configurations obtained by the algorithm cause the PV array reach almost the highest possible power generation at each time instant under almost any type of partial shading while the required switching numbers are reduced to the minimum possible

by eliminating the unnecessary switching actions which do not have any significant effect on PV array`s power generation.

### 4.2.1 Non-Identical Irradiance Profiles

The non-identical irradiance profiles or shading patterns which are utilized together with the reconfiguration algorithm for the desired analysis purposes are SDIPs generated based on the method presented in Chapter 3 using 4 different and independent sample sky images. The mentioned 4 different SDIPs are particularly selected in a manner that they represent an overcast sky condition along with three different irradiance profiles obtained based on three different cloud coverage and distributions in the sky. Cumulus clouds are considered to represent the existing cloud type during analyses due to their conformity to the selected sky images. Figure 4.9 shows different cloud shadow patterns and the resulting non-identical irradiance profiles or partial shading patterns representing the above mentioned 4 different shading scenarios.

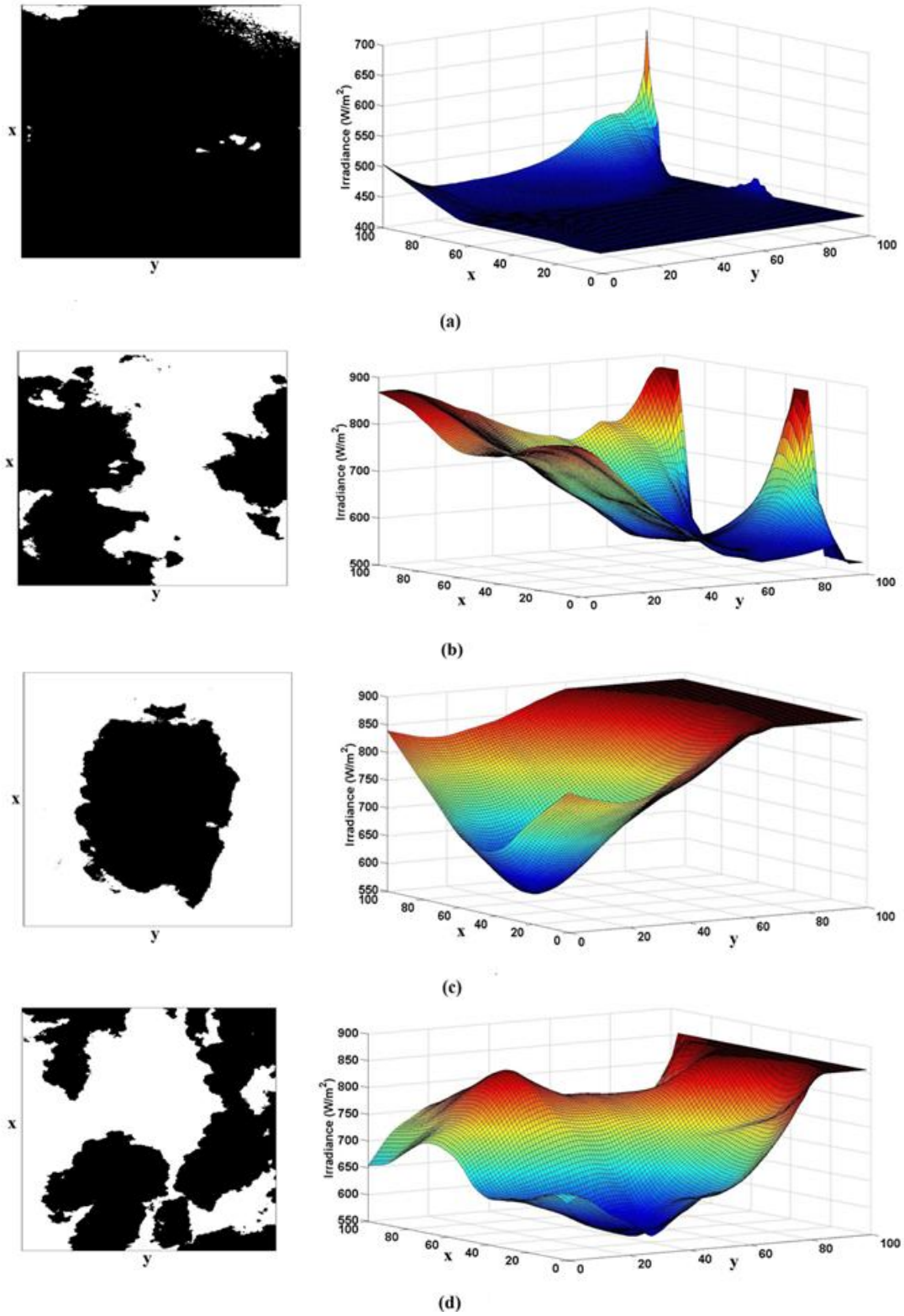


Figure 4.9: Cloud Shadow Patterns and SDIPs (Shading Scenarios) at 13:00 Local Time (LT) Considering Cumulus Clouds, (a) The 1st Shading Scenario, $cc = 96\%$ (b) The 2nd Shading Scenario, Partly Cloudy Sky, $cc = 44\%$ (c) The 3rd Shading Scenario 3, $cc = 34\%$ (d) The 4th Shading Scenario, $cc = 50\%$, for Berlin, Germany (Latitude: 52°33'56" N, Longitude: 13°18'39" E ) in July.

### 4.2.2 Working Principle of the Reconfiguration Algorithm

According to the previous discussions, the proposed reconfiguration algorithm works based on the irradiance equalization principle. The aim of the irradiance equalization method is to create series-connected rows of parallel-connected PV modules in a TCT interconnected PV array having similar or very close average irradiance values. The TCT interconnection is generally considered in PV array reconfiguration studies because, as also discussed earlier in the thesis, this array interconnection architecture provides the best performance under partial shading conditions.

According to the above mentioned discussions, significance of having precise information regarding the irradiance values incident on the surface of each individual PV module within the array is once again approved. Once the irradiance profiles are obtained and the desired array configuration is determined, the positions of PV modules should be changed and they should be relocated within the array in order to achieve the desired final array configuration. The task of allocation of PV modules with different irradiance levels to different rows within the PV array is performed and conducted by a flexible Switching Matrix which is controlled by the Reconfiguration Algorithm. Figure 4.10 presents the process of PV array reconfiguration.

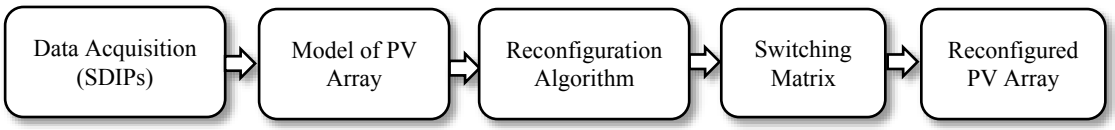


Figure 4.10: Flowchart of PV Array Reconfiguration System

As it is shown in the figure, the first step towards reconfiguration of a PV array is the data acquisition step. Information regarding solar irradiance values incident on the surface of individual PV modules within the PV array is gathered in the data

acquisition step. Data acquisition step earns a high significance due to high dependency of PV power production on the incident solar irradiance values, where precise data should be obtained regarding irradiance levels on the surface of PV modules within a PV array. Obviously the best method which can be utilized for data acquisition is to use one irradiance sensor or pyranometer per each individual PV module. However, economic considerations, equipment limitations, etc. cause the mentioned method be not always practically possible. As an alternative, estimation of solar irradiance values from module current, voltage and temperature measurements is considered in the literature [132,135]. The data acquisition task is held in this thesis using the previously described SDIPs as irradiance profiles on the surface of PV arrays providing irradiance levels for each individual PV module. The shading scenarios presented in Figure 4.9 are utilized as sources of irradiance data on the extent of PV arrays to be reconfigured.

One-Diode mathematical model of a PV cell, as defined in Chapter 2, is utilized in this thesis for modeling purpose of PV modules as the second step of the PV array reconfiguration process.

As it was mentioned previously, the reconfiguration algorithm works based on the irradiance equalization principle. The aim of the mentioned method is to create series-connected rows of parallel-connected PV modules with average irradiance values equal to the array`s average irradiance value. The average irradiance value of a row of parallel-connected PV modules, $\overline{G_\iota}$, is expressed as;

$$\overline{G_\iota} = \frac{\sum_{j=1}^{l} G_{ij}}{l} \tag{4.1}$$

Where;

$\bar{G}_i$ : Average irradiance value of the i$^{th}$ row of a PV array [W/m$^2$]

$G_{ij}$ : Irradiance value incident on the j$^{th}$ PV module of the i$^{th}$ row of a PV array [W/m$^2$]

$l$ : Total number of PV modules in a row of a PV array

According to the previous discussions of the thesis, the goal of irradiance equalization is to create series-connected rows of parallel-connected PV modules in a TCT interconnected PV array. Hence, the mentioned goal is considered to be achieved when similar $G_i$ values are obtained for all rows of a PV array as a result of array reconfiguration. Obviously, the ideal case from irradiance equalization point of view is the case under which the average irradiance of each individual row of parallel-connected PV modules is equal to the average irradiance value of the array ($\bar{G}_i = \bar{G}$). However, reaching this goal may not always be possible under real-world conditions due to highly variable and dispersed characteristics of the spatial distribution of irradiance values contained in an irradiance profile. Therefore, forcing the algorithm to find the optimal array configuration or in other words, the above mentioned ideal case in terms of irradiance equalization, may put the algorithm in an infinite loop. In order to overcome this problem, the developed reconfiguration algorithm tries to find the near-optimal array configuration from irradiance equalization point of view. The meaning of a near-optimal array configuration is a configuration that improves power generation in a PV array to approximately the highest possible level although the average row irradiance values are not necessarily equal to the array`s average irradiance value. The aim of the mentioned algorithm is to reduce the number of unnecessary switching actions by decreasing the number of reconfigured rows which

do not provide a significant contribution to power generation by the array. In this way, the lifetime of switching devices are preserved, the number of iterations of the algorithm is reduced and the operation speed of the algorithm is increased. In order to achieve this goal, an irradiance threshold, $\Delta G$, is defined and set in order to act as a tolerance against the limiting effect of the rows producing less amounts of current and hence limit power generation in a PV array. Once the mentioned irradiance threshold is set, the rows for which the average irradiance values fall within the mentioned threshold from the array`s average irradiance values are not reconfigured. The algorithm then reconfigures rows when $(\overline{G_i} > \bar{G} + \Delta G)$ or $(\overline{G_i} < \bar{G} - \Delta G)$. As an example, an irradiance threshold of $\Delta G = 0.05G$ implies 50 W/m$^2$ irradiance threshold under STC. Obviously, smaller values of irradiance threshold are expected to provide better results in terms of improvement of power generation in a PV array but there is always a tradeoff between the magnitude of the irradiance threshold and the number of switching actions to be performed and rows to be reconfigured. Therefore, it can be thought that smaller values of irradiance threshold cause higher costs whereas they may not necessarily provide much contribution to array`s power generation. On the other hand, considering a rational irradiance threshold causes the average row irradiance values and therefore, the power production by all rows and limiting effect of less power producing rows remain within tolerable limits. In this way, the less power generating rows will not impose significant reducing and limiting effects on power production by the other rows of the array. Also the number of rows to be reconfigured are reduced as well as the number of the switching actions to be performed and the lifetime of the switching devices is preserved. Taking the above mentioned example into consideration, considering an irradiance threshold of $\Delta G$ = 50 W/m$^2$ means that rows with average irradiance values 0 – 50 W/m$^2$ less or higher than the array`s average

irradiance value will not be reconfigured. The switching actions are performed by a flexible switching matrix. Once the appropriate array configuration is determined as a result of application of the reconfiguration algorithm, each switching action corresponds to a PV module reconfiguration determined by the algorithm. Switching actions are performed in order to relocate the corresponding PV modules and connect them to their new locations in the reconfigured array configuration.

According to the previous discussions, some of the rows within the array are not reconfigured by the algorithm as a result of application of the previously mentioned irradiance threshold. The algorithm considers irradiance values incident on the surface of PV modules within the array as a matrix having the same size (in terms of rows and columns) of the PV array. The rows which will not be reconfigured by the algorithm are primarily removed from the matrix and then, a new matrix of the rows to be reconfigured after removal of the non-reconfigured rows is formed. Obviously elements of the new matrix are PV modules which belong to the rows with average irradiance values falling out of the tolerable limits defined by the irradiance threshold. The elements of the new matrix or in other words, the PV modules to be reconfigured, are sorted column-wise in an ascending order based on their irradiance levels and a sorted matrix is formed. In this way, the first element of each column of the sorted matrix will be a PV module having the smallest irradiance value among the remaining unsorted ones. The obtained sorted matrix is then divided into two sub-matrices, each of size $k \times l/2$. Where, "$k$" denotes the matrix row numbers and "$l$" denotes the matrix column numbers. The algorithm then keeps the first sub-matrix of the size $k \times l/2$ unchanged and sorts the elements of the second $k \times l/2$ in a descending order. This implies that the first element of each column of the second $k \times l/2$ sub-matrix will

contain the PV module having the highest solar irradiance value among the remaining unsorted ones. The next step involves concatenating of the above mentioned two $k \times l/2$ sized sub-matrices. The final reconfiguration matrix is then formed as a result of integration of the non-reconfigured rows, as discussed earlier, to the concatenated sorted PV module matrix. The formation principle of the reconfiguration matrix can somehow be thought of as a queue in which the remaining PV modules to be reconfigured are assigned to the matrix elements according to their irradiance values. A pair of PV modules having respectively the remaining highest and lowest irradiance levels are assigned to elements of a row of the reconfiguration matrix at each reconfiguration step. In this way, balanced-irradiance rows of PV modules are formed in the reconfiguration matrix. Taking into account that the non-reconfigured rows are already balanced-irradiance rows falling within the determined tolerable limits, it can be expected that the resulting final reconfiguration matrix contains rows all having balanced-average irradiance values. Hence, the goals of the reconfiguration algorithm are expected to be reached in terms of finding the near-optimal array configuration from irradiance equalization point of view. On the other hand, it is not necessary to specifically determine the position of the reconfigured PV modules in a row since the order of the parallel-connected PV modules in a row does not affect current generation by the row. Figure 4.11 shows an example of application of the proposed reconfiguration algorithm to a $4 \times 4$ PV array with $G_1 < G_2 < \cdots < G_{16}$.

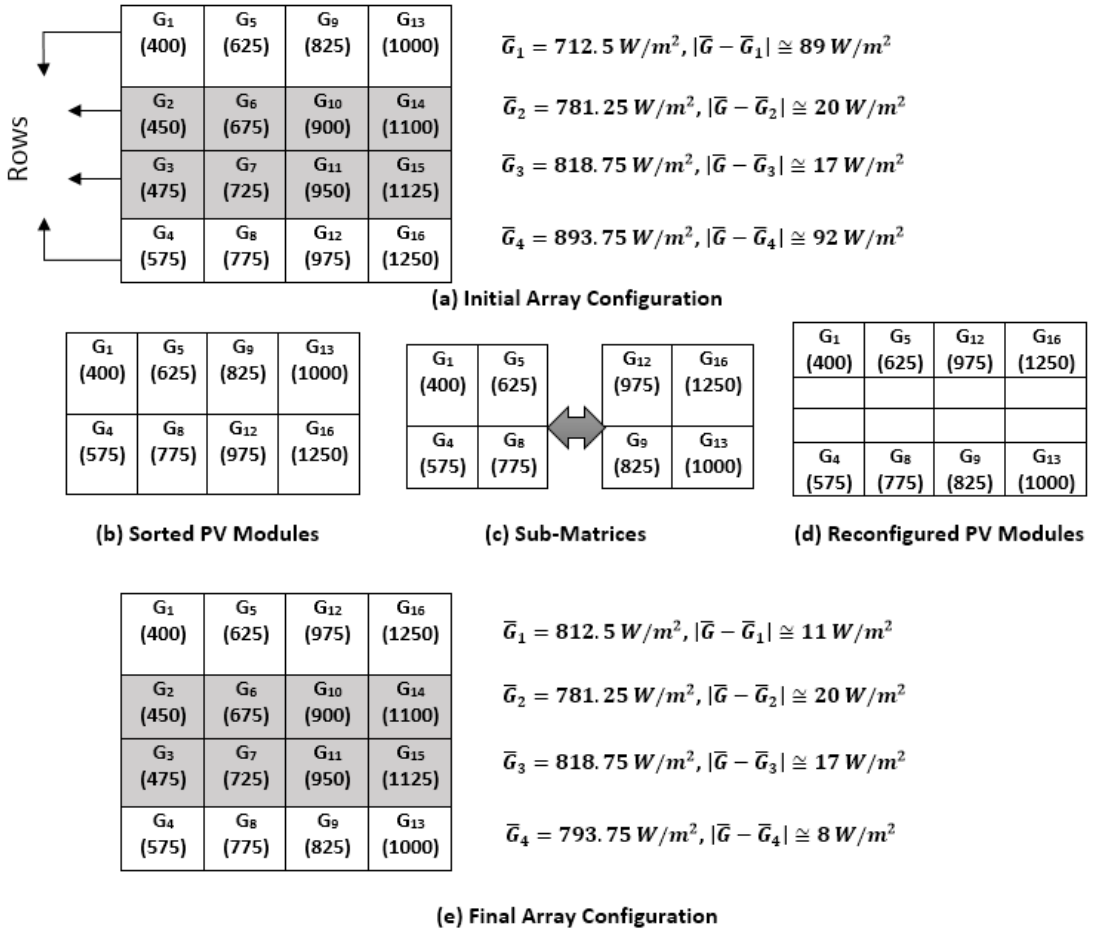


Figure 4.11: Example of Application of the Reconfiguration Algorithm to a $4 \times 4$ PV Array, $(G_1 < G_2 < \cdots < G_{16})$, $\bar{G} = 801.56\ W/m^2$, $\Delta G = 0.05\bar{G} \cong 40\ W/m^2$

The figure obviously shows the effects of application of the developed reconfiguration algorithm to the utilized PV array. It is shown in the figure that the highlighted 2nd and 3rd rows of the array are not reconfigured since their average irradiance value falls within the determined tolerable limits ($\Delta G = 0.05\bar{G} \cong 40\ \mathrm{W/m^2}$) from the array`s average irradiance value. The 1st and 4th rows of the PV array initially have average irradiance values which exceed the tolerable limits and hence are reconfigured by the algorithm. It is shown that, as a result of the reconfiguration, the average irradiance values of the 1st and 4th rows fall within the tolerable limits and the final reconfigured array includes rows with average irradiance values being within the determined tolerable limits.

As it was mentioned previously, the proposed PV array reconfiguration algorithm preserves the lifetime of switching devices by eliminating the unnecessary switching actions which do not have any significant impact on the array`s power generation. The motivation here is that due to the high dispersion of solar irradiance values contained within an irradiance profile, some PV modules may be replaced by other modules having the same irradiance values as a result of sorting of PV modules during the reconfiguration process. In this case, in fact only the place of some PV modules with the same irradiance levels are changed and the modules having the same irradiance values are replaced with similar ones from other rows of the array. Such a module reconfiguration does not actually provide any contribution in terms of irradiance equalization and hence does not affect the array`s power generation, but only causes the number of reconfigurations and the resulting switching actions to be increased. The mentioned increase in the number of PV module reconfigurations and the resulting required switching actions to be performed by the switching matrix reduces switching device lifetimes. Hence, in order to prevent the mentioned situation and preserve lifetime of switching devices, once the reconfiguration algorithm converges and the final reconfigured array configuration is determined, the algorithm searches for such unnecessary PV module replacements (if any) and cancels them in order to avoid unnecessary switching actions to be performed by the switching matrix.

### 4.2.3 Switching Matrix

Switching matrix in a reconfigurable PV array is responsible for performing the necessary switching actions in order to form the final reconfigured PV array configuration being previously determined as a result of application of the reconfiguration algorithm. A switching action can be defined as an action which is performed in order to disconnect a PV module from its initial position in the

non-reconfigured PV array and connect it to its new position in the reconfigured PV array configuration determined as a result of application of the reconfiguration algorithm. The switching matrix consists of two main parts being namely; switching devices and the matrix control mechanism. Switching devices are responsible for connecting and disconnecting PV modules within a PV array while the control mechanism is responsible for controlling of the mentioned actions by sending control signals to the switching devices.

*i. The Matrix Structure*

The structure of the switching matrix relies on utilization of electrical buses and switches. The mentioned control matrix allows for parallel interconnection of each PV module to each row of the PV array. The mentioned dynamic interconnections are made possible using totally $2 \times N_{PV}$ single-pole k-throw switches [114], where $N_{PV}$ indicates the total number of PV modules included within a PV array. Figure 4.12 shows an example of the structure of the utilized switching matrix.

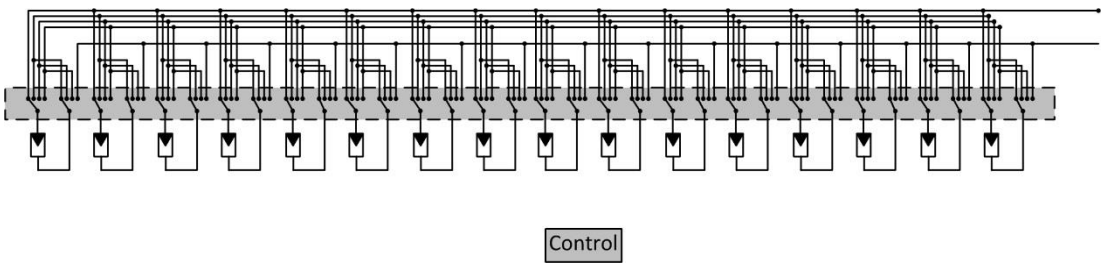


Figure 4.12: Structure of the Switching Matrix

*ii. Matrix Control*

The control mechanism of the switching matrix is responsible for triggering the utilized switching devices in order to perform the necessary reconfigurations and form the final PV array configuration determined as a result of application of the reconfiguration algorithm. The final reconfigured PV array configuration determined

by the reconfiguration algorithm forms the input of the matrix control mechanism. The control mechanism then sends triggering signals to the corresponding switching devices in order to execute the required switching actions and to form the final reconfigured array configuration upon determination of the reconfiguration plan by the reconfiguration algorithm.

### 4.2.4 Results and Discussion

The proposed PV array reconfiguration process is simulated in MATLAB/Simulink environment and applied to a $10 \times 10$ PV array including totally 100 Solarex MSX60 ($P_{max}$ = 60W, $V_{oc}$= 21.1V, $I_{sc}$ = 3.8A) type PV modules. The utilized PV modules are assumed to be located on the ground with equal distances to each other within the PV array. In this way, the distance between each pair of neighboring PV modules is considered to be 10% area of the geographical extent of the PV array. Simulations are performed for totally 4 different irradiance profiles or shading scenarios as defined in Figure 4.8. The simulation model firstly assigns the initial non-reconfigured irradiance values to the PV modules included in the array, as shown in Figure 4.13, in order to form the non-reconfigured PV array.

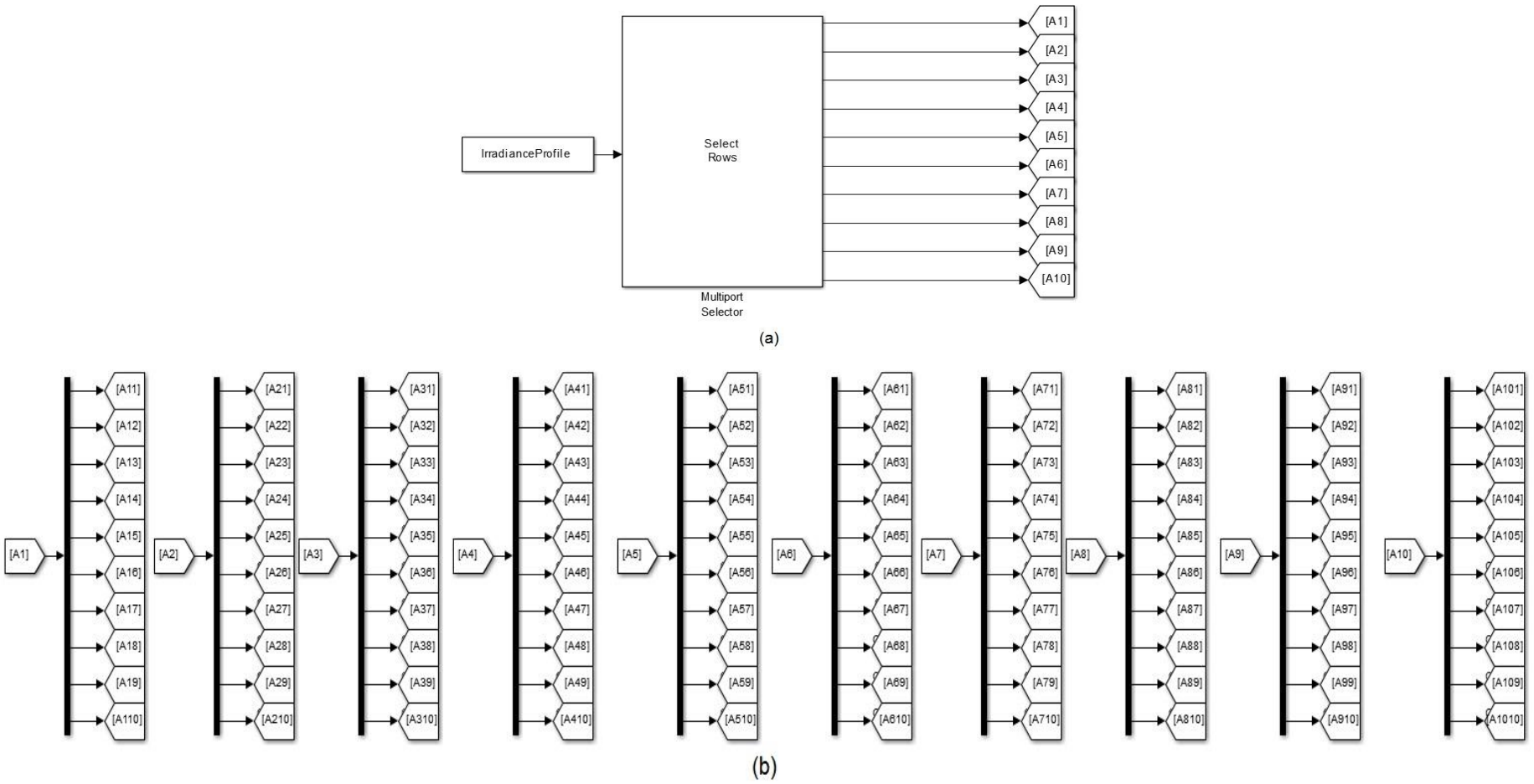


Figure 4.13: The Utilized Simulation Model to Assign Irradiance Values to Different PV Modules

As mentioned previously, the reconfiguration algorithm and the switching matrix are responsible for determination of the reconfigured PV array configuration and performing the necessary switching actions. Figure 4.14 shows the simulation model including the reconfiguration algorithm as a "MATLAB Function" together with the initial non-reconfigured irradiance profile.

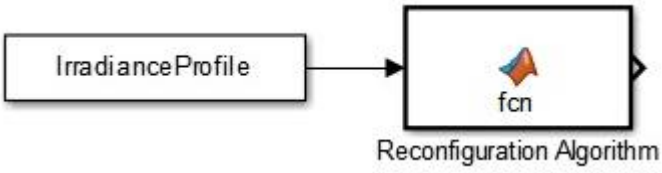


Figure 4.14: The Simulation Model for the Reconfiguration Algorithm

The reconfiguration algorithm shown in Figure 4.14 determines the reconfigured array configuration based on the non-reconfigured irradiance profiles or the shading scenarios which is provided as the input to the algorithm. Once the algorithm has determined the new reconfigured array configuration, it indicates the new positions of different PV modules included within the reconfigured PV array configuration. The output of the reconfiguration algorithm, which is sent to the "MatrixControlMechanismSubsystem", is a $100 \times 10$ matrix in which each row is considered as a triggering signal which controls the switching device connected to each individual PV module. Here, 100 denotes the total number PV modules included within the array and 10 denotes the array`s total row number. Figure 4.15 shows the internal structure of the "MatrixControlMechanismSubsystem" which is a sub-system having one input which is the previously mentioned $100 \times 10$ matrix and totally 100 outputs each being actually an individual row, or in other words the triggering signal, extracted from the input matrix. Each triggering signal consists of 0`s and 1`s and triggers a pair of switching devices connected to the terminals of the corresponding

PV modules in order to disconnect them from their initial non-reconfigured position and connect them to their new reconfigured row number within the array.

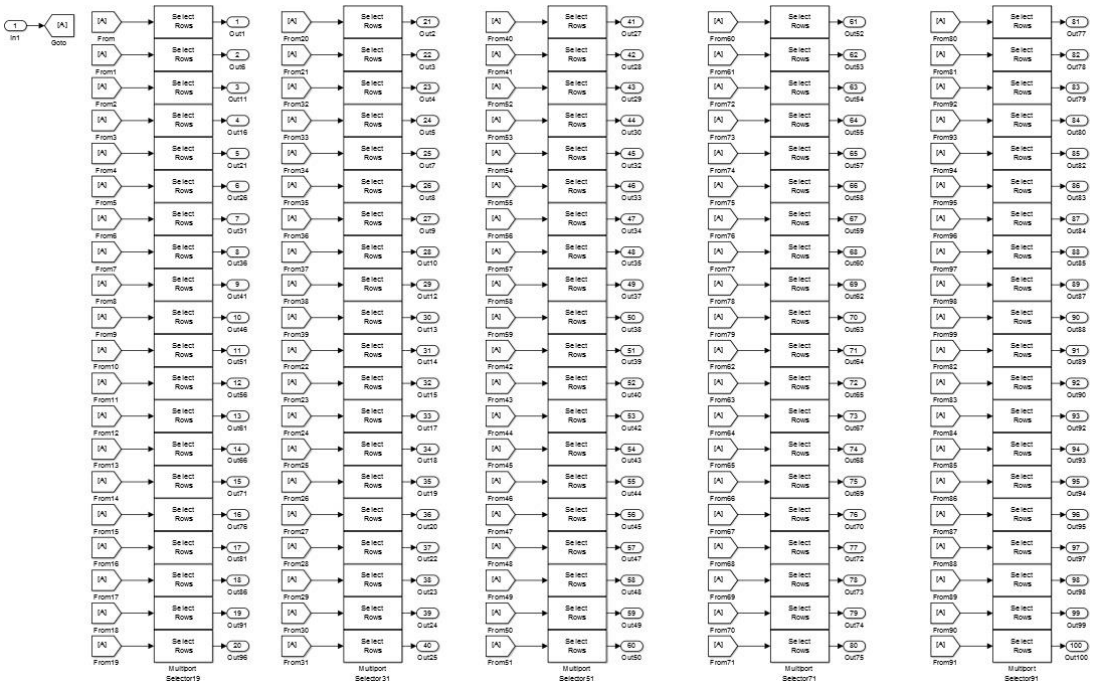

Figure 4.15: The Internal Structure of the "MatrixControlMechanismSubsystem"

Figure 4.16 shows a partial view of the PV array simulation model including totally one PV module along with their interconnections within the array. As it is shown in the figure, each PV module receives its irradiance value as a separate input and is connected to the electrical buses through a "Switching Sub-System". The simulation models for the PV modules are constructed based on the one-diode mathematical model of a solar cell, as previously described in Chapter 2.

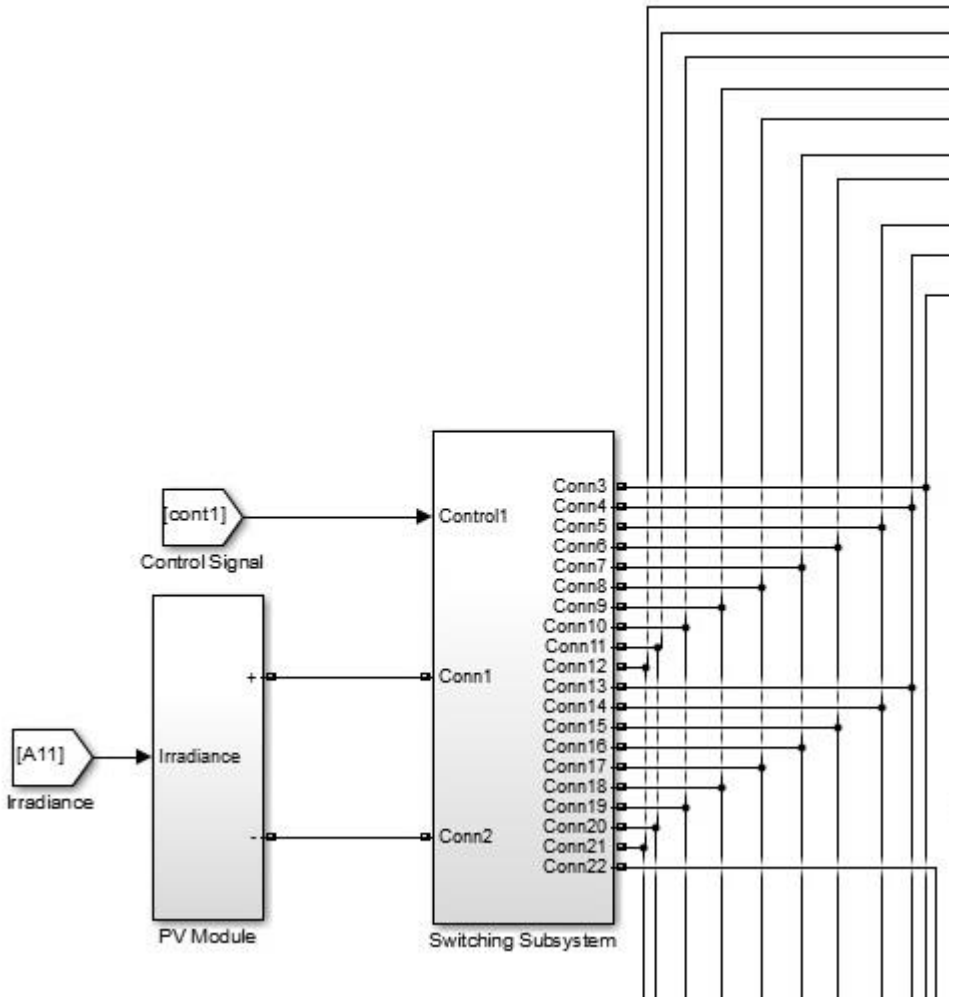


Figure 4.16: Simulation Model for PV Module Interconnections within the PV Array

The internal structure of the "Switching Subsystem" is presented in Figure 4.17. As it is shown in the figure, the input to the "Switching Subsystem" is the control signal or the triggering signal sent from the "MatrixControlMechanismSubsystem". The received control signal is simultaneously sent to the switching devices and triggers one pair of switching devices connected to the electrical buses which form the rows of the PV array. In this way, the triggered switches connect the PV module to its new reconfigured row number according to the received control signal generated as a result of application of the array reconfiguration algorithm.

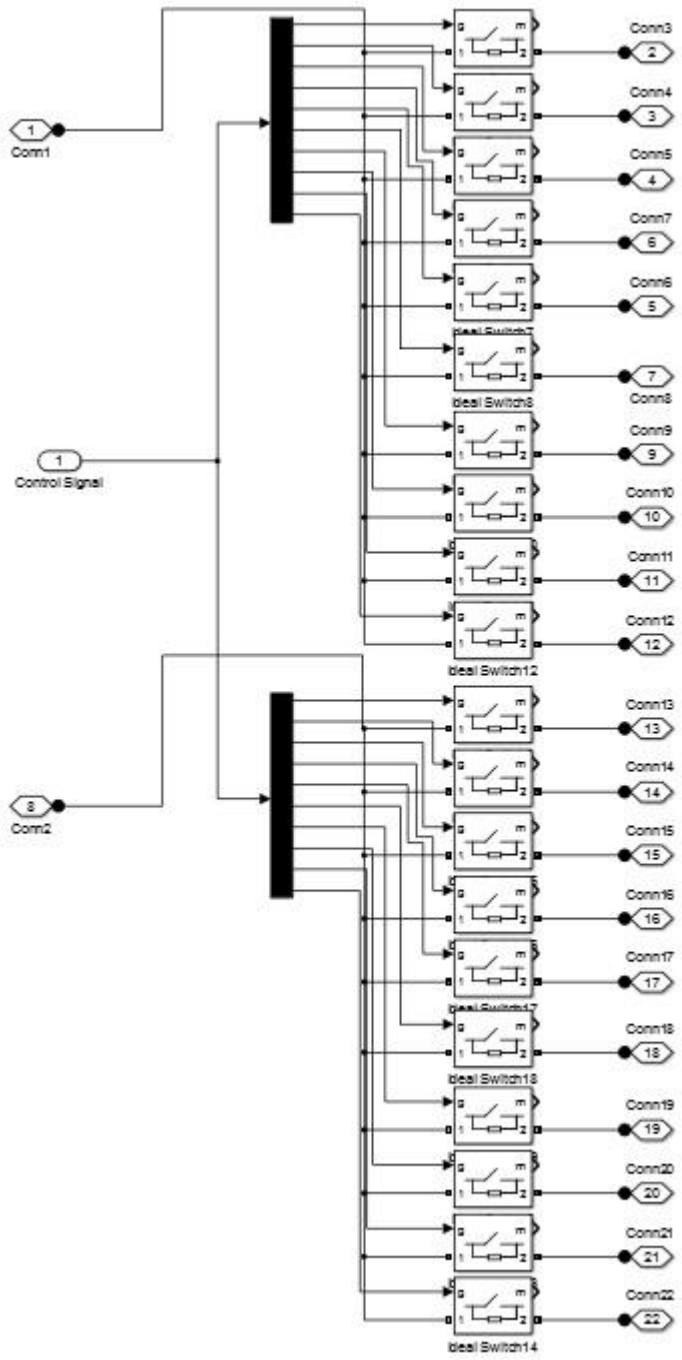


Figure 4.17: Internal Structure of the "Switching Subsystem"

The simulations are performed for 4 different shading scenarios or irradiance profiles as presented in Figure 4.9. Different irradiance threshold values, $\Delta G$, are utilized during simulations and the results are compared. The simulation results have shown that $\Delta G > 0.1\bar{G}$ almost does not provide any contribution to power generation by the PV array under all examined 4 different irradiance profiles. Thus, totally 4 different

irradiance thresholds between 0 and $0.1\bar{G}$ are utilized during simulations. The mentioned irradiance threshold values are considered as $\Delta G = 0.025\bar{G}$, $\Delta G = 0.05\bar{G}$, $\Delta G = 0.075\bar{G}$ and $\Delta G = 0.1\bar{G}$. It has been observed that array reconfiguration is not applicable under the 1st shading scenario representing overcast sky conditions due to almost uniform distribution of irradiance values. As it could be expected, the higher irradiance threshold values have resulted in lower number of module reconfigurations and therefore switching actions, while higher number of PV module reconfigurations and therefore switching actions are observed under lower irradiance threshold values. The simulation results have also shown that $\Delta G > 0.075\bar{G}$ and $\Delta G < 0.025\bar{G}$ do not provide any contribution to the array`s maximum power point, $P_{max}$, as a result of array reconfiguration under the 4th and 3rd irradiance profiles. The maximum improvement of the array`s power generation under the 2nd shading scenario has been achieved with $\Delta G = 0.05\bar{G}$ as a result of the existing irradiance distributions under the mentioned irradiance profile. Table 4.2 provides information regarding the PV array`s maximum power before array reconfiguration, $P_{NR}$, the array`s maximum power point under the ideal case in terms of irradiance equalization, $P_{OPT.}$, the number of switching actions performed by the switching matrix in order to form the final reconfigured array configuration, $N_{SW}$, and the achieved maximum power point, $P_{max}$, as a result of the array reconfiguration, corresponding to different irradiance threshold values under the previously mentioned irradiance profiles. The mentioned ideal case can be defined as the case under which the average irradiance values of all rows of the PV array are exactly equal to the array`s average irradiance value under each utilized irradiance profile or shading scenario.

Table 4.2: $P_{NR}$, $P_{OPT.}$, $P_{max}$ *(kW)* and $N_{SW}$ Corresponding to Different Irradiance Thresholds for the Utilized Irradiance Profiles

| $\Delta G$ | **2nd Shading Scenario** | | | **3rd Shading Scenario** | | | **4th Shading Scenario** | | |
|---|---|---|---|---|---|---|---|---|---|
| | **($P_{NR}$=3.695, $P_{OPT.}$=3.871, $P_{OPT.}/P_{NR}$= 1.047)** | | | **($P_{NR}$=4.449, $P_{OPT.}$=4.731, $P_{OPT.}/P_{NR}$=1.063)** | | | **($P_{NR}$=4.286, $P_{OPT.}$=4.406, $P_{OPT.}/P_{NR}$=1.027)** | | |
| | $N_{SW}$ | $P_{max}$ | $P_{max}/P_{NR}$ | $N_{SW}$ | $P_{max}$ | $P_{max}/P_{NR}$ | $N_{SW}$ | $P_{max}$ | $P_{max}/P_{NR}$ |
| $0.1\bar{G}$ | 17 | 3.74 | 1.012 | 42 | 4.68 | 1.053 | 9 | 4.28 | 1 |
| $0.075\bar{G}$ | 54 | 3.80 | 1.029 | 47 | 4.69 | 1.055 | 9 | 4.28 | 1 |
| $0.05\bar{G}$ | 68 | 3.86 | 1.044 | 57 | 4.72 | 1.061 | 66 | 4.39 | 1.025 |
| $0.025\bar{G}$ | 83 | 3.86 | 1.046 | 57 | 4.72 | 1.061 | 76 | 4.40 | 1.027 |

According to the results, the highest improvement of the array`s maximum power production has been observed with $\Delta G = 0.025\bar{G}$. The array`s maximum power point has been improved by 4.7%, 6.1% and 2.7% as a result of array reconfiguration under the 2nd, 3rd and 4th shading scenarios or irradiance profiles, respectively, for $\Delta G = 0.025\bar{G}$. Figure 4.18 shows variations of the array`s output power generation along with the switching numbers performed by the switching matrix in order to form the reconfigured PV array for different irradiance threshold values under different shading scenarios or irradiance profiles.

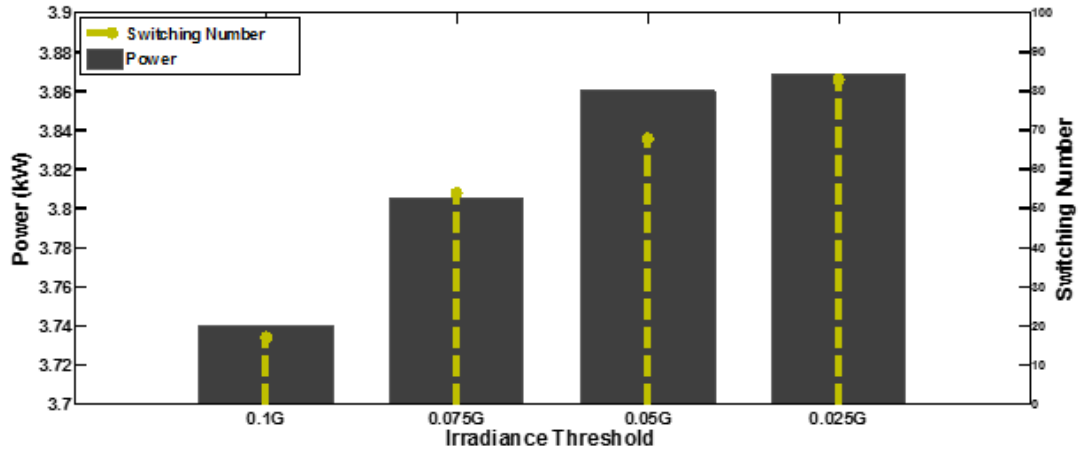


(a)

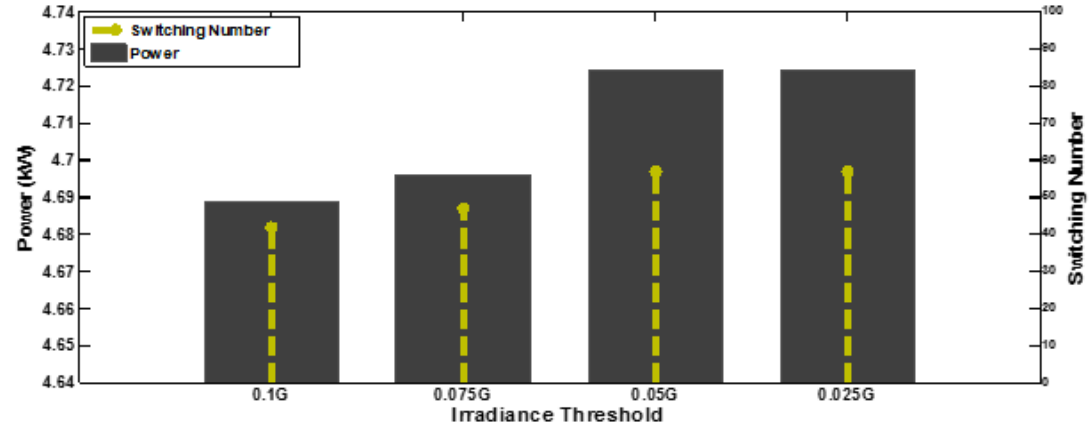


(b)

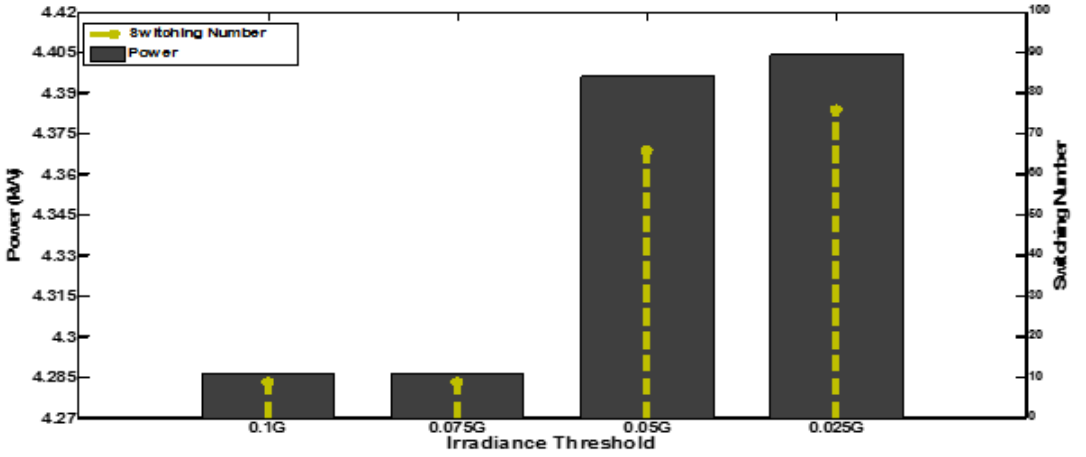


(c)

Figure 4.18: Switching Numbers, Array`s Maximum Power Point and Irradiance Threshold Values for (a) the 2nd, (b) the 3rd, (c) the 4th Shading Scenario

The obtained results suggest that $\Delta G = 0.05\bar{G}$ would be an appropriate irradiance threshold value for the irradiance profiles utilized during the analyses, taking into consideration both the number of switching actions and improvements of the array`s

power production. Obviously it can be expected that the proper irradiance threshold values and the corresponding improvements in array`s power generation may vary under different irradiance profiles obtained as a result of the existing cloud coverage and cloud distribution in the sky.

PV Array`s P-V characteristic curves are presented in Figure 4.19 before and after array reconfiguration for the utilized different shading scenarios and irradiance threshold values. The figure obviously puts forth the improving effects of array reconfiguration on array`s maximum power point values after reconfiguration under different irradiance profiles, where array reconfiguration is applicable. Also it has been observed that the applied irradiance threshold, $\Delta G$, has an smoothing effect on the array`s characteristic curves, where smaller values of irradiance threshold have resulted in closer characteristic curves to the ideal case, in terms of irradiance equalization. Obviously this is achieved to the cost of higher number of reconfigurations and switching actions performed by the switching matrix. The figure also presents the P-V characteristic curves for the ideal case from irradiance equalization point of view. It is shown that there is almost no difference between array`s maximum power point value, $P_{max}$, obtained as a result of the proposed array reconfiguration and the maximum power point obtained under ideal case, for each irradiance profile.

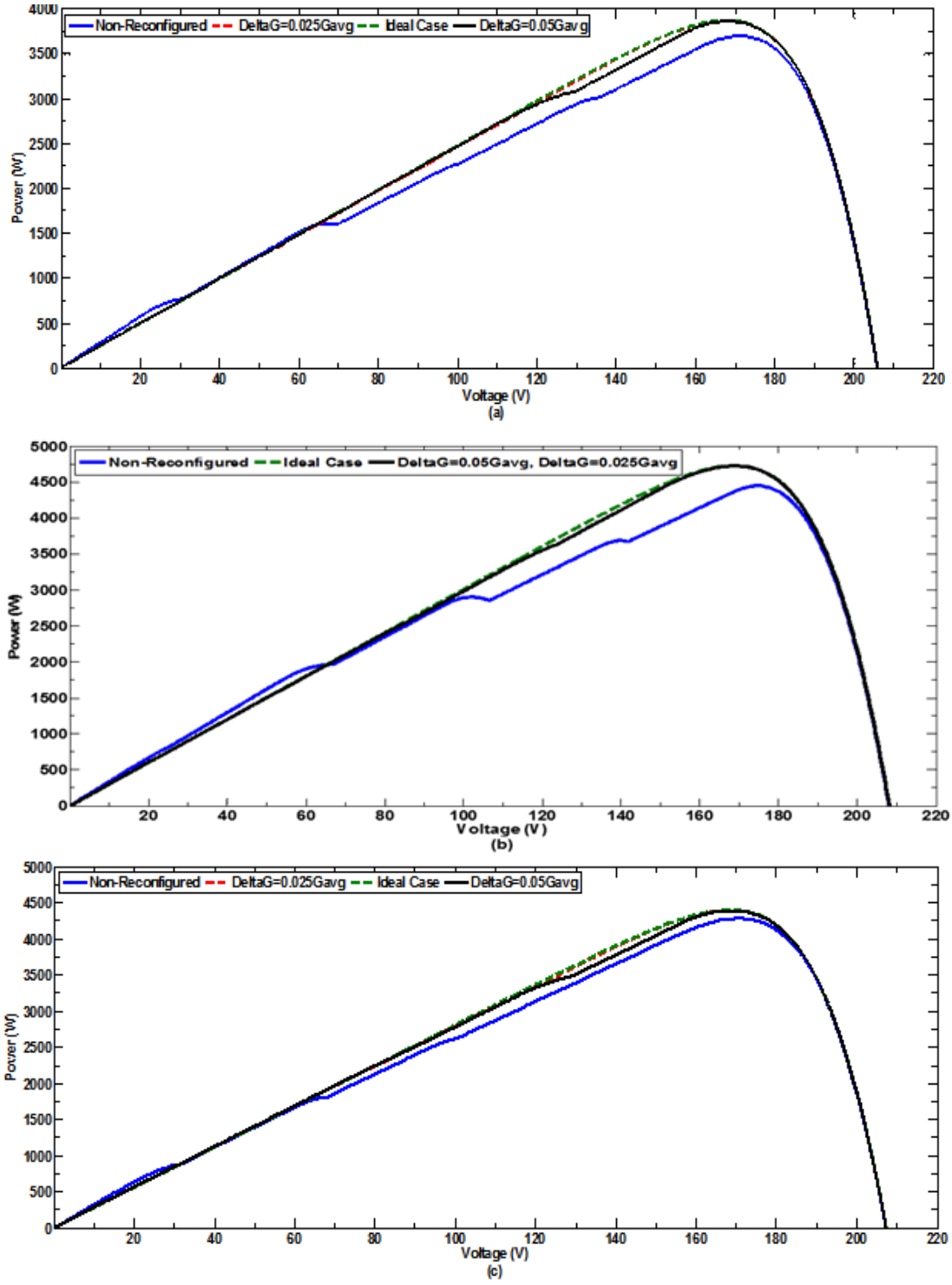


Figure 4.19: PV Array`s P-V Characteristic Curves Before and After Array Reconfiguration together with the Ideal Case for (a) the 2nd, (b) the 3rd, (c) the 4th Irradiance Profile

The developed PV array reconfiguration algorithm has been tested and the results have been provided for only one geographical location and an identical time instant.

However, the provided results are considered as representatives of the performance of the proposed reconfiguration strategy and its capability to improve array`s power generation under non-identical irradiance profiles. The reconfiguration model is provided as a global model which can be applied to any PV array at any geographical location subject to any irradiance profile. It is also expected that the proposed reconfiguration strategy will provide better performance when the existing irradiance profiles contain irradiance values with higher dispersion ranges as a result of the existing cloud coverage and its distribution in the sky.

As it was mentioned previously, application of an irradiance threshold can prevent reconfiguration of some rows of a PV array. Hence, it is obvious that all of the switching devices should not necessarily perform at the same time. On the other hand, elimination of unnecessary switching actions is another means by which performing of some switching devices under an existing irradiance profile is avoided. Taking both of the above mentioned factors into consideration, it can be concluded that the number of switching actions performed by the switching matrix as a result of application of array reconfiguration algorithm depends on the existing cloud coverage in the sky and the resulting irradiance profile incident on the extent of PV arrays. As an example, only 83 out of totally 200 switching devices should perform in order to form the final reconfigured array configuration under the 2$^{nd}$ irradiance profile with $\Delta G = 0.025\bar{G}$.

# Chapter 5

# CONCLUSIONS

Numerous methods have been introduced in the literature in order to analyze the performance of PV modules under variable environmental conditions. Mathematical modeling of a PV module is a widely utilized method in the literature for the mentioned analysis purposes. Various methods have been introduced among which, the one-diode mathematical model of a PV cell has a simple structure alongside the reliable results obtained with this modeling method. This thesis utilizes one-diode mathematical model of a PV cell for analysis purposes. A simple model for a PV module, as a combination a number of series and parallel connected PV cells, is developed in the thesis in MATLAB/Simulink environment based on one-diode mathematical model of a PV cell. The developed model for simulation of the performance of a PV module has been tested and successfully verified to be capable of simulation of the module`s performance under variable environmental conditions. It has been observed that performance of a PV module highly depends on the environmental conditions such as the incident solar irradiance as well as the module`s working temperature values. Once the simulation model for a PV module is developed successfully, PV arrays can also be simulated as a combination of a number of series and parallel connected PV modules having different interconnection architectures.

Performance of PV systems highly depends on the amounts of the incident solar irradiance and therefore partial shading of PV power plants mostly caused by cloud

passages can dramatically reduce power production in a PV power plant. Thus, having precise and accurate knowledge regarding the incident solar irradiance values on the surface of each individual PV module within a PV power plant is a mandatory factor for PV system design and management purposes. Also determination of strategies in order to combat the negative effects of partial shading requires detailed information regarding the irradiance values received by different PV modules in a PV power plant. This thesis introduces a novel modeling method in order to generate site-specific Spatially Dispersed Irradiance Profiles (SDIPs) based on the existing clouds in the sky. The proposed method utilizes real sky images in order to obtain cloud maps and cloud shadow patterns on the extent of application areas or PV power plants. Different cloud types and classes together with their light interaction characteristics or cloud transmission coefficients are also considered by the model in order to reflect the effect of sunlight interaction characteristics of each cloud type on the magnitude of the incident irradiance values. The performance of the proposed model has successfully been verified using various sets of measured data. The results obtained with the model has shown a wide dispersion range of irradiance values contained in spatially dispersed irradiance profiles at each time instant as a direct result of the existing cloud coverage and its distribution in the sky. The need for and significance of such an irradiance model which is capable of providing reliable site-specific irradiance data for different observation points based on the existing cloud coverage, its distribution in the sky and light interaction characteristics can obviously be observed for accurate PV system design and management purposes as well as power yield estimations in a PV power plant.

Once the PV modules are modeled and the incident irradiance profiles are obtained for the desired geographical areas, the performance of PV arrays can be analyzed under

the existing irradiance profiles or partial shading effects and proper measures can be taken in order to reduce or prevent the negative effects of partial shading or other factors that limit the performance of PV arrays such as module mismatch, etc. Numerous strategies and methods have been introduced in the literature for the mentioned purposes. Non-identical or variable electrical characteristics of PV modules caused by the utilized different materials and module manufacturing processes is defined as module mismatch. Obviously module mismatch is a factor which limits performance of PV arrays due to differences in power generation by different types of PV modules. Therefore, the ideal preventive measure in order to avoid the reducing effects of module mismatch is to utilize identical PV modules within each PV array. In this way, the performance of all PV modules will be similar under identical irradiance profiles and hence, none of the PV modules will limit power production by the other modules. However, under real-world conditions utilization of exactly similar PV modules may not always be possible and hence module mismatch may cause the array`s practical maximum power point be less than the sum of the maximum power points of all utilized PV modules within the array. Also partial or full shading of a number of PV modules in a PV array is another factor which limits the performance of the array as well as causing hotspot problems. Utilization of bypass diodes is a measure which can be taken against limiting effects of module mismatch or negative effects of partial or full shading of some PV modules and the resulting hotspot problems.

Utilization of dynamic reconfiguration strategies in order to improve array`s power generation under partial shading conditions is a leading-edge research area. This thesis introduces a simple adaptive dynamic reconfiguration algorithm for PV arrays. The adaptive nature of the mentioned algorithm comes from the fact that the proposed

algorithm performs array reconfiguration based on site-specific irradiance profiles generated using real sky images based on the existing cloud coverage and distribution in the sky. The analysis results have shown that application of the proposed reconfiguration algorithm has improved array`s power generation under all shading scenarios or irradiance profiles, where array reconfiguration is applicable. It has been observed that the magnitude of improvements in array`s power generation depends on the existing irradiance profiles. The results have shown that the proposed array reconfiguration algorithm has successfully been able to improve array`s power generation under all irradiance profiles as much as it would be possible under ideal case in terms of irradiance equalization. Although the reconfiguration algorithm has been tested and the results provided for a single geographical area at an identical instant of time, the algorithm is expected to be applicable in order to improve power generation in PV arrays located at any geographical location and under any type of irradiance profiles. The proposed reconfiguration algorithm is expected to provide higher performance under irradiance profiles containing wide range of highly dispersed irradiance values. The PV modules analyzed in this thesis are considered to be identical in terms of their electrical characteristics and hence, the negative effects of module mismatch, wiring, etc. has not been taken into consideration. The main advantages of the proposed algorithm can be considered as its simple structure, high performance, being not limited by the number of the utilized PV modules, conformity to the TCT interconnection and saving the lifetime of switching devices. The proposed algorithm provides higher performance when applied to PV arrays including high number of PV modules, large-scale rooftop PV systems and Building Integrated PV Systems (BIPV) under wide range of irradiance values contained in an irradiance profile, rather than small-scale PV systems utilized for residential purposes.

# REFERENCES


[1] S. S. Hegedus and A. Luque, *Handbook of photovoltaic science and engineering*. West Sussex, UK: Wiley, 2003.

[2] V. M. Fthenakis, "Chapter IV-1 – Overview of Potential Hazards," in *Practical Handbook of Photovoltaics*, 2012, pp. 1083–1096.

[3] D. Feldman, D. Boff, and D. R. Margolis, "Q2/Q3 2016 Solar Industry Update, Sunshot, U.S. Department of Energy (DOE)," 2016.

[4] SolarPowerEurope, "Solar Photovoltaics Jobs & Value Added in Europe," pp. 1–36, 2015.

[5] D. Feldman, R. Margolis, A. Goodrich, G. Barbose, R. Wiser, and N. Darghouth, "Photovoltaic (PV) Pricing Trends: Historical, Recent, and Near-Term Projections," 2012.

[6] K. Vandeligt, P. Sophie, and P. Yves, *Assessment of the Environmental Performance of Solar Photovoltaic Technologies*. 2012.

[7] K. Kaygusuz, "Environmental Impacts of the Solar Energy Systems," *Energy Sources, Part A Recover. Util. Environ. Eff.*, vol. 31, no. 15, pp. 1376–1386, 2009.

[8] S. Jazayeri, P. Kralovic, A. Honarvar, A. Naini, J. Rozhon, R. Shabaneh, and T. Walden, “Comparative Life Cycle Assessment (LCA) of Base Load Electricity Generation in Ontario,” 2008.

[9] N. C. McDonald and J. M. Pearce, “Producer responsibility and recycling solar photovoltaic modules,” *Energy Policy*, vol. 38, no. 11, pp. 7041–7047, Nov. 2010.

[10] R. Mcmonagle, “The Environmental Attributes of Solar PV in the Canadian Context Summary of Findings,” 2006.

[11] M. Raugei, M. Isasa, and P. Fullana Palmer, “Potential Cd emissions from end-of-life CdTe PV,” *Int. J. Life Cycle Assess.*, vol. 17, no. 2, pp. 192–198, Feb. 2012.

[12] C. A. Wolden, J. Kurtin, J. B. Baxter, I. Repins, S. E. Shaheen, J. T. Torvik, A. A. Rockett, V. M. Fthenakis, and E. S. Aydil, “Photovoltaic manufacturing: Present status, future prospects, and research needs,” *J. Vac. Sci. Technol. A Vacuum, Surfaces, Film.*, vol. 29, no. 3, p. 30801, May 2011.

[13] M. Raugei and V. Fthenakis, “Cadmium flows and emissions from CdTe PV: future expectations,” *Energy Policy*, vol. 38, no. 9, pp. 5223–5228, Sep. 2010.

[14] A. J. McEvoy, T. Markvart, and L. Castañer, *Practical handbook of photovoltaics : fundamentals and applications*. Academic Press, 2012.

[15] P. Sinha, C. J. Kriegner, W. A. Schew, S. W. Kaczmar, M. Traister, and D. J. Wilson, "Regulatory policy governing cadmium-telluride photovoltaics: A case study contrasting life cycle management with the precautionary principle," *Energy Policy*, vol. 36, no. 1, pp. 381–387, Jan. 2008.

[16] V. Fthenakis and H. C. Kim, "Life-cycle uses of water in U.S. electricity generation," *Renew. Sustain. Energy Rev.*, vol. 14, no. 7, pp. 2039–2048, Sep. 2010.

[17] D. Schüler, M. Buchert, R. Liu, S. Dittrich, and C. Merz, "Study on Rare Earths and Their Recycling," Darmstadt, 2011.

[18] D. Kammen, J. Nelson, A. Mileva, and J. Johnston, "An Assessment of the Environmental Impacts of Concentrator Photovoltaics and Modeling of Concentrator Photovoltaic Deployment Using the SWITCH Model | Renewable and Appropriate Energy Laboratory." [Online]. Available: http://rael.berkeley.edu/old_drupal/node/781. [Accessed: 08-Sep-2017].

[19] V. Fthenakis and H. C. Kim, "Land use and electricity generation: A life-cycle analysis," *Renew. Sustain. Energy Rev.*, vol. 13, no. 6–7, pp. 1465–1474, Aug. 2009.

[20] K. Zweibel, "The Impact of Tellurium Supply on Cadmium Telluride Photovoltaics," *Science (80-. ).*, vol. 328, no. 5979, 2010.

[21] W. D. Grossmann, I. Grossmann, and K. Steininger, “Indicators To Determine Winning Renewable Energy Technologies with an Application to Photovoltaics,” *Environ. Sci. Technol.*, vol. 44, no. 13, pp. 4849–4855, Jul. 2010.

[22] M. Graebig, S. Bringezu, and R. Fenner, “Comparative analysis of environmental impacts of maize–biogas and photovoltaics on a land use basis,” *Sol. Energy*, vol. 84, no. 7, pp. 1255–1263, Jul. 2010.

[23] D. Turney and V. Fthenakis, “Environmental impacts from the installation and operation of large-scale solar power plants,” *Renew. Sustain. Energy Rev.*, vol. 15, no. 6, pp. 3261–3270, Aug. 2011.

[24] “Solar parks – Opportunities for Biodiversity Background information from the German Renewable Energies Agency,” 2010.

[25] L. Krueger, “Overview of Firts Solar`s Module Collection and Recycling Program,” in *2nd International Conference on PV Module Recycling*, 2011.

[26] J. H. Wohlgemuth, “Standards for pv modules and components – Recent developments and challenges,” *27th Eur. Photovolt. Sol. Energy Conf. Exhib.*, vol. 16560, no. October, pp. 2976–2980, 2012.

[27] Y. T. Tan, D. S. Kirschen, and N. Jenkins, “A Model of PV Generation Suitable for Stability Analysis,” *IEEE Trans. Energy Convers.*, vol. 19, no. 4, pp. 748–755, Dec. 2004.

[28] A. Kajihara and T. Harakawa, “Model of photovoltaic cell circuits under partial shading,” *Proc. IEEE Int. Conf. Ind. Technol.*, vol. 2005, pp. 866–870, 2005.

[29] Weidong Xiao, W. G. Dunford, and A. Capel, “A novel modeling method for photovoltaic cells,” in *2004 IEEE 35th Annual Power Electronics Specialists Conference (IEEE Cat. No.04CH37551)*, pp. 1950–1956.

[30] N. Celik and N. Acikgoz, “Modeling and experimental verification of the operating current of mono-crystalline photovoltaic modules using four- and five-parameter models,” *Appl. Energy*, vol. 84, no. 1, pp. 1–15, 2007.

[31] C. Carrero, J. Amador, and S. Arnaltes, “A single procedure for helping PV designers to select silicon PV module and evaluate the loss resistances,” *Renew. Energy*, vol. 32, no. 15, pp. 2579–2589, 2007.

[32] S. Liu and R. A. Dougal, “Dynamic multiphysics model for solar array,” *IEEE Trans. Energy Convers.*, vol. 17, no. 2, pp. 285–294, 2004.

[33] M. G. Villalva, J. R. Gazoli, and E. R. Filho, “Comprehensive Approach to Modeling and Simulation of Photovoltaic Arrays,” *IEEE Trans. Power Electron.*, vol. 24, no. 5, pp. 1198–1208, 2009.

[34] M. Jazayeri, S. Uysal, and K. Jazayeri, “A simple MATLAB/Simulink simulation for PV modules based on one-diode model,” in *High Capacit. Opt. Networks Emerging/Enabling Technol. HONET-CNS*, pp. 44–50, Dec. 2013.

[35] J. a. Gow and C. D. Manning, “Development of a photovoltaic array model for use in power-electronics simulation studies,” *IEE Proc. - Electr. Power Appl.*, vol. 146, no. 2, p. 193, 1999.

[36] S. Chowdhury, G. A. Taylor, S. P. Chowdhury, A. K. Saha, and Y. H. Song, “Modelling, simulation and performance analysis of a PV array in an embedded environment,” in *2007 42nd International Universities Power Engineering Conference*, 2007, pp. 781–785.

[37] K. Ishaque, Z. Salam, and Syafaruddin, “A comprehensive MATLAB Simulink PV system simulator with partial shading capability based on two-diode model,” *Sol. Energy*, vol. 85, no. 9, pp. 2217–2227, 2011.

[38] K. Ishaque, Z. Salam, and H. Taheri, “Simple, fast and accurate two-diode model for photovoltaic modules,” *Sol. Energy Mater. Sol. Cells*, vol. 95, no. 2, pp. 586–594, 2011.

[39] S. K. Kim, J. H. Jeon, C. H. Cho, E. S. Kim, and J. B. Ahn, “Modeling and simulation of a grid-connected PV generation system for electromagnetic transient analysis,” *Sol. Energy*, vol. 83, pp. 664–678, 2009.

[40] C. Sah, R. Noyce, and W. Shockley, “Carrier Generation and Recombination in P-N Junctions and P-N Junction Characteristics,” *Proc. IRE*, vol. 45, no. 9, pp. 1228–1243, Sep. 1957.

[41] H. Tian, F. Mancilla-David, K. Ellis, P. Jenkins, and E. Muljadi, "A Detailed Performance Model for Photovoltaic Systems: Preprint," 2012.

[42] W. Desoto, S. Klein, and W. Beckman, "Improvement and validation of a model for photovoltaic array performance," *Sol. Energy*, vol. 80, pp. 78–88, 2006.

[43] M. Jazayeri, S. Uysal, and K. Jazayeri, "A simple MATLAB/Simulink simulation for PV modules based on one-diode model," in *High Capacity Optical Networks and Emerging/Enabling Technologies, HONET-CNS*, pp.44-50, Dec. 2013.

[44] L. T. Wong and W. K. Chow, "Solar radiation model," *Appl. Energy*, vol. 69, no. 3, pp. 191–224, 2001.

[45] ASHRAE, *ASHRAE Handbook*. Atalanta: HVAC publications, 1999.

[46] Iqbal, *an introduction to solar radiation*. Toronto: Academic press, 1983.

[47] J. A. Davies and D. C. McKay, "Evaluation of selected models for estimating solar radiation on horizontal surfaces," *Sol. Energy*, vol. 43, pp. 153–168, 1989.

[48] C. Gueymard, "Mathematically integrable parametrization of clear-sky beam and global irradiances and its use in daily irradiation applications," *Sol. Energy*, vol. 50, no. 5, pp. 385–397, 1993.

[49] B. Y. h. Liu and R. C. Jordan, “The inter-relationship and characteristic distribution of direct, diffue and total solar radiation,” *Sol. Energy*, vol. 4, no. 3, pp. 1–19, 1960.

[50] D. G. Erbs, S. A. Klein, and J. A. Duffie, “Eastimation of the diffuse radiation fraction for hourly, daily and monthly-average global radiation,” *Sol. Energy*, vol. 28, no. 4, pp. 293–302, 1982.

[51] D. T. Reindl, W. A. Beckman, and J. A. Duffie, “Diffuse fraction corrections,” *Sol. Energy*, vol. 45, no. 1, pp. 1–7, 1990.

[52] A. Skartveit and J. A. Olseth, “A model for diffuse fraction of hourly global radiation,” *Sol. Energy*, vol. 38, no. 4, pp. 271–274, 1987.

[53] A. Louche, G. Notton, P. Poggi, and G. Simonnot, “Correlations for direct normal and global horizontal irradiations on a French Mediterranean site,” *Sol. Energy*, vol. 46, no. 4, pp. 261–266, 1991.

[54] C. A. Gueymard, “Clear-sky irradiance predictions for solar resource mapping and large-scale applications: Improved validation methodology and detailed performance analysis of 18 broadband radiative models,” *Sol. Energy*, vol. 86, no. 8, pp. 2145–2169, 2012.

[55] K. Scharmer and J. Greif, *The European Solar Radiation Atlas, Vol.1: Fundamentals and Maps*. Paris, France: Les Presses de l`Ecole des Mines, 2000.

[56] G. Notton, C. Cristofari, M. Muselli, P. Poggi, and N. Heraud, “Hourly Solar Irradiations Estimation : From Horizontal Measurements to Inclined Data,” in *2006 First International Symposium on Environment Identities and Mediterranean Area*, 2006, pp. 234–239.

[57] K. Jazayeri, S. Uysal, and M. Jazayeri, “MATLAB/simulink based simulation of solar incidence angle and the sun’s position in the sky with respect to observation points on the Earth,” in *Proceedings of 2013 International Conference on Renewable Energy Research and Applications, ICRERA*, pp.173-177, pp.173-177, Oct. 2013.

[58] M. Jazayeri, S. Uysal, and K. Jazayeri, “A case study on solar data collection and effects of the sun’s position in the sky on solar panel output characteristics in Northern Cyprus,” in *Proceedings of 2013 International Conference on Renewable Energy Research and Applications, ICRERA*, pp.184-189, Oct. 2013.

[59] P. Jones, “Cloud-cover distribution and correlations,” *J. Appl. Meteorol.*, vol. 31, pp. 732–741, 1992.

[60] A. Ångström, “Solar and terrestrial radiation,” *Q. J. Roy. Met. Soc.*, vol. 4, pp. 121–126, 1924.

[61] J. A. Prescott, “Evaporation from a water surface in relation to solar radiation,” *Trans. Roy. Soc. South Aust.*, vol. 64, pp. 114–125, 1940.

[62] M. R. Rietveld, “A new method for estimating the regression coefficients in the formula relating solar radiation to sunshine duration,” *Agric. Meteorol.*, vol. 19, pp. 243–352, 1978.

[63] K. K. Gopinathan, “A general formula for computing the coefficients of the correction connecting the global solar-radiation to sunshine duration,” *Sol. Energy*, vol. 41, no. 6, pp. 449–502, 1988.

[64] C. Gueymard, P. Jindra, and V. Estrada-Cajigal, “A critical look at recent interpretations of the Ångström approach and its future in global solar radiation predictions,” *Sol. Energy*, vol. 54, no. 5, pp. 357–363, 1995.

[65] “Nasa Langley Research Center,” 2016. [Online]. Available: https://eosweb.larc.nasa.gov/cgi-bin/sse/sse.cgi?+s01+s07#s07. [Accessed: 01-Jan-2016].

[66] A. M. G. Klein Tank, “Daily dataset of 20th-century surface air temperature and percipitation series for the European Climate Assessment.,” *Int. J. Clim.*, no. 22, pp. 1441–1453, 2002.

[67] A. Lanetz, V. Lyubanski, I. Setter, B. Kriheli, E. G. Evseev, and A. I. Kudish, “Inter-comparison of different models for estimating clear sky solar global radiation for the Negev region in Israel,” *Energy Convers. Manag.*, vol. 48, pp. 259–268, 2007.

[68] K. Kondratyev, *Radiation in the atmosphere*. New York: Academic Press, 1969.

[69] A. J. Biga and R. Rosa, "Estimating solar irradiation sums from sunshine and cloudiness observations," *Sol. Energy*, vol. 25, pp. 265–272, 1980.

[70] A. Padovan and D. Del Col, "Measurement and modeling of solar irradiance components on horizontal and tilted planes," *Sol. Energy*, vol. 84, no. 12, pp. 2068–2084, 2010.

[71] S. Nijmeh and R. Mamlook, "Testing of two models for computing global solar radiation on tilted surfaces," *Renew. Energy*, vol. 20, no. 1, pp. 75–81, 2000.

[72] D. T. Reindl, W. A. Beckman, and J. A. Duffie, "Evaluation of hourly tilted surface radiation models," *Sol. Energy*, vol. 45, pp. 9–17, 1990.

[73] V. Badescu, "3D isotropic approximation for solar diffuse irradiance on tilted surfaces," *Renew. Energy*, vol. 26, pp. 221–223, 2002.

[74] Y. Q. Tian, R. J. Davies-Colley, P. Gong, and B. W. Thorrold, "Estimating solar radiation on slopes of arbitrary aspect," *Agric. For. Meteorol.*, vol. 109, pp. 67–74, 2001.

[75] P. S. Koronakis, "On the choice of the angle of tilt for south facing solar collectors in the Athens basin area," *Sol. Energy*, vol. 36, pp. 217–225, 1986.

[76] B. Liu and R. Jordan, “Daily insolation on surfaces tilted towards the equator,” *Trans ASHRAE*, vol. 41, pp. 67–526, 1962.

[77] R. Perez, P. Ineichen, and R. Seals, “Modelling daylight availability and irradiance components from direct and global irradiance,” *Sol. Energy*, vol. 44, pp. 271–289, 1990.

[78] J. E. Hay, “Calculation of monthly mean solar radiation for horizontal and inclined surfaces,” *Sol. Energy*, vol. 23, pp. 301–330, 1979.

[79] A. Skartveit and J. A. Olseth, “Modelling slope irradiance at high latitudes,” *Sol. Energy*, vol. 36, pp. 333–344, 1986.

[80] M. D. Steven and M. H. Unsworth, “The angular distribution and interception of diffuse solar radiation below overcast skies,” *Q. J. R. Meteorol. Soc.*, vol. 106, pp. 57–61, 1980.

[81] R. C. Temps and K. L. Coulson, “Solar radiation incident upon slopes of different orientations,” *Sol. Energy*, vol. 19, pp. 179–184, 1977.

[82] “WRMC-BSRN,” 2016. [Online]. Available: http://bsrn.awi.de/. [Accessed: 20-May-2016].

[83] R. Posselt, R. Müller, R. Stöckli, and J. Trentmann, “CM SAF Surface Radiation MVIRI Data Set 1.0 - Monthly Means / Daily Means / Hourly Means.,” 2011.

[84] K. Behrens, “Expanded measurements from station Lindenberg (2007-07),” Jan. 2016.

[85] H. Morf, “A stochastic solar irradiance model adjusted on the Ångström-Prescott regression,” *Sol. Energy*, vol. 87, no. 1, pp. 1–21, 2013.

[86] W. Schüepp, “Direct and scaterred radiation reaching the earth, as influenced by atmospheric, geographical and astronomical factors,” in *Solar Radiation*, N. Robinson, Ed. Amesterdam: Elsevier, 1966, pp. 111–160.

[87] M. Jazayeri, K. Jazayeri, and S. Uysal, “Generation of spatially dispersed irradiance time-series based on real cloud patterns,” *Sol. Energy*, vol. 158, pp. 977–994, 2017.

[88] J. S. G. Ehnberg and M. H. J. Bollen, “Simulation of global solar radiation based on cloud observations,” *Sol. Energy*, vol. 78, no. 2, pp. 157–162, 2005.

[89] H. Morf, “The stochastic two-state irradiance model (STSIM),” *Sol. Energy*, vol. 62, pp. 101–112, 1998.

[90] V. Badescu, “A new kind of cloudy sky model to compute instantaneous values of diffuse and global solar irradiance,” *Theor. Appl. Climatol.*, vol. 72, pp. 127–136, 2002.

[91] H. Yang, B. Kurtz, D. Nguyen, B. Urquhart, C. W. Chow, M. Ghonima, and J. Kleissl, "Solar irradiance forecasting using a ground-based sky imager developed at UC San Diego," *Sol. Energy*, vol. 103, pp. 502–524, 2014.

[92] C. W. Chow, B. Urquhart, M. Lave, A. Dominguez, J. Kleissl, J. Shields, and B. Washom, "Intra-hour forecasting with a total sky imager at the UC San Diego solar testbed," *Sol. Energy*, vol. 85, pp. 2881–2893, 2011.

[93] R. Perez, S. Kivalov, J. Schlemmer, K. Hemker Jr., D. Renne, and T. E. Hoff, "Validation of short and medium term operational solar radiation forecasts in US.," *Sol. Energy*, vol. 84, no. 12, pp. 2161–2172, 2010.

[94] M. C. Allmen and W. P. Kegelmeyer, "The computation of cloud-base height from paired whole-sky imaging cameras," *J. Atmos. Ocean. Technol.*, vol. 13, pp. 97–113, 1996.

[95] A. Heinle, A. Macke, and A. Srivastav, "Automatic cloud classification of whole sky images," *Atmos. Meas. Tech.*, vol. 3, no. 3, pp. 557–567, 2010.

[96] J. Huo and D. Lu, "Cloud determination of all-sky images under low visibility conditions," *J. Atmos. Ocean. Technol.*, vol. 26, no. 10, pp. 2172–2180, 2009.

[97] J. Huo and D. Lu, "Preliminary retrieval of aerosol optical depth from allsky images," *Adv. Atmos. Sci.*, vol. 27, no. 2, pp. 421–426, 2010.

[98] E. Kassianov, C. Long, and J. Christy, "Cloud base-height estimation frompaired ground-based hemispherical observations," *J. Appl. Meteorol.*, vol. 44, pp. 1221–1233, 2005.

[99] C. Long, J. Sabburg, J. Calbo, and D. Pages, "Retrieving cloud characterisitcs from ground-based daytime color all-sky images," *J. Atmos. Ocean. Technol.*, vol. 23, no. 633–652, 2006.

[100] G. Pfister, R. McKenzie, J. Liley, and A. Thomas, "Cloud coverage based on all-sky imaging and its impact on surface solar irradiance," *J. Appl. Meteorol.*, vol. 42, no. 1421–1434, 2003.

[101] G. Seiz, J. Shields, U. Feister, E. Baltsavias, and A. Gruen, "Cloud mapping with ground-based photogrammetric cameras," *Int. J. Remote Sens.*, vol. 28, no. 9, pp. 2001–2032, 2007.

[102] D. Nguyen and J. Kleissl, "Stereographic methods for cloud base height determination using two sky imagers," *Sol. Energy*, vol. 107, pp. 495–509, 2014.

[103] A. Nguyen, M. Velay, J. Schoene, V. Zheglov, B. Kurts, K. Murray, B. Torre, and J. Kleissl, "High PV penetration impacts on five local distribution networks using high resolution solar resource assessment with sky imager and quasi-steady state distribution system simulations," *Sol. Energy*, vol. 132, pp. 221–235, 2016.

[104] G. M. Lohmann, A. Hammer, A. H. Monahan, T. Schmidt, and D. Heinemann, "Simulating clear-sky index increment correlations under mixed sky conditions using a fractal cloud model," *Sol. Energy*, vol. 150, pp. 255–264, 2017.

[105] M. J. Harris, "Real-time cloud simulation and rendering," *ACM SIGGRAPH 2005 Courses - SIGGRAPH '05*, p. 222, 2003.

[106] A. Kokhanovsky, "Optical properties of terrestrial clouds," *Earth-Science Rev.*, vol. 64, no. 3–4, pp. 189–241, 2004.

[107] R. Tapakis and A. G. Charalambides, "Equipment and methodologies for cloud detection and classification: A review," *Sol. Energy*, vol. 95, pp. 392–430, 2013.

[108] J. A. Duffie and W. A. Beckman, *Solar Engineering of Thermal Processes*. Hoboken, New Jersey: Wiley, 2006.

[109] R. W. Johnson, J. E. Shields, and T. L. Koehler, "Analysis & Interpretation of Simultaneous Multi-station Whole Sky Imagery," 1991.

[110] R. Johnson, W. Hering, and J. Shields, "Automated visibility and cloud cover measurements with a solid-state imaging system," 1989.

[111] W. Jewell and R. Ramakumar, "The effect of moving clouds on electric utilities with dispersed photovoltaic generation," *IEEE Trans. Energy Convers.*, vol. EC-2, no. 4, pp. 570–576, 1987.

[112] *International Cloud Atlas*. World Meteorological Organization, 1987.

[113] J. S. Stein, M. J. Reno, and C. W. Hansen, "The variability index: a new and novel metric for quantifying irradiance and PV output variability," in *Word Renewable Energy Forum, Denver, CO.*, 2012.

[114] G. Velasco-Quesada, F. Guinjoan-Gispert, R. Piqué-López, M. Román-Lumbreras, and A. Conesa-Roca, "Electrical PV array reconfiguration strategy for energy extraction improvement in grid-connected PV systems," *IEEE Trans. Ind. Electron.*, vol. 56, no. 11, pp. 4319–4331, 2009.

[115] M. Jazayeri, S. Uysal, K. Jazayeri, and S. Yapici, "Experimental Analysis of Effects of Connection Type on PV System Performance," in *Proceedings of 2013 International Conference on Renewable Energy Research and Applications, ICRERA*, pp.190-195, Oct. 2013.

[116] S. Dezso, "Aalborg Universitet Real-time Modelling, Diagnostics and Optimised MPPT for Residential PV Systems," 2009.

[117] D. P. Hohm and M. E. Ropp, "Comparative study of maximum power point tracking algorithms using an experimental, programmable, maximum power point tracking test bed," in *Conference Record of the Twenty-Eighth IEEE Photovoltaic Specialists Conference - 2000 (Cat. No.00CH37036)*, pp. 1699–1702.

[118] A. A. J. Al Nablusi, “Efficiency Optimization of a Standalone Solar Energy System Using Fuzzy Based MPPT,” 2012.

[119] A. K. Abdelsalam, A. M. Massoud, S. Ahmed, and P. N. Enjeti, “High-Performance Adaptive Perturb and Observe MPPT Technique for Photovoltaic-Based Microgrids,” *IEEE Trans. Power Electron.*, vol. 26, no. 4, pp. 1010–1021, Apr. 2011.

[120] N. Femia, G. Petrone, G. Spagnuolo, and M. Vitelli, “Optimization of Perturb and Observe Maximum Power Point Tracking Method,” *IEEE Trans. Power Electron.*, vol. 20, no. 4, pp. 963–973, Jul. 2005.

[121] K. Ishaque, Z. Salam, M. Amjad, and S. Mekhilef, “An Improved Particle Swarm Optimization (PSO)–Based MPPT for PV With Reduced Steady-State Oscillation,” *IEEE Trans. Power Electron.*, vol. 27, no. 8, pp. 3627–3638, Aug. 2012.

[122] Qian Zhang, Changsheng Hu, Lin Chen, A. Amirahmadi, N. Kutkut, Z. J. Shen, and I. Batarseh, “A Center Point Iteration MPPT Method With Application on the Frequency-Modulated LLC Microinverter,” *IEEE Trans. Power Electron.*, vol. 29, no. 3, pp. 1262–1274, Mar. 2014.

[123] M. Jazayeri, S. Uysal, and K. Jazayeri, “Evaluation of maximum power point tracking techniques in PV systems using MATLAB/Simulink,” in *2014 Sixth Annual IEEE Green Technologies Conference*, pp.54-60, Apr. 2014.

[124] B. N. Alajmi, K. H. Ahmed, S. J. Finney, and B. W. Williams, "Fuzzy-Logic-Control Approach of a Modified Hill-Climbing Method for Maximum Power Point in Microgrid Standalone Photovoltaic System," *IEEE Trans. POWER Electron.*, vol. 26, no. 4, 2011.

[125] A. K. Rai, N. D. Kaushika, B. Singh, and N. Agarwal, "Simulation model of ANN based maximum power point tracking controller for solar PV system," *Sol. Energy Mater. Sol. Cells*, vol. 95, no. 2, pp. 773–778, Feb. 2011.

[126] R. Ramaprabha and B. L. Mathur, "A comprehensive review and analysis of solar photovoltaic array configurations under partial shaded conditions," *Int. J. Photoenergy*, vol. 2012, 2012.

[127] D. Picault, B. Raison, S. Bacha, J. DeLaCasa, and J. Aguilear, "Forecasting photovoltaic array power production subject to mismatch losses," *Sol. Energy*, vol. 84, pp. 1301–1390, 2010.

[128] D. Picault, B. Raison, S. Bacha, J. Aguilera, and J. De La Casa, "Changing photovoltaic array interconnections to reduce mismatch losses: A case study," *2010 9th Conf. Environ. Electr. Eng. EEEIC 2010*, pp. 37–40, 2010.

[129] M. Jazayeri, S. Uysal, and K. Jazayeri, "A comparative study on different photovoltaic array topologies under partial shading conditions," in *Proceedings of the IEEE Power Engineering Society Transmission and Distribution Conference*, Apr. 2014.

[130] M. Z. Shams El-Dein, M. Kazerani, and M. M. a Salama, "Optimal photovoltaic array reconfiguration to reduce partial shading losses," *IEEE Trans. Sustain. Energy*, vol. 4, no. 1, pp. 145–153, 2013.

[131] P. Wilson, J. Storey, and D. Bagnall, "Improved optimization strategy for irradiance equalization in dynamic photovoltaic arrays," *IEEE Trans. Power Electron.*, vol. 28, no. 6, pp. 2946–2956, 2013.

[132] D. Nguyen and B. Lehman, "A reconfigurable solar photovoltaic array under shadow conditions," *Conf. Proc. - IEEE Appl. Power Electron. Conf. Expo. - APEC*, pp. 980–986, 2008.

[133] M. Alahmad, M. A. Chaaban, S. K. Lau, J. Shi, and NealJ., "An adaptive utility interactive photovoltaic system based on a flexible switch matrix to optimize performance in real-time," *Sol. Energy*, vol. 86, no. 3, pp. 951–963, 2012.

[134] M. Jazayeri, K. Jazayeri, and S. Uysal, "Adaptive photovoltaic array reconfiguration based on real cloud patterns to mitigate effects of non-uniform spatial irradiance profiles," *Sol. Energy*, vol. 155, no. C, pp. 506–516, 2017.

[135] B. Patnaik, J. D. Mohod, and S. D. Duttagupta, "Distributed multi-sensor network for real time monitoring of illumination states for a reconfigurable solar photovoltaic array," in *Physics and Technology of Sensors (ISPTS), 2012 1st International Symposium on*, 2012, pp. 106–109.

# APPENDICES

# Appendix A: Generation of Spatially Dispersed Irradiance Time-Series Based on Real Cloud Patterns

Moein Jazayeri, Kian Jazayeri, Sener Uysal, "Generation of spatially dispersed irradiance time-series based on real cloud patterns", *Solar Energy*, vol.158, pp.977-994, 2017.


A B S T R A C T

Clouds, being complex components of the atmosphere, have significant effects on power generation by photovoltaic (PV) systems. For example, shadows caused by the cloud coverage over a geographically distributed PV power plant may cause significant fluctuations in power generation by leaving a number of PV panels unable to generate power and contribute to power generation by the plant at each time instant. Thus, investigation of the mentioned effects on PV power generation requires realistic spatial irradiance information. Such information should be evaluated based on the existing real cloud coverage and its light transmission characteristics. This also provides the opportunity to select appropriate coping strategies against the mentioned negative effects of partial shading on PV plant's power output. This paper presents a modeling approach which generates Spatially Dispersed Irradiance Profiles (SDIPs) for PV arrays based on existing cloud patterns derived from local sky images taken at the application sites. The model gets the direct, diffuse and global irradiance values incident on a horizontal surface, which are primarily obtained utilizing a solar irradiance model (the Morf (2013) model), along with local sky images captured at the application sites and cloud transmittance values, as input data and yields site-specific Spatially Dispersed Irradiance Profiles (SDIPs) incident on the surface of inclined PV panels within PV application areas, as a result of process of the inputs. Utilization of local sky images and cloud transmittance values for different cloud types creates the opportunity for precise analysis of interactions of sunlight with the existing cloud type and hence, obtaining unique and site-specific irradiance profiles according to the existing cloud type and distribution in the sky. The model firstly detects the cloudy and clear-sky parts in the sky image and then instantly utilizes the most appropriate ellipse on the cloud layer associated with each solar panel through which the beam irradiance is received by the panel. The model also considers the light transmission characteristics of different cloud types as the parameter affecting the beam irradiance. The diffuse and ground-reflected irradiance components are assumed to be spatially constant and thus identical for all solar panels. Cloud base heights, as provided in the International Cloud Atlas (1987), are also utilized to calculate the ground area covered by each sky image. Daily irradiance sequences for different observation points in a PV array are simulated under partly cloudy sky conditions using a set of sky images and utilized for validation purpose of the proposed algorithm. It is demonstrated that instantaneous irradiance values, as well as daily irradiance sequences, differ from point to point in a geographically distributed PV application site depending on the distribution of clouds in the sky. The mentioned variable characteristic of the irradiance sequences received at different observation points, as well as the model's capability to reflect the mentioned variabilities, is verified using irradiance data derived from satellite observations. The performance of the proposed model is validated using variability index (VI) metric as a measure of irradiance variability during a day. The modeled VI values are validated against the measured VI values for a reference point located at the center point of the generated irradiance profiles. Daily VI values calculated for both measured and simulated 1-min global horizontal irradiance (GHI) data are compared for a population of totally 117 days during April – August time period. The results of comparison show statistics of mean bias error (MBE) of 0.16, root mean square error (RMSE) of 2.394, correlation coefficient of 0.94 and mean absolute error (MAE) of 1.91. The validation results demonstrate capability and accuracy of the proposed model for estimation of irradiance values under cloudy sky conditions.

# Appendix B: Adaptive Photovoltaic Array Reconfiguration Based on Real Cloud Patterns to Mitigate Effects of Non-Uniform Spatial Irradiance Profiles

Moein Jazayeri, Kian Jazayeri, Sener Uysal, "Adaptive photovoltaic array reconfiguration based on real cloud patterns to mitigate effects of non-uniform spatial irradiance profiles", *Solar Energy*, vol. 155C, 99.506-516, 2017.


ABSTRACT

This paper proposes a simple and dynamic reconfiguration algorithm for photovoltaic (PV) arrays in order to mitigate negative effects of non-uniform spatial irradiance profiles on PV power production. Spatially dispersed irradiance profiles incident on inclined PV module surfaces at each application site are generated based on real sky images. Models of PV modules are constructed in MATLAB/Simulink based on one-diode mathematical model of a PV cell. The proposed dynamic reconfiguration algorithm operates based on irradiance equalization principle aiming for creation of balanced-irradiance series-connected rows of PV modules. The proposed algorithm utilizes an irradiance threshold to obtain near-optimal configurations in terms of irradiance equalization and number of switching actions under any type of non-uniform spatial irradiance profile. The algorithm provides no limits on the number of PV modules within the array. The reconfiguration algorithm is examined with different irradiance profiles and significant improvements, almost equivalent to the ideal case corresponding to equal irradiance for all panels, are achieved for each shading pattern. The advantages of the algorithm are simplicity and providing significant improvements in array's power generation alongside with reduced number of switching actions.

# Appendix C: Artificial Neural Network-Based All-Sky Power Estimation and Fault Detection in Photovoltaic Modules

Kian Jazayeri, Moein Jazayeri, Sener Uysal, "Artificial neural network-based all-sky power estimation and fault detection in photovoltaic modules," *Journal of Photonics for Energy*, vol. 7, no. 2, 2017.

**Abstract.** The development of a system for output power estimation and fault detection in photovoltaic (PV) modules using an artificial neural network (ANN) is presented. Over 30,000 healthy and faulty data sets containing per-minute measurements of PV module output power (W) and irradiance ($W/m^2$) along with real-time calculations of the Sun's position in the sky and the PV module surface temperature, collected during a three-month period, are fed to different ANNs as training paths. The first ANN being trained on healthy data is used for PV module output power estimation and the second ANN, which is trained on both healthy and faulty data, is utilized for PV module fault detection. The proposed PV module-level fault detection algorithm can expectedly be deployed in broader PV fleets by taking developmental considerations. The machine-learning-based automated system provides the possibility of all-sky real-time monitoring and fault detection of PV modules under any meteorological condition. Utilizing the proposed system, any power loss caused by damaged cells, shading conditions, accumulated dirt and dust on module surface, etc., is detected and reported immediately, potentially yielding increased reliability and efficiency of the PV systems and decreased support and maintenance costs.  [DOI: 10.1117/1.JPE.7.025501]

**Keywords:** artificial intelligence; artificial neural networks; fault detection; renewable energy sources; solar energy; sustainable development.

Paper 17017 received Jan. 24, 2017; accepted for publication Apr. 4, 2017; published online Apr. 19, 2017.

# Appendix D: Comparative Analysis of Levenberg-Marquardt and Bayesian Regularization Backpropagation Algorithms in Photovoltaic Power Estimation Using Artificial Neural Network

Kian Jazayeri, Moein Jazayeri, Sener Uysal, "Comparative analysis of levenberg-marquardt and bayesian regularization backpropagation algorithms in photovoltaic power estimation using artificial neural network", in *Proceedings - Lecture Notes in Computer Science (including subseries Lecture Notes in Artificial Intelligence and Lecture Notes in Bioinformatics*), vol. 9728, pp.80-95, New York City, NY, USA, June 2016.

**Abstract.** This paper presents a comparative analysis of Levenberg-Marquardt (LM) and Bayesian Regularization (BR) backpropagation algorithms in development of different Artificial Neural Networks (ANNs) to estimate the output power of a Photovoltaic (PV) module. The proposed ANNs undergo training, validation and testing phases on 10000+ combinations of data including the real-time measurements of irradiance level ($W/m^2$) and PV output power (W) as well as the calculations of the Sun's position in the sky and the PV module surface temperature (°C). The overall performance of the LM and the BR algorithms are analyzed during the development phases of the ANNs, and also the results of implementation of each ANN in different time intervals with different input types are compared. The comparative study presents the trade-offs of utilizing LM and BR algorithms in order to develop the best ANN architecture for PV output power estimation.

## Appendix E: A Comparative Study on Different Photovoltaic Array Topologies under Partial Shading Conditions

Moein Jazayeri, Sener Uysal, Kian Jazayeri, "A comparative study on different photovoltaic array topologies under partial shading conditions", in *Proceedings - IEEE PES T&D Conference and Exposition*, Chicago, IL, USA, April 2014.

***Abstract*—This paper mainly analyzes the performance of different photovoltaic array configurations under various shading patterns. A Matlab/Simulink based simulation model of a PV module is utilized as the smallest building block of the mentioned topologies. The model is validated using the datasheet parameters of the `SOLAREX MSX-60` PV module. The performance and output characteristics of `Series-Parallel`, `Total-Cross-Tied` and `Bridge-Link` array topologies are analyzed and compared using a 6x6 PV array under 6 different shading scenarios. The effects of bypass diodes during partial shading conditions are considered and the analysis results are presented and compared with and without bypass diodes. The mentioned shading scenarios are defined in such a way to simulate the passage of a cloud in different patterns. The results show that all the mentioned topologies have similar performances under identical illuminations while the `Total-Cross-Tied` (TCT) configuration, despite the high complexity of the system, outperforms both `Series-Parallel` (SP) and `Bridge-Link` (BL) structures under partial shading conditions. `Bridge-Link` and `Series-Parallel` configurations stand on the 2nd and 3rd performance stages respectively while a Series-Parallel connection presents the least system complexity. The analyses and results provide detailed information on the characteristics of different array topologies which can be utilized by system designers to estimate the power yield and choose the most appropriate system configuration with respect to the existing environmental conditions to improve the overall efficiency.**

***Keywords*—*array configuration, bridge-link, module characteristics, series-parallel simulink, solar cell, solar energy, solar module, total-cross-tied,***

## Appendix F: Evaluation of Maximum Power Point Tracking Techniques in PV Systems Using MATLAB/Simulink

Moein Jazayeri, Sener Uysal, Kian Jazayeri, "Evaluation of Maximum Power Point Tracking Techniques in PV Systems Using MATLAB/Simulink", in *Proceedings - Sixth Annual IEEE Green Technologies Conference*, pp.54-60, Corpus Christi, TX, USA, April 2014.

***Abstract*— This paper mainly focuses on the performance evaluation of "Perturb&Observe" and "Incremental Conductance" algorithms as the most commonly utilized two Maximum Power Point Tracking (MPPT) techniques for photovoltaic systems. Matlab/SIMULINK platform is used to model and simulate the entire system. The simulation model of a PV module is constructed based on the one-diode mathematical model of a solar cell and the model is validated using the manufacturer`s datasheet parameters for a commercially available PV module. A boost type DC/DC converter topology is utilized and modeled and simulation models for "P&O" and "IncCond" algorithms are constructed. According to the results, both of the algorithms have shown almost similar performances under identical test conditions. Despite its relatively high complexity, the IncCond algorithm has been slightly more efficient and has reached to the MPP in a shorter time period, while most probably the simple structure of the P&O algorithm has caused it to be the most preferred MPPT algorithm. The paper provides reliable information on the performance and characteristics of the mentioned two MPPT techniques which can be used by system designers to improve the overall efficiency and reduce the cost of PV system applications.**

***Keywords- DC/DC converter, boost converter, incremental conductance, MPPT, perturb&observe, PV module, solar energy, solar cell.***

## Appendix G: A Simple MATLAB/Simulink Simulation for PV Modules Based on One-Diode Model

Moein Jazayeri, Sener Uysal, Kian Jazayeri, "A simple MATLAB/Simulink simulation for PV modules based on one-diode model", in *Proceedings - High Capacity Optical Networks and Emerging/Enabling Technologies, HONET-CNS*, pp.44-50, Famagusta, North Cyprus, December 2013.

***Abstract*—This paper proposes a simple and practical simulation model for solar modules using MATLAB/Simulink. The model is based on a single-diode mathematical model of a solar cell and is capable of accurate modeling of I-V and P-V characteristics of a solar module. Model parameters are obtained from manufacturer`s datasheets and series and shunt resistances are calculated using a simple method based on open-circuit voltage, short-circuit current and irradiance values. The model is interfaced with SimPowerSystems toolbox. This feature makes the model capable of being used with power electronic devices and elements for advance analyses. The model is validated using measured I-V characteristics of a commercially available crystalline silicon solar module and the effects of environmental conditions (temperature and irradiance) as well as the effects of cell parameters like series and shunt resistances on module characteristics are investigated. The proposed model is capable of being used by solar energy researchers, system analysts and designers as a simple and helpful tool for advance analysis requirements.**

***Keywords*—*solar energy, solar cell, solar module, module characteristics, simulink.***

## Appendix H: Experimental Analysis of Effects of Installation Alignment and Solar Insolation on Power Generation by Solar Panels

Moein Jazayeri, Sener Uysal, Kian Jazayeri, "Experimental analysis of effects of installation alignment and solar insolation on power generation by solar panels", in *Proceedings of the 3rd IEEE Global Humanitarian Technology Conference, GHTC 2013 (2013)*, pp.35-40, San Jose, CA, USA, October 2013.

***Abstract*— This paper mainly focuses on the effects of variations of solar irradiance on PV panel power outputs and considers the importance of choosing the right orientation for system installations. The analyses are based on real-time measured data collected during a 6-Month period (October/2012-March/2013) in Northern Cyprus. The mentioned data presents the months with the lowest solar insolation and the results clearly illustrate the direct relationship between the amounts of the solar irradiance and power generation by PV panels. The results can be utilized for effective use of PV systems, especially for rural areas and locations with relatively less amounts of available solar irradiance.**

***Keywords*— *photovoltaics, solar energy, solar insolation, solar power generation, solar data collection, sun`s position in the sky***

# Appendix I: MATLAB/Simulink Based Simulation of Solar Incidence Angle and the Sun's Position in the Sky with Respect to Observation Points on the Earth

Kian Jazayeri, Sener Uysal, Moein Jazayeri, "MATLAB/simulink based simulation of solar incidence angle and the sun's position in the sky with respect to observation points on the Earth", in *Proceedings of 2013 International Conference on Renewable Energy Research and Applications, ICRERA*, pp.173-177, Madrid, Spain, October 2013.

*Abstract*— **This paper proposes a simulation model for calculation of the sun`s position in the sky and the incidence angle of sunlight beams on the surface of solar modules with any tilt angle, located at any geographical location on the Earth`s surface. The electrical power generated by a solar panel directly depends on the amount of the received solar irradiance on panel surface where the received irradiance is directly proportional to the sun's position in the sky. Therefore, it is of great importance for solar energy researchers and system designers to have a precise knowledge about the movement and position of the sun in the sky with respect to any specific observation point on the earth. A simple and practical simulation model of the sun's position in the sky is designed using MATLAB/Simulink platform. The model simulates the sun`s position in the sky and solar angle of incidence based on the latitude and longitude of the observation point, solar module`s azimuth and tilt angle values, the Julian day number and the local clock time. The proposed model provides the possibility of instantaneous or continuous determination and tracking of the sun's position in the sky for any geographical location on earth and can be considered as a helpful tool for sun tracking and other system planning purposes.**

*Keywords— photovoltaic, photovoltaic simulation, solar altitude, solar angle of incidence, solar azimuth, solar energy, sun`s position in the sky, sun tracking,*

## Appendix J: Experimental Analysis of Effects of Connection Type on PV System Performance

Moein Jazayeri, Sener Uysal, Kian Jazayeri, Seyda Yapici, "Experimental analysis of effects of connection type on PV system performance" in *Proceedings of 2013 International Conference on Renewable Energy Research and Applications, ICRERA*, pp.190-195, Madrid, Spain, October 2013.

*Abstract* — **This paper mainly focuses on experimental performance analysis of solar modules under different irradiance values. Also effects of interconnection types and bypass diode application on module output characteristics under variable shading patterns are analyzed. The mentioned analyses are based on and supported by real-time measurement data and the results confirm the direct relationship between the power generation by solar modules and the incident solar irradiance. According to the results, although higher voltage values are obtained, series strings of solar cells/modules, without bypass diodes, show a higher sensitivity to shading effects and string output power is subjected to higher amounts of reduction compared with the parallel connection conditions. On the other hand, parallel connected solar cells/modules provide higher values of generated current amounts while the output voltages are equivalent to that of each individual cell/module. Experimental results also show that application of bypass diodes in series connected module strings has a great improving effect on power production by the string. The significance of the results arises during design and planning procedures of solar energy systems, where detailed knowledge of system characteristics under different shading patterns creates the opportunity to take the required measures and obtain optimum system performance.**

*Keywords— I-V characteristics, photovoltaic cell interconnection, photovoltaic power generation, P-V characteristics, solar energy, solar modules*

## Appendix K: A Case Study on Solar Data Collection and Effects of the Sun's Position in the Sky on Solar Panel Output Characteristics in Northern Cyprus

Moein Jazayeri, Sener Uysal, Kian Jazayeri, "A case study on solar data collection and effects of the sun's position in the sky on solar panel output characteristics in Northern Cyprus", in *Proceedings of 2013 International Conference on Renewable Energy Research and Applications, ICRERA*, pp.184-189, Madrid, Spain, October 2013.

*Abstract*—**This paper mainly focuses on methods of calculations of sun`s position in the sky and analyses of its effects on solar panel output characteristics collected during a case study. Methods for calculations of sun`s position in the sky and measurement of solar panel output characteristics are reviewed and then followed by a case study on an experimental data collection system in Northern Cyprus. During the case study, the collected ground measured data are analysed and the results are compared. The solar angle of incidence and the sun`s position in the sky are calculated and compared for different time intervals along with panel output characteristics. The short-term data sets belong to three sample days representing sunny, rainy and cloudy conditions in May-2012. The results highlight the effects of sun`s position in the sky and the incidence angles of sunlight, during different time intervals and dates, on module output characteristics. The results provide helpful information for researchers and system designers for system yield estimation purposes.**

*Keywords*— *photovoltaics, solar angle of incidence, solar energy, solar data collection, solar radiation, sun`s position in the sky*

## Appendix L: Determination of Power Losses in Solar Panels Using Artificial Neural Network

Kian Jazayeri, Sener Uysal, Moein Jazayeri, "Determination of Power Losses in Solar Panels Using Artificial Neural Network", in *Proceedings - IEEE AFRICON Conference*, Port Luis, Mauritius, September 2013.

*Abstract*— **The main purpose of this paper is on developing an intelligent system which provides real time monitoring and fault detection for solar panels. Utilizing artificial neural network technology, the solar panel fault detection system is capable of perceiving sun's position in the sky and estimating the corresponding output power of a solar panel based on the algorithms derived by the artificial neural network which has been trained on solar data at several time intervals. The system is capable of operating in any geographical location providing 24-hour monitoring and fault detection as well as future power estimations for solar panels.**

*Keywords—artificial neural networks, fault detection, photovoltaic cells, photovoltaic systems, solar energy, solar power generation.*

## Appendix M: Analysis of Effects of Sun's Position in the Sky on Solar Radiation and Solar Panel Output Power

Moein Jazayeri, Sener Uysal, Kian Jazayeri, "Analysis of effects of sun's position in the sky on solar radiation and solar panel output power", in *Proceedings - IEEE AFRICON Conference*, Port Luis, Mauritius, September 2013.

*Abstract* — **It is basically approved that the output power of a solar cell/module directly depends on the amount of solar irradiance which it receives from the sun. Also it is known that the irradiance values are not constant at any specific time interval. The changes in the position of the sun with respect to earth are one of the main reasons causing the variations in the amount of incoming sunlight and its energy to the earth's surface. The main focus of this paper is to analyze the effects of changes in the position of the sun in the sky on the incoming solar radiation during a whole year. Also the effects of such changes on the hourly values of solar radiation as well as the effects on the output power generated by a solar panel during a specific sample day is analyzed.**

*Keywords—solar energy, solar power generation, solar radiation, irradiance, photovoltaic cells, data acquisition, data analysis*